A CONCEPTUAL METHODOLOGY FOR THE PREDICTION OF ENGINE EMISSIONS

A Dissertation
Presented to
The Academic Faculty

by

Reza Rezvani

In Partial Fulfillment
of the Requirements for the Degree
Doctor of Philosophy

School of Aerospace/ College of Engineering
Georgia Institute of Technology
December 2010

Copyright © 2010 by Reza Rezvani

A CONCEPTUAL METHODOLOGY FOR THE PREDICTION OF ENGINE EMISSIONS

Approved by:

Prof. Dimitri N. Mavris,
Faculty Advisor and Committee Chair
School of Aerospace Engineering
Georgia Institute of Technology

Prof. Jeff Jagoda
School of Aerospace Engineering
Georgia Institute of Technology

Dr. Jimmy Tai
School of Aerospace Engineering
Georgia Institute of Technology

Prof. Brian German
Scholl of Aerospace Engineering
Georgia Institute of Technology

Mr. William J. Haller
Glenn Research Center
National Aeronautics and
Astronautics Administration (NASA)

Date Approved: November, 2011

To my dear parents and my dear wife

for their support and encouragement

ACKNOWLEDGEMENTS

Finally here I am, about to finish my long journey of dissertation; however, I could not have finished this journey without the help and companionship of many individuals.

First, I wish to thank my advisor Prof. Dimitri Mavris. Without his support and willingness to give me a chance to be a member of the Aerospace Systems Design Laboratory, I would not be writing this now. I would also like to thank Prof. Jeff. Jagoda who accepted me as a graduate student in the School of Aerospace Engineering and supported me as the school graduate coordinator and a member of my defense committee. Thanks to Dr. Jimmy Tai who mentored me during my research endeavor and thought me how to perform efficiently in the ASDL. Many times he stayed late with me in the lab discussing my research results and reviewing this dissertation. I would like to thanks Prof. Brian German who always motivated me about this work. I would also like to thank Mr. William J. Haller from NASA Glenn Research Center who made this whole research possible by funding it through the Advanced Emissions Modeling project under the NASA/GRC sponsorship.

I wish to thank those who once were or still are the residents of the room 308 and 310 at the Weber building: Mandy Goltsch, Simone Briceno, Kyle Collins, Fredric Villeneuve, Stephane Dufresne, Keith Becker, Joseph Iacobucci and Woong Je Sung; many of them are doctor now or on their way to become one. I've had a good time with them through all this years and learned a lot from them.

To my best friends in the lab, Ousmane Diallo, Bassem Nairouz and Brian Kestner: Thank you for your support, advice and giving me hope and encouragement to

move on. I am so glad that at difficult times, I could find you who could understand what I was going through and show me the way out.

I would like to thank my mom and dad who always encouraged and supported me and scarified their own life so I could have a better and brighter future. I hope I deserved it. Thanks to my other family members who have been patient enough, supportive and always believed in me.

Last but not least, special thanks to my dear wife, Tina who supported me with all the decisions I made all the way to the end and put up with me during my graduate study years.

At the end, I would also like to thank many other friends, colleagues, faculty members and staff whose names are not mentioned here for their advice, help and friendship.

I thank you all and wish you happiness and health.

Reza Rezvani

Atlanta, Fall 2010

TABLE OF CONTENTS

ACKNOWLEDGEMENTS ..... **IV**

LIST OF TABLES ..... **X**

LIST OF FIGURES ..... **XIII**

LIST OF ABBREVIATIONS ..... **XVIII**

LIST OF SYMBOLS ..... **XX**

SUMMARY ..... **XXII**

1 INTRODUCTION **1**

1.1 Design Process 1

1.2 Emissions Prediction and Combustor Design Considerations 4

1.3 Motivations 9

1.3.1 Environmental Concerns 10

1.3.2 Aviation Growth and Regulations 14

1.3.3 Shortcomings of Emissions Prediction Models 21

1.4 Research Objective and Research Questions 24

2 THEORETICAL BACKGROUND AND LITERATURE REVIEW **26**

2.1 Internal Flow-field Models 29

2.1.1 CFD Approach 29

2.1.2 Network Approach 31

2.1.3 Control Volume Approach 33

2.1.4 Component Modeling Approach 33

2.1.5 Assessment of Internal Flow-field Analysis Approaches 40

2.2 Combustion Models 41

2.2.1 Combustion Mechanism 43

2.2.2 Chemical Reactors Network Approach 51

2.3 Assessment of Current Emissions Prediction Approaches 59

2.4 Uncertainty Analysis 61

3 INTERIM SUMMARY AND HYPOTHESIS FORMULATION 64

3.1 Review of Research Objective and Research Questions 64

4 GENERAL DESCRIPTION OF RQL COMBUSTOR CONCEPT 71

4.1 Fuel Management 74

4.1.1 Variable Geometry 74

4.1.2 Fuel Shifting 76

4.2 Mixing Methods 77

4.3 Atomizer and swirler 79

5 PROPOSED METHODOLOGY 80

5.1 One Dimensional Internal Flow-Field Model 83

5.1.1 Chemical Equilibrium Analysis 84

5.1.2 Flow Properties 86

5.1.3 Diffuser Model 87

5.1.4 Snout Model 92

5.1.5 Flow Partitioning Model 93

5.1.6 Combustor Zones 99

5.1.7 Combustor Configuration and Orientation 110

5.1.8 Volume of Combustor Zones 112

5.1.9 Annulus Zone 113

5.1.10 Combustor 2D View Model 114

5.2 Droplet Evaporation and Diffusion Burning Model 114

5.3 Non-Uniform Mixture Model 120

5.4 Chemical Reactors Network Model 124

5.4.1 A Chemical Reactor's Network Model for Single Annular Combustor 127

5.4.2 A Chemical Reactor's Network Model for RQL Combustor 128

5.5 Post Processing 132
5.6 Challenges 132
5.6.1 Design Perspective versus Analysis Perspective 132
5.6.2 Disciplinary Models/Tools and Their Integration 133
5.6.3 Limited Available Data 133
5.6.4 Combustion Mechanism 134
5.7 Emissions Prediction Approach and Skin Friction Coefficient Calculation Analogy 134
6 INTEGRATED ENVIRONMENT 137
6.1 1D Internal Flow-Field Model 138
6.2 CRN Model 139
6.3 Linking All Components Together 142
7 APPROACH IMPLEMENTATION AND RESULTS 146
7.1 Surrogate Model for Chemical Equilibrium Analysis 148
7.2 Fuel Combustion Mechanism 151
7.3 Experiment 1: Emissions Prediction of Single Annular Combustor 158
7.3.1 Emission Model for the CFM56-7B27 Combustor 158
7.3.2 Emission Model for the Energy Efficient Engine Combustor 170
7.3.3 SAC Emission Model Results and Discussion 177
7.3.4 Generalized Non-Uniform Mixture Model 193
7.4 Experiment 2: Further Analysis of the CFM56 Combustor Emissions Model . 198
7.4.1 Uncertainty Analysis 198
7.4.2 Sensitivity Analysis 206
7.5 Experiment 3: Emissions Prediction of an RQL Combustor 218
8 DISCUSSION AND CONCLUSION 235
8.1 Review 235

8.2 Revisiting Research Questions and Hypotheses 236
8.2.1 Research Questions 236
8.2.2 Hypotheses 236
8.3 Contributions 239
8.4 Limitations and Future Works 241
8.5 Final Remarks 245
APPENDIX A. TRANSIENT DROPLET EVAPORATION MODEL 247
APPENDIX B. COMPONENT SCRIPTS AND CODES 252
APPENDIX C. EMISSION MODELS OUTPUTS 269
REFERENCES 273

LIST OF TABLES

Table 1: Combustor design conflicting requirements [14] 9
Table 2: Major potential impacts of chemical compounds released by aircraft [19].....13
Table 3: Outcomes of past CAEP meetings [3] 18
Table 4: ICAO/LTO cycle duration and thrust setting at each mode 19
Table 5: Inputs and design parameters in Genetic algorithm optimization 32
Table 6: Comparison between internal flow-field analysis methods.....41
Table 7: Surrogate model of JP-4 [16].....46
Table 8: MATHALB functions used in the 1D flow-field Model 138
Table 9: Components of the SAC CRN (left) and RQL CRN (right) model.....140
Table 10: Main commands used in the CHEMKIN CRN model 141
Table 11: Design and operating parameters.....142
Table 12: Inputs to the 1D flow-field model 144
Table 13: Inputs to the Droplet Evaporation and Diffusion Burning model 145
Table 14: Inputs to the CRN Model.....145
Table 15: Input range of training data for the CEA neural network models 150
Table 16: Number of hidden nodes of the CEA neural network models.....151
Table 17: Cycle parameter values determined in EDS project for the CFM56-7B27.....160
Table 18: Measured geometrical information of the CFM56 SAC combustor 160
Table 19: Mean radius of compressor exit and turbine inlet of the CFM-56 engine.....161
Table 20: The CFM56 SAC diffuser inlet Mach number at four ICAO/LTO modes 161
Table 21: Known information and parameters of the CFM56 SAC.....163
Table 22: The CFM56 SAC variables considered in the Monte Carlo filtering for geometry matching 163
Table 23: Filtered set of inputs of the CFM56 SAC 1D flow-field model determined from MCF for geometry matching 166
Table 24: Final set of inputs of the CFM56 SAC 1D flow-field model 166
Table 25: Comparison of the model predicted and actual geometrical data of the CFM56 SAC.....167
Table 26: Considered range of unmixedness degree and cooling flow fractions for the CFM-56 SAC model in the Monte Carlo simulation 168

Table 27: The CFM-56 SAC final set of unmixedness degree and cooling flow fractions 169
Table 28: The CFM-56 SAC predicted emission indices using parameters obtained from the Monte Carlo simulation 169
Table 29: Measured or published geometrical information of the E^3 SAC 171
Table 30: The E^3 cycle parameter values [18] 171
Table 31: The E^3 SAC diffuser inlet Mach number at four ICAO/LTO modes 172
Table 32: Known information and parameters of the E^3 SAC.....172
Table 33: The E^3 SAC variables considered in the MCF for geometry matching.....173
Table 34: Filtered set of inputs of the E^3 SAC 1D flow-field model determined from MCF for geometry matching 173
Table 35: Final set of inputs of the E^3 SAC 1D flow-field model 175
Table 36: Comparison of the model predicted and actual geometrical data of the E^3 SAC 175
Table 37: Considered range of unmixedness degree and cooling flow fractions for the E^3 SAC model in Monte Carlo filtering 176
Table 38: E^3 SAC final set of unmixedness degree and cooling flow fractions 177
Table 39: E^3 SAC predicted emission levels using parameters that are obtained from the Monte Carlo simulation 177
Table 40: E^3 SAC and CFM56 SAC model results based on GNUM model and Monte Carlo simulation unmixedness values 195
Table 41: Input ranges and definitions of on-design parameters for the Monte Carlo simulation 199
Table 42: Input ranges and definitions of off-design parameters for the Monte Carlo simulation 200
Table 43: Range of on-design parameters for the sensitivity analysis.....207
Table 44: Range of off-design parameters for the sensitivity analysis 209
Table 45: Geometry information of the Wall-Jet RQL combustor [1] 221
Table 46: RQL combustor engine cycle parameters [1]. 222
Table 47: Inputs of the RQL combustor 1D flow-field model 225
Table 48: Comparison of the 1D flow-field model outputs and actual values 226

Table 49: swirler area and associated parameters' variation 226
Table 50: Predicted emission indices and unmixedness degrees of the Wall-Jet RQL combustor 226
Table 51: Additional outputs of the CFM56-7B27 SAC emission model.....270
Table 52: Additional outputs of the E^3 SAC emission model 271
Table 53: Additional outputs of the Wall-Jet RQL combustor emission model.....272

LIST OF FIGURES

Figure 1: Basic modules in the design process [6] 1
Figure 2: General design process steps from problem definition to detail design [6] 2
Figure 3: Cost, knowledge and design freedom during design Process 3
Figure 4: Aircraft, engine and combustor hierarchical connectivity 5
Figure 5: NO_x and CO Correlation [4].....6
Figure 6: Forecast of aviation continuous growth [12].....14
Figure 7: Air fleet expansion demand due to growth in aerial transportation and need to replace the retired aircrafts [12] 15
Figure 8: Reduction trend of aircraft emissions in the past [12].....15
Figure 9: NO_x ICAO regulation based on engine rated thrust and OPR [11].....17
Figure 10: ICAO/LTO cycle [10] 17
Figure 11: A generic layout of a single annular combustor [7] 29
Figure 12: A network generated for an annular combustor [21] 32
Figure 13: Droplet size distribution 35
Figure 14: Axial and radial swirlers.....37
Figure 15: An example of elementary reactions 44
Figure 16: Distillate curve of JP-4 [16] 45
Figure 17: An example of a network of elementary chemical reactors [8] 51
Figure 18: Perfect Stirred Reactor (PSR) and its parameters [2].....53
Figure 19: Plug Flow Reactor (PFR) and its parameters 55
Figure 20: Steps in Monte Carlo analysis 62
Figure 21: Relation between the research questions and hypotheses 69
Figure 22: Equivalence ratio of an RQL combustor at different axial locations [15] 71
Figure 23: An RQL combustor concept [9] 73
Figure 24: Fuel operating schedule of a variable geometry RQL combustor [1] 75
Figure 25: NASA HSR fuel-shifting RQL concept [1] 75
Figure 26: Fuel operating schedule of a fuel-shifting RQL combustor [1] 76
Figure 27: An RQL combustor with Wall-Jet mixing zone in the middle section [1].....77
Figure 28: Reduced scale quench concept with convoluted liner [1] 78
Figure 29: Reduced scale quench concept with quench vanes [1].....78

Figure 30: Combustor zones and flow partitions 81
Figure 31: The flow chart of the emission prediction model 82
Figure 32: Main combustor elements in 1D internal flow-field model 83
Figure 33: Diffuser model and its parameters 88
Figure 34 : The flowchart of sizing the diffuser at design condition. 90
Figure 35: Snout section located between the diffuser and liner 93
Figure 36: Primary zone and swirler 100
Figure 37: Secondary zone and its main parameters and features 103
Figure 38: Transition zones and their main parameters and features 110
Figure 39: Combustor with different inlet and exit mean radii 111
Figure 40: Zone volume in annular combustor configuration as a combination of incomplete cones 113
Figure 41: Droplet size distribution 117
Figure 42: Time variation of three droplet parameters 119
Figure 43: Droplet size distribution at the beginning (blue) and the end (red) of the ignition delay time 120
Figure 44: Heywood unmixedness parameter [9] 121
Figure 45: The unmixedness degree diagram [13] 122
Figure 46: Truncated and discretized normal distribution of equivalence ratio [13] 124
Figure 47: Network of reactors based on combustor zones 125
Figure 48: A chemical reactors' network with implementation of diffusion burning and unmixedness degree in CHEMKIN software environment [13] 126
Figure 49: A proposed CRN for the single annular combustor configuration 127
Figure 50: A proposed CRN for the RQL combustor configuration 129
Figure 51: Velocity profile in boundary layer [5] 136
Figure 52: Integrated emission model in the Model Center environment 143
Figure 53: Relation between the research questions, hypotheses and experiments 147
Figure 54: Structure of NPSS model to run CEA analysis 149
Figure 55: Cold flow neural net training results for c_p (top figure) and γ (bottom figure) 152

Figure 56: Cold flow neural net training results for μ (top figure) and R (bottom figure) 153
Figure 57: Reacting-Flow neural net training results for c_p (top figure) and γ (bottom figure) 154
Figure 58: Reacting-Flow neural net training results for μ (top figure) and R (bottom figure) 155
Figure 59: Reacting-Flow neural net training results for exit temperature.....156
Figure 60: Kollrack combustion mechanism for aviation fuel (Jet-A) 157
Figure 61: SAC combustor of the CFM56-7B27 engine with dimensions measured in inches [18, 22] 159
Figure 62: 1D flow-field and CRN models of a single annular combustor in the CHEMKIN 162
Figure 63: Scatter plot matrix of inputs and outputs of the CFM-56 SAC 1D flow-field model (top figure) and MCF (bottom figure) in JMP 165
Figure 64: The CFM-56 SAC actual and 1D flow-field model drawings 168
Figure 65: SAC combustor of the E^3 with dimensions measured in inches [20].....170
Figure 66: The E^3 SAC 1D flow-field scatter plot matrix (top figure) and MCF (bottom figure) in the JMP 174
Figure 67: The E^3 actual and 1D flow-field model drawings 176
Figure 68: The CFM56 SAC cooling flow budget 178
Figure 69: The E^3 SAC cooling flow budget 178
Figure 70: Predicted and actual NO_x emission indices of the CFM56 SAC 181
Figure 71: Predicted and actual NO_x emission indices of the E^3 SAC 181
Figure 72: Predicted and actual CO emission indices of the CFM56 SAC 182
Figure 73: Predicted and actual CO emission indices of the E^3 SAC.....182
Figure 74: The CFM-56 SAC droplet distribution at time zero (blue) and at the ignition time (red) and the time variation of droplet parameters at take-off and climb 184
Figure 75: The CFM-56 SAC droplet distribution at time zero (blue) and at the ignition time (red) and the time variation of droplet parameters at approach and idle 185

Figure 76: The E3 SAC droplet distribution at time zero (blue) and at the ignition time (red) and the time variation of droplet parameters at take-off and climb.....186
Figure 77: The E^3 SAC droplet distribution at time zero (blue) and at the ignition time (red) and the time variation of droplet parameters at approach and idle.....187
Figure 78: CFM56 SAC droplet distributions 188
Figure 79: E^3 SAC droplet distributions 188
Figure 80: The CFM-56 premixed equivalence ratio distribution in the primary zone...189
Figure 81: The E^3 premixed equivalence ratio distribution in the primary zone. 190
Figure 82: The CFM-56 SAC axial temperature variations across combustor zones.....191
Figure 83: The E^3 SAC axial temperature variations across combustor zones.....192
Figure 84: A generalized model for the unmixedness degree.....194
Figure 85: Comparison of the CFM56 SAC EI NO_x values.....196
Figure 86: Comparison of the CFM56 SAC EI CO values 196
Figure 87: Comparison of the E^3 SAC EI NO_x values.....197
Figure 88: Comparison of the E^3 SAC EI CO values 197
Figure 89: Frequency distribution of EI NO_x and EI CO at take-off.....202
Figure 90: Frequency distribution of EI NO_x and EI CO at climb 203
Figure 91: Frequency distribution of EI NO_x and EI CO at approach.....204
Figure 92: Frequency distribution of EI NO_x and EI CO at idle 205
Figure 93: Relative contribution of input parameters to EI NO_x at take-off.....210
Figure 94: Relative contribution of input parameters to EI NO_x at the climb condition.211
Figure 95: Relative contribution of input parameters to EI NO_x at the approach condition.....212
Figure 96: Relative contribution of input parameters to EI NO_x at the idle condition....213
Figure 97: Relative contribution of input parameters to EI CO at the take-off condition216
Figure 98: Relative contribution of input parameters to EI CO at the climb condition...217
Figure 99: Relative contribution of input parameters to EI CO at the approach condition.....218
Figure 100: Relative contribution of input parameters to EI CO at the idle condition....219
Figure 101: Quick mixing in RQL combustor to bypass the high NO_x stoichiometric region [17] 220

Figure 102: The NASA HSR Wall-Jet RQL single module and final configuration [1].221
Figure 103: The 1D flow-field and CRN models of the RQL combustor configuration in CHEMKIN 222
Figure 104: The Wall-Jet RQL combustor actual and 1D flow-field model produced drawings 225
Figure 105: The Wall-Jet RQL combustor predicted and actual NO_x emission indices .227
Figure 106: The Wall-Jet RQL combustor droplet distributions 228
Figure 107: The Wall-Jet RQL combustor predicted and actual CO emission indices ...229
Figure 108: The Wall-Jet RQL combustor premixed equivalence ratio distribution in the rich zone 230
Figure 109: The Wall-Jet RQL combustor axial temperature variation across combustor zones 231
Figure 110: The pdf of temperature, NO, CO, CO2 and H2O at the output of the PaSR at supersonic cruise condition 232
Figure 111: Effect of changing the mixing to rich zone area ratio on the emission indices.....233

LIST OF ABBREVIATIONS

AEDT	Aviation Environmental Design Tool
ASC	Air Staged Combustor
ASDL	Aerospace Systems Design Laboratory
CAEP	Committee on Aviation Environmental Protection
CCD	Computational Combustion Dynamics
CDF	Cumulative Distribution Function
CFD	Computational Fluid Dynamics
CO	Carbon Monoxide
CRN	Chemical Reactor's Network
DEDB	Droplet Evaporation and Diffusion Burning
DLN	Dry Low NO_x
DOE	Design Of Experiments
DZ	Dilution Zone
EDS	Environmental Design Space
EI	Emission Index
EPA	Environmental Protection Agency
EPAP	Environmental Protection Agency Parameter
FAA	Federal Aviation Administration
FAR	Fuel to Air Ratio
GNUM	Generalized Non-Uniform Mixture
HSCT	High Speed Civil Transport
HSR	High Speed Research
ICAO	International Civil Aviation Organization
LDI	Lean Direct Injection
LPP	Lean Premixed Pre-Vaporized

LTO	Landing/Take-off
MCF	Monte Carlo Filtering
MCS	Monte Carlo Simulation
MMD	Mass Median Diameter
MZ	Mixing Zone
NO_x	Nitrogen Oxides
NPSS	Numerical Propulsion System Simulation
NUM	Non-Uniform Mixture
ODE	Ordinary Differential Equation
OPR	Overall Pressure Ratio
PaSR	Partially Stirred Reactor
pdf	Probability Density Function
PFR	Plug Flow Reactor
PSR	Perfect Stirred Reactor
PZ	Primary Zone
RQL	Rich Quench Lean
SAC	Single Annular Combustor
SMD	Sauter Mean Diameter
SO_x	Sulfur Oxides
SZ	Secondary Zone
TALON	Technology for Advanced Low NO_x
TAPS	Twin Annular Premixed Swirler
TZ	Transition Zone
UHC	Unburned Hydro Carbons
VOP	Volatile Organic Particulates

LIST OF SYMBOLS

A	Area
a	Cooling mechanism Technology Factor
AR	Diffuser Aspect Ratio
B	Droplet's Spalding Transfer Number
C_d	Orifice's Flow Coefficient
C_P	Diffuser Pressure Recovery Coefficient
c_p	Specific Heat at Constant Pressure
D	Droplet Diameter
d	Jet or Orifice diameter
FN	Injector Flow Number
G	Gibbs Energy
H	Cross Section's Height
h	Latent Heat of Evaporation
J	Flow Momentum Ratio
K_{sw}	Swirler Discharge Parameter
K	Equilibrium Constant/ Droplet Evaporation Constant
k	Thermal Conductivity/Reaction Rate
L	Length
M	Mach Number
n	Number of dilution orifices or Injectors
Pr	Prandtl Number
Q	Dynamic Pressure/Volume Fraction in the Rosin-Rammler Equation
q	Flow Momentum/ Shape Factor in the Rosin-Rammler Equation
r	Radius
R	Gas Constant

Re	Reynolds Number
S	Unmixedness Degree/ Optimum Distance between Quenching Orifices
SW	Swirl Number
T	Temperature
V	Velocity/Volume
X	Scale Factor in the Rosin-Rammler Equation
Y	Jet Penetration Depth/ Species Mass Fraction
α	Swirler Area Coefficient
α_{sw}	Swirl Angle
β	Divergence or Convergence Angle of Transition Zone
γ	Specific Heat Ratio
ΔP_{tot}	Total Pressure Loss
η	Efficiency
θ	Dilution Jet Penetration Angle
μ	Dynamic (Absolute) Viscosity/Zone's Flow Fraction
ν	Kinematic Viscosity
ρ	Density
σ	Surface Tension/ Standard Deviation
τ	Characteristic Time
Φ	Cooling Effectiveness
φ	Equivalence Ratio

SUMMARY

Current emission prediction models in the conceptual design phase are based on historical data and empirical correlations. Two main reasons contributing to the current state of emission models are complexity of the phenomena involved in the combustor and relatively low priority of having a more detailed emissions model at the conceptual design phase. However, global environmental concerns and aviation industry growth highlight the importance of improving the current emissions prediction approaches. There is a need to have an emission prediction model in the conceptual design phase to reduce the prediction uncertainties and perform parametric studies for different combustor types and operating conditions.

The research objective of this thesis is to develop a methodology to have an initial estimate of gas turbines' emissions, capture their trends and bring more information forward to the conceptual design phase regarding the emission levels. This methodology is based on initial sizing of the combustor and determining its flow-fractions at each section using a 1D flow analysis. A network of elementary chemical reactors is considered and its elements are sized from the results of the 1D flow analysis to determine the level of emissions at the design and operating conditions. Additional phenomena that have significant effects on the prediction of emissions are also considered which are: 1) droplet evaporation and diffusion burning, and 2) fuel-air mixture non-uniformity. A simplified transient model is developed to determine the evaporation rate for a given droplet size distribution and to obtain the amount of vaporized fuel before they ignite. A probabilistic unmixedness model is also employed to consider the range of equivalence ratio distribution for the fraction of the fuel that is vaporized and mixed with air.

An emission model is created for the single annular combustor (SAC) configuration and applied to two combustors to test the prediction and parametric

capabilities of the model. Both uncertainty and sensitivity analyses are performed to assess the capability of the model to reduce the prediction uncertainty of the model compared to the simpler models without considering the droplet evaporation and mixture non-uniformity. The versatility of the model is tested by creating an emission model for a Rich-Quench-Lean (RQL) combustor, and the results are compared to limited actual data.

In general, the approach shows a good performance predicting the NO_x emission level compared to CO emission level and capturing their trends. Especially in the RQL combustor case, a more detailed model is required to improve the prediction of the CO emission level.

CHAPTER 1

INTRODUCTION

1.1 Design Process

The main subject of this thesis is emissions prediction at the conceptual design phase; however, it is beneficial to explain the general design process in general and how it is related to the emissions prediction.

The design is defined as a plan to develop and build a product, process, component or system of components to achieve a certain objective(s) while satisfying given requirements and constraints[6]. A good design comprises of analysis and synthesis. The synthesis involves the design components identification and break down and combining them back together to the whole design. The analysis deals with modeling and predicting the behavior of components using mathematical, physical and computational tools [6]. Designing is an iterative process and sometime due to lack of knowledge, inaccurate physical models, change of conditions and many other factors, it is necessary to go back to earlier steps to update or change inputs based on a newly acquired experience and information that have been obtained through the process (Figure 1).

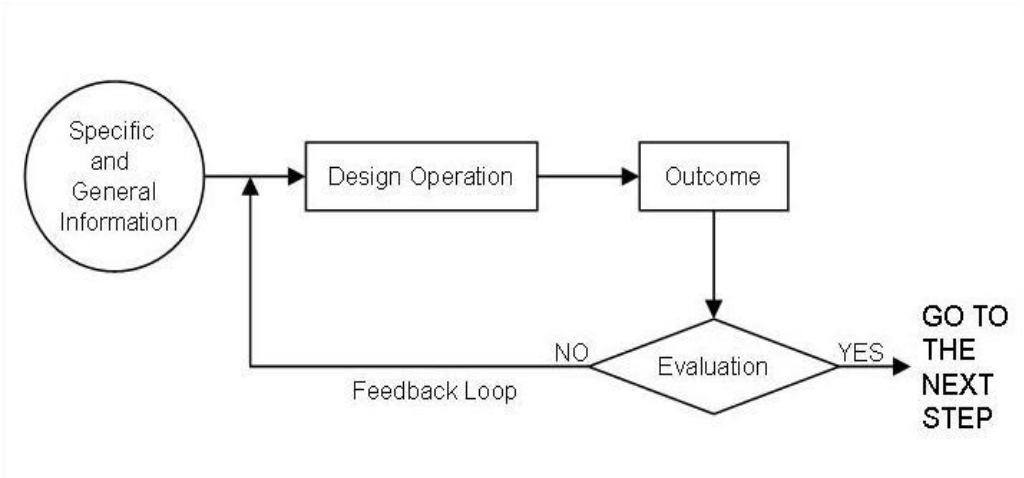

Figure 1: Basic modules in the design process [6]

As shown in Figure 2, design process consists of three major steps, *conceptual*, *preliminary* or *embodiment* and *detailed* design.

The conceptual design which is the first step in the design process starts with defining the requirements obtained from customer reviews, market studies, a request for proposal (RFP) or a mission profile. It is crucial to have a set of well defined, inclusive, non-conflicted, technically feasible and economically viable requirements. Poorly defined requirements can introduce a large amount of uncertainty into the process. Lists of unsuccessful designs that suffered from unrealistic requirements from technical or economical perspective is long.

The requirements are translated to a set of engineering characteristics and then the main characteristics and elements of the design are determined. Initially a number of possible design alternatives are created and based on given criteria and the analysis and synthesis results the best alternative among them will be selected. At this stage, there is enough freedom to change or modify the design at relatively low cost. Decisions that are made in the conceptual design phase have the most significant effect on the design characteristic. They shape the overall design architecture and will propagate to the later steps and even to manufacturing and production levels. With progressing in the design

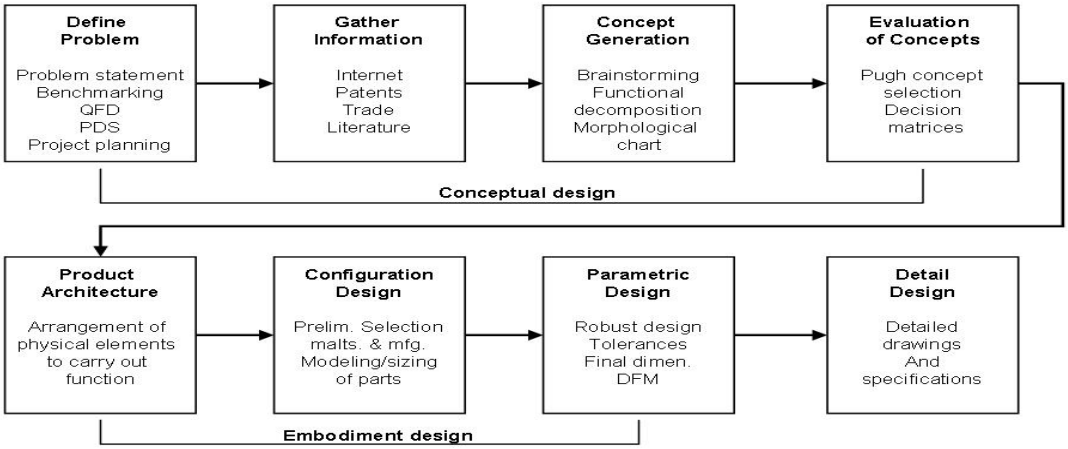

Figure 2: General design process steps from problem definition to detail design [6]

process, a freedom to change the design is shrinking, and it becomes more expensive to perform major changes. If a design change deems necessary, then one should go back to previous levels and start the process again (Figure 2). To have a better picture of a problem and its scope, it is important to provide designers with enough knowledge to make timely decisions because changing a design in the earlier design phase is easier than later phases. In the earlier design phases more freedom exists to change the design and less cost is committed to the design process. As a result, it is desired to provide as much knowledge as possible to the designer to make a correct decision at early design phases (Figure 3).

In the preliminary design phase, with utilizing a high fidelity analyses, more unknown aspects of the design are explored and more design characteristics are determined. Better prediction of the design behavior and its performance is possible at this step. Decision about the shape, placement and size of the components are made in this step; therefore, performing major design changes after this point becomes expensive.

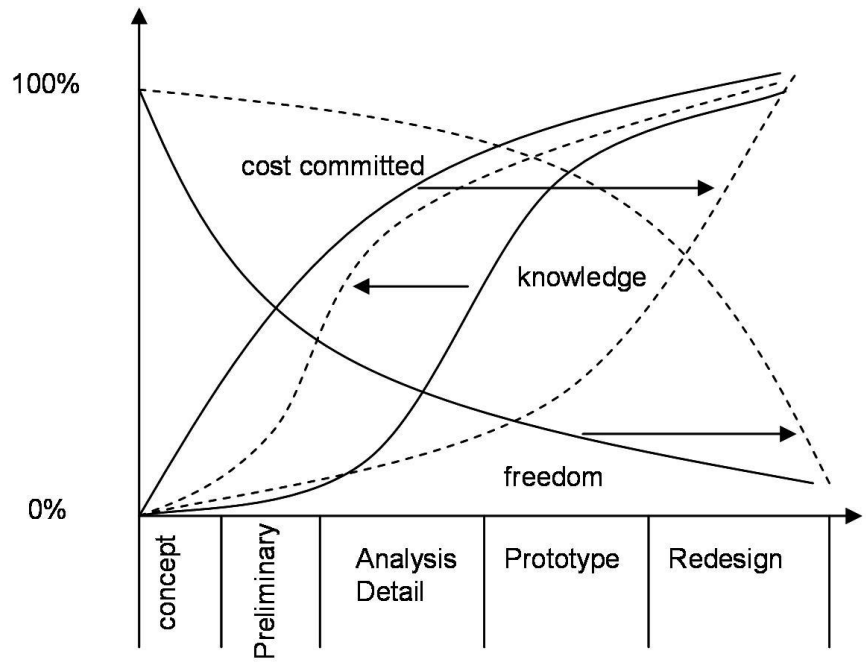

Figure 3: Cost, knowledge and design freedom during design Process

There are three main steps in the preliminary design phase which are the product architecture, configuration design and parametric design [6]. In the product architecture, the overall shape and components of the design are studied while configuration design is more focused on shape and placement and other features of each component and subsystem. In the parametric design, the effort will be focused on modeling the behavior of the system and predicting its response under non-ideal circumstances to find a set of parameters that ensures the optimality or robustness of the design.

In the detailed design, decisions about the finest details of a design have to be made. Materials, manufacturing process guidelines and accurate part dimensions are created to make it ready for production and manufacturing process.

1.2 Emissions Prediction and Combustor Design Considerations

The emission levels, combustor features and geometry are closely related to each other. To develop an emissions prediction model, a level of knowledge about the combustor and its features are required. The level of knowledge increases as the design moves from the early design phases to the final stages. As a result, the accuracy of the emissions prediction increases and the prediction uncertainty decreases by moving from the conceptual design phase to the detail design phase and experiments.

In this work, the intention is not to provide a methodology to design a combustor, but due to the close relation between the emission levels and the combustor characteristics, a brief description of the combustor and its design characteristics is provided in this section. The goal is to make the reader familiar with the complexity involved in the combustor design and the relation between the combustor design characteristics and the fidelity of the emissions prediction model.

Combustors are integral part of gas turbine engines. Any change of characteristics and parameters at higher level would propagate to lower levels and have direct or indirect implications on the combustor design and emission levels (Figure 4).

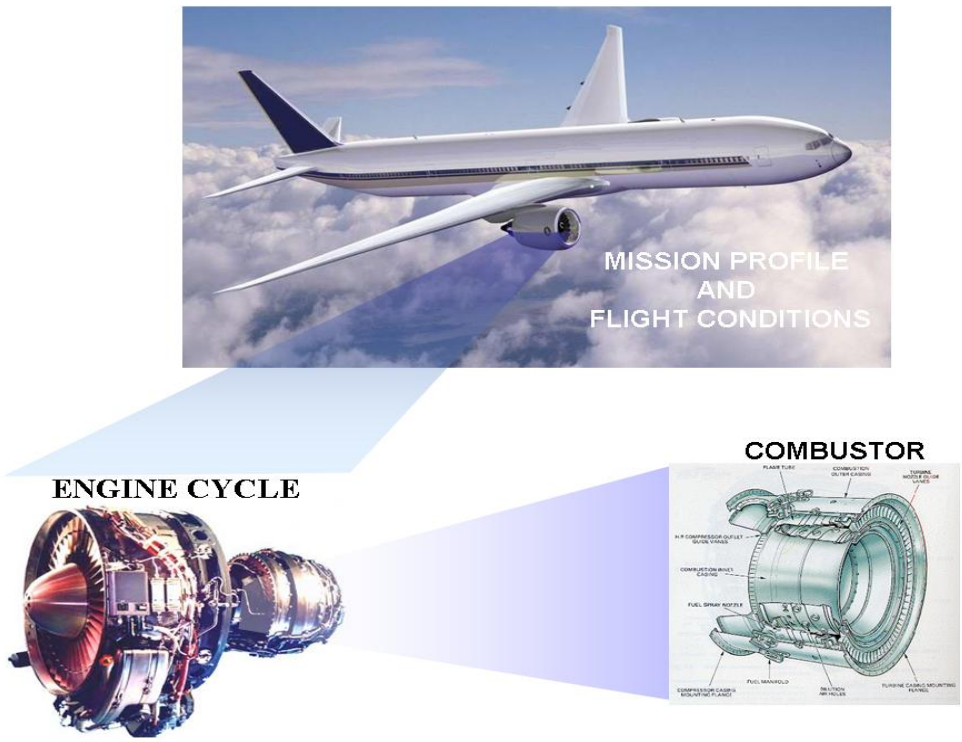

Figure 4: Aircraft, engine and combustor hierarchical connectivity

Designing and analyzing a combustor presents a major challenge to designers and researchers due to the followings:

- Complexity and nonlinearity of physical and chemical phenomena
- Conflicting requirements

At the initial gas turbine engine design phase, a combustor is considered as a black box that has a sole purpose of giving certain amount of thermal energy to the high pressure flow that comes from the compressor. In this perspective, a combustor model is a thermodynamics equation that calculates the required amount of fuel flow for a required temperature rise and no emission consideration is involved. However, in reality there are additional tasks that must be accomplished by a combustor. It should extract maximum amount of chemical energy from the fuel, convert it into heat and transfers it to the incoming air at the best efficiency. A combustor design must assure flame endurance, stability and relightability, even in most unfavorable conditions. The combustor has to

provide a favorable exit temperature profile tailored to the needs of first row of turbine blades. At the same time the combustor should keep its emission levels below the maximum allowable limits.

Difficulties exist to control the combustor emissions due to its chemo-physical complexity and the presence of conflicting requirements. For example, while it is desired to have high combustion efficiency which is attainable at maximum flame temperature, it is in conflict with having low NO_x emission levels which is achievable at lower temperatures. On the other hand, if the flame temperature is lowered to reduce NO_x emissions, it causes CO, UHC and particulate emissions to rise. It means that at low engine power settings where the flame temperature is not at its peak and mixing is poor, the CO emission is dominant and at high power settings the NO_x emissions become dominant (Figure 5).

Having adequate amount of total pressure loss in a combustor is another issue. While any kind of pressure loss in combustor due to heat addition and friction reduces the overall propulsion efficiency, certain amount of pressure loss is needed. This pressure loss forces the annulus dilution flow to penetrate into the combustor's core section. In addition, the pressure difference makes the turbine cooling flow to move through the cooling holes located on the blades.

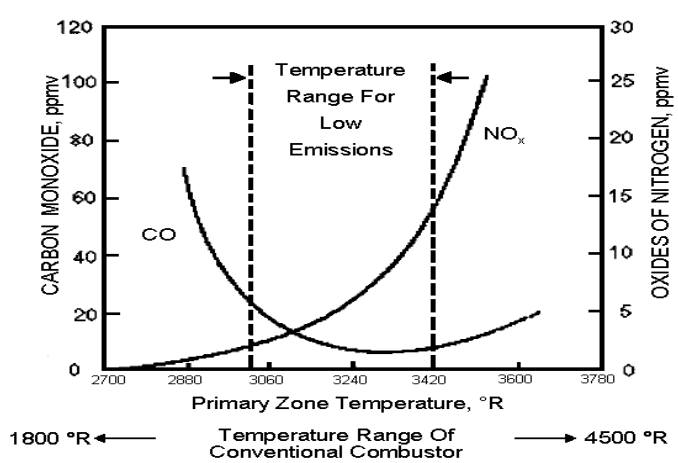

Figure 5: NO_x and CO Correlation [4]

Many of the issues mentioned above cannot be addressed properly in the initial design phases because many aspects of the combustor design are not known yet and without knowing them, modeling the aforementioned phenomena is not possible. As mentioned, in the first design phase of a combustor, only a simple enthalpy calculation in engine cycle analysis is considered. With this calculation, the amount of thermal energy required for a required amount of thrust or power is determined. Consequently, this calculation provides the first estimate of the required amounts of fuel flow and air flow. To determine the general combustor geometry in the next step, the combustor type and configuration must be known. The combustor type and configuration is often preselected as a priori based on the technology level and the engine manufacturer experience. The most common types of combustors are listed below, but some of these types are not being used in today aero turbine engines. Currently in aero-turbine engines, the preferred choice is the single or double annular combustor type due to the volume of the available data about them, experience using them and their low weight and compact size. There are undergoing attempts to develop other type of combustors to be used in aero-turbine engines.

- Can type
- Can-Annular type
- Reverse flow
- Single Annular Combustor (SAC)
- Double Annular Combustor (DAC)
- Rich-Quench-Lean (RQL)
- Lean Premixed Pre-vaporized (LPP)
- Dry Low NO_x (DLN)

The obtained information can be used to determine an overall shape of the combustor and first estimate of its dimensions to satisfy part of the requirements without

violating the constraints. A comprehensive list of combustor design conflicting requirements is shown in Table 1 [14]. The key point to satisfy the stated requirements is to have a desired flow distribution which itself depends strongly on the geometry of the combustor and its features. The flow-field inside the combustor affects the combustion process meaning that what happens inside a combustor is a physiochemical phenomenon [23] and modeling any type of combustor should be based on the following two major disciplines and the interactions between them:

- Flow-field analysis
- Combustion analysis

It is not possible in the conceptual design phase to take all these requirements into account and some of them can only be considered and determined in the detail or experiment phase.

A general understanding of the flow distribution inside the combustor can be obtained in the conceptual design phase and these results open a way to initially size the combustor elements. All this information may be used to develop an emission model that provides the first-hand estimate of the emission levels of the combustor in early design phases. The emphasis in the conceptual design phase is more on having a tool to capture the trend, interdependencies and relative changes of the emission levels by varying different parameters and there is less focus on the prediction accuracy.

More detailed information about the combustor can be obtained by further refining the design in the preliminary and detail design phases. In these phases, more phenomena and higher fidelity models are considered and the focus is on the details of the combustor elements and optimizing their performance. More combustor requirements can be taken into account in these phases. All these additional information can be used to improve the emission model and increase its accuracy.

One of the final design stages is combustor testing, where initially a sector of a combustor is tested, such a process is known as sector rig test. Many tests are conducted

at different conditions that are sometimes different from real operating conditions due to the cost and complexity of the process, and the data are then extrapolated to real conditions [18, 24-28]. When all the potential design and technical problems are discovered and resolved, a full-scale combustor rig test is performed to better assess its performance and make it ready for the integration with other engine components. At these stages the emission levels are measured and the assessment is performed to test whether all the requirements are met or not. A correlation-based emission model may be developed at this phase.

After providing a brief explanation of design process and the relation of the emissions prediction fidelity and the combustor design phase, the motivations to predict the emission levels at the conceptual design phase are discussed in depth in the following section.

1.3 Motivations

Motivations of this thesis are provided in three groups or levels in a hierarchical form. The highest level is related to the environmental concerns. The second level is aviation growth and regulations, and the last one is emissions models uncertainty and

Table 1: Combustor design conflicting requirements [14]

Design Requirements	Conflicts
Maximum combustion efficiency	NO_x
Minimum pressure loss	Pattern factor, NO_x, smoke, turbine back-flow margin
Combustor exit temperature quality	T_{wall}, ΔP, combustor length and channel height, number of fuel nozzles
Cool combustor walls, long life	Pattern factor, low-power CO and HC
Wide flight envelope	Ignition, stability, pattern factor, smoke
Minimum NO_x and smoke	CO, HC, ignition, stability, complexity
Simple construction, light weight and low cost	T_{wall}, pattern factor variation, emissions
Minimum size and length	Operating range, pattern factor
Minimum number of fuel nozzles, simple fuel injection system	Pattern factor, ignition, stability, emissions

their limited parametric capabilities. Each group of motivations is related to the previous group.

1.3.1 Environmental Concerns

Aircraft's engine exhaust products are made of water vapor (H_2O), carbon dioxide (CO_2), carbon monoxide (CO), oxides of nitrogen (NO_x), oxides of sulfur (SO_x), unburned or partially burned hydrocarbon (UHC), volatile organic particulates (VOP), soot and, particulates. Among these pollutants, NO_x and CO_2 emissions need special attention due to their contribution to total aviation emissions, effect on the global warming, climate change and atmospheric ozone formation/depletion. The level of CO_2 production is directly related to the specific fuel consumption of engine and combustion efficiency. The level of combustion efficiency for majority of the operation conditions is above 99%; therefore, little gain in term of CO_2 reduction can be obtained by increasing the combustion efficiency. On the other hand, there is more area of improvement to reduce the engine's specific fuel consumption and efforts to reduce the CO_2 emission are focused on this area. The discussion of those efforts is outside of the scope of this study. Contrary to CO_2 emissions, the level of NO_x emission is directly related to the engine combustion mechanism and combustor design. Aviation related NO_x emission represent 2% of the total NO_x produced by all sources (power generation 19%, ground transport 70%, and marine engines 9%) [29] and comprises 86% of total turbine engine exhaust emissions by mass. The other pollutant contributions are 12.4% for CO, 1.5% for UHC and 0.1% for soot. The aviation NO_x emission contribution to the total NO_x emission (2%) compared to those from other sources is small; however, it needs special attention because NO_x has a potential damaging effects on atmospheric ozone through the following elementary reaction [29-30].

$$NO+O_3 \leftrightarrow NO_2+O_2$$

A good practice to understand the effects of aviation emissions on the environment are to read case studies. One of these case studies is the high speed airplane study. Although the high speed airplane research is conducted in the past, it provides valuable lessons which can be used for similar current and future efforts. Those efforts show the effect of the economical/environmental concerns and technology barriers on the success or failure of the project.

The amount of emissions that high speed/high altitude airplanes produce become more important than those airplanes that fly at lower speeds/altitudes because around 30% of aviation pollutants end up in the lower stratosphere [31] where high speed/high altitude airplanes fly. Part of the importance of the high speed/high altitude emissions is linked to the uncertainties of assessing the impact of emissions on higher atmospheric layers and the higher risk of any change in those layers as a result of the aviation emissions. The emissions of high speed airplanes (and any jet powered airplane in general) are directly related to the combustor design of their propulsion system and their engine cycle parameters. Consequently, the combustors of high speed transportation engines are a high risk element due to the need for advanced technologies [32]. At supersonic cruise conditions, high speed aircraft propulsion systems operate at high inlet pressures and temperatures at the combustor inlet that lead to a high level of NO_x formation. For example, for the Concorde Olympus 593 gas turbine engine operating at cruise condition, the level of NO_x emission index is about 20 g/kg-fuel [33] which is comparable to the maximum level of NO_x emission level of a subsonic aircraft at sea-level take-off condition. If the current combustor technology is applied to future supersonic transport aircrafts, the estimation of their NO_x emission index would be around 30-80 g/kg-fuel [34]. This level of NO_x formation for a fleet of 500 HSCT would result in a loss of 8% of the Ozone layer [35]. To control the extent of such damage, the NO_x emission at cruise conditions should be kept between 3-8 g/kg-fuel to limit its effect

on the Ozone layer to be less than 1% which is not attainable by current conventional combustor technologies [36-38].

A research conducted by the Pratt & Whitney and General Electric to design an advanced low emission combustor (NO_x emission index of 5 g/kg-fuel at supersonic cruise) under NASA sponsored High Speed Research (HSR) program [1]. The Pratt & Whitney came up with an RQL concept and General Electric with Lean Direct Injection (LDI) concept. Something worth noticing in those programs is the lack of any initial assessment or emission models to be used as a road map for the rest of the research.

Depending on whether the aircraft cruise altitude is in troposphere/lower stratosphere or in the higher stratosphere, presence of NO_x can lead to ozone production in the former [39] or ozone depletion in the latter case [19, 31]. Ozone formation is not desirable at troposphere, which are in the range of cruise altitudes of subsonic and some supersonic airplanes. On the other hand, ozone depletion is undesirable in stratosphere, where supersonic airplanes will fly. Table 2 lists the effects on the atmosphere that are studied under Atmospheric Effects of Stratospheric Aircraft (AESA) project.

The Panel on Atmospheric Effects of Aviation (PAEAN) has made recommendations in [40] about HSCT project that is relevant to this research. Some of the recommendations are provided herein:

"Although recent decisions by aircraft manufacturers make it unlikely that a fleet of HSCTs will be flying anytime soon, there is still substantial interest in supersonic aviation and it seems inevitable that it will be considered again at some point in the future. The fundamental reaction processes that occur in engines are not understood well enough to determine the potential magnitude, phase, and composition of emissions. Without this information, plume and wake processes cannot be quantified. PAEAN recommends more investigation of fundamental engine chemistry and particle formation processes, including laboratory, modeling, and field studies."

"Because future high-speed aircraft have not yet been fully built and tested, the emission indices of many critical species are not known with certainty. It important to keep in mind that any future changes in fuel composition (such as new lubricant compounds) and engine design (such as the new LPP design) can greatly affect emissions. PAEAN recommends that assessment studies continue to include a realistic range of potential emission indices, particularly for NO_x and soot compounds."

"Because the proposed HSCTs would at times operate sub-sonically in both the stratosphere and troposphere, and subsonic aircraft sometimes fly in the lower stratosphere, there are common issues important for assessing the atmospheric effects of both the proposed HSCT fleet and the existing subsonic fleet."

Table 2: Major potential impacts of chemical compounds released by aircraft [19]

Species	Environmental Impacts
CO_2	Infrared radiative forcing and associated climate impact
H_2O	Infrared radiative forcing and associated climate impact Formation of contrails and cirrus clouds and associated climate impact Formation of polar stratospheric clouds and related impact on heterogeneous chemistry Source of HO_x and impact on atmospheric chemistry
NO_x	Formation of ozone in the upper troposphere and lower stratosphere Increase in the abundance of tropospheric OH Enhanced catalytic ozone destruction in the middle stratosphere Reduction in stratospheric ozone depletion by HO_x, ClO_x, BrO_x Conversion to HNO_3 and formation of type I polar stratospheric clouds with potential chlorine activation and ozone depletion
SO_x	Source of H2SO4 in young plume Source of sulphate aerosols and associated climate impact Change in cirrus cloud properties and related climate impact Activation of soot as cloud condensation nuclei and ice nuclei Increase in particle surface area with NO_x reduction, chlorine activation, and ozone depletion
Soot	Condensation nuclei and ice kernels Increased surface area for heterogeneous reactions Radiative absorber and associated climate impact
CO	Perturbation in tropospheric ozone and HO_x budgets
HC	Formation of tropospheric and lower stratospheric ozone Conversion of ClO_x to HCl Conversion of NO_x to PAN (peroxy acetyl nitrate)

Based on the above discussions about the effects of aviation emissions on the environment, the following observations are made:

Observation I: Aviation emissions may have significant effects on the environment and atmosphere. These effects are not completely modeled due to the lack of emissions and atmospheric models or the uncertainties of the current models.

Observation II: There is an uncertainty about the design of the future airplane (especially the high speed, high altitude aircraft) and their propulsion systems as well as their emissions.

1.3.2 Aviation Growth and Regulations

Aviation growth and regulations is the other motivation of this thesis. Domestic and worldwide aviation is expected to have continuous growth for the foreseeable future (Figure 6) which translates to expansion of the current aircraft fleet, replacement of retired aircrafts, and expansion of airports in the future (Figure 7). These developments will lead to growth in aviation emission levels [12]. However, one way or another, all the aviation emissions are related to aircraft engines and their combustor. Reducing the aviation emission levels in local (around airports) and global (at altitude) scale is

Figure 6: Forecast of aviation continuous growth [12]

achievable through a better engine and combustor design with low emissions (especially NO_x, CO, UHC, soot and particulates). Transitioning from fleet level to engine level, in addition to the aviation growth, engine overall pressure ratio (OPR) has continuously increased over the past few decades to reduce specific fuel consumption (SFC) and increase turbine engine performance, but this increase in OPR has been achieved at cost of higher combustor inlet temperatures and pressure, which are directly related to the NOx emission level [41]. To compensate for the effects of fleet growth and increase in OPR, efforts have been made to reduce aircraft engine emissions by modifying the combustor design.

Figure 8 shows amount of emission reduction of the main pollutants in term of emission

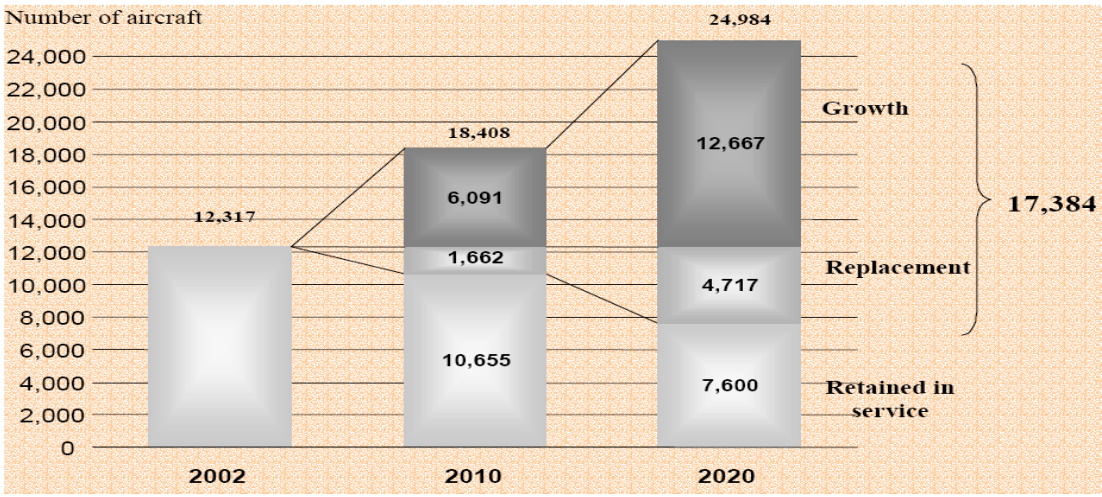

Figure 7: Air fleet expansion demand due to growth in aerial transportation and need to replace the retired aircrafts [12]

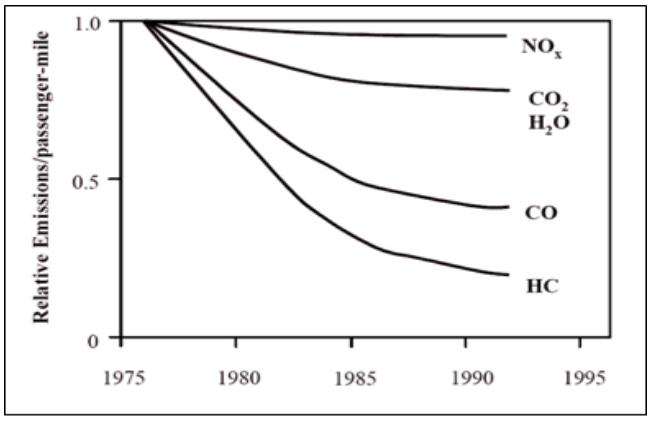

Figure 8: Reduction trend of aircraft emissions in the past [12]

per passenger carried by aircrafts. Looking at the figure, it can be seen that there is a considerable reduction in the emission levels of CO and UHC; however, small reductions in NO_x emission level indicates the challenge that designers are facing to control it. Great reduction in CO and UHC emission is a result of increasing the combustion efficiency through enhancement of atomization and mixing. Although these enhancements can reduce NO_x emissions to some extent, the main factor contributing to NO_x production is the flame temperature, which could not be lowered significantly in the past efforts. Reduction of flame temperature and NO_x level through the use of lean or rich combustion has negative correlation with CO and UHC levels, as shown in the Figure 5. It can be predicted that further reduction in the NOx emissions might stop or reverse the decreasing trend of CO and UHC emission levels. Finally in spite of overall reduction of combustion products per passenger, their overall emission levels have gone up due to the continuous growth in aviation transportation [12].

To control the local emission levels in vicinity of airports, the International Civil Aviation Organization (ICAO) sets regulations that specify all aircraft emissions to be lower than certain values, and these regulations should be met by all member countries. For example, for NOx emissions, a model is used to determine the maximum permitted amount of NO_x as a function of engine OPR and thrust rating (Figure 9). Since the inception of regulations in 1986, ICAO has incrementally lowered the emission levels and, they are expected to be more stringent in coming years. To coordinate ICAO's environmental regulations, the Committee on Aviation Environmental Protection (CAEP) was created in 1983, and has been establishing noise and emission standards through its meetings. Table 3 shows the NO_x standard level set forth by CAEP since 1986 which indicates a decreasing trend in the allowable level of NO_x emission, reflecting more stringent regulations.

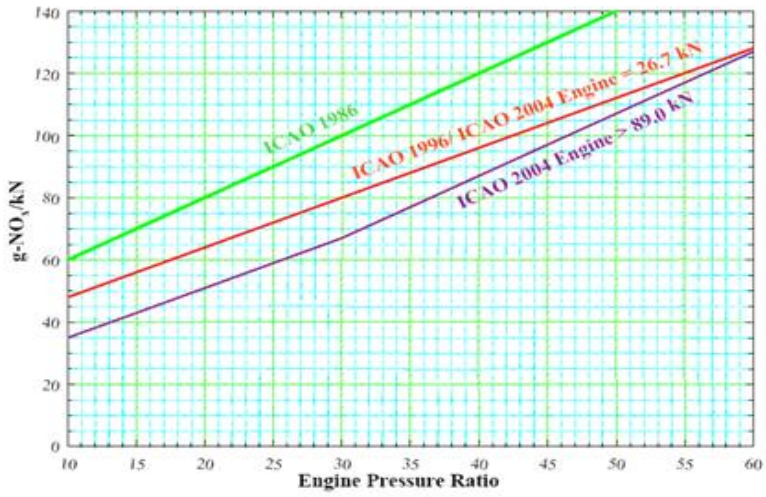

Figure 9: NO_x ICAO regulation based on engine rated thrust and OPR [11]

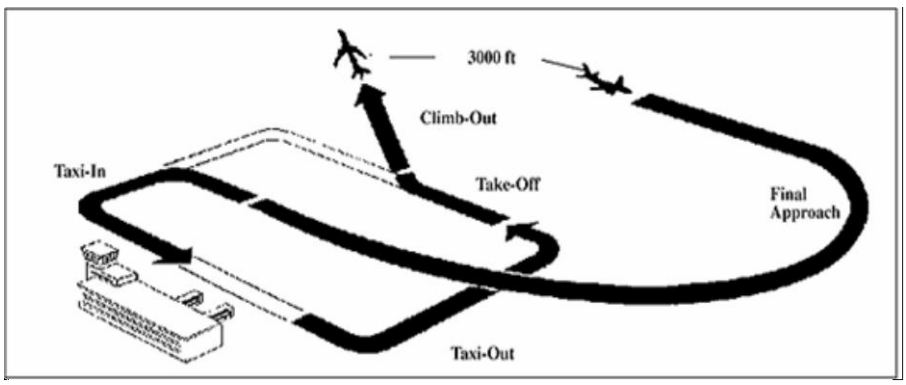

Figure 10: ICAO/LTO cycle [10]

Gas turbine emissions are defined in two ways. One way is to express them in term of amount of pollutant produced in grams to fuel spent in kilogram which is called emission index (EI). The second definition which is based on emission index is defined by the Environmental Protection Agency (EPA). The EPA is responsible for setting emissions regulations in the US based on the CAEP standards. These standards then will be enforced by Federal Aviation Administration (FAA). The Environmental Protection Agency Parameter (EPAP) is based on the Landing/Take-off (LTO) cycle (Figure 10) and is the primary figure of merit for evaluating emissions. EPAP quantifies the level of emissions in the vicinity of airports and consists of different phases with specified duration as shown in Table 4. Equation (1) shows how to calculate EPAP.

Table 3: Outcomes of past CAEP meetings [3]

Meeting	Year	NO_x Standard
CAEP/1	1986	Initial NO_x standard set (chapter 2)
CAEP/2	1991	New NO_x standard,20% below CAEP/1
CAEP/3	1995	New NO_x standard,16% below CAEP/2
CAEP/4	1998	No reductions
CAEP/5	2001	No reductions
CAEP/6	2004	New NO_x standard,12% Below CAEP/3
CAEP/7	2007	No reductions

$$EPAP\left(\frac{g}{kN}\right) = \sum_i \frac{w_{f_i} \cdot \Delta t_i}{T_i} EI_i = \sum_i SFC_i EI_i \Delta t_i \tag{1}$$

where:

w_f : Fuel flow (kg/sec)

Δt: Duration of each phase (sec)

T_i: Rated thrust at each phase (kN)

EI: Emission Index (g/kg-fuel)

SFC: Specific Fuel Consumption (1/hr)

Similar to the parameter in the Equation (1), the International Civil Aviation Organization (ICAO) has defined an emission metric (DP/F_{oo}). The difference between ICAO parameter and EPA parameter is in the definition of the thrust term. In EPA parameter the thrust is specified at each phase while in ICAO parameter the thrust is set to its value at sea level static take-off condition. In either case, in order to reduce the EPA parameter or DP/F_{oo}, one can reduce SFC, emission index or time durations in a given ICAO/LTO cycle. To reduce the CO_2 level, the efforts are mainly focused on reducing SFC since there is not much work that can be done in term of CO_2 emission index reduction. On the other hand, reduction in the NO_x or CO emissions can be achieved by either lowering SCF or their EI which is directly related to the chemical process inside the combustor. In general, the level of the emission index is the indicative of the combustor technology and its internal physics while DP/F_{oo} or EPA parameters are indicative of the engine technology in addition to the combustor technology.

Whether the aircraft is operating in vicinity of an airport or at high altitudes, exhaust gases are categorized as local air pollution or green-house gases [12]. In the past the main focus was on the level of the emissions in the vicinity of airports, but it is now going to include the emission levels at cruise conditions and altitude, where emissions may contribute to climate change and ozone layer depletion. Reference [42] describes researches to find an appropriate metric to capture the emissions of the aircraft while they are flying at the cruising altitude. In the same reference the methods used by the ICAO to certify the emissions of the aircrafts in the airport vicinity and at altitudes are listed. Currently, the ICAO certification methodology is based on the measuring the engine emissions in a controlled environment as sea-level static conditions in the ground-based test vehicle. Then the measured values are corrected for the change in the test condition and ideal sea-level static of ISA standard day using the equation below (for EI NO_X).

$$EI_{NOX_{SLS,ISA}} = EI_{NOx_{Measured}} \left(\frac{P_{SLS,ISA}}{P_{Measured}} \right)^n \left(\frac{FAR_{SLS,ISA}}{FAR} \right)^m e^{(19(h-0.00629))} \qquad (2)$$

where P is the pressure at combustor inlet and FAR is the overall fuel to air ratio. The parameter h in the exponential term is the altitude for humidity correction. Certification of an aircraft engine at cruising altitude is more challenging due to the technical limitations to measure the emission at those altitudes. Based on the same reference as above, the available methods to measure the emissions at altitude or simulated cruise conditions such as: 1) the in-flight measurement, 2) the in-altitude test facility (ATF) measurement, 3) measuring the aircrafts emissions by a chase aircraft that follows it are not practical either due to the cost or technical limitations. An alternate methodology is to

Table 4: ICAO/LTO cycle duration and thrust setting at each mode

Operating Mode	% Static Thrust	Δt (min.)
Taxi	7	26
Take-off	100	0.7
Climb	85	2.2
Approach	30	4

use correlation equations to correlate the amount of the emissions in the cruising altitude to the ground based measurements, fuel flow or combustor internal condition and characteristics. The first two methods are considered for altitude emissions calculations. The first one is to use correlation equation similar to the one shown in equation (2) to find the emissions at altitude using the measured emission values at test conditions and then correcting it using pressure and fuel to air ratios at the cruise and test conditions and the exponential humidity correction factor. In this method the exponents of the ratios (n and m) depend on the combustor type, for example it is 0.4 for conventional combustors. The other more simplified method to calculate NO_x emission is to assume a correlation between the fuel flow and NO_x emission level; however, the method shows some limitations when it is applied to the dual annular combustor (DAC) type [42]. An important point about all these correlations is that they are all based on either an empirical correlations or test facility measurements. Although these correlations are accurate for the type of the combustor that are defined, however for other combustor type they may generate significant errors. Consequently, such correlation and methods are not useful when there is a need to quantify the levels of the emissions of a new combustor type.

Another good example to further highlight the importance of using an emissions prediction model in the conceptual design for the future engines is Environmental Design Space (EDS) project which is described below.

Federal Aviation Administration (FAA) is conducting an effort to develop an integrated environment and set of tools to quantify the aviation environmental impacts and capture the interdependencies between parameters of interest in the aircraft such as noise and emissions [43]. The EDS is a system model that is being developed in Georgia Institute of Technology to model aircraft and engine for given operating conditions and determine the level of environmental impacts in conjunction with Aviation Environmental Design Tool (AEDT). The EDS captures the interdependencies between

noise and emissions. In fact one of the goals of the project is to predict the environmental impacts of aircraft fleets in the future. The achievement of this goal depends on the availability of an emission (as well as noise) model able to predict the pollutants level of future technologies based on the given requirements and physics-based models [44]. The current models that are being used in emissions prediction and the EDS, are empirical models that correlate the emission levels with compressor exit temperature and pressure (P_3 and T_3). Although they are effective models for current class of engines and combustors, they do not take into account other design aspects of a combustor and based on available experimental data. Since there are not any experimental databases available for future technologies with which to build an empirical model, the need for a physics-based emissions prediction model for combustor conceptual design is substantiated. Such a tool can be used to enhance the policy making process for government agencies to set realistic limits on the level of environmental impacts of the future fleet [45].

Observations III through V highlight the importance of finding a way to model aviation emissions produced by the current and future aircrafts around airports and at altitude. These observations also have some links to environmental concerns as well.

Observation III: Environmental and health concerns has led to increasingly more stringent regulations.

Observation IV: There is a need to model aircraft emissions in the vicinity of airports and at cruise conditions to capture interdependencies between aircraft, engine and combustor parameters and emissions. The model may be used to capture the effects of future technologies on the environment and set some realistic constraints to limit those effects.

1.3.3 Shortcomings of Emissions Prediction Models

In the previous sub-sections the importance of prediction of aircraft emissions and their impact on the environment is highlighted. In addition, a need is identified to have an

emission model in the conceptual design phase to correctly capture the trend of the emission variations and reduces the uncertainty of the emissions prediction of combustors for which not enough experimental data exist. Since the application of this model is in the conceptual design phase, the simplicity and execution speed are important factors, and detailed and high fidelity models (like CFD) are not a good candidate. Currently, emissions prediction in initial design phases relies on empirical and historical trends [46], but the empirical data have limited range of applicability and they are valid for combustor types that are similar in performance and configuration to the one from which the data are extracted. The empirical or semi-empirical models have limited capability to link various design aspects of combustor or engine design and technology levels to combustor performance or emission levels. In empirical correlations, these possible variations are lumped into a constant coefficient in the model or they are absent from the model. One of the major shortcomings of the empirical correlations for emissions prediction is that they are not parametric enough to capture the effects of design feature variations on the emission levels. Experimental correlations are unable to model more than one combustor type at a time and any attempt to use them for a type that is different than what they are originally derived from, increases the prediction uncertainty. In additions, empirical correlations are based on experiments with a certain range of operating conditions (due to hardware and cost constraints) which limits the general predictive capability of empirical correlations when they are used for broader range of operating conditions (i.e. cruise conditions).

Detailed emissions analysis can be considered an option when many design aspects of a combustor have been selected or determined, and the emissions studies are performed through CFD with a simplified chemistry or rig test runs. In spite of all the advancements in CFD methods, complete CFD modeling of the combustion process including all the species interactions, turbulence and heat transfer, is still not a viable option for design purposes due to the extensive computational resources that are required

[14]. In addition to the absence of detailed geometry and combustor characteristics, cost and execution time are other two important factors that limit the extensive use of CFD analysis in the initial design phases. As a result, these detailed analyses cannot be considered in the conceptual design phase.

The same issues identified above also exist in performing sector or full scale rig tests. They are very expensive, labor intensive and usually conducted to obtain the final characteristics of a combustor in term of performance and emissions parameters and should not be considered as a tool to greatly modify the design. Besides, sometimes combustors are tested under conditions that are not exactly the same as operating conditions due to hardware and cost limitation. The data obtained from such tests are extrapolated to obtain the characteristics at the desired operating conditions.

The above discussion results into the following observations regarding the current approaches to calculate the engine emissions. These observations are presented in a hierarchical form

Observation V: Current emissions prediction models that are used in the conceptual phase are reliant on historical data and empirical correlations. At advanced design stages, CFD analysis with simplified chemistry and rig test data are used to predict the emissions.

Observation VI: Empirical correlations are only reliable in the situation under which the tests are performed and have a limited range of applicability. Any attempt to extrapolate them beyond their valid operating range should be exercised with caution.

Observation VII: There is a need for a parametric emissions prediction model in the conceptual design phase that is more physics-based to captures the interdependencies between aircraft, engine and combustor parameters for different combustor types and operating conditions in a relatively easy and fast way in the presence of the conceptual phase uncertainties.

1.4 Research Objective and Research Questions

From all the mentioned motivations and observations, the research objective of this thesis is deduced as follows:

There is a need to develop an approach to model emissions of gas turbine engines at the conceptual design phase. The emphasis is on a relatively fast and simple emissions prediction method to reduce prediction uncertainties in early design phases. This design oriented prediction method could be used to develop parametric and versatile models for conventional or unconventional combustor concepts at different operating conditions. These models should be able to capture the interdependencies between combustor parameters, engine parameters and emission levels. To achieve that goal, the models should capture the important physical phenomena inside the combustor and may be used to identify the main contributors to the emission levels.

The following research questions are deduced from the observations. They serve as sub-level objectives of this research. From observations I through IV related to environmental concerns, aviation growth and regulation stringency the first research question is derived:

Research Question 1 (RQ1): How can an emissions prediction approach be made more parametric in a way that a variation in a combustor design parameter is reflected in the emission levels?

From observations III and IV related to more stringent regulations the second research question is derived:

Research Question 2 (RQ 2): How can different combustor architectures be accommodated in an emissions-prediction approach and their effects on emission levels be captured at different operating conditions?

From observations V, VI and VII related to the current state of the emissions prediction model in the conceptual design phase, the third group of the research questions is derived:

Research Question 3.1 (RQ 3.1): How can the uncertainties of emissions prediction model be reduced in the conceptual design phase?

Research Question 3.2 (RQ 3.2): How can the uncertainties in the emissions prediction model and the important factor affecting it be captured and quantified?

The rest of this thesis is based on the provided research objective and the research questions and is organized as follows: in Chapter 2, a literature review of past and current efforts to model gas turbine combustor emissions along with a theoretical background are provided to highlight the shortcomings of past works in this field. In Chapter 3 after the literature review, the research questions are restated and reminded in the context of the information provided in the literature review. In the same chapter, the hypotheses are formulated to address the problems posed by the research questions. In Chapter 4, a general description of a less known RQL combustor is provided. In Chapter 5, based on the theoretical background and literature review, a proposed methodology is provided. Next chapter introduces the integration environment created for emissions prediction. In Chapter 7, the designed experiments based on the proposed methodology to prove or disprove the hypotheses are introduced, and their results are provided and discussed. The thesis overview, contributions, limitations, recommendation for future works and final remarks are the subjects of Chapter 8. Additional information, data and codes are provided in the Appendices.

CHAPTER 2

THEORETICAL BACKGROUND AND LITERATURE REVIEW

The subject of this thesis focuses on the emission related aspects of combustors and their associated uncertainties. Since the oxides of nitrogen (NO_x) and carbon monoxide (CO) are among the most important emissions of gas turbine engines, they are considered in this thesis. Other aspects, such as structural analysis, thermal stress, acoustic and cost are not considered here. Several methods are available to model combustor emissions. These methods can be categorized in three groups:

- Correlation-based (empirical or semi-empirical)
- High fidelity physics-based
- Hybrid

Correlation-based models use experimental data obtained from the combustor sector or full-scale rig tests. Based on test results and experiences, a correlation is assumed between certain parameters and emission levels. Then, a curve fitting procedure is performed to define emission levels as a function of a group of identified parameters. In empirical models which are the first type of the correlation-based models, the selected parameters are usually the operating parameters such as temperature and pressure. The combustor characteristics are not included in empirical models. The semi-empirical models are the second type of the correlation-based models. Although the semi-empirical models are still based on experimental data, this data is utilized in the form of physical models. Semi-empirical models contain more parameters representative of the combustor characteristics than empirical models, such as characteristic time and volume [7, 47]. Also, due to the limited capabilities of the test facilities to generate the data within the entire range of operation, sometimes the experimental data are extrapolated to real conditions, which may increase the uncertainty of the prediction. A limited number of tests and the ability of the test facility to simulate the real flight environment limit the

predictive capability of these models. The correlations-based models are design specific, or they can be applied to similar type or class of combustors; therefore, the ability of correlation-based models to predict emission levels of new combustors or those that are different from the levels the model is based on, may be reduced. The other concern related to the correlation-based models is their scalability. Unless there is large volume of test data for combustors with different size, the correlation-based models are based on a specific size and geometry and their accuracy may go down when they are used for combustors with different size.

Using high fidelity physics-based approaches (such as CFD) to predict combustor emissions has its own drawbacks. Despite of continuous development of CFD methods and computational power of the processors, high fidelity models require long set-up time, demanding computational resources and high cost, which make them inappropriate in the conceptual design phase [14]. Currently, CFD models are considered a tool that can be used more for analysis and limited sensitivity analysis and less for design purposes. They can be used to model and analyze particular design at advanced design phases where many aspect of the design is determined and detail geometrical information and initial or boundary condition are defined. The CFD methods are considered most detailed models in flow-field analysis, but their intensive computational burden makes them impractical for the conceptual design phase where Design Of Experiments (DOE) runs and trade-off studies are an essential part of the process. However, with the continuous increase in the processing capabilities of computers and the development of more efficient CFD methods, it is likely that the CFD methods will be used *in the future* as a parametric design tool in the earlier design phases. Another point is that in CFD methods the fidelity of the combustion chemistry is lowered in favor of the higher flow-field fidelity. The fidelity of the combustion reactions used in CFD models is usually limited to a few elementary reactions out of hundreds or thousands. Researchers have made an effort to employ simplified and efficient CFD methods to predict combustor emissions.

For example, Mongia [14] used a CFD model combined with empirical correlations to analyze combustor flow-field and emission distributions of 10 combustor types. In his work, he used empirical models for NO_x, CO and UHC emissions, and radiative, convective and conductive heat transfer models. No species reaction is modeled in his works [48-49]. Danis et al. used the anchored Computational Combustor Dynamics (CCD) method with simplified finite rate chemistry combined with equilibrium radical concentration to predict NO_x and CO emission distributions in a combustor [50].

The third group of emission models is hybrid models. These models are based on employing simplified physical and chemical models to analyze the internal flow-field of a combustor and combustion process. In hybrid models, the correlations are used in the component and flow-field levels and can be used independent of combustor type. In other words, the use of experimental data in hybrid models is at a level where they are being used as a coefficient or tuning factors. Mattingly et al. [4] and Lefebvre [7, 51] provided a good approach to be used in the hybrid emissions models in the conceptual design phase. Many physics-based models (including the one used in this thesis) are based on their work. Rizk et al. [52-53], Shakariyants et al. [54-57] provided different methods for emissions prediction considering combustion, flow-field, droplet evaporation and etc.

In all the emission models, at least two main fields are identified; the first one is the combustor internal flow-field and the second one is combustion or chemical process. The species formation and destruction processes in a combustor are dependent on the internal flow-field of the combustor and one cannot be analyzed without considering the effects of the other one; however, depending on the application and the priorities of the research, the presence of one discipline may be stronger than the other one.

The rest of this chapter provides the methods to model the combustor internal flow-field, the combustion process and chemistry and, the integration of these methods to predict the emissions. The materials provided in this chapter are discussed based on their

usefulness to predict the emission (not designing the combustor) in the conceptual design phase and emphasis is placed on those methods that are suitable for that purpose.

2.1 Internal Flow-field Models

In the conceptual design phase, the internal flow-field model provides information such as dilution and cooling flow fractions and location of cooling and dilution holes in the combustor by employing physics-based and semi-empirical equations [54-55, 58]. Due to the interdependencies between the combustion and geometry models, it is likely that iteration is required in order to reach to an acceptable solution. Depending on the combustor type and architecture, different zones are present in the combustor; for example Figure 11 shows the basic components of a conventional combustor that are considered in the internal flow-field model. It is essential to know the combustion type and configuration to model the flow-field. All combustor types contain some or all of the elements that are shown in the figure; however, the order or configuration of the elements may vary. In the following section, the internal flow-field models recognized in the literature are described.

2.1.1 CFD Approach

Extensive work has been done on CFD analysis of the combustor's internal flow-

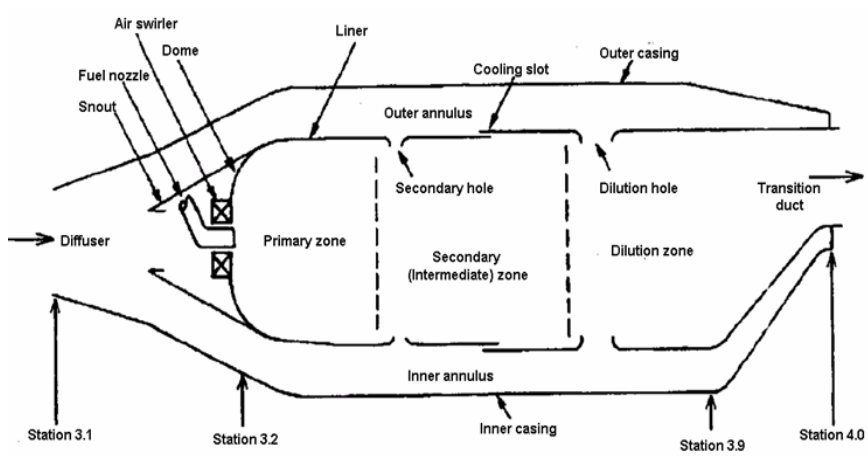

Figure 11: A generic layout of a single annular combustor [7]

field. As mentioned earlier, this approach is not appropriate in the conceptual design phase because of the lack of flexibility, high cost, high computational resource requirement, long set-up time and long execution time. Also detailed modeling of the flow-field inside the combustor is difficult due to the complexity of the turbulent and multi-phase flow models [50].

In analyzing the internal flow-field of a combustor, depending on the level of complexity and available computational resources, two CFD approaches are identified. In the first approach, known as “cold flow”, the flow-field is modeled without taking into account the effect of combustion heat release. In this approach, the computational burden is reduced by assuming that the flow-field pressure and velocity fields are independent of the heat release process and the effect of the heat release on the flow-field is minimal. Such an approach is not applicable for modeling the flame and heat transfer effects. The second approach known as the “reacting flow” approach, takes into account the heat release effects on the flow-field by adding a source or sink term in the Navier-Stokes energy equation. The addition of the energy source or sink term should be accompanied by the addition of additional species conservation equations that are present in the flow and react with each other. The numbers of species in the CFD simulation is limited to the main reactants and products to reduce the model complexity and execution time. The complexity of a CFD model will also have a direct effect on the convergence of the simulation to the final solution. To reduce the execution time, additional information or equations such as empirical or semi-empirical models, combustion efficiencies, and convective and radiative thermal effects can be used in conjunction with the CFD model. Rizk and Mongia used reacting flow CFD analysis, which incorporated Lefebvre’s correlation models into their analysis [14, 59-60]. Considering the reactive flow in the CFD analysis necessitates making additional assumptions about the type of reaction in the model. Assumptions such as laminar flamelet that considers infinitely fast reaction or the equilibrium reaction can reduce the complexity of the reacting flow CFD simulation.

Lebedev et al. used the methane-fueled combustor with equilibrium chemical model to obtain temperature and mixture fraction distribution inside a combustor [61].

2.1.2 Network Approach

In the network approach, the internal flow-field of a combustor is approximated by a series of sub-flows and co-annular flow tubes and 1D reacting streamlines. The network approach is a quasi one dimensional method that uses a network of flow elements and nodes built based on the geometry of the combustor (Figure 12) to determine the flow characteristic inside the combustor. In this method, the elements represent the physical features of the combustor and nodes connect these elements to one another. The governing equations are implemented in each node and each element is described by the semi-empirical or physics-based equations. When the governing equations of all the nodes are put together, a system of linear equations is obtained that is solved by using linear algebra methods to obtain the temperature, heat transfer, pressure, mass flow and equilibrium specie concentration profiles through the combustor. The chemical equilibrium calculation is used in this method to avoid solving differential equations. However making this simplification has a direct effect on emission calculations where finite rate chemistry is important. The method initially used by Grevenstein and Laurie to analyze the flow in a pipe network [62]. Stuttaford and Rubini employed the network approach to model the flow-field in a reverse flow turbine engine combustor [63]. Finally Despierre et al. used this approach combined with the Genetic algorithm to optimize the design of a dual annular combustor [21]. In their study, they fixed the geometry and performed the Genetic algorithm optimization to reach eight design targets by varying six input parameters (Table 5).

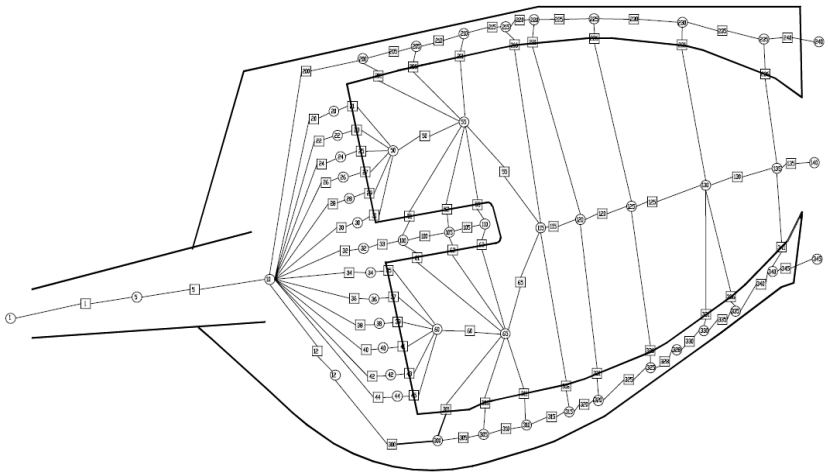

Figure 12: A network generated for an annular combustor [21]

The network method provides detailed information about the combustor internal flow-field, with the desired level of accuracy depending on the number of nodes and accuracy of the semi-empirical correlations. In this approach, a compromise exists between the execution time and accuracy. Increasing the number of elements and nodes makes the accuracy of the model closer to that of the CFD analysis and at the same time, increases its execution time. Providing an efficient solver to solve the system of equations has a direct effect of the accuracy and execution time of the approach. The network approach does not provide the flexibility of using a network of one combustor (with moderate change) for another combustor with a different configuration. Using this approach to design and size a combustor based on the required flow-field presents some

Table 5: Inputs and design parameters in Genetic algorithm optimization

Input Design Variables	Design Parameter Targets
Primary holes area	Injector fuel/air ratio
Dilution holes area	Primary zone fuel/air ratio
Injector area	Intermediate zone fuel/air ratio
Primary effusion cooling holes area	Dilution zone fuel/air ratio
Intermediate effusion cooling holes area	Primary zone wall temperature
Dilution effusion cooling holes area	Secondary zone wall temperature
	Dilution zone wall temperature
	Overall pressure drop

complications as changing the size and shape of the combustor might necessitate modifying the number and configuration of nodes and elements.

2.1.3 Control Volume Approach

In this approach, the combustor is divided into a finite number of axial zones or control volumes, where each zone communicates with neighboring zones through a number of flow parameters. The analysis moves forward by solving governing equations in the integral form for each control volume and obtaining the average flow properties in that zone. The process starts from the combustor inlet and ends at the combustor exit. If a particular condition is desired at the combustor exit plane, iteration will be required to converge to the desired target condition. The accuracy of the control volume method depends on the size of the control volumes and their boundaries. This method was used by Rodriguez and O'Brien [64] to analyze the flow-field inside single annular and reverse-flow combustors. They built their approach on the previous work done by Davis who sequentially modeled a turbine engine's compressor [65]. This 1D approach provides the flow variation in the direction of the flow in the core and annulus section of the combustor, but it does not take into account the flow property variations normal to the flow direction. Comparing this approach to the network and CFD approaches, the control volume approach loses its 2D or 3D observability while providing a simpler, faster and more versatile modeling technique with less computational burden.

2.1.4 Component Modeling Approach

The component modeling approach can be considered as a simplified control volume approach with some modifications. In this approach, partitioning the combustor into smaller control volumes is not completely user defined and has some constraints. The partitioning is based on pre-defined combustor elements where each element is contained within a control volume [4, 51]. The boundaries of each element are either

physical boundaries or are defined in accordance with the location of the dilution holes or points where flow properties are changed significantly. The advantage of this approach over the control volume approach is in its modular characteristics, where components can be combined in various ways to resemble the configuration of the combustor type of interest. Each component is modeled separately and then all components are linked to each other to form the whole combustor. The component models may be empirical, semi-empirical, or physics-based. Some of the models in this approach are non-linear; thus, the equations cannot be represented in matrix form where linear algebra methods can be used to solve them. Figure 11 shows the elements that are used to model a conventional single annular combustor. These elements are the basic building blocks that can be used to model different combustor types with various configurations. This modular feature is the strength of this approach that makes it attractive for 1D internal flow-field analysis.

Much of the work on the component modeling approach uses models and methods that are similar to those suggested by Mattingly and Pratt [4] and Lefebvre [7] and many definitions and equation in this thesis is based on the mentioned authors' work as well. Shakariyants et al. used this method in their work to size a single annular combustor of CF6-80 engine emissions [54-57]. Andreini and Facchini used the approach to model the emissions of several types of combustors, but they did not go into detail about the internal flow-field analysis process [66].

A brief explanation of the combustor elements used in the component modeling approach is provided here. These components can be looked at as pre-built objects that can be used to construct a whole combustor. The mathematical models and associated equation of each component wills be provided in the Chapter 5.

2.1.4.1 Diffuser

The job of the diffuser is to slow the air flow coming from the compressor and provide a smooth and well-distributed flow to the combustor core and annulus. The

diffuser component is sized for on-design condition to slow the flow to the desired Mach number at the diffuser exit and increase the static pressure with a minimum total pressure loss. In addition to the on-design condition, the diffuser must have an acceptable performance at off-design operating conditions. The diffusers used in combustors have different types. They can have a flat or curved wall, gradual or sudden expansion, and single or multiple passages.

2.1.4.2 Atomizer

Fuel atomization and spray droplet size have important effects on combustor performance and emission levels [52]. When liquid fuel (JP-9 or Jet-A) is injected to the combustor core, the initial jet of the fuel converts to various-sized droplets through aerodynamic and hydraulic instabilities [67-68]. The heat that exists in the vicinity of the droplets quickly evaporates some of them, but some of the droplets are large enough to get into the flame zone before they evaporate. The existence of droplets in the flame region creates a specific different kind of flame called diffusion flame In contrast to the

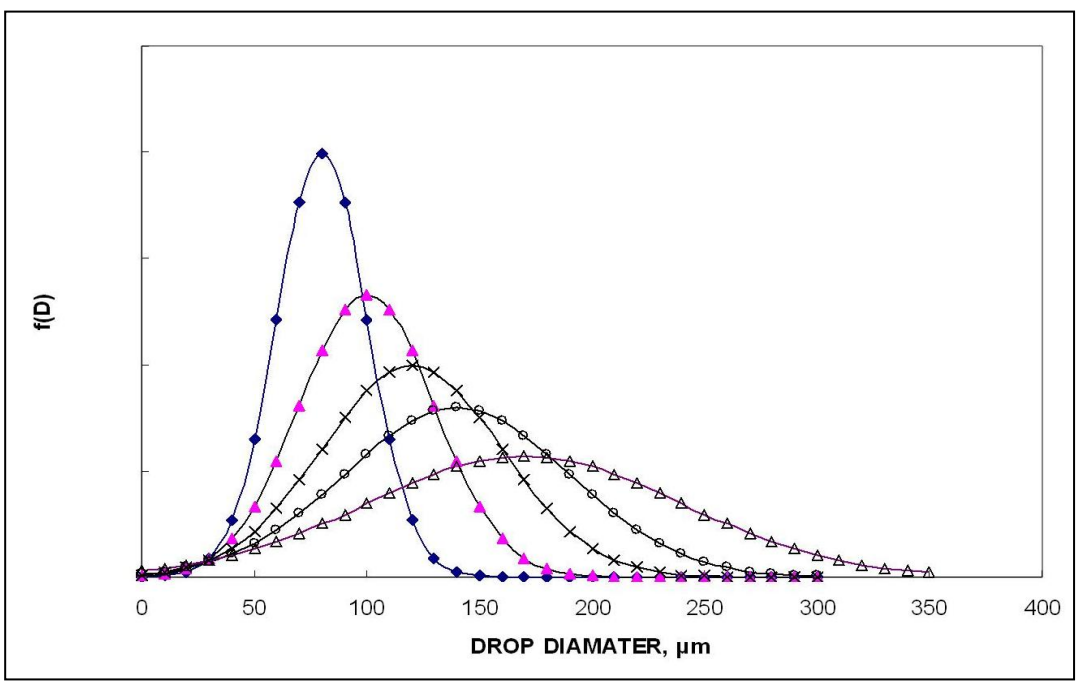

Figure 13: Droplet size distribution

premixed flame, where the fuel and oxidizer (air) are mixed together before burning, in the diffusion flame, the fuel and air are separate and encounter the flame from opposite directions through the diffusion process. The diffusion flame positions itself between incoming air and fuel streams, where the fuel to air ratio is stoichiometric and results in the maximum flame temperature. There is a range of droplet diameters in the fuel spray for which various droplet diameter distribution models have been proposed. The droplet size distribution depends on many factors such as atomizer type, flow-field around the fuel jet, and upstream fuel line conditions (Figure 13). It is convenient to work with mean droplet diameter instead of droplet distribution. Among many different definitions available for the droplet mean diameter, the Sauter mean diameter (SMD) is the one that is widely used in combustion applications and is defined as the diameter of a droplet whose ratio of volume to surface is the same as that of the whole fuel spray. The SMD can be viewed as an average or mean value diameter of all droplets present in the spray. Droplet models are usually defined in terms of the SMD as a function of atomizer type. Lefebvre in [7] and Mellor in [46] have provided droplet models for simplex and air blast atomizers.

2.1.4.3 Swirler

The other element that has a direct effect on the structure of the flame, emission levels and overall combustor efficiency is the swirler. The main job of the swirler is to convert part of the axial velocity component of the core flow to the tangential component. Imposing a tangential motion to the flow creates a flow recirculation that brings the hot gases back to the flame front which increases flame stability and prevents flame blow-off. At the same time the toroidal motion of the flow reduces the flame length [69]. The amount of swirling that a swirler imposes to the flow is quantified by the *Swirl* number which is shown in equation below as [70].

$$SW = \frac{G_\phi}{G_x \, r_0} \tag{3}$$

where G_φ is the axial flux of angular momentum, G_x is the axial flux of momentum (axial thrust) and r_0 is the outer radius of the swirler. Flow recirculation is obtained for strong Swirl number greater than 0.6 [4].

The other job of the swirler is to enhance the mixing of the fuel with air [69]. Swirlers can be axial, radial or a combination of both (Figure 14). Many studies are conducted to model the swirler, its interaction with fuel spray and its effects on the flow and combustion process [71-76]. A significant part of the success associated with modern combustor concepts such as twin annular premixed swirler (TAPS) or LDI combustors are associated with the way their swirler is designed to better mix the fuel with air. The swirler can be looked at as a stationary single stage fan or an inlet guide vanes. The following parameters defined the characteristics and performance of a swirler:

- Blade positioning angle
- Blade curvature
- Number of blades
- Hub and tip radii

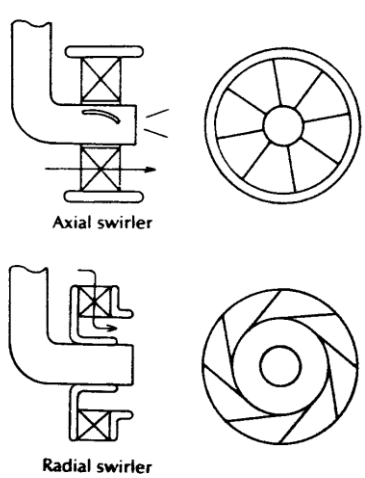

Figure 14: Axial and radial swirlers

- Blade solidity (Chord to length ratio)
- Blade thickness
- Axial, radial or hybrid swirler
- Flow coefficient

2.1.4.4 Combustor Core Zones

The number and type of zones in the core section of a combustor depend on the type of the combustor and its design. As a basic rule, the zone is defined as a region in the combustor where no flow is added to it or there is a uniform characteristic across that region. For example, in the single annular combustor, the number of rows of dilution orifices is used to define the zones in the core section of the combustor. Depending on the combustor type, there are one, two, or three rows of orifices, and each region between the rows is considered as one zone.

Often the core section of a single annular combustor is divided into three major axial parts. These parts are distinguished from each other by introducing additional air that comes from the annulus in the form of jets through dilution holes and crosses the main core flow. In the SAC, the three distinguishable zones are 1) the primary zone, 2) the secondary zone, and 3) the dilution zone. In other combustor types, depending on their internal flow-field and architecture, additional zones can be defined. In the RQL combustor, which would be another combustor type, additional zones such as rich zone, mixing zone and lean zone can be defined. Specific tasks should be accomplished in each zone. The primary zone in a SAC or the rich zone in an RQL combustor is a place where the flame is anchored. In this region, the flow is characterized as a highly intensive turbulent flow. The main task of the primary or rich zone is to sustain the flame at all conditions. A swirler-induced recirculation is contained in these zones to recirculate part of the hot gases back to the flame region to prevent flame blow-off or extinction. In SAC, the primary zone fuel to air ratio is often close to the stoichiometric value to have a stable

flame. To burn off the unburned fuel and hydrocarbons coming from the primary zone, additional air from the annulus is introduced to the core section through the first row of dilution orifices. The region between the first and next set of dilution orifices is called the intermediate or secondary zone. The primary and secondary zones make significant contributions to the total NO_x and CO emission levels [77-78]. The addition of additional air from the annulus to the core section through the second row of dilution orifices identifies the beginning of the dilution zone where it ends at the combustor exit plane.

The flow in this post-flame region is relatively calm. The task of the dilution zone and its dilution jets is to provide a desired exit temperature and velocity profile for the first stage of the turbine blades. The exit profiles are tailored to the needs of the turbine blade in terms of thermal and mechanical stress management. In an RQL combustor, the task of the rich zone is similar to that of the primary zone; however, the fuel to air ratio at the rich zone is significantly above one. The rich zone is followed by a mixing zone in which the exhaust of the rich zone quickly mixes with quench jets coming from the combustor annulus. The mixing zone is a turbulent region and the quality of mixing and quenching in this zone has a significant effect on the level of the emissions. The lean zone burns the unburned hydrocarbon coming from the mixing zone in a lean condition and is followed by a dilution zone. A more detailed description of the SAC and RQL combustor types is provided in Chapter 4.

2.1.4.5 Flow Partitioning

The flow partitioning model is a virtual model that divides the air flow between different zones of the combustor, and based on the amount of the flow going into each zone and corresponding pressure drop, the dimensions of the combustor elements will be determined. After the diffuser, air flow is divided between the combustor core and annulus. The placement of liners and their distance from the casing and the amount of pressure loss through the dilution orifices and swirler determine the amount of the flow

that goes into the combustor core and annulus. It is important to have an adequate amount of flow in the primary or rich zones to control the equivalence ratio, the burned gas temperature, emission formation, and to prevent flame blow-off. Also it is equally important to send sufficient air to the annulus for liner cooling and air dilution. On the one hand, sending more air than necessary to the primary zone makes the fuel and air mixture very lean and prone to flame instability and blow-off while leaving little air for liner cooling and dilution. On the other hand, having little air going into the primary zone results in a stoichiometric and sometimes rich mixture that could deviate the temperature from the desired value and increase the UHC and CO emission levels. It can also result in additional air going to the annulus that could spoil the mixing pattern of the secondary and dilution zones, which could result in an undesired temperature profile at the combustor exit. The situation for the rich zone in the RQL combustor type is different from that of the primary zone. Sending more air than necessary to the rich zone may result in an equivalence ratio close to unity, which is undesirable for the RQL combustor. Because of the criticality of the amount of the air that goes to the rich zone in the RQL design, concepts like the variable geometry swirler or fuel shifting are considered [1].

The size of the mixing, secondary, and dilution zone orifices is important for having adequate mixing and for preventing short or long jets. Orifices with a small diameter provide jets with low momentum that are unable to penetrate deep enough into the core section and mix well with hot gases. Large diameter orifices, on the other hand may impinge the jets coming from the opposite inner and outer liners, leading to uneven temperature distribution [79-80].

2.1.5 Assessment of Internal Flow-field Analysis Approaches

Table 6 shows a qualitative comparison of the four methods mentioned to model the combustor internal flow. Four criteria in the conceptual phase are considered which are: 1) execution time, 2) set-up time, 3) versatility, and 4) fidelity. The execution time

and set-up time have a direct correlation with cost, which is an important issue in combustor design. Also, a design-friendly model should be reasonably flexible to incorporate design types with different architecture and design. The fidelity of a model has less importance compared to the other three criteria; however, the more accurate and realistic a model, the better the final emissions prediction. From the table, it can be seen that component modeling is good candidate for the purpose of this thesis.

Table 6: Comparison between internal flow-field analysis methods

Approach	Execution Time	Set-up Time	Versatility	Fidelity
CFD	⊗	⊗	⊗	●
Network	◉	○	○	◉
Control Volume	◉	○	◉	○
Component Modeling	●	◉	●	○

Excellent ● Good ◉ Fair ○ Poor ⊗

2.2 Combustion Models

The next step in the combustor emissions prediction process is the introduction of the methods used in combustion or chemistry analysis. The combustion model inputs include geometry information, flow conditions at combustor inlet and flow-field information. The most well-known methods to model the combustion process are detailed models like reacting flow CFD or computational combustion dynamics (CCD) [50]. The CFD methods were discussed in the previous sections; therefore, the focus here will be on the methods that have not yet been discussed.

There is always a correlation between the fidelity of the flow-field analysis and the chemistry analysis due to resource limitations. In CFD methods the chemistry analysis is simplified, while in the other methods, the flow-field analysis is simplified to have a higher fidelity chemistry analysis. To simplify the combustion model and reduce the CFD workload, simplified assumptions are made. The most well-known models used in reacting flow simulations (especially turbulent flow) are the *fast-chemistry*, *flamelet*, and *equilibrium* models [81-82]. In the first two models, the Damkohler number is

assumed to be large. As shown in the equation below, a large Damkohler number means that the reaction time scale is much shorter than the flow time scale.

$$Da = \frac{\tau_{fluid}}{\tau_{reaction}} \tag{4}$$

The fast-chemistry models are widely used for diffusion flame modeling while the flamelet models can be used for diffusion, premixed or partially premixed turbulent flames where a thin flamelet is wrinkled by the turbulent flow. The flamelet models are used by researchers to model the turbulent combustion process [83-85]. Since flamelet models assume fast chemistry in the flame regions, they are not suitable for slow reactions like NO_x formations and sometime the use of finite rate chemistry models is necessary [61]. The equilibrium model also assumes very large residence time such that the combustion has enough time to go into equilibrium condition. Although such a model is appropriate to determine the temperature distribution in the combustor (as the heat release is a fast process). There are many reactions and species in the combustion that do not reach to equilibrium conditions and such an assumption can produce significant prediction errors. Another way to model a combustion process is the *Chemical Reactors Network (CRN)* approach. In this approach, a combustor is divided into smaller regions with similar flow properties and each region modeled by a single or a set of elementary chemical reactors [86]. In the CRN approach the chemistry fidelity is increased at the cost of lowered flow analysis fidelity. A more detailed description of the approach is provided in section 2.2.2.

No matter what assumptions are used in the combustion or chemistry analysis, the first step to model a combustion process is to model how the species in the process react with each other. Such a model is called c*ombustion mechanism*. The following section provides an overview of the combustion mechanism.

2.2.1 Combustion Mechanism

To start modeling a combustion process, it is essential to provide a model of fuel combustion with air. Although at a global level the reaction of the fuel with air can be written as a single line of a chemical equation with reactants at one side and products at the other side, this is just an overall picture of what really happens and does not tell the whole story. This type of chemical equation, which is called a global reaction, gives the main end products of a chemical process without mentioning the intermediates steps and those species produced in small quantities. The formation of products, however, is not a direct result of the fuel and air molecules collision. In fact, the possibility of having final products as a result of direct collision between the fuel and air molecules is extremely low and it is more probable to have some intermediate molecular and atomic collisions responsible of forming the final products. These reactions are called elementary reactions and represent a picture that is closer to what really happens in the combustion process on molecular scales (Figure 15).

Elementary reactions show how unstable and short lived molecules and radicals can react with each other through a complex chain of elementary reactions to create the final stable products. Many species (e.g. CH, OH, HO and O) that are present in elementary reactions are unstable and have a very short life. The presence of these species in the flame is proved by various experiments. These intermediate species have an important effect on the formation or destruction rate of the final products [87].

Every elementary reaction has a forward or forward/reverse reaction direction, and each direction, as shown in Figure 15, has forward and reverse reaction rates k_f and k_r. In a chemical equilibrium condition, these coefficients are used to determine the concentration of species. In non-equilibrium conditions, the coefficients are used to find the rates at which species are produced or consumed using the relation similar to equation (5) which gives the reaction rate of CO in the combustion mechanism shown in Figure 15.

$$CO + O_2 \underset{k_r}{\overset{k_f}{\Leftrightarrow}} CO_2 + O$$

$$O + H_2O \underset{k_r}{\overset{k_f}{\Leftrightarrow}} OH + OH$$

$$CO + OH \underset{k_r}{\overset{k_f}{\Leftrightarrow}} CO_2 + H$$

$$H + O_2 \underset{k_r}{\overset{k_f}{\Leftrightarrow}} OH + O$$

$$O + N_2 \underset{k_r}{\overset{k_f}{\Leftrightarrow}} NO + N$$

$$N + O_2 \underset{k_r}{\overset{k_f}{\Leftrightarrow}} NO + O$$

Figure 15: An example of elementary reactions

$$\frac{d[CO]}{dt} = -k_f[CO][O_2] + k_r[CO_2][O] - k_f[CO][OH] + k_r[CO_2][H] \tag{5}$$

Reaction rates are a function of pressure, temperature and order of reaction. To take into account these parameters, reaction rates are defined as a function of pre-exponential factor or frequency factors *A*, reaction order *n* and activation energy *E* which are used in the equation below to calculate the reaction rate.

$$k = AT^n \; e^{-E/RT} \tag{6}$$

To find the concentration of species at a given time, a system of differential equations with a range of time scales (stiff system of ordinary differential equations) must be solved. This system of differential equations contains the reaction rate equations of all the species listed in the combustion mechanism.

The combustion of every fuel with air has its own combustion mechanism. Many investigations, experiments and studies have been conducted to find the combustion mechanism of different fuels with air. Even in some cases there are several mechanisms for a fuel describing the combustion mechanism for different conditions like rich or lean mixtures. As fuel molecules become more complex and larger with a higher number of carbon atoms, more intermediate species become involved in the process which increases

the number of elementary reactions and makes it more difficult to model the complete combustion mechanism.

To reduce the complexity of the combustion mechanism of large fuel molecules, initial elementary reactions responsible for breaking large fuel molecule into smaller ones (Pyrolysis process) are lumped into a few global chemical equations [87-89]. In this method, the available combustion mechanisms of smaller molecules are combined with the global reactions of larger molecules to model the combustion mechanism of the fuel. Besides the difficulty of modeling the combustion mechanism of single-component fuels with a high number of carbon molecules, another problem is associated with the actual fuels being used in industry. Most hydrocarbon-based fuels in industry (including aviation fuels) are derivatives of petroleum and are a mixture of many hydrocarbons. For example, aviation fuels consist of more than 300 components, and it is very difficult to model their physical or chemical properties and combustion mechanisms. The percentage of species present in these fuels varies based on the oil wells and refineries they come from or the time of the year when they are extracted and refined [90-91]. To reduce the number of components to a manageable size (10 to 15), a surrogate model can be created

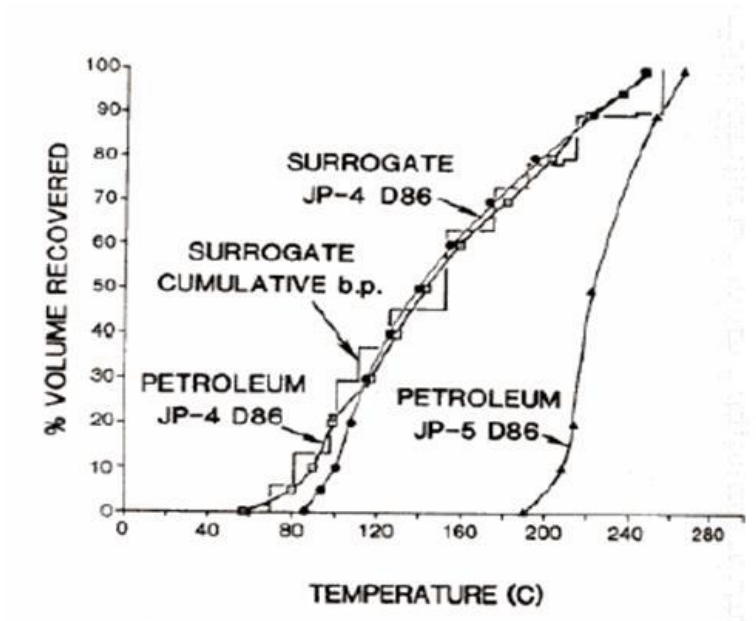

Figure 16: Distillate curve of JP-4 [16]

that mimics the same physical and chemical properties and distillate curve of the original fuel as much as possible while having fewer components than the original fuel. Figure 16 shows the distillate curve and Table 7 shows a surrogate model of JP-4 consisting of 14 components. Surrogate models are used in modeling the spray combustion, internal flow-field, combustion mechanism and laboratory tests [16, 91-93].

Although in surrogate models the number of components has been reduced, considering the current available computational resources, it is still difficult to model the combustion mechanism of a surrogate model and even if it is possible, it would be hard to use them in a combustion analysis [90]. The solution is to use the major components of a surrogate that have the largest fractions of the fuel. For most common aviation fuels (JP-8 or Jet-A), the major constituents are paraffins and aromatics; therefore, it is possible to create a very simple model of a fuel using a mixture of one alkane and one aromatic that exhibits chemical structures similar to the ones in the original fuel. For Jet-A, Lindstedt

Table 7: Surrogate model of JP-4 [16]

Compound Class	Petroleum JP-4 % volume	Surrogate JP-4 % volume	Surrogate Components
Paraffin	61.2	61.5	n-Hexane n-Heptane n-Octane n-Nonane n-Decane n-Dodecane n-Tetradecane
Monocycloparaffins	24.2	24.0	Cyclohexane Methylcyclohexane Cyclo-octane
Dicycloparaffins	4.9	5.0	Decalin
Alkyl benzenes	8.2	8.0	Toluene
Indans and tetralins	1.1	1.0	Tetralin
Indenes and dihydronaphtalenes	0.0	0.0	-
Naphthalene	0.4	0.5	1-Methylnaphthalene
Total paraffin	90.3	90.5	
Total aromatics	9.7	9.5	

and Maurice [94-95] suggested using 89-mol% n-decane ($C_{10}H_{22}$) representing alkane and 11-mol% of an aromatic fuel. The aromatic fuel can be benzen (C_6H_6), toluen ($C_6H_5CH_3$), ethyl-benzene ($C_6H_5C_2H_5$) or naphtalene ($C_{10}H_8$). Benzen is not a good choice as an aromatic component since it does not provide a good prediction of the aromatic concentration in the flame. Other three aromatics give the same result and any one of them may be selected as an aromatic constituent based on the availability of the data [90].

To further simplify a fuel surrogate model and make it applicable to fast combustion analysis, aviation fuels can be represented by a component that has the highest percentages in the mixture [87]. In the case of aviation fuels, the main constituent is $C_{12}H_{22}$ or $C_{12}H_{24}$ or a representative formula of aviation fuel (like $C_{12}H_{23}$). The combustion mechanism of a jet fuel is generated based on its major constituent and defining the global reaction for larger molecules that convert to smaller ones through the Pyrolysis process [96-97].

Every fuel has a unique combustion mechanism, but all or part of the pollutant formation sub-mechanisms remain unchanged in different fuel combustion mechanisms. Certain elementary reactions and reaction paths are present in combustion mechanisms that are responsible for pollutant formations. The formation sub-mechanism of carbon monoxide (CO) and nitrogen oxides (NO_x) are among the reactions that almost remain the same in different combustion mechanisms. Since unburned hydrocarbon (UHC) emissions consist of various hydrocarbon-based molecules coming from different sources based on fuel type and combustion condition, it is hard to find a common mechanism among them. A description of these pollutant elementary reactions common in all combustion mechanisms is provided in the following.

2.2.1.1 Thermal NO Formation

Thermal NO_x formation is the main NO_x formation mechanism and is produced by the oxidation of atmospheric nitrogen in the high temperature region of the flame and post-flame regions. Zeldovich proposed the following elementary reactions for NO formation:

$$O+N_2 \leftrightarrow NO+N$$

$$N+O_2 \leftrightarrow NO+O$$

The first reaction has strong temperature dependency and is slow, while the second reaction is faster. Due to the overall slow rate of these reactions, compared to the fuel oxidation, thermal NO is being formed in the post-flame region. The Zeldovich mechanism is extended by adding the following reaction to the previous elementary reactions:

$$N+OH \leftrightarrow NO+H$$

The reverse rates of the above reactions are very slow and sometimes are ignored.

2.2.1.2 Prompt NO Formation

The prompt (Fenimore) NO formation was discovered by Fenimore [98]. This mechanism is particularly important in rich conditions. However, its contribution is less than that of the thermal NO formation. The prompt NO formation is related to the interaction of atmospheric nitrogen with hydrocarbon radicals in the early stage of the flame region, which makes it totally different from the thermal formation sub-mechanism. In this mechanism, the interaction of atomic nitrogen with HC radicals creates amines and cyano compounds that are converted to some intermediate compounds and ultimately to NO. The formation mechanism of the prompt NO is not as simple as the thermal NO formation mechanism due to the presence of a high number of hydrocarbon radicals and different reaction paths, but its complexity may be reduced by considering HC radicals as the main radical interacting with the nitrogen and skipping the process that

leads to the formation of HC. The following reactions initiate the Prompt NO formation mechanism:

$$CH+N_2 \leftrightarrow HCN+N$$

$$C+N_2 \leftrightarrow CN+N$$

After this point, the mechanism depends on the value of the equivalence ratio. For equivalence ratios less than 1.2, NO formation is based on the following reactions [68]:

$$HCN+O \leftrightarrow NCO+H$$

$$NCO+H \leftrightarrow NH+CO$$

$$NH+H \leftrightarrow N+H_2$$

$$N+OH \leftrightarrow NO+H$$

For richer conditions, the mechanism is too complex to be presented in a few elementary reactions. Implementing the prompt NO formation in a fuel combustion mechanism requires a set of elementary reactions representing a complex interaction between the hydrocarbon and nitrogen species. Since these kinds of elementary reactions do not show up in a simplified combustion mechanism (especially those that are based on the Pyrolysis process), implementing prompt NO formation in a simple combustion mechanism is not possible.

2.2.1.3 Nitrous Oxide Intermediate Formation

The nitrous oxide (N_2O) mechanism is important in fuel lean and low temperature conditions and consists of three steps [68]:

$$O+N_2+M \leftrightarrow N_2O+M$$

$$H+N_2O \leftrightarrow NO+NH$$

$$O+N_2O \leftrightarrow NO+NO$$

2.2.1.4 Nitrogen Dioxide Formation

A significant part of the NO produced by the mechanisms described above is converted to NO_2 in the low-temperature region of combustors; therefore, at the combustor exit, a mixture of NO and NO_2 exists, which is called NO_x. The NO_2 formation or destruction elementary reactions are:

$$NO+HO_2 \leftrightarrow NO_2+OH$$

$$NO_2+H \leftrightarrow NO+OH$$

$$NO_2+O \leftrightarrow NO+O_2$$

The first reaction is a formation reaction and is significant at low temperature. The next two reactions are responsible for NO_2 destruction and are significant at high temperatures; therefore, the NO_2 formation rate is higher at low temperature regions (combustor exit) and lower at high temperature regions.

2.2.1.5 Carbon Monoxide Oxidation

Unlike NO_x formation mechanisms, which do not produce significant heat and may be separated from the other chemical reactions, the CO oxidation is the main source of heat release in the combustion of hydrocarbon fuels. In simplified form, hydrocarbon fuel combustion can be divided in two steps; the first step is CO formation based on fuel and air interaction, and the second step is CO oxidation to CO_2. The presence of water or hydrogen significantly enhances the CO oxidation rate. The first step is a complex mechanism and is fuel specific and is not completely known to researchers; however, the second step is simple and can be modeled by the following reactions with water as a source of hydroxyl radicals (OH):

$$CO+O_2 \rightarrow CO_2+O$$

$$O+H_2O \rightarrow OH+OH$$

$$CO+OH \rightarrow CO_2+H$$

$$O_2+H \rightarrow OH+O$$

In addition to the above reactions, in the presence of hydrogen molecules, the following reactions are also considered for the formation of hydroxyl radicals:

$$O+H_2 \rightarrow OH+H$$

$$OH+H_2 \rightarrow H_2O+H$$

2.2.2 Chemical Reactors Network Approach

As mentioned earlier, the chemical reactors' network (CRN) approach is used to model the finite-rate combustion process. This method is based on dividing the combustion area into smaller regions in which physical and chemical characteristic variations are small. Each region can be replaced by a single or several simple elementary chemical reactors. The characteristic of each reactor and its connections with other reactors depend on the flow-field. From this brief description, the link between the flow-field and CRN is obvious. The reactors are linked together by flows coming from other reactors or flow inlets (Figure 17). After building the network of reactors, the fuel combustion mechanism is introduced to the network. The governing equations of elementary reactors are relatively simple and consist of algebraic and differential equations. Solving the governing equation of the network of reactors will yield species

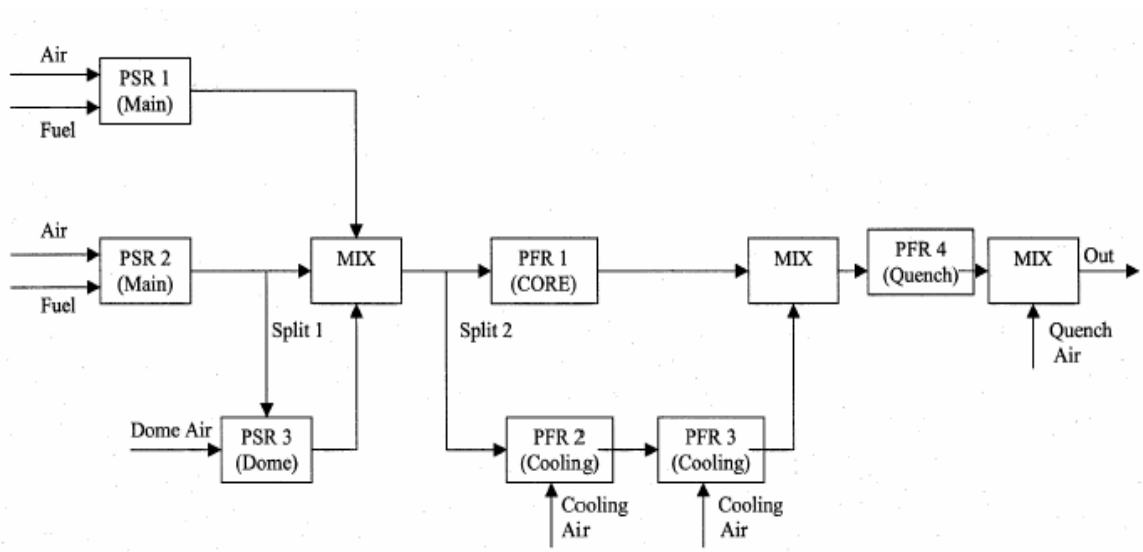

Figure 17: An example of a network of elementary chemical reactors [8]

concentration and exit temperature at the exit of each reactor. The CRN models need more time to run than empirical or semi-empirical models, but they are faster than CFD models. In contrast to CFD models with high fidelity internal flow analysis and low fidelity chemistry analysis, the CRN models have simplified flow-field and detailed chemical analysis.

Three main types of reactors used in constructing CRNs are the perfect (well) stirred reactor (PSR), the plug flow reactor (PFR) [68] and partially stirred reactor (PaSR) [99]. The PSR and PFR reactors were introduced by S. L. Bragg [100] and initially used in CRNs by Swithenbank [58]. The PaSR is an additional type of reactor that was formulated later by Chen [99] and Correa [101]. If the flow inside a combustor is considered to span a wide range of regimes from a fully turbulent to a one dimensional laminar flow, then each PSR and PFR reactor represents the ends of this range. As described in the next sections, the PSR represents combustion in a high-intensity turbulent flow, where mixing time is much shorter than the reactors' residence time, while the PFR represents combustion in a one-dimensional calm flow, where mixing time is much longer than the residence time. The PaSR is located between the PSR and the PFR, where the fuel and air are neither totally mixed nor totally segregated, which means the mixing time of fuel and air and the reactor's residence time are on the same order.

2.2.2.1 Perfect Stirred Reactor (PSR)

The Perfect Stirred Reactor is a 0D ideal reactor in which instantaneous perfect mixing of fuel and air as well as products occurs and the mixture exiting the reactor has the same concentrations as the mixture inside the reactor [2]. It is assumed that the Damkohler number inside the PSR is zero. In a PSR, combustion takes place uniformly in a control volume and there is no spatial or temporal variation of parameters (Figure 18). The reactor was initially used in flame stabilization and reaction rate studies [86, 102]. The important parameter in PSR is the residence time which represents the available time

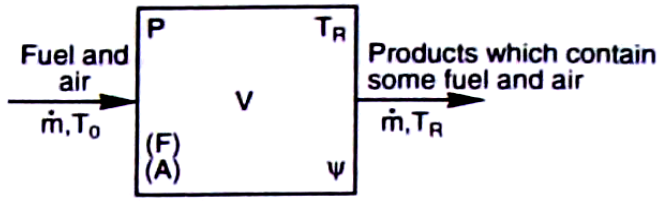

Figure 18: Perfect Stirred Reactor (PSR) and its parameters [2]

that reactants have in a reactor. The relative magnitude of the residence time compared to the reaction time determines the degree of the reaction progress in the reactor before the mixture comes out of it. The following describe the mathematical model of the PSR. All the equations are extracted from reference [68]. The relation between reactor volume (*V*), mixture flow rate ($\dot{m}$) and residence time (τ) is shown in equation (7). Any two of these parameters define the third one.

$$\tau_{res} = \frac{\rho_{mix} V}{\dot{m}} \tag{7}$$

where ρ_{mix} is the mixture density. Equation (8) shows the species conservation equation in the PSR:

$$\frac{dm_{i,cv}}{dt} = \dot{m}_i''' V + \dot{m}_{i,in} - \dot{m}_{i,out} \tag{8}$$

where

$\dot{m}_i''' V$: ith species production rate

$\dot{m}_{i,in}$: ith species inlet mass flow rates

$\dot{m}_{i,out}$: ith species exit mass flow rates

$\frac{dm_{i,cv}}{dt}$: The accumulation rate of ith species inside the reactor volume V.

The volumetric rate of generation or destruction of the ith species is shown below:

$$\dot{m}_i''' = \dot{\omega}_i MW_i \tag{9}$$

where

$\dot{\omega}_i$: The net production rate of the ith species

MW_i : The molecular weight of the ith species.

The mass flow of the ith species into the control volume is:

$$\dot{m}_{i,in} = \dot{m}Y_{i,in} \tag{10}$$

where:

$Y_{i,in}$:The initial mass fraction of ith species

The equation for the mass flow rate out of the control volume is similar to the above equation as well. Substituting the term in the right hand side of equation (8) with equations (9) and (10) and assuming steady condition results in a series of species conservation equations:

$$\dot{\omega}_i MW_i V + \dot{m}(Y_{i,in} - Y_{i,out}) = 0 \;\; i = 1...N \tag{11}$$

Equation (11) provides N equations for N species with N+ 1 unknown (N mass fractions and temperature). The addition of energy equation is needed for problem closure which for steady-state condition is:

$$\dot{Q} = \dot{m}(h_{out} - h_{i,in}) \tag{12}$$

where $\dot{Q}$ is the rate of heat release and $h_{i,in}$ and $h_{i,out}$ are i^{th} species enthalpies (formation and sensible). $\dot{Q}$ is expressed by individual species as:

$$\dot{Q} = \dot{m}(\sum_{i=1}^{N} Y_{i,out} h_i(T) - \sum_{i=1}^{N} Y_{i,in} h_i(T_{in})) \tag{13}$$

Although perfect mixing cannot occur in reality and it results in flame extinction, PSRs are good candidates to model parts of a combustor where the turbulence intensity and micro/macro mixing degree are high. The primary and secondary zones fall into this category.

2.2.2.2 Plug Flow Reactor (PFR)

The Inside the PSR (PFR) is a 1D reactor in which flow properties change in the axial direction while remaining uniform in the radial direction (Figure 19). No mixing takes place in the axial direction but the properties change in that direction so the value of the flow parameters at the exit plane is different than their value inside the reactor.

The conservation equations of the Inside the PSR are provided below [68]. All equations are one dimensional (x-direction). Equations (14), (15), (16) and (17) show the mass conservation, momentum conservation, energy conservation, and species conservations in the x-direction.

$$\frac{d(\rho u_x A)}{dx} = 0 \tag{14}$$

$$\frac{dp}{dx} + \rho u_x \frac{du_x}{dx} = 0 \tag{15}$$

$$\frac{dY_i}{dx} - \frac{\dot{\omega}_i MW_i}{\rho u_x} = 0 \tag{16}$$

$$\frac{d(h + u_x^2/2)}{dx} + \frac{\dot{Q}'' P}{\dot{m}} = 0 \tag{17}$$

where ρ is density, p is pressure, u_x is axial velocity, P is perimeter, $\dot{Q}''$ is heat flux per unit area, h is enthalpy and c_p is specific heat at constant pressure.

Combining the above equations with ideal gas assumptions, relations between species mass fractions, concentrations, and molecular weight and reaction rates and

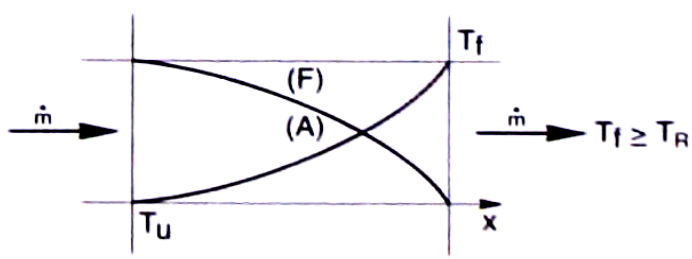

Figure 19: Plug Flow Reactor (PFR) and its parameters

assuming zero heat flux, the rate of temperature change, species mass fractions, and density can be obtained as

$$\frac{dT}{dx} = \frac{u_x^2}{\rho c_p}\frac{d\rho}{dx} + \frac{u_x^2}{c_p}\left(\frac{1}{A}\frac{dA}{dx}\right) - \frac{1}{u_x \rho c_p}\sum_{i=1}^{n} h_i \dot{\omega}_i MW_i = 0 \tag{18}$$

$$\frac{dY_i}{dx} = \frac{\omega_i MW_i}{\rho u_x} \tag{19}$$

$$\frac{d\rho}{dx} = \frac{\left(1 - \frac{R_u}{c_P MW_{mix}}\right)\rho^2 u_x^2\left(\frac{1}{A}\frac{dA}{dx}\right) + \frac{\rho R_u}{u_x c_P MW_{mix}}\sum_{i=1}^{N} MW_i \dot{\omega}_i\left(h_i - \frac{MW_{mix}}{MW_i} c_P T\right)}{p\left(1 + \frac{u_x^2}{c_P T}\right) - \rho u_x^2} \tag{20}$$

The above equations can be solved with appropriate initial boundary conditions to obtain the mass fraction and temperature profile across the reactor. The residence time across the PFR is calculated from the following equation.

$$\frac{dt_{res}}{dx} = \frac{1}{u_x} \tag{21}$$

Regions of the combustor where flow is one-dimensional and calm and turbulence intensity is low can be modeled by PFRs. Part of the secondary zone and dilution zone are the best candidates to be modeled by PFRs.

2.2.2.3 Partially Stirred Reactor

A Partially Stirred Reactor is useful when the turbulent mixing time is on the same order as the reactor residence time; therefore, it does not have the limitations of the PSR which assumes the instantaneous turbulent mixing assumption. On the limits, when the mixing time is much shorter than the residence time, its behavior approaches the PSR and when the mixing time is much longer than the residence time, its behavior approaches the PFR [103]. In PaSR the Damkohler number is on order of unity where the interaction between the chemical and fluid dynamics is strong. The interaction of

turbulent mixing and chemical reaction is defined through the definition of the turbulent mixing time:

$$\tau_{mix} = C_D \frac{\kappa}{\varepsilon} \tag{22}$$

where C_D is a constant, k is the turbulent kinetic energy, ε is the turbulent intensity and the ratio of turbulent kinetic energy over turbulent intensity is the time scale of the energy containing eddies in the turbulent flow. For the first order models, finding the value of turbulent intensity is not possible as it is a local variable, therefore in this study the mixing time is calculated based on the height of the mixing zone.

To address the issues of modeling the chemical reaction in the turbulent flow, averaging techniques introduces a significant error in the calculation of the mean species concentrations. The non-linearity in the turbulent mixing problem can be addressed by the joint probability distribution function (pdf) of the flow properties. A transport equation for this joint pdf is proposed by Pope [104] in which a joint velocity-composition pdf can be degenerated to single-point scalar pdf by ignoring the velocity fluctuation and spatial homogeneity [101]. Finally due to the large dimension of the single-point scalar pdf, Pope [105] developed a Monte Carlo method to sample the pdf distribution randomly (Equation(23)) and showed that for a sufficient number of samples the ensemble average of samples will converge to the density-weighted average.

$$\phi^{(1)}, \phi^{(2)}, ..., \phi^{(n)}, ..., \phi^{(N)} \tag{23}$$

The samples are randomly selected and governing equations will be applied to them. Samples interact with each other through a mixing term (first term) in equations (24) and (25). They show the rate of change of temperature in the nth sample and rate of change of the kth species mass fraction in the nth sample.

$$\frac{dY_k^{(n)}}{dt} = \frac{1}{\dot{m}_o \tau_{mix}} \sum_{i=1}^{M} [\dot{m}_o (Y_{i,kt} - \langle Y_k \rangle] + \frac{MW_k \dot{\omega}_k^{(n)}}{\rho^{(n)}} \tag{24}$$

$$\frac{dT^{(n)}}{dt} = \frac{1}{C_p^{(n)} \dot{m}_o \tau_{mix}} \sum_{i=1}^{M} \dot{m}_i \left(\sum_{k=1}^{k_g} Y_{i,k} (h_{i,k} - \langle h_k \rangle) \right) - \sum_{k=1}^{k_g} \frac{MW_k \dot{\omega}_k^{(n)} h_k^{(n)}}{\rho^{(n)} C_p^{(n)}} \tag{25}$$

In the above equations the mixing term is simplified using the Interaction-by-Exchange-with-the-Mean (IEM) model or Linear-Mean-Squares-Estimation model (LMSE) [106]. The other mixing model is the Modified Curl's model. Chen [99] provided the analytical form for LSME or Modified Curl's models as a basis for validating the PaSR model. In his model the unmixedness degree (S) is defined as

$$S = \frac{\langle \widetilde{f''f''} \rangle}{(1 - \langle \tilde{f} \rangle)\langle \tilde{f} \rangle} \tag{26}$$

where $\tilde{f}$ is the density weighted average and f'' is the fluctuation. The unmixedness value is bounded by 0 and 1, 0 being completely segregated and 1 being completely mixed. The unmixedness degree is linked to the residence and mixing time scales in the LMSE and Modified Curl's models by:

$$S_{MC} = \frac{1}{1 + \tau_{res} / 3\tau_{mix}} \tag{27}$$

$$S_{LMSE} = \frac{1}{1 + C_\phi \tau_{res} / 3\tau_{mix}} \tag{28}$$

where residence time is defined as:

$$\tau_{res} = \frac{\rho_{mix} V}{\dot{m}} \tag{29}$$

Equation (27) is used for the Modified Curl's model and equation (28) for the LMSE model. The value of C_φ is usually 2. Inside the PaSR the samples are randomly selected at each time marching step and their governing equations are solved. This random selection of the samples inside the PaSR is the reason of the stochastic nature of the reactor's outputs. After sampling and solving the governing equations, the exit

composition of the species and the exit temperature of the PaSR are provided in term of probability density functions (pdf).

2.3 Assessment of Current Emissions Prediction Approaches

As the analysis methods move from high fidelity approaches to simplified physics-based approaches, the fidelity of the internal flow-field analysis goes down and changes from a mesh of small cells or grids to the averaged spatial zones. Due to this change, more computational power may be diverted to a detailed finite rate chemistry analysis. In combustion analysis a trend can be seen that indicates the move from equilibrium, fast chemistry, flamelet, or simple 2-3 step-finite-rate chemistry in high-fidelity flow-field approaches to a detailed combustion mechanism with more species and elementary reactions in the CRN approach.

The CRN approach has disadvantages too, one of which is the absence of a solid rule or guideline to build a CRN. Ad-hoc methods are used by researchers to build CRNs [66]. These methods are based on CFD analysis [107] or experimental measurements of flow-field parameters that are conducted for a cold or reacting flow. Tonouchi et al. used a two-reactor model to predict the emissions of a combustor with heptane [108]. Shakariyants et al. used 1D flow modeling, global combustion model of Jet-A along with simple emissions formation models in a series of finite rate chemistry models to determine the emission levels of the CF6-80 combustor and compared it with CFD results [54-57]. In their study, they did not explicitly consider the mixture non-uniformity and existence of fuel droplets. Mellor [47] and Mellor and Fritsky [109] used semi-empirical correlations based on different time scales to size a single annular combustor with a known architecture. Novosselov et al. used the temperature and velocity distributions generated by a CFD analysis to build a CRN [110-111]. Vedula et al. used experimental data to build a CRN for a ceramic matrix composite (CMC) liner combustor and modeled its emissions [112]. Lebedev et al. built a CRN based on 3D CFD results and employed

the flamelet concept in one of the PSRs in the CRN to account for the existence of a diffusion flame for the CIAM methane fueled combustor [61]. Rizk et al. used a CRN to implement the diffusion flame concept as well as a mixture non-uniformity into the emissions-prediction of a single annular combustor [53] with a propane combustion mechanism [89] to predict NO_x emission of set of combustors. In their work, no details are provided about the flow-field modeling, diffusion modeling or reactors' sizing. Part of the overall droplet evaporation and diffusion burning process used in this thesis is similar to the one provided in reference 112; however, all the relations and equations used here are developed independently without any knowledge about the equations employed in [53].

The other issue related to the CRN approach is that the PSR and PFR reactors represent two end-of-flow regimes, which are the high intensity 0D turbulent flow and the laminar 1D flow. The validity of the model is questionable if it is applied to a region in a combustor that is somewhere between these two extreme ends, i.e., a partially mixed, medium intensity turbulent flow. One way to bridge the gap between the PSR and PFR concepts is to use the Partially Stirred Reactor (PaSR) concept, but PaSR execution time is long and it is sensitive to initial conditions or guess provided to it [103].

In almost all the above methods, the fuel is gaseous fuel; however, in real liquid-fueled combustion the effect of droplet evaporation should be considered as well. Part of this thesis' contribution is the assumption of developing and integrating different models and disciplines together and creating a model for emissions prediction and initial combustor sizing in the conceptual design phase. The other contributions is about capturing the effects of the uncertainty of the inputs and considering different combustion phenomena on the final emission levels and their distributions. To that end, the following section provides a background about the uncertainty concept.

2.4 Uncertainty Analysis

Many sources of uncertainty exist when physical phenomena are modeled. They originate from uncertain inputs, boundary conditions, calibration, or lack of sufficient fidelity in the model [113]. The uncertainty can be viewed as the difference between available knowledge and complete knowledge and can be classified into two groups: Aleatory and epistemic. They are also classified as random and nonrandom uncertainties [114]. The aleatory uncertainty is related to the variability and uncertainty of the inputs to a system or the system characteristics [115-116]. This type of uncertainty can be modeled by probability theory. If enough information is available, the inputs to the model can be modeled as random variables with a defined probability density function.

The objective of the sensitivity analysis is to determine the contribution of individual parameters on the aleatory uncertainty level. The aleatory uncertainty can be modeled, but it is not necessarily reducible. The state of the inputs to the system cannot be completely certain and they are random in nature; therefore, a degree of aleatory uncertainty always exists in the predictions. On the other hand, epistemic uncertainty is inherent in the structure of the model itself. The fidelity of the model and the type of assumptions made define the degree of epistemic uncertainty. Different theories such as evidence theory, possibility theory, and fuzzy set theory are used to model epistemic uncertainty [117].

Often it is not possible to find an analytical solution for the output probability density function (pdf) or cumulative distribution function (CDF) as a function of input uncertainties. The common practice in uncertainty analysis to capture the effect of the uncertainty of inputs on the output is the Monte Carlo simulation approach. The approach is briefly described next.

A relation between an output and inputs of a model can be described by:

$$Y = f(x_1, x_2, ..., x_n) \tag{30}$$

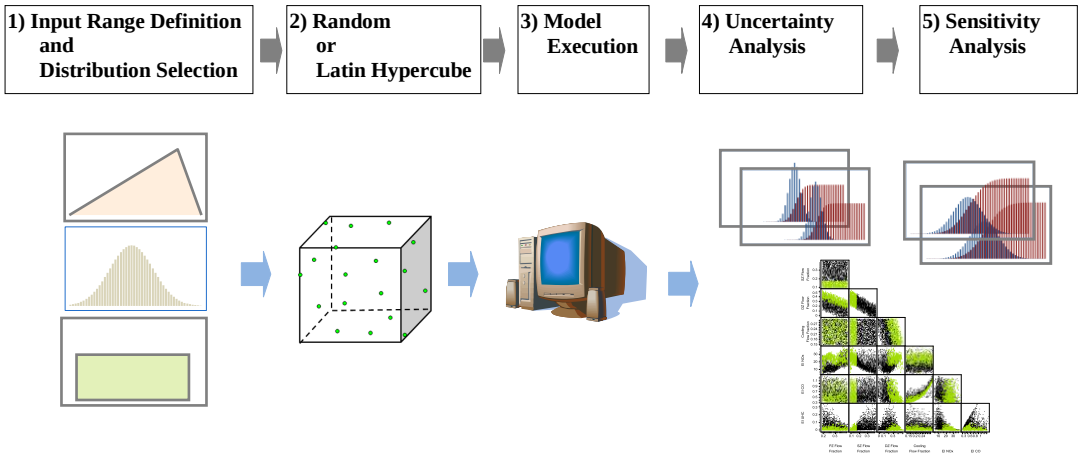

Figure 20: Steps in Monte Carlo analysis

where Y is the model output and $x_1 \ldots x_n$ are model inputs. The function f can represent a very simple relation or a non-linear behavior of a complex system. The Monte Carlo simulation can be defined in five steps[118]:

1. Selection of the range and type of input distributions (unifrom, loguniform, triangular etc.)
2. Sample generation from the input ranges and distributions that are defined in step 1 (random or latin hypercube) to create a sample space X_i of size m

$$X_i = [x_{i,1}, x_{i,2} \ldots\ldots x_{i,n}] \quad i = 1 \ldots m \tag{31}$$

3. Execution of samples in X_i to generate the response sequence $Y_i = f(X_i)$
4. Processing the data for uncertainty analysis using expected value E(y) and variance of V(y):

$$E(y) = \sum_{i=1}^{m} \frac{y_i}{m} \quad and \quad V(y) = \sum_{i=1}^{m} \frac{[y_i - E(y)]^2}{m-1} \tag{32}$$

The other way to process the data is to plot the histogram or frequency plot of Y which shows the variability of Y.

5. Sensitivity analysis through the use of scatter plot matrices, analysis of variance (ANOVA), screening or other methods to obtain the sensitivity of Y to the inputs *X* and the contribution of the uncertainty of inputs to the variability of the output.

Figure 20 shows the steps listed in Monte Carlo analysis.

After completing the theoretical background and literature review, the next chapter provides a review of the research objective and research questions. Based on this information, a set of hypotheses is formulated.

CHAPTER 3

INTERIM SUMMARY AND HYPOTHESIS FORMULATION

This chapter provides an overview of the main points of the previous chapters and summarizes what has been discussed thus far. In this chapter, based on the research questions developed in the first chapter and the literature review, hypotheses are formulated to answer the posed research questions. Then, the introduction of the RQL concept is provided in Chapter 4 and the proposed methodology is explained in Chapter 5. In the next chapter the integrated environment to predict the emissions is introduced. The methodology implementation and validation are provided in Chapter 7. Discussion and conclusion is the subject of the last chapter before appendices.

3.1 Review of Research Objective and Research Questions

In Section 1.4 a research objective and a set of research questions are provided based on the observations. To demonstrate the thought process leading to the hypotheses, they are restated here. In the research objective, the need for an approach to predict the combustor emissions, parametric assessment and capturing the relation between the combustor characteristics and system level parameters and emissions at the conceptual design phase are highlighted. The goal is to reduce the prediction uncertainties and avoiding high fidelity combustion analysis.

In Chapter 2, a literature review and theoretical background are provided and as a result, a deeper understanding of the available methods and their shortcomings in modeling gas turbine emissions is acquired. Here, research questions are restated with the additional knowledge gained from the previous chapter. The hypotheses are based on the available methods introduced in Chapter 2 and their weaknesses and strengths. To support the hypotheses, a methodology is developed in Chapter 5 and experiments are designed to prove or disprove the hypotheses.

The first research questions (RQ 1) is the result of the concerns related to aviation growth and emissions regulations. Future regulation will be more stringent as a result of aviation growth and environmental concerns. Also, the regulations may expand to operating conditions beyond the ICAO/LTO cycles to cruise altitudes. An emissions-prediction model is needed to predict the aviation emissions at different operating conditions and to be used in conjunction with other engine or aircraft analysis/design tools to model pollutants around airports and at cruising altitudes. A parametric capability of such a model is important to reflect the change of design features and operating conditions in the emission levels of the current and future aircraft fleet.

Research Question 1(RQ 1): How can an emissions prediction approach be made more parametric in a way that a variation in a combustor design parameter is reflected in the emission levels?

The required criteria are expected to be satisfied through the use of hybrid emissions prediction models. In such a model, important phenomena are modeled using hybrid equations that are independent of combustor type and architecture. Separating disciplines and phenomena in the emissions formation process and modeling them using simple physics-based or semi-empirical models can provide the needed parametric capability while keeping the complexity of the model at a moderate level.

The second research question (RQ 2) is based on the observed environmental and aviation growth concerns and regulations. Such concerns identify a need to model the emissions of current and future aircrafts at any operating conditions with minimum need for experimental data. Such a model will be used to assess the impact of emissions on the environment and study the feasibility and viability of the future combustor concepts.

Research Question 2(RQ2): How can different combustor architectures be accommodated in an emissions prediction approach and their effects on emission levels be captured at different operating conditions?

The second research question emphasizes the flexibility or versatility of an emission model. In order to accommodate different combustor architectures, the emissions model should be modeled in modular fashion. A set of elementary modules or components is required such that by putting them together based on the given combustor architecture and configuration, the emission model can be created. In such a modular approach, reconfiguring the elements in a different configuration can resemble different combustor types. Reviewing sub-sections 2.1.5 and 2.2.2 shows that the component modeling and the chemical reactor network (CRN) approaches are the most versatile approaches to be used for the 1D flow and combustion analysis. The component modeling approach is the best candidate for internal flow-field analysis because it is simple, fast, and flexible and can be used to model different types of combustors by changing the architecture of its elements. The CRN approach is the best way to model the combustion process. The architecture and characteristics of CRN depend on the combustor type as well as the result of the internal flow-field analysis.

As a result, the first hypothesis (H1) is formulated as a potential answer to the first and second research questions (RQ 1 and RQ 2).

***Hypothesis 1 (H1)*:** The addition of combustor internal flow-field analysis using modular component modeling approach to the combustion analysis using the chemical reactors' network (CRN) approach results in a more versatile and parametric emissions prediction approach for different combustor types, different operating conditions, and different combustor design parameters.

The third group of research questions (RQ 3.1 and SRQ 3.2) are deduced from studying the shortcomings of current emissions prediction models (sub-section 1.3.3). Since empirical data are not always available (especially in the conceptual design phase and for the future technologies), and using correlation-based emission models to predict engine emissions is not a reliable approach. In addition, the correlation-based emission models are design specific. These drawbacks of current emissions prediction models (correlation-based) in the conceptual design phase introduce a level of uncertainty in predictions. Therefore, the final research question can be stated as follows.

Research Question 3.1 (RQ 3.1): How can the uncertainties of emissions prediction model be reduced in the conceptual design phase?

A research question 3.2 (RQ 3.2) follows the research question 3.1. The first step is to find a way to capture and quantify these uncertainties.

Research Question 3.2 (RQ 3.2): How can the uncertainties in the emissions prediction model and the important factor affecting it be captured and quantified?

As it was pointed out in the literature review, current emission models do not model some important disciplines with enough fidelity. The absence of an important disciplinary analysis necessitates adding additional inputs to the model to compensate for this deficiency. The value of these combustion-specific inputs should be provided by a field expert. As a conclusion, integrating these inputs at such a fidelity level with engine or combustor level inputs can cause complications in the smooth execution of analysis and prediction of emissions. These additional inputs may increase the uncertainties of the model if their value cannot be determined correctly. A lack of knowledge about a correct value of a particular parameter might lead to making erroneous assumptions about the input values, which translates to uncertainty in the outputs. To eliminate this problem, important disciplines in the emissions formation process must be correctly identified and

modeled to avoid unnecessary or erroneous assumptions about the inputs. The important disciplines identified in the theoretical background and literature review as making a significant contribution to the emission levels are internal flow-field, chemical process, droplet evaporation/burning, and fuel/air mixture non-uniformity. A parametric emissions model must consider these disciplines. It is hypothesized that integrating these models in an emissions prediction approach can be used for parametric studies of emission levels and their interdependencies with combustor design variables for conventional and advanced combustor concepts. At the same time addition of droplet evaporation/burning, and fuel/air mixture non-uniformity will reduce emissions prediction uncertainties compared to simple models that do not considers these disciplines. The second hypothesis (H2), therefore, is formulated as follows.

***Hypothesis 2 (H2)*:** An integrated emissions-prediction approach with reduced uncertainties can be developed by modeling and integrating important phenomena in the emissions formation process using hybrid models. The most important phenomena are assumed to be droplet evaporation/burning and air/fuel mixture non-uniformity. An interface provides a line of communication between the disciplines. Therefore, the first secondary hypothesis is formulated as:

***Secondary Hypothesis 2A (SH 2A)*:** The following simplified models are expected to reduce epistemic uncertainties of the emissions prediction**:**

- Probabilistic unmixedness model
- Droplet evaporation model
- Diffusion burning based on un-vaporized fuel flow

To capture the epistemic uncertainties in an emissions prediction model, first the important disciplines must be modeled and included in the approach and then an uncertainty analysis through a Monte Carlo simulation must be performed to find the

contribution of the different phenomena on the uncertainty of the emission levels. The Monte Carlo simulation process can be performed for a complete model and models lacking a discipline to quantify the improvement in the emission levels prediction.

To capture the aleatory uncertainty, a sensitivity analysis must be performed. The result of the sensitivity analysis shows the contribution of the inputs' variation (uncertainty) on the emission levels.

Therefore, the second secondary hypothesis is formulated as:

Secondary Hypothesis 2B (SH 2B): The Monte Carlo analysis can model the epistemic uncertainties. A comparison of the uncertainty analysis of a complete model with deficient models can capture the potential improvement or deterioration of emission uncertainties. A sensitivity analysis can model the aleatory uncertainties and show the effect of the inputs' uncertainty (variation) on the emission levels.

Figure 21 shows the relation among research questions, hypotheses and designed experiments.

The suggested hypotheses should be tested and validated in this thesis by

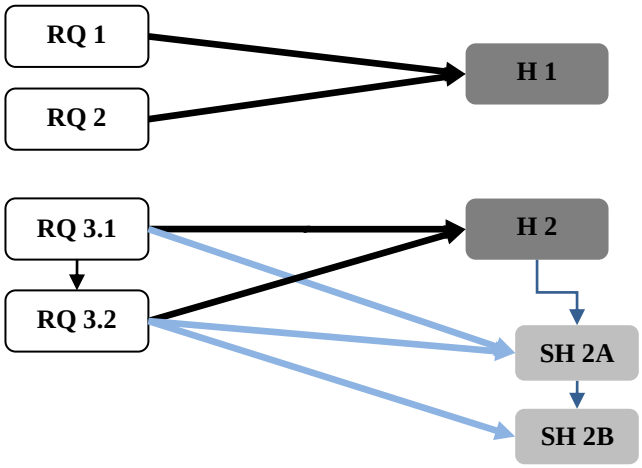

Figure 21: Relation between the research questions and hypotheses

constructing a suitable methodology and experiments. The next chapter introduces general information about an RQL combustor used in one of the experiments. Chapter 5 introduces the proposed methodology, which is based on the stated hypotheses. In Chapter 7 a set of experiments will be used to test and prove/disprove the hypotheses.

CHAPTER 4

GENERAL DESCRIPTION OF RQL COMBUSTOR CONCEPT

Since one of the experiments in this thesis is to model the emissions of a Rich-Quench-Lean (RQL) combustor, a brief description of it is provided here.

The RQL combustor is a type of air staged combustor (ASC) in which the combustor air flow is distributed in a way to create a fuel rich mixture in the first zone of the combustor (Figure 22). A fuel rich combustion results in a lower flame temperature than stoichiometric combustion which results in a lower thermal NO_x level. Existence of the rich flame in RQL combustor will also increase the flame stability and reduces the chance of the flame blow-off. On the one hand, the Oxygen starved environment in the rich zone cannot convert all of the chemical energy of the fuel to thermal energy and a considerable unburned hydrocarbons and carbon monoxide exist in the rich zone exhaust gases; on the other hand, a big portion of the total air flow that is coming from the compressor is remained in the combustor annulus and needs to be mixed with burned rich zone products. A major consideration here is that the addition of the annulus air into the core section in usual manner will change the mixture equivalence ratio from rich to lean value in a slow rate which gives enough time for combustion to take a path that goes through the stoichiometric region [28, 119] where local equivalence ratio can approach

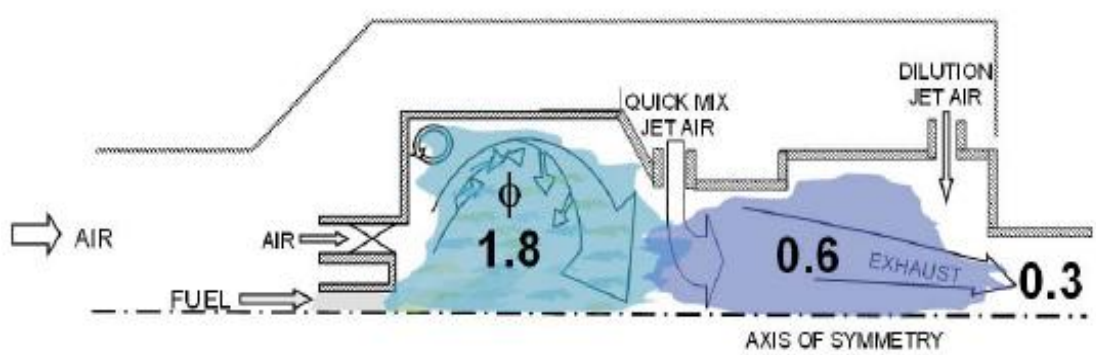

Figure 22: Equivalence ratio of an RQL combustor at different axial locations [15]

unity. The result is a high flame temperature and thermal NO_x formation. Such an event negates the effect of burning the mixture in the rich condition. The solution is to mix the dilution jet with the rich zone exhaust gases so fast and efficient that not enough time would be available for the combustion to go through the stoichiometric condition. Quick mixing will bring the total equivalence ratio of the mixture below unity to the lean condition where the flame temperature and thermal NO_x production is low while keeping the combustion to go through the stoichiometric beurning. The rich combustion also introduces a second path to NO_x production through the complex prompt (Fennimore) NO_x production mechanism [98].

Number of considerations should be addressed in the RQL concept. The first one is the type of the liner cooling technology that is used in the rich zone. The conventional cooling methods (film or effusion cooling) are not a good choice for rich section of the combustor. Addition of cooling flow to the rich mixture may create local stoichiometric mixtures near the liner wall with high flame temperature and thermal NO_x production; therefore, using cooling techniques that introduce a film of cooling air into the rich zone should be minimized or possibly be avoided. The lower flame temperature of the rich combustion in the rich zone eases the cooling requirement compared to the cooling requirement in the primary zone of a conventional combustor. This makes it easier to find alternate cooling techniques for the RQL combustor.

The candidates for cooling methods could be non-metallic materials such as monolithic ceramic or ceramic matrix composite (CMC) with maximum allowable liner temperature of 2500 F [9] or metallic nickel based Haste alloy with maximum allowable temperature of 2100 F. An inner coating of the combustor liner in the rich zone section is another option [120]. A cooling technology other than non-metallic alloys is Float-Wall cooling technology used in the P&W TALON combustor. In general, any cooling technology that prevents or minimizes the exposure of the cooling flow to the rich zone hot gases is preferable for the RQL concept.

The second consideration is quick mixing of dilution jets with the hot rich zone gases. It is important to design the dilution orifices and the mixing section in such a way that mixing of the cross flow jets with rich zone exhaust gases takes place in a short time. Number, size and the shape of the mixing orifices and the cross section of the mixing section have significant effects on the quality and speed of the mixing [78-80, 119, 121-123]. One way to enhance the mixing is to reduce the mixing cross section area (Figure 23) which reduces the mixing time through the reduction of the size of the largest energy containing eddies present in the flow. Reduction in eddy size also enhances the mixing and makes it possible for the coming jets to penetrate deeper into the hot gases and mix with them [28]. Care must be taken in the reduction of cross section to avoid very high core gas velocity which can disrupt the downstream flow or cause the flame to blow-off.

The third consideration is the mixing quality of air and fuel in the atomizer/swirler. The existence of droplets or non-uniformity in the fuel/air mixture can create local high temperature packets and increase the NO_x production.

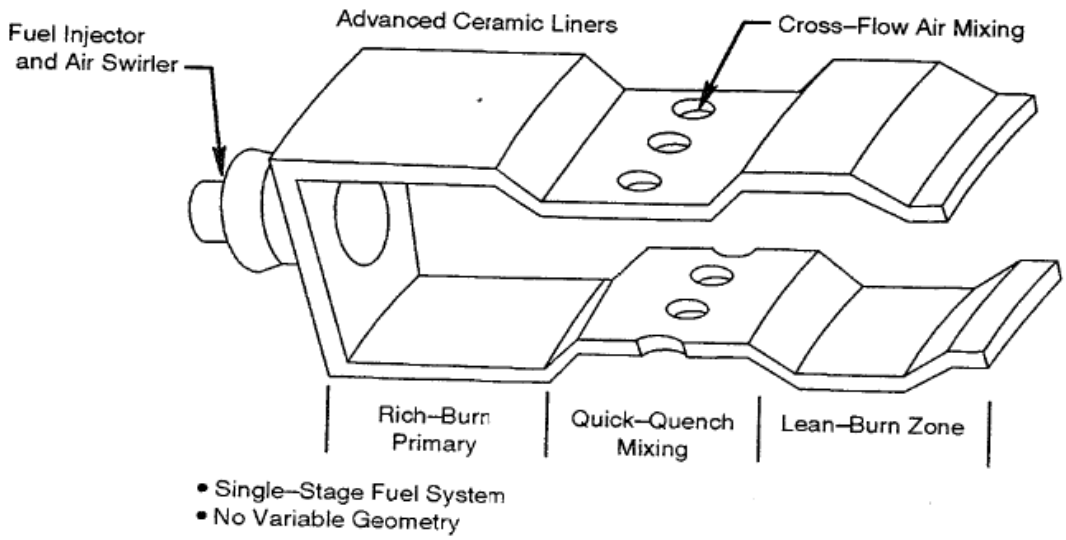

Figure 23: An RQL combustor concept [9]

4.1 Fuel Management

Since RQL combustors are designed to have rich flame in the first zone at on-design condition (take-off or supersonic cruise), the reduction of the fuel to air ratio by reduction of power setting may reduce the rich zone equivalence ratio down to the unity. Therefore, in contrast to the conventional combustor, if the RQL combustor has a fixed geometry, it is possible that it ends up having higher NO_x emission level at lower power settings. For this reason, some concepts employ the variable geometry or fuel shifting concepts to modulate the amount of the fuel that goes into the rich section. The objective is to keep the rich zone equivalence ratio away from one (rich or lean) at all power settings. Each concept is described in the following.

4.1.1 Variable Geometry

In a variable geometry RQL combustor, a mechanism changes the effective area of the swirler to change the portion of the air that is going into the rich zone and keeping that away from the stoichiometric region. The swirler area may be increased or decreased to keep the rich zone equivalence ratio above or beyond one depending on the level of engine power. Figure 24 shows the operating fuel schedule of NASA High Speed Research RQL combustor for a variable geometry RQL combustor.

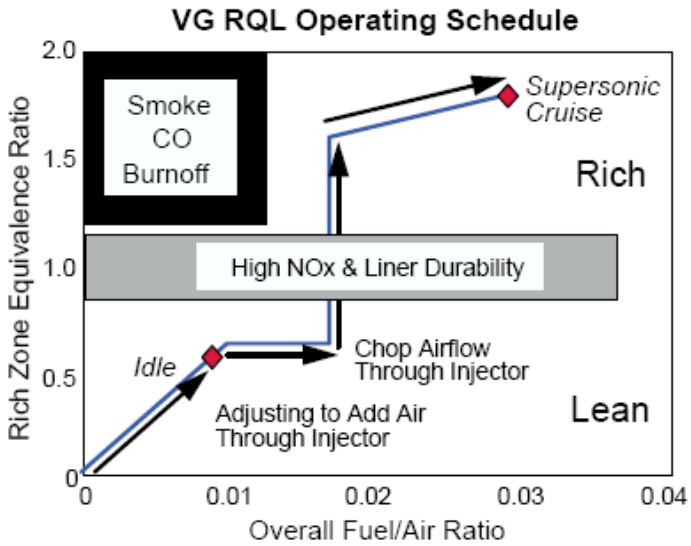

Figure 24: Fuel operating schedule of a variable geometry RQL combustor [1]

In the variable geometry concept, changing the swirler area will change the pressure drop across the swirler. This change will affect the combustor flow distribution through the change of the burner pressure loss coefficient and it cannot be considered

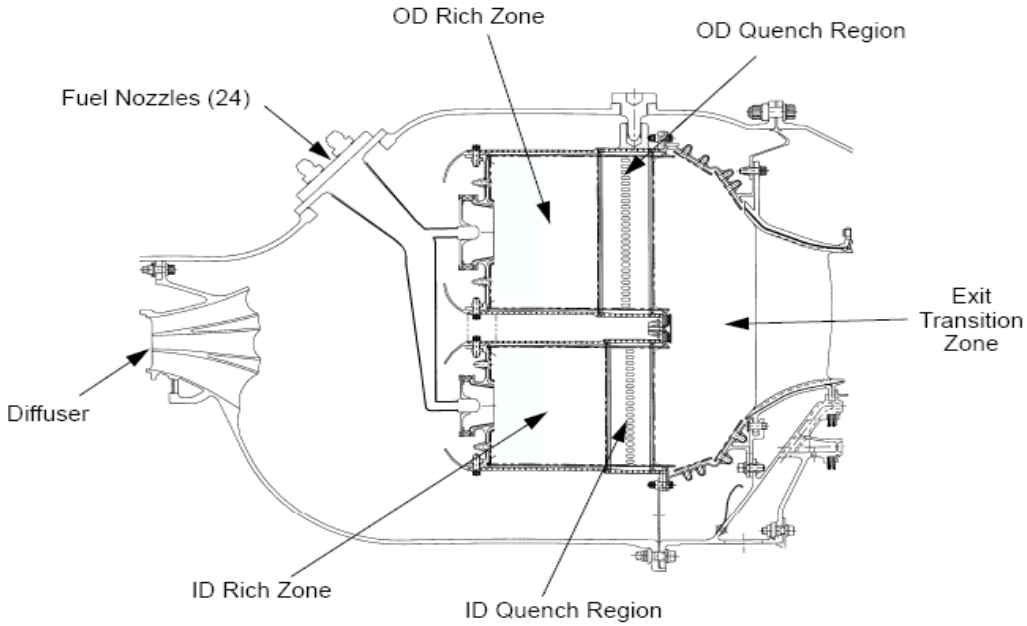

Figure 25: NASA HSR fuel-shifting RQL concept [1]

constant as power setting changes (an assumption that is true for the fixed geometry combustor). While the variable geometry RQL may take less space than the other concept (fuel shifting combustor), but the complexity of the variable geometry mechanism creates some reliability concerns in the harsh combustor environment.

4.1.2 Fuel Shifting

In fuel shifting concept, there are two similar RQL combustors that are placed radially next to each other (Figure 25) and their exhausts are mixed at the end section of the combustor. This concept is similar to conventional dual annular combustor with respect to its configuration. At each power setting, the amount of fuel that goes to each section (inner and outer) is scheduled to keep each section at rich or lean condition (Figure 26).

Since modulating the fuel flow is easier than modulating the airflow that is going to rich zone (as it happens in the variable geometry), the reliability of the fuel shifting concept is higher than the variable geometry and it has less operability problem. However, the size of the fuel shifting RQL combustor tends to be bigger than the variable

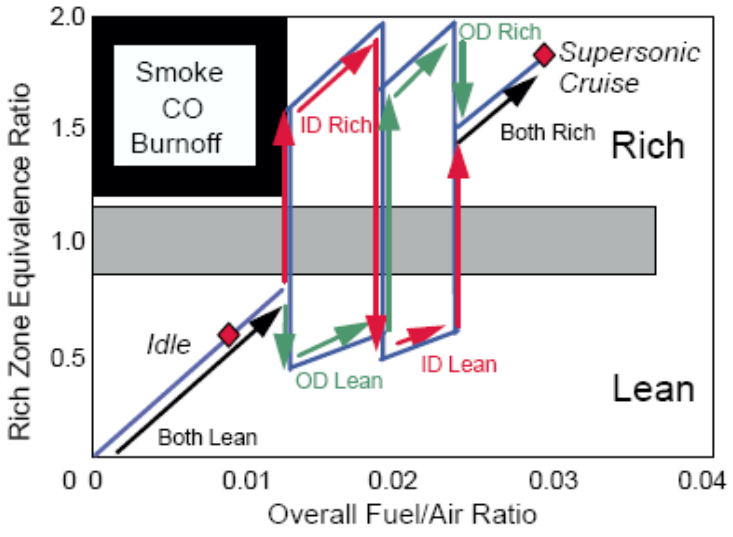

Figure 26: Fuel operating schedule of a fuel-shifting RQL combustor [1]

geometry combustor and the internal flow field is more complex.

4.2 Mixing Methods

Several types of combustors based on the RQL concept have been proposed, designed and built. They range from designs like NASA HSR combustor [9, 124] to more conventional looking such as P&W TALON series [17]. The types of RQL combustors can be categorized based on the type of the device that is being used to mix the air with the hot core gases. Three types of mixing are identified in the literature review and they are described below.

The first type is the "Wall-Jet" concept. In this concept the end section of the rich zone is narrowing down to a smaller area of the mixing zone and the air is introduced to the hot gases in the mixing zone through a series of orifices. The size and placement of the orifices are optimized for maximum mixing (Figure 27). In the second and third concepts which are referred to "reduced scale quench (RSQ)" concept, in order to enhance the mixing process, the mixing flow is introduced to the hot gases through a large number of very small orifices in a narrow channel.

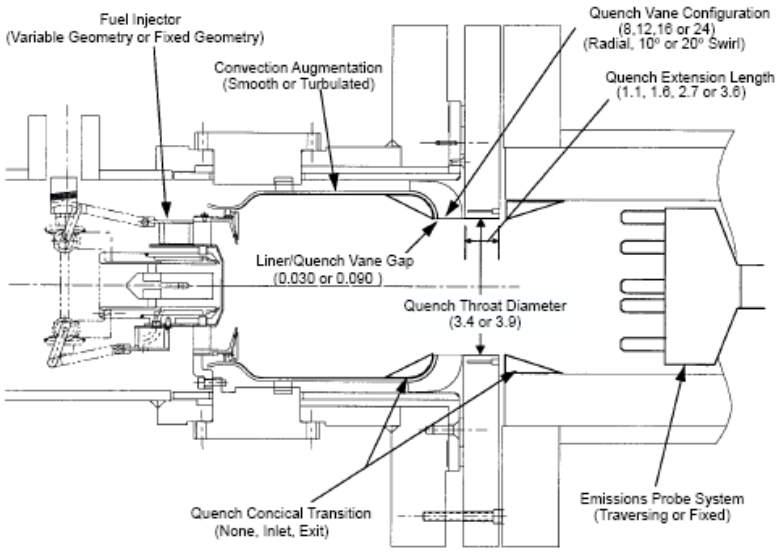

Figure 27: An RQL combustor with Wall-Jet mixing zone in the middle section [1]

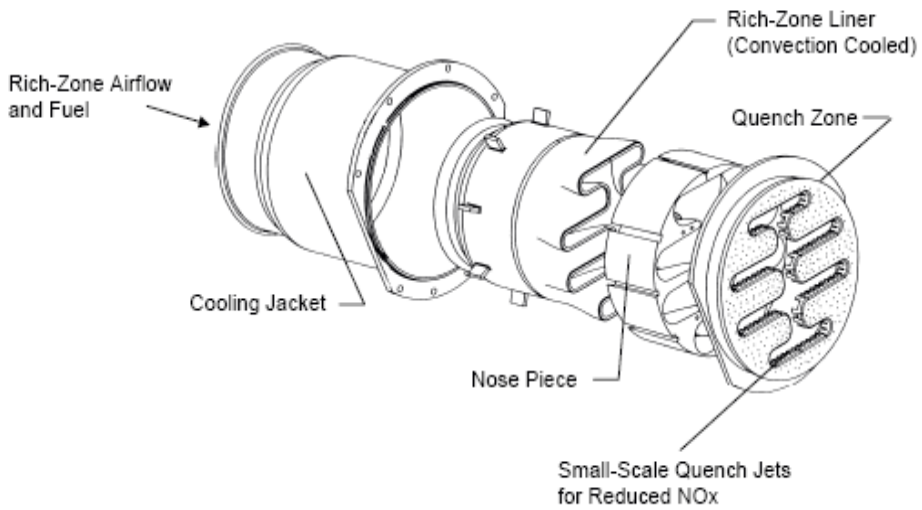

Figure 28: Reduced scale quench concept with convoluted liner [1]

In the "Convoluted Liner" concept, the rich zone exhaust gases are directed to a narrow convoluted channel and jets that are coming out of a large number but the very small orifices are mixed with the hot gases (Figure 28).

The third mixing concept which is another type of RSQ concept is called "Quench Vane", in which the cold annulus flow is mixed with the hot gases in a narrow channels

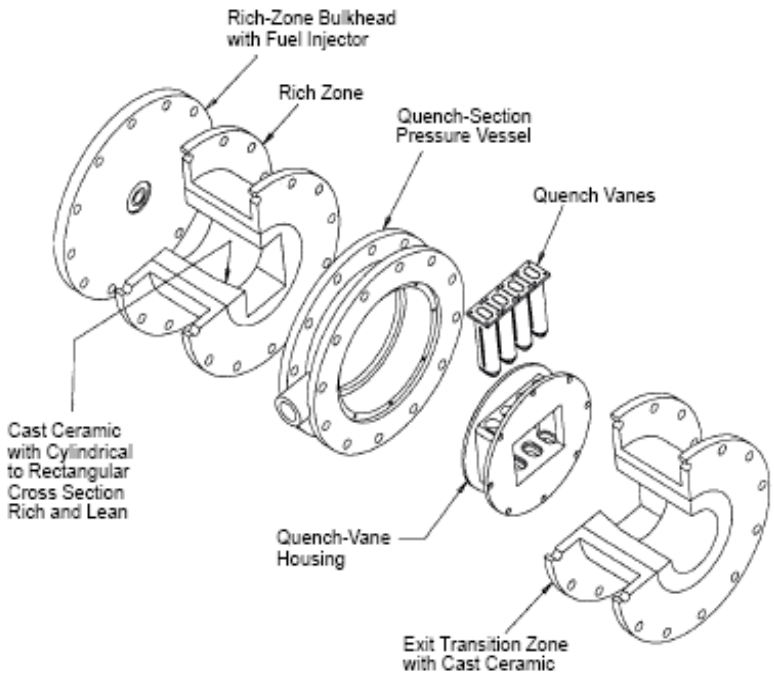

Figure 29: Reduced scale quench concept with quench vanes [1]

created by the vertical vanes and the mixing flow is directed to the channels through a large number of small holes drilled on the side of the vertical vanes (Figure 29). The RSQ concepts provide better mixing than the Wall-Jet concept and it results into a lower NO_x level, but at the same time the small narrow channel may increase the pressure losses. Between the two RSQ concepts of the Convoluted Liner and Quench Vane, the Quench Vane is preferable due to its simpler geometry compared to the convoluted liner. Also due to the better mixing process in the RSQ concepts, they can provide a good level of mixing in a shorter length than the Wall-Jet concept length.

In the Wall-Jet method, the mixing efficiency is not as good as RSQ concept due to the size of the Quench jets. The advantage of the RSQ over Wall-Jet is that due to the very narrow passage of the mixing zone, the mixing jets can be much smaller than the Wall-Jet concept and mix enough with the hot gases. The bigger size of the mixing jets in the Wall-Jet concepts comes at the price of the lower efficiency in mixing process. In such a case, the size of the large energy containing eddies are bigger than those of the RSQ concept which increases the time required for the complete mixing.

4.3 Atomizer and swirler

To have a better atomization in RQL combustor, an integrated high shear swirler can be used. An interaction between counter rotating swirling flows and a fuel film can produce very fine droplets. The complexity of such a combination makes its simple modeling impossible; therefore, in this report the conventional pressure-swirl Simplex atomizer with single axial swirler is used.

The materials and topics that are provided up to this point are used to construct a new methodology to model the combustor emissions in the conceptual design phase which is the subject of Chapter 5.

CHAPTER 5

PROPOSED METHODOLOGY

In this chapter a methodology is provided to obtain the first estimate of a combustor size and predict its emissions with acceptable accuracy and reasonable execution time. Two main areas that are addressed in this methodology are:

- Flow-field analysis
- Combustion analysis

The methodology is based on a combined 1D internal flow-field model of a combustor and a chemical analysis model based on the methods that are provided and discussed in Chapter 2. The internal flow-field of a combustor is a function of its shape and geometry; therefore, initial size and geometrical information of the combustor is required to determine its internal flow-field. Since the application of this methodology is limited to the conceptual design phase where the combustor geometry is not available, the initial geometry and size must be estimated based on the initial design requirement, combustor configuration and design conditions. Many factors, criteria and constraints affect the combustor geometry and size of its components; the reader is referred to Section 1.2 and Table 1 for more information. Many of these criteria cannot be evaluated when a combustor is initially sized and their evaluation is postponed to detail design or rig test phases. The most important criteria at the initial design phase of a combustor are: 1) geometrical constraint, 2) equivalence ratio at different zones, 3) the dilution jet penetration depth, 3) the velocity or Mach number inside the zone and, 4) cooling requirements based on the temperature level of hot gases. The values that are obtained for these parameters are first-hand estimate. As the design process progresses, the higher fidelity models and experiments are used to refine the design and obtain more accurate prediction. Additional criteria such as temperature profile factor and temperature pattern

factor, local hot spots, mixing quality, combustion dynamics, blow-off and ignition are considered at detail design phases as the design process proceeds.

To meet the set of criteria and constraints at the conceptual phase, determining how much flow goes to each section/zone of the combustor and consequently sizing the components is required (Figure 30). The task of splitting and directing specific fractions of the air flow that is coming from the diffuser to different sections is called *flow partitioning*.

Flow partitioning begins with analyzing the diffuser characteristics and diffuser exit flow conditions. The first step is to determine the flow properties of the compressor exit. The compressor exit flow properties are determined from the engine cycle analysis. The required properties are total pressure and temperature at the compressor exit (P_{31} and T_{31}), Mach number (M_{31}) and air mass flow ($\dot{m}_{31}$). The condition at which components are sized is called *on-design* condition. In design condition, one or more combustor parameters reach their maximum value and the combustor and its relevant component must be sized for that condition. For subsonic aircrafts, the flow properties reach their maximum condition at the take-off condition; however, other parameters such as relightability at altitude and blow-off condition may become critical at other conditions such as cruise or idle. Due to these reasons, the design point of the different combustor

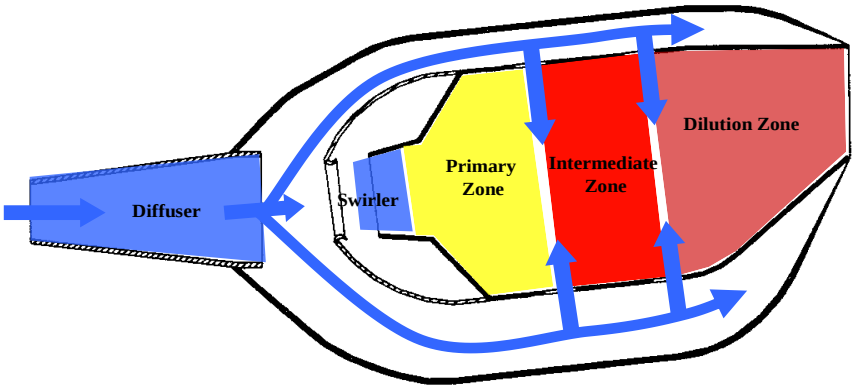

Figure 30: Combustor zones and flow partitions

components may be different depending on the considered criteria. For supersonic aircrafts, the flow properties (especially T_{31}) may be more critical at supersonic cruise than take-off and it should be considered in sizing the components (e.g., the liner cooling) too. In this research the components will be sized for maximum flow conditions and other criteria such as flame blow-out or altitude ignition will not be considered. After sizing components for on-design condition, the next step is to determine the flow fractions and internal-flow filed information for the given operating conditions (which could be other than the design condition).

The next step is to use the geometrical and flow-field information obtained from the 1D internal flow-field model in the chemical reactors' network (CRN) to determine

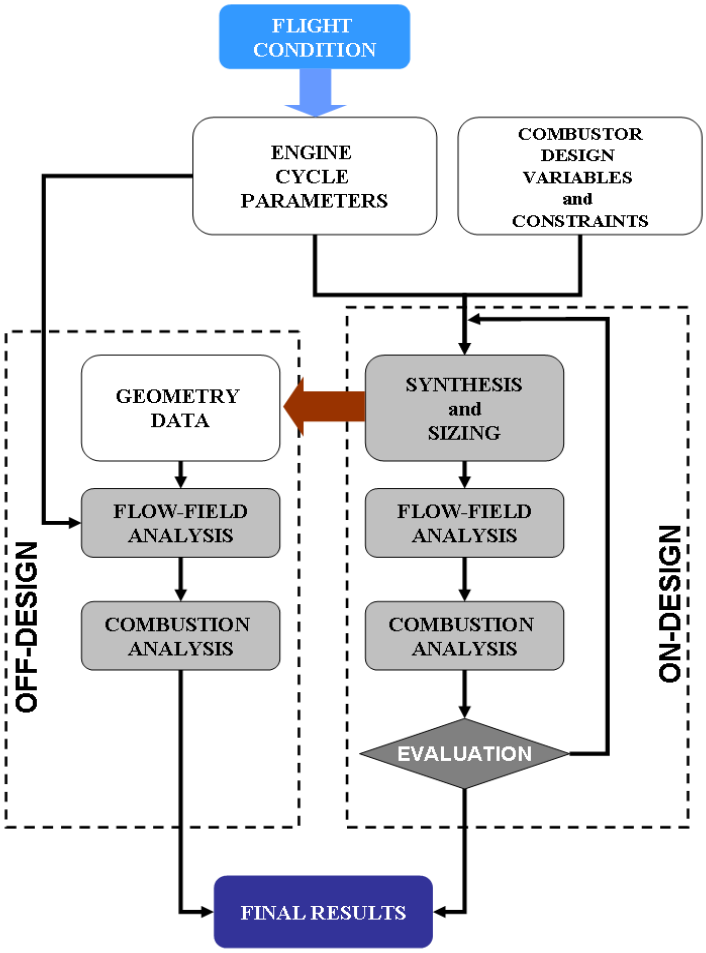

Figure 31: The flow chart of the emission prediction model

the size, fuel to air ratio, residence time, inlet flow rate and volume of the elementary reactors. Then the governing equations of the CRN will be solved to obtain the mass fraction of the species of interest at the exit of the combustor. The iteration may be needed if some criteria, such as the maximum difference between exit temperature calculation of 1D model and CRN model, are needed to be satisfied. The species mass fraction will be post-processed to obtain the parameters of interest such as emission index or ICAO DP/Foo. Figure 31 shows the flowchart of the described process.

The next section describes the process to build a 1D internal flow-field model. Since it is intended for the model to work at both design (on-design) and operating (off-design) modes, required models for both modes will be described. For the majority of the components, the equations and relations between the parameters are the same for both modes; however, they are rearranged based on parameters which are considered as known inputs and those which are considered unknown and are needed to be determined.

5.1 One Dimensional Internal Flow-Field Model

The 1D flow-field model assumes that a combustor consists of a number of elemets/components and that the flow inside of each one of them is uniform. In that

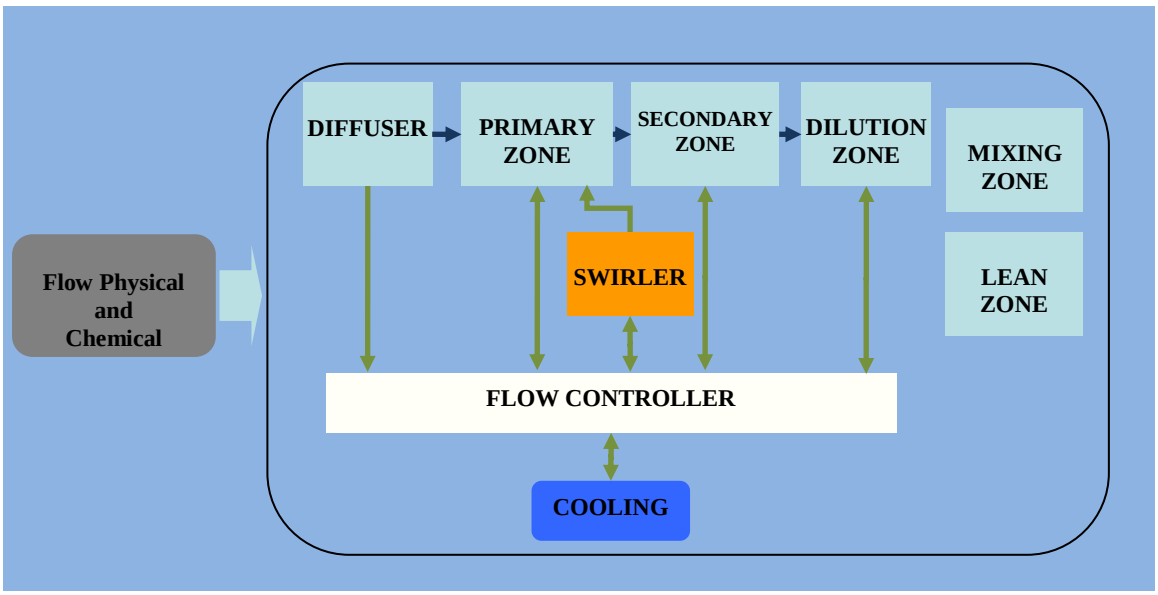

Figure 32: Main combustor elements in 1D internal flow-field model

sense, the elements are considered 0D models, but their integration together creates a 1D or 1½D model. Since the 1D flow-field model will be applied to SAC and RQL concepts, the emphasis will be on the elements that exist in those combustors. Figure 32 shows the main elements that are considered in this thesis and their relation with each other. In the figure, the model depicts a conventional combustor and additional elements of the mixing zone and lean zone are shown that are used in conjunction with others to build a 1D flow-field model for an RQL combustor concept. In the same figure, some of the elements are actual elements (e.g., zones and swirler) while others (i.e., the cooling element, flow controller and flow properties) are virtual elements. These virtual elements enable the calculation of the required cooling and the flow fractions that go into each zone.

The rest of this section introduces the combustor's main elements that are required to build the 1D flow-field models of SAC and RQL combustors. Also the relevant physical or hybrid equations for design and off-design modeling of these elements are provided.

5.1.1 Chemical Equilibrium Analysis

Chemical equilibrium analysis (CEA) is considered as the first building block of the 1D flow-field model. The model is used to calculate the temperature and flow properties of fuel and air mixture and burned mixture in the combustor.

Often in simple combustion analysis an enthalpy balance between reactant (air and fuel mixture) and products (burned mixture) is used to determine the temperature of the burned mixture. The gas properties such as specific heats (c_P and c_v) and gas constant (R) are defined as a function of temperature and fuel to air ratio (FAR) using the following equation:

$$\dot{m}_f \eta_{comb} LHV + \dot{m}_a c_{p\,in} T_{in} = (\dot{m}_f + \dot{m}_a) c_{p\,out} T_{out} \tag{33}$$

where η_{comb} is combustion efficiency which is the ratio of the released to available chemical energy and *LHV* is the fuel low heating value.

The enthalpy equation assumes that the amount of heat release (LHV) is always constant and it is equivalent to the complete combustion that produces H_2O, CO_2, N_2, O_2 or unburned fuel. In reality, the amount of heat release is not constant, and the combustion products are not just the ones that are mentioned above. In addition, equation (35) predicts the continuous increase in the exit temperature by increasing the fuel flow. However, combustion temperature reaches its maximum value at a point around unity equivalence ratio (stoichiometric fuel to air ratio) and it declines afterward. Also the reactant and product dissociation changes the exit temperature. As a result, equation (35) range of validity is for mixtures that have an equivalence ratio of less than one. In the 1D flow-field model, at some points (especially in RQL combustor concept) the equivalence ratio goes well beyond unity; thus, using above enthalpy equation would provide a significant error for temperature (and consequently gas properties) calculation. As a result, in this thesis, the more advanced chemical equilibrium analysis (CEA) approach is used to calculate the burned gas temperature and properties.

In the CEA approach, the assumption is that reactants and products have enough time to reach the equilibrium condition where the rate of the production and destruction of species becomes equal. Although this assumption cannot be used in the emissions prediction; however, it produces satisfactory result for temperature calculation.

In this approach, first a group of species believed to significantly contribute to the process is selected and their thermodynamic properties are defined as analytical equations. The most common form of the thermodynamic property equation is the 7 coefficient (a_1-a_7) NASA polynomial form, where the specific heat at constant pressure (c_p), enthalpy (H) and entropy (S) are defined as in the equations below:

$$\begin{aligned}
\frac{c_P}{R} &= a_1 + a_2 T + a_3 T^2 + a_4 T^3 + a_5 T^4 \\
\frac{H}{RT} &= a_1 + a_2 \frac{T}{2} + a_3 \frac{T^2}{3} + a_4 \frac{T^3}{4} + a_5 \frac{T^4}{5} + \frac{a_6}{6} \\
\frac{S}{R} &= a_1 \ln T + a_2 T + a_3 \frac{T^2}{2} + a_4 \frac{T^3}{3} + a_5 \frac{T^4}{4} + a_7
\end{aligned} \tag{34}$$

With the thermodynamic properties, the concentration of the species and the mixture temperature are determined by minimizing the Gibbs energy of formation ($\Delta_f G^0(T)$) of the species which corresponds to maximizing the entropy [125]. The number of Gibbs energy equations is equal to the number of species and the energy conservation equation is added to determine the mixture temperature. The Gibbs energy equation is based on the species equilibrium constants (K).

$$Log_{10}K = \frac{-\Delta_f G^0(T)}{RT} \tag{35}$$

A NASA CEA code is available to perform CEA approach[126]. The following properties are considered in this thesis as the output of the CEA given the inlet air and fuel flow rates, temperature, pressure and combustion efficiency.

- Exit Temperature
- Specific heat at constant pressure (c_p)
- Specific heat ratio (γ)
- Gas constant (R)

In the CEA analysis, the combustion efficiency is defined as the ratio of the actual temperature rise to maximum attainable temperature rise.

5.1.2 Flow Properties

The second level of the 1D flow-field model follows is based on the results of the CEA model described above. At this level, depending on the condition and requirements (on-design and off-design), the following flow properties and geometric information at each component of the combustor are determined:

- Mach number
- Velocity
- Weight flow function

$$wff = \sqrt{\frac{\gamma g}{R}} M \left(1 + \frac{\gamma - 1}{2} M^2\right)^{-\frac{\gamma+1}{2(\gamma-1)}} \tag{36}$$

- Area

$$A = \frac{\dot{m}\sqrt{T_{tot}}}{P_{tot} wff} \tag{37}$$

- Total-to-Static Pressure Ratio

$$\frac{P_{tot}}{P_{st}} = \left(1 + \frac{\gamma - 1}{2} M^2\right)^{\frac{\gamma}{\gamma-1}} \tag{38}$$

- Static Pressure and Temperature
- Dynamic Pressure

$$P_{dyn} = P_{tot} - P_{st} \tag{39}$$

The change in the density and Mach number in the annulus is very small meaning that dynamic pressure variation in the annulus and the liner (before entering the core section and flame area) is very negligible. Nonetheless, the variation in the density and Mach number is captured in the dynamic pressure because its calculation is based on equation 41 and the flow-function (Equation 38).

At on-design condition, when the Mach number and total pressure and temperature is known, the flow function (*wff*) value can be determined and from equation (36) and the cross section area of the component is calculated from equation (37). In off-design conditions, knowing cross section area (*A*) and total pressure and temperature, the flow function (*wff*) value is obtained from equation (39). By solving equation (38), the Mach number can be determined.

5.1.3 Diffuser Model

The diffuser is the first component of the combustor that is located after the compressor exit. The diffuser's primary job is to decrease the flow Mach number

(velocity) and increase its static pressure with minimum pressure losses. In this thesis, the diffuser's objective is to slow-down the flow. The equations used in this section are extracted from reference [4]. Figure 33 shows the simple diffuser elements and its associated parameters used in this thesis.

5.1.3.1 <u>On_Design Mode</u>

In this mode, the goal is to determine the diffuser geometry that results in slowing down the flow to a given Mach number at on-design condition. The diffuser model receives the following design variables and engine cycle parameters:

- Type (straight-wall, dump or a combination of both)
- Number of splitter plates
- Divergence half angle (straight-wall diffuser)
- Maximum area ratio of straight-wall diffuser (sweet-spot)
- Inlet mean radius (r_{m31})
- Exit mean radius (r_{m32})
- On-design inlet Mach number (M_{31})
- On-design exit Mach number (M_{32})

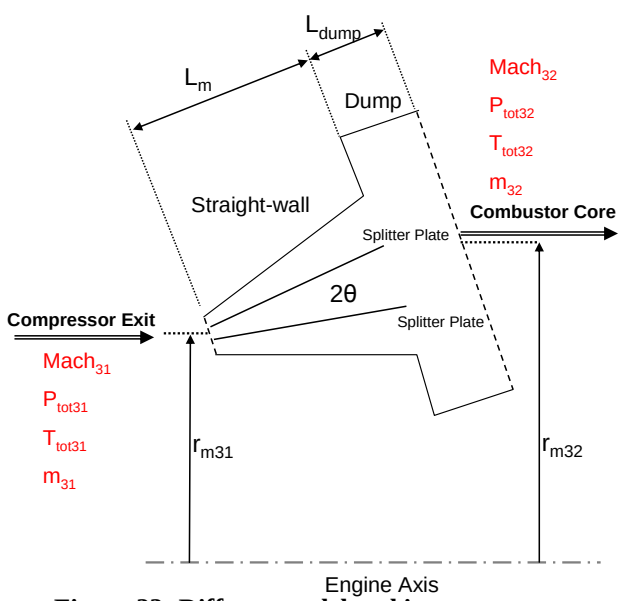

Figure 33: Diffuser model and its parameters

- On-design air flow ($m\square_{31}$)
- On-design inlet total temperature (T_{tot31})
- On-design inlet total pressure (P_{tot31})

The process starts with the calculation of the diffuser efficiency (η_{eff}). The initial sizing is performed for straight-wall diffuser. In this case, the diffuser efficiency will be a function of its divergence half angle (θ). The efficiency of the straight-wall diffuser is calculated from following equation [127]:

$$\begin{aligned}\eta_{straigh-wall} &= 1.1138 - 0.017701(2\theta) + 1.99925\times10^{-4}(2\theta)^2 \\ &\quad - 9.3068\times10^{-7}(2\theta)^3 + 1.5722\times10^{-9}(2\theta)^4\end{aligned} \tag{40}$$

The process of sizing the diffuser is shown in Figure 34 and described here. The process starts with sizing the straight-wall section. First the diffuser inlet area (A_{31}) is calculated using equation (39). Because the Mach number at station 32 is known, the flow function (*Wff*) can be determined from equation (38) for station 32. Also the total to static pressure ratio can be determined from equation (40). However total pressure at station 32 is not known and it is not possible to determine the static pressure, dynamic pressure and flow velocity at station 32. The total pressure at station 32 (and total pressure drop) is a function of the Ideal Pressure Recovery coefficient ($C_{P.Ideal}$) through the following equations [4]:

$$AR = \frac{A_{32}}{A_{31}} = \sqrt{\frac{1}{1 - C_{P.ideal}}} \tag{41}$$

$$C_P = \frac{P_{st32} - P_{st31}}{P_{dyn}} = C_{P.ideal}\eta_{diff} \tag{42}$$

$$\Delta P_{st} = C_P P_{dyn31} \tag{43}$$

$$P_{st32} = P_{st31} + \Delta P_{st} \tag{44}$$

$$P_{tot32} = P_{tot31} \frac{P_{tot32}}{P_{tot31}} \tag{45}$$

The total pressure and temperature (assuming constant temperature process) and area at station 32 (diffuser exit) are calculated from equations (41) to (45) by having an initial guess for $C_{P\ ideal}$. Weight flow fraction at station 32 can be recalculated using

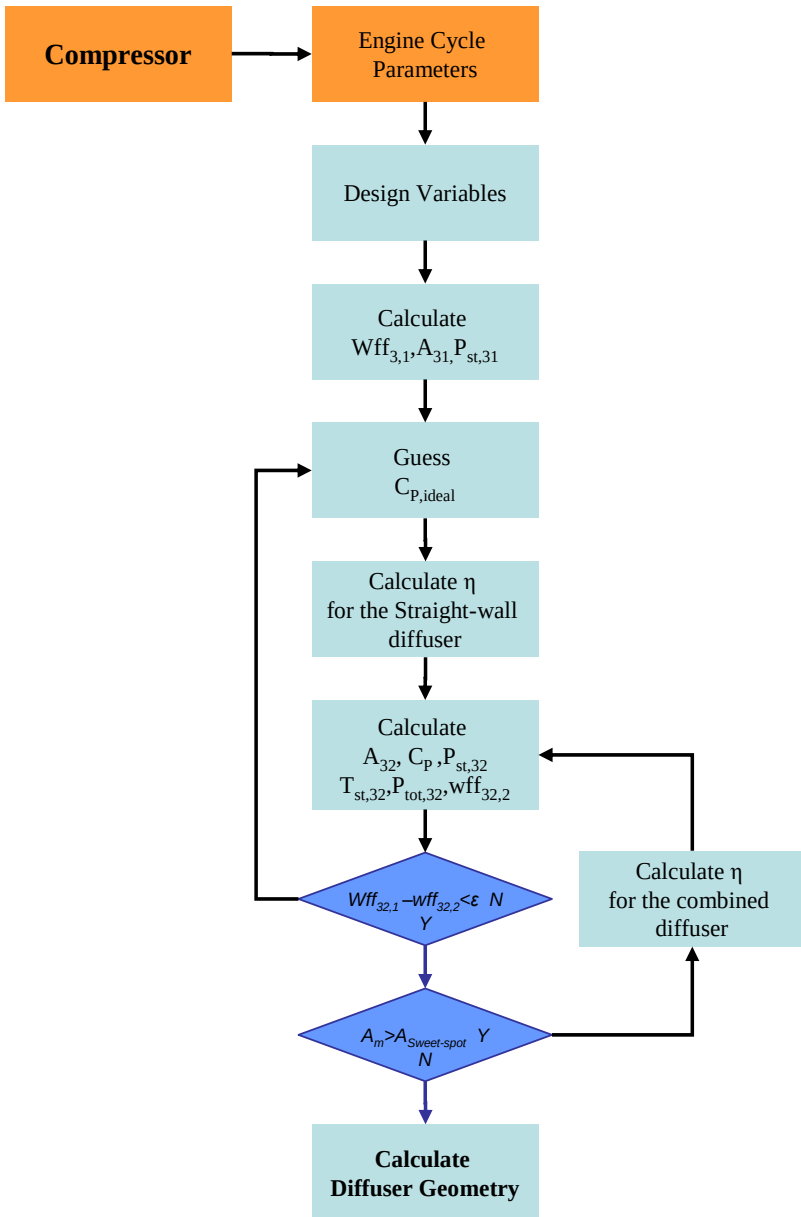

Figure 34 : The flowchart of sizing the diffuser at design condition.

equation (39). If the values of *wff* that are calculated at the beginning and end of the process are within the defined threshold, then the process stops; otherwise, an iteration with new value for $C_{P,ideal}$ is performed until convergence is achieved.

If the calculated value of A_{32} is bigger than the maximum value assigned for the straight-wall diffuser (sweet-spot, A_m), then the diffuser will be considered as a combination of straight-wall and dump diffusers. The following equation is thus used to calculate the total diffuser efficiency [4]:

$$\eta_{total} = \frac{\eta_{straight-wall} AR(1 - AR_m) + 2(AR_m AR - 1)}{AR^2 - 1} \tag{46}$$

where AR is the total diffuser area ratio (A_{32}/A_{31}) and AR_m is the area ratio of the straight-wall section of the diffuser (A_m/A_{31}). Other than the difference in the calculation of diffuser efficiency, the rest of the calculation for the combined diffuser will be the same. At the end, the area at station 31, 32 and at the end of the straight-wall section (between 31 and 32) and mean radii at 31 and 32 will be used to determine the height at each station and length of straight-wall and dump sections. The length of the straight-wall section is obtained from the divergence half angle (θ) and inlet and exit height of the straight-wall section by using a simple trigonometric equation. The length of the Dump section is set to be equal to its height [4].

5.1.3.2 <u>Off-Design Mode</u>

After the diffuser dimensions are determined at the on-design model, the geometrical information can be used to obtain the diffuser's exit flow properties at off-design conditions. Most of the equations that are used in on-design model are used in off-design model too; however, this time the geometry information is known and the flow properties (i.e. Mach number, pressure etc.) are unknowns. The following list shows the inputs to off-design geometry model:

- Geometrical Information (A_{31},A_{32}, divergence angle θ, sweet-spot value, number of splitter plates)
- Off-design inlet Mach number (M_{31})
- Off-design air flow ($\dot{m}_{31}$)
- Off-design inlet total temperature (T_{tot31})
- On-design inlet total pressure (P_{tot31})

The flow properties at station 31 will be calculated using equations (38), (39) and (40). To calculate the pressure loss (P_{t31}-P_{t32}) and total pressure (P_{t32}) at station 32, $P_{dyn,31}$ will be calculated from equation (41). Using that calculation and the pressure recovery coefficient (C_P), the increase in static pressure from station 31 to 32 is determined (Equation (42)). Finally, the value of P_{s32} is determined using equation (44).

Since the value of the pressure loss coefficient (Equation (47)) in the diffuser is assumed to be constant and since it is available from on-design calculations, P_{t32} can be determined from it. Further, using equations (36) and (39), the wff_{32}, $Mach_{32}$ and velocity at station 32 will be calculated.

$$\left(\frac{\Delta P_{tot}}{Q}\right)_{diff} = \frac{P_{tot31} - P_{tot32}}{P_{dyn31}} \tag{47}$$

5.1.4 Snout Model

The snout section is the section between diffuser and the beginning of the combustor core (primary or rich zones). The task of the snout is to streamline the flow coming from the diffuser to the combustor annulus and core section (Figure 35). As will be described later, there is a specific Mach number at the annulus section that maximizes the dilution jet penetration at the first dilution holes. The job of the snout is to take the right amount of the flow required at the annulus section and accelerate it to the optimum Mach number at annulus section entry. In the 1D flow-field model, the snout input and

exits Mach numbers (M_{32} and M_{liner}) are given based on the burner required pressure loss coefficient and required Mach number in the beginning of the burner (combustor core).

5.1.5 Flow Partitioning Model

The flow partitioning model of the 1D flow-field model determines the partition of the airflow in the combustor. At the same time, it assures the conservation of mass, momentum and energy. Since this model is used for two different combustor concepts of SAC or RQL, some of the inputs may be renamed based on their usage.

5.1.5.1 On-Design Mode

At on-design mode, the flow partitioning model determines the fraction of the total airflow that each zone needs to meet the required criteria. It also calculates the bulk temperature of each zone to determine the amount of the cooling flow that is required at on-design condition to keep the temperature of the combustor liner below the liner's material limit. The total flow is divided into two parts, the first part goes to the core section (burner) and it is determined by the required equivalence ratio in the first zone of the burner (which is either the primary zone in the SAC or the rich zone in the RQL combustor). The second part is diverted around the main burner to the annulus section and will be added to the core section through the cooling holes and dilution orifices. The

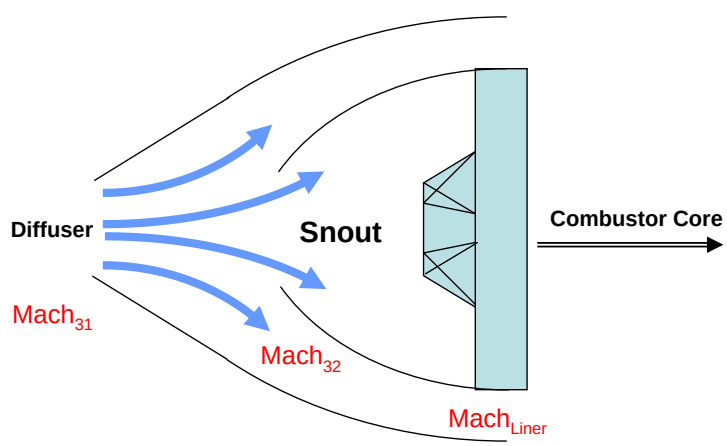

Figure 35: Snout section located between the diffuser and liner

mass flow that goes into each zone is used to size that zone's cross section area or dilution orifices, which are described later in this chapter. For the on-design condition, following input parameters are needed:

- Diffuser inlet and exit total pressures (P_{tot31} and P_{tot32})
- Total pressure loss across the core section/burner (ΔP_{tot})
- Maximum liner temperature ($T_{liner\text{-}max}$)
- On-design fuel flow ($\dot{m}_f$)
- Primary zone efficiency (η_{PZ})
- Secondary zone efficiency (SAC, η_{SZ}) or lean zone efficiency (RQL, η_{LZ})
- Dilution zone efficiency (η_{DZ})
- Cooling mechanism factor (a)
- On-design primary or rich zone Equivalence Ratio (φ_{PZ})
- Diffuser exit Mach number (M_{32})
- Cooling flow temperature ($T_{st\text{-}cool}$)
- Zone's cooling flow fraction

In the above inputs, the total pressure loss across the liner (ΔP_{tot}) is considered constant in the liner. The value is provided from the engine cycle analysis at on-design condition. In the engine cycle analysis, the amount of pressure loss is determined to have adequate cooling in the turbine section. The cooling flow temperature is considered to be the same as the static temperature at station 32 (T_{st32}). The other group of inputs that needs further description is the zone's cooling flow fraction. The zone's cooling flow fraction determines what fraction of the cooling flow will be mixed with hot gases at each section and how much of that goes to the next section. The zone's cooling flow fraction is different than the cooling fraction introduced in the next paragraph which is the ratio of the total cooling flow to total air flow. The zone's cooling flow fraction affects the gas temperature value at the exit of each zone as well as the levels of the emissions.

With the given values for the equivalence ratios at each zone, their combustion efficiencies and the input temperature and pressure, the exit temperature at the end of each zone is determined using the CEA model. Initially the temperatures are calculated without considering the mixed cooling flow; this calculation gives the maximum core gases temperature at each zone which is necessary to calculate the amount of required cooling flow. If the maximum temperature between the zones is higher than the maximum allowable liner temperature ($T_{liner\text{-}max}$), then cooling is required. The cooling flow effectiveness (ϕ_{cool}) and cooling flow fraction (μ_{cool}) is determined from following equations [4]:

$$\phi_{cool} = \frac{T_{zone\ Max} - T_{liner\ Max}}{T_{zone\,max} - T_{st-cool}} \tag{48}$$

$$\mu_{cool} = \frac{\dot{m}_{cool}}{\dot{m}_{tot}} = a\frac{\phi_{cool}}{1-\phi_{cool}} \tag{49}$$

After determining the cooling fraction, the fraction of the cooling flow that is assigned to a particular zone can be considered in temperature calculation of that zone by adding that fraction to the total flow in each zone.

The secondary or zone (in SAC) or lean zone (in RQL) dilution flows going through the dilution orifices should be enough to burn off the unburned fuel or UHC or provide the required temperature profile or equivalence ratio. The rest of the flow enters the dilution zone through dilution zone orifices. The following equations are used to determine the flow fraction of the primary zone (μ_{PZ}), secondary zone (μ_{SZ}) and the dilution zone.

$$\mu_{PZ} = \frac{\dot{m}_{PZ}}{\dot{m}_{tot}} = \frac{\varphi_{tot}}{\varphi_{PZ}} \tag{50}$$

$$\mu_{SZ} = \frac{\dot{m}_{SZ}}{\dot{m}_{tot}} = \frac{\varphi_{tot}}{\varphi_{SZ}} - \frac{\varphi_{tot}}{\varphi_{PZ}} \tag{51}$$

$$\mu_{DZ} = \frac{\dot{m}_{DZ}}{\dot{m}_{tot}} = 1 - \mu_{PZ} - \mu_{SZ} - \mu_{cool} \tag{52}$$

where φ is the equivalence ratio. The above equations can be used in RQL combustor as well where the primary zone is replaced by the rich zone and secondary zone by the lean zone. However, in the RQL combustor the lean zone dilution flow is not added to the lean zone directly but through orifices in the mixing zone.

Additional parameters of interest can also be determined. The first one is the pressure loss coefficient (Equation (53)):

$$\left(\frac{\Delta P_{tot}}{Q}\right)_{burner} = \frac{P_{t40} - P_{t32}}{P_{dyn\ 32}} \tag{53}$$

The pressure dynamic in the denominator of the above equation is based on station 32 (diffuser exit) where the swirler feels the coming flow. The above value should always be bigger than the minimum pressure loss coefficient to ensure that the residence time in the primary zone is greater that the micro-mixing time [4]. The minimum value for the pressure loss coefficient is:

$$\left(\frac{\Delta P_{tot}}{Q}\right)_{burner\ min} = \left(\frac{\dot{m}_{PZ}}{\dot{m}_{tot}}\right)^2 \left(\frac{A_{ref}}{A_{liner}}\right)^2 \tau_{PZ}(2\tau_{PZ} - 1) \tag{54}$$

The pressure loss coefficient is a function of combustor geometry and as long as the geometry is not changing, the value of the coefficient remains constant; therefore for combustor configurations that have fixed geometry, the value of the pressure loss coefficient determined at on-design condition can be used in other operating conditions as prior knowledge to determine the amount of the pressure loss in the burner at off-design conditions. Such an assumption is valid for the SAC. However, if the combustor geometry changes, the value of the coefficient changes too; therefore, a change in the geometry should be considered at each off-design condition to recalculate the coefficient and then determine the new pressure loss in the burner. The derivation of the relation will

be provided in the next section that describes the off-design mode of the flow partitioning model.

The other parameter calculated in the on-design mode of the flow partitioning model is the ratio of the liner to reference area. The reference area is the maximum area in the combustor which is set to be the casing area at the beginning of the burner (end of the snout).The liner area is at the beginning of the burner, which is the beginning of the primary or rich zone. Reference [4] suggests the following equation in order to maximize the ratio of dilution jet penetration per jet diameter:

$$\left(\frac{A_{Liner}}{A_{Casing}}\right)_{optimum} = 1 - \left(\frac{\dot{m}_{PZ}}{\dot{m}_{tot}}\right)^{3/2} \left(\frac{\Delta P_{tot}}{Q}\right)_{burner}^{-1/3} \tag{55}$$

At the end, the flow properties at the combustor exit (station 40) will be calculated using flow properties relations.

5.1.5.2 <u>Off-Design Mode</u>

This mode of the flow partitioning model is based on the combustor components sizes calculated in on-design condition; therefore, this part of the flow partitioning model is executed after the on-design part of the sub-section 5.1.6, which provides the sizes of the combustor elements. The previous sub-section explains that if the geometry of the combustor is not constant then its pressure loss coefficient is not constant either. However, this coefficient can be calculated if enough information is available about the combustor geometry and its changes. Equation (58) shows the relation between the combustor total airflow and the combustor geometry.

$$\dot{m}_{tot} = \sum_{i=1}^{n} \rho_{32} V_i c_{di} A_i = \sum_{i=1}^{n} \rho \sqrt{\frac{2\Delta P_t}{\rho_{32}}}_{t} c_d A_i = \sum_{i=1}^{n} \sqrt{2\rho_{32}.\Delta P_t}\, c_d A_i = \sqrt{2\rho_{32}.\Delta P_t} \sum_{i=1}^{n} c_{di} A_i \tag{56}$$

where c_d is the flow coefficient and ρ is the density at station 32, assumed to be the same for all the dilution jets, and where A_i is the flow passage area of the ith flow. Also from the mass conservation:

$$\dot{m}_{tot} = \rho_{32} V_{32} A_{32} \tag{57}$$

Combining equations (53), (56) and (57) yields:

$$\left(\frac{\Delta P_{tot}}{Q}\right)_{burner} = \left(\frac{A_{32}}{\sum_{i=1}^{n} c_{di} A_i}\right)^2 \tag{58}$$

Therefore, if any of the flow passage areas (such as the swirler area in the RQL combustion) changes at off-design condition, the new pressure loss coefficient can be determined from the above equations. Finally, by knowing the dynamic pressure at station 32 from the diffuser off-design calculation, the burner pressure loss at off-design condition can be obtained using the pressure loss coefficient.

The amount of the mass flow that goes through different passages (primary zone, cooling holes and dilution orifices) is given by equation (59):

$$\dot{m} = c_d \rho_{32} V_j A = c_d \frac{A}{A_{32}} \sqrt{\left(\frac{\Delta P_{tot}}{Q}\right)_{burner}} \tag{59}$$

For the dilution holes, the above equation can be written in the following form:

$$\frac{\dot{m}_{dil}}{\dot{m}_{tot}} = \frac{n_{orifice} \pi d_j^2 V_j}{4 A_{32} V_{32}} \tag{60}$$

where n is the number of dilution holes and d_j and V_j are the dilution jet diameter and velocity, determined in the on-design mode of the zone models as will be shown later.

Finally, knowing the airflow distribution and off-design fuel flow, the temperature at each zone is determined using the CEA analysis. Initially the cooling flow distribution is not considered in the zones to determine the maximum temperature. These temperatures are used to determine the amount of the cooling flow that is required at the given condition using equations (48) and (49). The obtained values will be compared against the value that is obtained based on equation (59) to assure that the adequate amount of cooling is available at the given off-design condition. Finally after cooling

flow calculation, the exit temperature from each zone is calculated so as to account for the fraction of the cooling flow that is considered to be mixed with the core flow. For the RQL combustor, the addition of the cooling flow to the rich mixture pushes the mixture equivalence ratio closer to the stoichiometric value and increases the mixture's temperature. For the SAC combustor, the mixture goes farther away from the stoichiometric value and the exit gas temperature will be lower.

5.1.6 Combustor Zones

The combustor zones are designed at on-design condition by knowing the amount of the air and fuel flow that goes into them and by setting the design variables. At off-design conditions, the size of each zone is used to determine the Mach number, velocity, static pressure and temperature at the end of each zone. Most of the off-design calculations of the combustor zones are performed in the off-design mode of the flow partitioning model.

In this section, the zones of SAC and RQL combustors are introduced. Since the task of the primary zone in SAC and the rich zone in RQL concepts are essentially the same, they are described under the title of primary zone. Also due to similarity, secondary and dilution zones are described together. Finally the RQL specific components of mixing zone and lean zone are described at the end.

In the on-design mode, the flow fractions determined in the flow partitioning model are used to determine the cross sectional area of the core section and the annulus of the combustor, their length and the size and number of dilution orifices. The dimensions of the combustor elements will be used to calculate their volume. In off-design mode, Mach number, velocity, static pressure and temperature are determined using the flow properties relations.

5.1.6.1 Primary Zone

The task of the primary zone is to anchor the flame and provide a good mixing between fuel and air. The main feature of the primary zone is its swirler. The swirler creates a recirculation bubble in the primary zone by imparting a rotation to the (Figure 36). Due to this action, the total pressure of the flow will be dropped too.

5.1.6.1.1 On-Design Mode

Since the amount of the pressure drop at on-design condition is provided from the engine cycle analysis, the swirler is sized to provide the given amount of the pressure drop. The following equation is used to determine the physical area of the swirler [4, 7]:

$$A_{SW} = \sqrt{\frac{K_{sw}}{Cos(\alpha_{sw})^2} \frac{1}{\frac{2\rho_{32}\Delta P_{burner}}{\dot{m}_{sw}} + \left(\frac{n_{inj}}{A_{liner}}\right)^2}} \tag{61}$$

where:

- A_{sw}: swirler flow passage area
- K_{sw}: swirler discharge parameter (1-3)

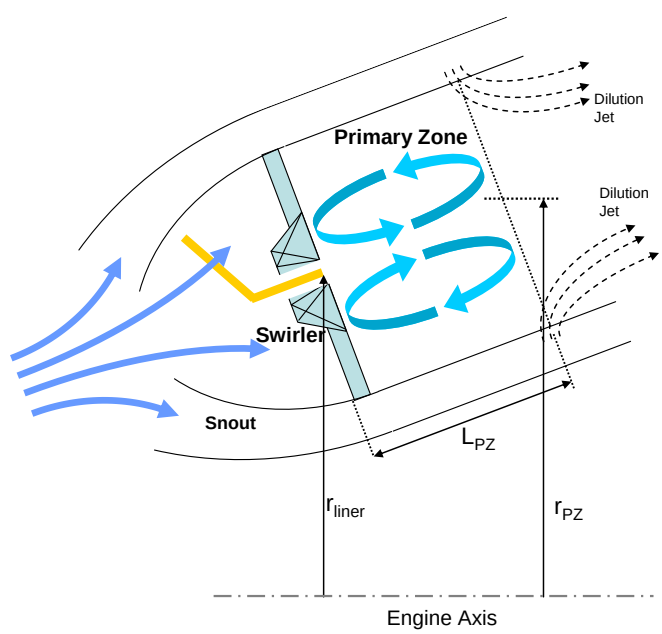

Figure 36: Primary zone and swirler

- α_{sw}: swirler vane angle (50-65 degrees)
- n_{inj}: combustor injector number
- A_{liner}: Liner area after the swirler
- $\dot{m}_{sw}$: Air flow going through the swirler

The amount of the air that goes through the swirler is:

$$\dot{m}_{sw} = \frac{\dot{m}_{PZ}\,(1 - \frac{\dot{m}_{inj}}{\dot{m}_{fuel}})}{n_{inj}} \tag{62}$$

The $\frac{\dot{m}_{inj}}{\dot{m}_{fuel}}$ is the ratio of the air that goes through the injector (in air-blast and air-assisted type injectors) and it is zero for plain or pressure swirl injectors.

If the value of the inner radius of the swirler (r_{hub}) is known from the size of the injector or atomizer, then the outer radius of the swirler (r_{tip}) can be determined from geometrical relations. Equations (63) and (64) provide the swirl number value and the length of the recirculation zone in the primary zone, which is defined as L_{PZ} in Figure 36 [4, 7, 51].

$$SW = \frac{2}{3} Tan(\alpha_{sw}) \frac{1 - \left(\frac{r_{hub}}{r_{tip}}\right)^3}{1 - \left(\frac{r_{hub}}{r_{tip}}\right)^2} \tag{63}$$

$$L_{PZ} = 2 r_{tip} SW \tag{64}$$

Form the flow property relation, the cross section area at the exit of the primary zone is determined. The cross section area can be sized for fixed Mach number or fixed cross section.

In summary, the following design parameters in the primary zone model are provided by the user based on the available knowledge and commonly used values:

- swirler vane angle (α_{sw})
- swirler discharge parameter (K_{sw})
- Number of injectors in the combustor (n_{inj})
- swirler hub radius (r_{hub})
- Ratio of the injector air flow to fuel flow $\frac{\dot{m}_{inj}}{\dot{m}_{fuel}}$

The other parameters required by the primary zone model such as total pressure loss, temperature and pressure in the zone are provided by diffuser, snout or flow partitioning models.

5.1.6.1.2 Off-Design Mode

In the off-design mode of the primary zone model, Mach number, velocity, static pressure and temperature are determined using the flow property relations. The mass flow that goes through the swirler in off-design condition can be obtained by:

$$\dot{m}_{swirler} = \sqrt{\frac{2\rho\Delta P_{tot}}{K_{sw}\left(\sec(\alpha_{sw})/\alpha A_{sw}\right)^2 - \frac{n_{inj}}{A_{liner}^2}}} \tag{65}$$

The parameter α in the above equation is the swirler area coefficient for the variable geometry swirler (in RQL combustor) that changes the area of the swirler at Off-design conditions. Originally, this equation is used in the off-design mode of the flow partitioning method, but due to its relevance to primary zone, it is mentioned in this sub-section.

5.1.6.2 <u>Secondary and Dilution Zones</u>

The main feature of the secondary and dilution zones that are present in either the SAC or RQL combustors are the dilution jets that penetrate the main core flow from the dilution orifices. The pressure difference between the annulus and the core section is the main driver of the annulus flow to the core section in form of the dilution jets (Figure 37).

5.1.6.2.1 On-Design Mode

In on-design mode, the model sizes the dilution orifices' diameter and number based on the required penetration depth to jet diameter ratio. The exit cross section of the zone is calculated from the given exit zone temperature and pressure using the flow properties values. The cross section area can be sized for fixed Mach number or fixed cross section.

The length of the zone is determined based on the given length to height ratio of the zone. The exact determination of the length is outside of scope of this research since it requires the exact modeling of the mixing process and detailed flow modeling using criteria such as temperature and flow profile. Based on the available information in the public domain and reports the length ratio is considered between 0.5 and 1 [4, 18, 20, 25].

Sizing the orifices is based on the maximum penetration depth to dilution jet's

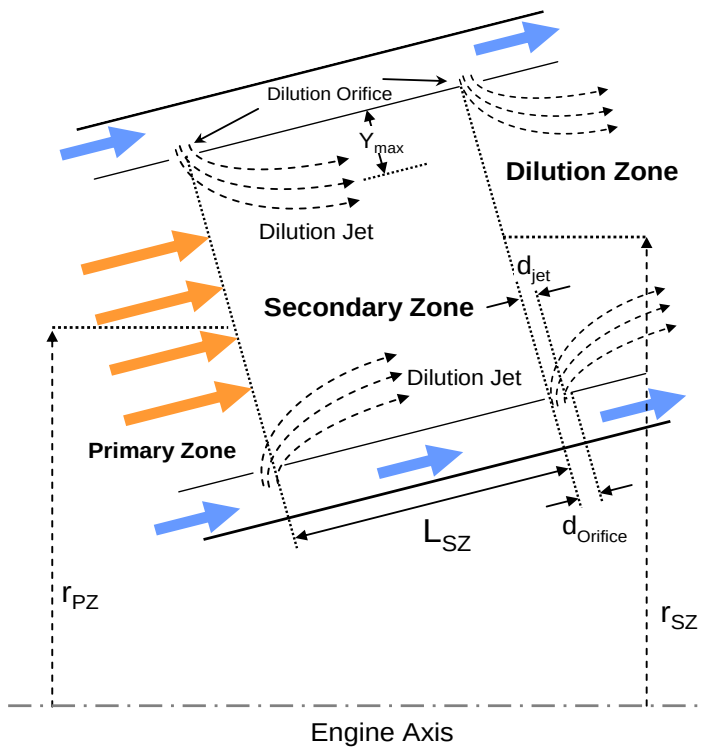

Figure 37: Secondary zone and its main parameters and features

diameter artio, $\frac{Y_{\max}}{d_{jet}}$ which is [7, 128]:

$$\frac{Y_{\max}}{d_j} = 1.25\sqrt{\frac{q_j}{q_{core}}}\frac{\dot{m}_{core}}{\dot{m}_{core} + \dot{m}_{jet}} \tag{66}$$

where:

q_j: Momentum of the jet flow

q_{core}: Momentum of the liner (core) flow

d_j: Jet diameter

Y_{max}: Maximum penetration

The jet and core mass flow values are available from the flow partitioning model. To find the jet to liner flow momentum ratio $\frac{q_j}{q_{core}}$, the following equation is used:

$$\frac{q_j}{q_{core}} = \frac{\left(\frac{\Delta P_{tot}}{Q}\right)_{burner}}{\frac{T_{core}}{T_{32}}\left(\frac{\dot{m}_{core}}{\dot{m}_{tot}}\frac{A_{case}}{A_{Liner}}\right)^2} \tag{67}$$

The value of T_{core} is the value of temperature at the end of the previous zone. The casing area value (A_{case}) is also obtained from the equation (55). To obtain the penetration depth, jet diameter and consequently the size and number of the orifices, the design value of $\frac{Y_{\max}}{H_{liner}}$ needs to be provided. This value is based on the design criteria of how much penetration in the core section is required and is provided by the user. The H_{liner} is the liner height at the beginning of the zone (secondary or dilution zone) which can be obtained from the cross section area and the combustion configuration (annular or tubular). The detail of calculating the height of the core section at different stations based on the combustor configuration is given in the next section.

The dilution jet diameter value is obtained as follows:

$$d_j = \left(\frac{Y_{max}}{H_{liner}}\right)\left(\frac{Y_{max}}{d_j}\right)^{-1} H_{liner} \tag{68}$$

Since the dilution jet area is an effective area that is smaller than the physical area by factor of the flow coefficient c_d, the dilution orifice diameter is:

$$d_{orifice} = \frac{d_j}{\sqrt{c_d}} \tag{69}$$

The value of c_d depends on the orifices shape and flow condition, but as a first approximate, it is considered constant [4] and its value is considered between 0.6-0.65 [129-130]. The number of dilution orifices is obtained by dividing the total flow that goes through the orifices (secondary or dilution flow) by the flow that goes through a single orifice. Simplifying the relation yields the following:

$$n_{orifices} = \frac{\dot{m}_{dilution}}{\dot{m}_{tot}}\frac{\dot{m}_{tot}}{\dot{m}_{jet}} = \frac{\dot{m}_{dilution}}{\dot{m}_{tot}}\frac{4A_{32}}{\pi d_j^2}\frac{V_{32}}{V_j} \tag{70}$$

For very slow flow inside the combustor, it is assumed that the total pressures drop is the same as the difference between the static pressures between annulus and the liner flow, and the density in the annulus section is almost constant. Therefore, the jet velocity can be obtained from the following relation:

$$V_j = \sqrt{\frac{\Delta P_{tot}}{\frac{1}{2}\rho_{32}}} = V_{32}\sqrt{\frac{\Delta P_{tot}}{\frac{1}{2}\rho_{32}V_{32}^2}} = V_{32}\sqrt{\left(\frac{\Delta P_{tot}}{Q}\right)_{burner}} \tag{71}$$

Finally, to determine the penetration angle of the jet, the following equation is used [7, 131].

$$Sin\theta = \sqrt{1-\frac{q_{ann}}{q_j}} = \frac{\left[\dfrac{(1-\dot{m}_{core})/\dot{m}_{tot}}{\left(1-A_{liner}/A_{casing}\right)}\right]^2}{\left(\dfrac{\Delta P_t}{Q}\right)_{burner}} \tag{72}$$

where q_{ann} and q_j are annulus and jet flow momentums and penetration angle θ is measured from the combustor axis.

5.1.6.2.2 Off-Design Mode

In off-design mode, the amount of the flow that goes through the orifices is determined using the known values of the orifices size and number. I addition, in this mode, the penetration ratio of dilution jets and their penetration angle are determined. Since it is assumed that flow coefficient c_d is constant, the jet diameter is the same for all conditions. By using equations (66), (67) and (68) the penetration depth to liner height ratio ($\frac{Y_{\max}}{H_{liner}}$) will be obtained. The penetration angle is obtained from equation (72). The Mach number, velocity, static temperature and pressures are obtained using the flow property relations.

5.1.6.3 Mixing Zone

The mixing zone is a component that is specially designed for the RQL combustor in which the annulus air should mix quickly with the fuel rich hot gases coming out from the rich zone section. Some similarities exist between this component and secondary zone and dilution zone components; however, the mixing process in the mixing zone is required not only to be faster but also to have a higher quality. Due to these requirements, the design process of the holes in the mixing zone is different. Due to the different application, the dilution orifices in the mixing zone are called quenching orifices.

As described in Chapter 4, different mixing methods in the mixing zone include: 1) the Wall-Jet, 2) the reduced scale quenching-Convoluted Liner and, 3) the reduced scale quenching-Quench Vanes. This research is limited to the use of the Wall-Jet mixing method due to the geometrical complexity of the other concepts. Although the flow regime of the Wall-Jet and RSQ concepts are not the same, they can be described by the

same theory. The formulas to model them; however, will not be the same. The method to design the orifices in the Wall-Jet concept is known as NASA method which is described here.

5.1.6.3.1 On-Design Mode

In the Wall-Jet method, the number of quench orifices is optimized for the best mixing. Holdeman et al. and others [15, 79-80, 119, 121] suggested the following equations for the optimum number of quenching orifices in the tubular (equation 73) and annular (equation (74)) combustor configurations:

$$n = \frac{\pi\sqrt{2J}}{C} \tag{73}$$

$$\frac{S}{H} = \frac{C}{\sqrt{J}} \tag{74}$$

where n is the optimum number of orifices, J is the jet-to-core flow momentum ratio and C is the empirical constant, which is 2.5 for tubular configuration, 1.25 for in-line orifices in annular configuration and 5 for staggered orifices in annular configuration. S is the optimum distance between orifices in annular configuration and H is the mixing zone height. The orifices are circular. The momentum flux ratio is determined from equation (67). The rest of the mixing zone calculation is the same as the secondary and dilution zone calculations. With the known value for the number of orifices, the jet diameter is obtained from equations (69), (70) and (71). Then the penetration ratio ($\frac{Y_{\max}}{H_{liner}}$) and penetration angle are obtained from equations (66), (67), (68) and (72).

The inlet cross section area of the mixing zone is determined by multiplying the exit cross section of the previous zone (rich zone) by a coefficient. The coefficient is called mixing zone to rich zone area ratio. As the coefficient becomes smaller, the mixing quality enhances due to the smaller size of the energy containing eddies; however, the casing area at the mixing zone remains the same as at the exit of the rich zone. The exit

area of the mixing zone is determined based on the fixed Mach number or fixed area criteria. The length is determined based on the ratio of the given length to height ratio.

There is an exception in determining the exit temperature based on the equivalence ratio in the mixing zone. The assumption in the 1D-flow model is that mixing of the quenching jets with the hot gases coming from the rich zone is so fast that no reaction occurs until the mixtures goes to the lean zone. (This assumption will be removed in the CRN model). Therefore for the mixing zone, instead of using the CEA analysis to calculate its exit temperature, a simple sensible enthalpy balance equation will be used to determine the final temperature of the non-reacting mixture using the following equation:

$$T_{t\,MZ} = \frac{\dot{m}_{MZ} c_P T_{32} + \dot{m}_{RZ} c_P T_{t\,RZ}}{\dot{m}_{MZ} + \dot{m}_{RZ}} \tag{75}$$

5.1.6.3.2 Off-Design Mode

Similar to the secondary and dilution models, at this mode the penetration ratio and angle as well as static temperature and pressure at the end of the zone are determined.

5.1.6.4 Lean Zone

The task of the lean zone is to burn (or burn off) the lean mixture coming from the mixing zone. After the mixing zone, the lean zone area will be increased by the same ratio that the rich zone area is decreased (mixing to rich zone area ratio). The bigger area slows down the flow providing enough time for the combustion to take place and be completed. Other than the cooling flow that may mix with the core section, there is no introduction of additional flow in the lean zone. The lean zone can be considered as a long tube with a calm flow after the mixing zone.

The lean zone model is very simple. Since its total temperature (like other zones) is calculated in the flow partitioning section, the only remaining calculations in on-design

mode are: 1) to determine the exit area based on the temperature, pressure and fixed Mach or area criteria and, 2) to determine the length from the length to height ratio.

In off-design mode, the model calculates the flow properties using the flow properties equations.

5.1.6.5 Transition Zone

In RQL concepts, there could be a significant reduction in the cross section area from the rich zone to mixing zone and increase from the mixing zone to the lean zone. To smooth out this transition, converging or diverging transition zones are used between the mixing zone and neighboring zones (Figure 38). In this thesis, it is considered that these zones increase the residence time of the rich zone or the lean zone; therefore, the volume of the transition zone is added to the rich or lean zone volume. The equation to calculate the length of the transition zone depends on the combustor configuration. If the cross section area ratio of the mixing zone to the rich zone is given for the tubular configuration, the length of the zone is defined as:

$$L_{TR} = H_{RZ} \frac{1 - \sqrt{A_{MZ} / A_{RZ}}}{2Tan\beta} \tag{76}$$

where L_{TR} is the length of the transition zone. The expression inside the square root is the cross section area ratio of the mixing to rich zone, where β is the divergence or convergence angle of the transition zone.

For annular configuration, the transition zone length is the positive solution of a quadratic equation multiplied by the rich zone height:

$$L_{TR} = H_{RZ} \frac{-b \pm \sqrt{b^2 - 4ac}}{2a} \tag{77}$$

where a,b and c are defined as:

$$a = \frac{2H_{RZ}}{r_{m\ RZ}} Sin(\alpha) Tan(\beta)$$

$$b = 2Tan(\beta) - \frac{H_{RZ}}{r_{m\ RZ}} Sin(\alpha) \tag{78}$$

$$c = \frac{A_{MZ}}{A_{RZ}} - 1$$

5.1.7 Combustor Configuration and Orientation

The annular and tubular configurations are considered in the 1D flow-field model. Depending on the selected configuration, some of the equations (e.g. in mixing zone model) should be replace by others. Also the height of the zones depends on the combustor configuration. Equation (79) is used to determine the height of a zone when the configuration is annular while equation (80) is used for tubular configuration.

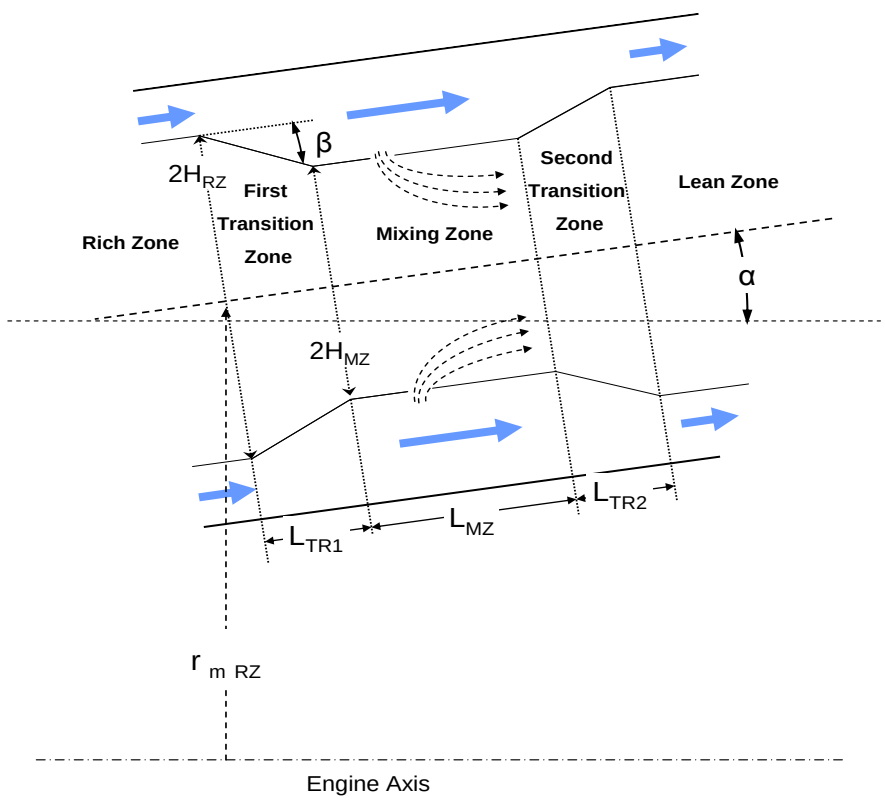

Figure 38: Transition zones and their main parameters and features

$$H_{annular} = \frac{A}{2\pi\, r_{mean}} \tag{79}$$

$$H_{tubular} = \sqrt{\frac{4A}{\pi\, n_{inj}}} \tag{80}$$

The height of the zones in the annular configuration depends on their distance from engine centerline (mean radius, r_m). In the tubular configuration, as long as all the tubes can be fitted in a given perimeter, they are independent from the mean radius but the height is dependent on the number of tubes (injectors, n_{inj}). This difference has an implication when the length of the zones and jet penetration ratios are calculated since they are defined based on the height of the zone. Thus, the height of the zones and their penetration ratios are different for these two configurations (although the difference is not large).

The other consideration in the 1D flow-field model is the orientation of the combustor with respect to the engine centerline. Often the compressor and turbine requirements result in a different inlet and exit radii for combustor. Although the issue is

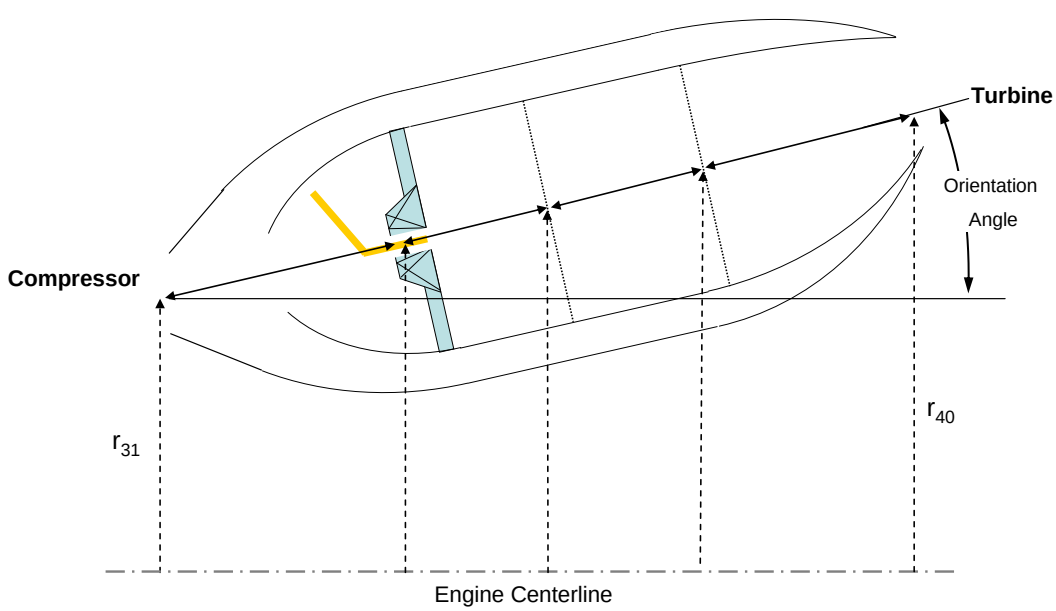

Figure 39: Combustor with different inlet and exit mean radii

simple for tubular combustor (as its values are independent of the mean radius), some complications arise in geometrical calculation of the annular combustor. To keep the cross-section area fixed, the height of the section increases or decreases as the combustor moves away from or toward the centerline. This change in the height directly affects the length of the zones which results in a different combustor length. The combustor length is not a priori knowledge; therefore, the orientation angle (Figure 39) and the mean radii of different zones are not known either. Iteration is required to address the problem. In the 1D flow-field model, the whole design process starts with an initial guess for each zone's mean radius and also for orientation angle. The iteration continues until the whole process converges to a final value where all the zones have the same orientation angle as the combustor and the last zone's mean radius is the same as the turbine inlet mean radius.

In the model the diffuser and the last zones are always considered to be annular to match to compressor exit or turbine inlet.

5.1.8 Volume of Combustor Zones

The volumes of the zones are required in the chemical reactor's network (CRN) model for finite-rate chemistry calculation. Just as described in the previous sub-section, the calculation of the volume is straightforward for the tubular configuration: the volume of a cylinder (same inlet and exit area) or an incomplete cone (different inlet and exit area) is multiplied by the number of the modules (tubes/cans).

However, for the annular configuration, the geometry becomes complex and the calculation of the zone is not simple anymore. The shape of a zone in the annular configuration is a combination of incomplete cones (front face, rear face, outer face and inner face) as seen in Figure 40. The addition and subtraction of these incomplete volumes will give the volume of the zone. If there is a dilution jet with a penetration angle, volume will be added (if the dilution jet at the end of the zone) or subtracted (if the

dilution jet at the beginning of the zone) from the zone volume. A MATLAB code is written to calculate the volume of an annular zone (Appendix B) with the following input:

- Inlet and exit mean radii
- Inlet and exit heights
- Zone length
- Inlet and exit penetration angle
- Injectors number
- Combustor orientation angle
- Configuration

5.1.9 Annulus Zone

As the last part in the 1D flow-field model, an additional model is created to determine the area between the liner and casing (annulus) and to find annulus height, Mach number, static pressure and temperature at various axial locations. The area can be determined based on the fixed area criteria (same as the area in the previous section) or

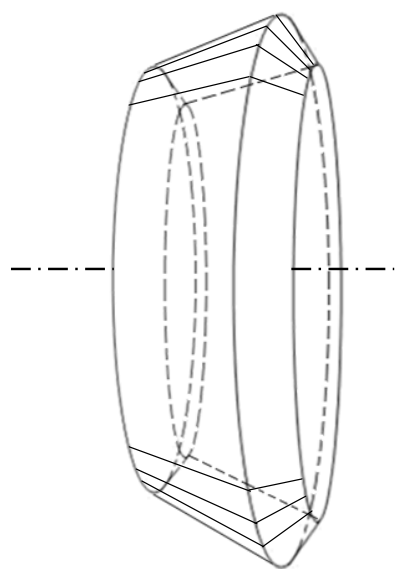

Figure 40: Zone volume in annular combustor configuration as a combination of incomplete cones

fixed Mach number (same Mach number as the Mach number in the previous section).

The differences of heights at the outer annulus and inner annulus in the annular configuration are considered to have the equal amount of annulus flow going into outer and inner annulus sections. Since the inner annulus is closer to the engine centerline, its height must be bigger than the outer annulus to have the same area and receive the same amount of the airflow.

5.1.10 Combustor 2D View Model

Finally after the size of the annulus and zones, their height, length and mean radii are determined, this information is used to generate a 2D view of the combustor. It also shows the location and size of the dilution orifices and geometry features.

5.2 Droplet Evaporation and Diffusion Burning Model

The following section suggests a method to model the droplet evaporation and diffusion burning (DEDB) in the combustor. The existence of the droplet burning and the diffusion flame has significant effect on the emission levels. While high temperature diffusion flames can burn off carbon monoxide (CO) and unburned hydrocarbons (UHC), they will simultaneously enhance one of the NO_x formation mechanisms and result in a higher level of NO_x emissions [53].

Droplet burning in the combustor is the major source of NO_x emissions and it is important to find a way to consider it in the emissions prediction model. The presence of fuel droplets in the flame zone creates a diffusion flame in addition to the premixed flame. The diffusion flame results in a local high temperature mixture and a high NO_x formation [53]. A complete and detailed model for droplet evaporation and burning is computationally intensive and time consuming; however, for the current task, a fast model is required to determine the quantity of evaporated fuel and the effect of fuel

droplets on the species concentrations. In this thesis, the assumption is that there is a diffusion flame around each droplet and that they are separated from the premixed flame. This assumption greatly simplifies the model. Another assumption is that the droplets coming from the atomizer will be in pure evaporation phase before the ignition time which is given by equation (81) [46-47, 109].

$$\tau_{ignition} = 10^{-4} \frac{e^{\frac{21000}{RT}}}{\phi} \tag{81}$$

where φ is the mixture equivalence ratio, T in the exponent term is temperature (K) which is assumed to be the same as a bulk temperature in the primary zone. Since the all the ignition time models that are available are for lean to stoichiometric mixtures [132], the above equation for rich mixtures should be used with caution. The above equation provides a continuous decrease in ignition time beyond stoichiometric ratio which cannot be right and it is modified to have the same rate of decrease after the stoichiometric ratio as before it. The next step is to calculate the droplet sizes and determine the percentage of them that are evaporated before they reach the ignition time. After that, the droplets ignite and burn at the stoichiometric ratio which is the characteristic of the diffusion flame.

Often the droplet model for various injectors is given in the form of the Sauter mean diameter [7, 46]. The SMD models are a function of fuel physical properties, injector type, geometry and fuel flow. For brevity and lack of additional data, in this research SMD model of the pressure-swirl atomizer will be used which is given below [7].

$$SMD = 2.25\sigma_L^{0.25}\mu_L^{0.25}\dot{m}_L^{0.25}\Delta P_L^{-0.5}\rho_A^{-0.25} \tag{82}$$

where :

σ_L: Fuel (Jet-A) surface tension (N/m)

μ_L: Fuel (Jet-A) dynamic (absolute) viscosity (Poise, Pa.s)

$\dot{m}_L$: Fuel flow rate (kg/s)

ΔP_L: Liquid pressure loss across atomizer (Pa)

ρ_A: Gas density (kg/m3)

The value of ΔP_L is defined based on the injector Flow Number (FN) which is a unique and fixed number for each injector and is defined as:

$$FN = \frac{\dot{m}_l}{\sqrt{\Delta P_L \rho_L}} \tag{83}$$

The combination of equations (84) and (83) would provide the SMD for the given fuel flow (power setting).

In reality, an injector produces a range of droplet diameters, which is represented by SMD. To better capture the droplet evaporation, this thesis considers the droplet size distribution. It is a common practice to model the droplet distribution with the Weibull distribution. In the combustion community, this distribution is more known as the Rosin-Rammler equation [133]:

$$Q = 1 - e^{-\left(\frac{D}{X}\right)^q} \tag{84}$$

where Q is the fraction of the total volume of the droplets whose size is less than D. Parameters X and q are scale and shape factors of the distribution. The parameter q is the measure of the droplet spread with value between 1.8 and 3 and X the size value at which 63.2% droplet diameters are smaller than that.

If the SMD of a distribution is known from the injector model, by assuming a value for q, the following equation gives the value of mass median diameter (MMD) [7]. The MMD is a diameter where Q is 0.5.

$$MMD = SMD \times 0.6931^{\frac{1}{q}} . \Gamma\left(1 - \frac{1}{q}\right) \tag{85}$$

where Γ is the Gamma function. By solving equation (84) when Q is 0.5 and D is set equal to MMD, the value for X can be obtained, revealing the droplet size distribution.

Figure 41 shows an example of the Rosin-Rammler distribution for different shape factor (q) values.

To determine the vaporized fraction for a droplet with a specified diameter before it ignites, the new distribution of droplet size at the end of ignition delay time will be obtained. This calculation can then be integrated to obtain the percentage of the droplets' volume that is vaporized and the percentage that has been left in liquid form.

The final size of a droplet at end of the ignition delay time with a given initial diameter is given by the following equation [68, 134]:

$$\frac{dD}{dt} = -4\frac{k_g \, ln(1+B_M)}{\rho_f c_{Pg} D} \tag{86}$$

where:

B_M :The Spalding number controlled by mass transfer

k_g: Gas conductivity

ρ_f: Fuel density

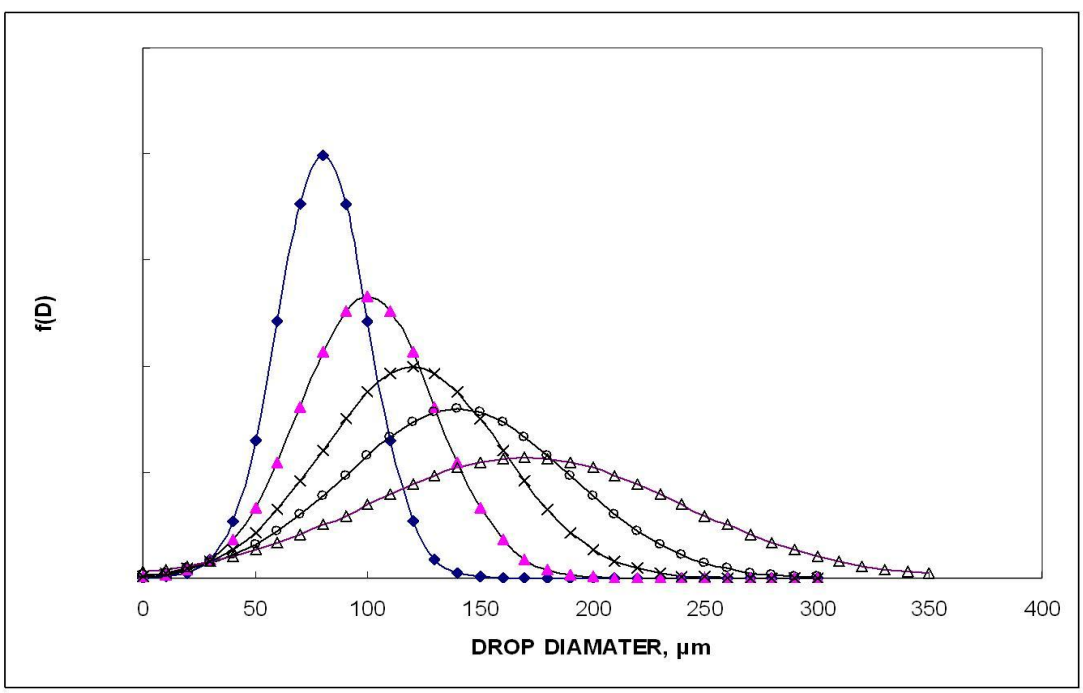

Figure 41: Droplet size distribution

c_{pg}: Gas specific heat at constant pressure

The convection effect is also considered in the model using the droplet's Reynolds and Prandtl numbers using the following equation which is multiplied to the droplet's vaporization rate [135-136]:

$$C_{convection} = 1 + 0.3\,\mathrm{Re}_D^{0.5}\,\mathrm{Pr}_g^{0.33} \tag{87}$$

The Reynolds number is based on the droplet diameter and the turbulent intensity fluctuation U_{turb}.

The reference [134] provides the details of this process, including the right temperature and composition to be used to determine k_g , c_{pg} , Reynolds and Prantl numbers.

The rate of change of droplet surface temperature is given by:

$$\frac{dT_s}{dt} = \frac{\dot{m}_l h_{fg}\left(B_T / B_M - 1 \right)}{c_{Pf}\, m_D} \tag{88}$$

where:

B_T: The Spalding number controlled by heat transfer

h_{fg}: Fuel latent heat

m_D: Fuel droplet mass

c_{pf}: Fuel specific heat at constant pressure

The Spalding numbers B_T and B_M definitions are:

$$B_M = \frac{Y_{fS}}{1 - Y_{fS}} \tag{89}$$

$$B_T = c_{Pg} \frac{T_\infty - T_s}{h_{fg}} \tag{90}$$

where $Y_{f,S}$ is the droplet vapor mass fraction at the surface. T_∞ in this work is defined as the temperature of the air flow coming from the compressor.

The physical properties of fuel and air mixtures are obtained from aviation fuel properties handbook [137-139] and those that are not available are approximated by n-dodecane ($C_{12}H_{26}$) fuel. A detailed description of the process is provided in Appendix A.

Using initial surface temperature as the fuel temperature and initial diameter and gas temperature and pressure, the differential equations (86) and (88) can be solved.

The above method is used to obtain the droplet size after a given ignition delay time for a range of droplet sizes. The method provides a history of surface temperature (T_s), droplet diameter squared (D^2) and evaporation constant (k) during the evaporation as well as their value at the time of ignition (Figure 42), which is used to calculate a new droplet size distribution after the evaporation (Figure 43). Then the new distribution will be integrated to find the remaining droplet in liquid form as follows:

$$\frac{\dot{m}_{f\,liq}}{\dot{m}_{f\,tot}} = \frac{V_{liq}}{V_{tot}} = 1 - \int_0^{D_{max}} \frac{Q}{X}\left(\frac{D}{X}\right)^{q-1} e^{-\left(\frac{D}{X}\right)^q} \left(1 - \left(\frac{D_f}{D}\right)^3\right) dD \tag{91}$$

$$evaporation\ degree = \frac{\dot{m}_{f\,vapor}}{\dot{m}_{f\,tot}}$$

where D_{max} is set to be a very large number where initial Q value is 1. A MATLAB

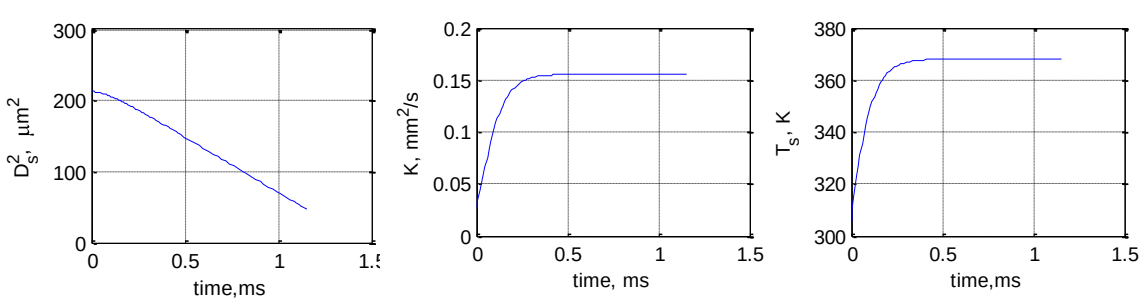

Figure 42: Time variation of three droplet parameters

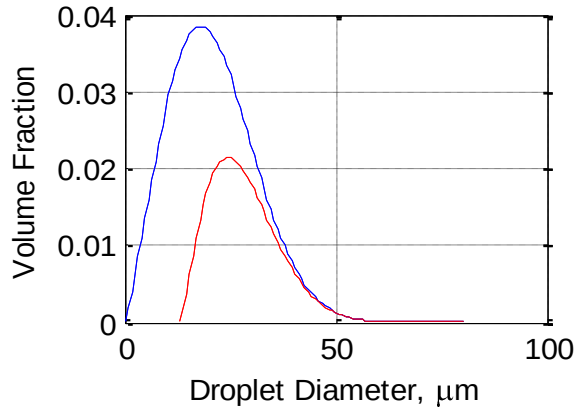

Figure 43: Droplet size distribution at the beginning (blue) and the end (red) of the ignition delay time

code is written to solve the equations and determine the percentage of the vaporized and liquid fuel (Appendix B).

An adequate amount of air will be assigned to the part of the fuel flow remained in liquid form to make the ratio stoichiometric to resemble the diffusion flame. The rest of the airflow and vaporized fuel flow is assumed to be pre-mixed before ignition. The pre-mixed mixture is not uniform in the combustor and this non-uniformity should be considered because it has a potential significant effect on flame temperature and pollutant levels.

5.3 Non-Uniform Mixture Model

A Non-Uniform Mixture (NUM) model is proposed in this section to compensate for the non-uniformity and equivalence ratio dispersion that exist in the combustor. To that end the (Heywood) mixing parameter *S*, also known as the unmixedness degree, is used. The unmixedness degree in equation (92) defines the distribution of the flow fraction over the interval of equivalence ratio [9, 140] and is equivalent to the coefficient of variation in probability.

$$S = \frac{\sigma}{\overline{\varphi}} \tag{92}$$

where:

σ: Standard deviation

$\overline{\varphi}$: Mean equivalence ratio

The unmixedness degree is not a spatial distribution; rather it shows the degree of non-uniformity and dispersion of the equivalence ratio in the combustor in a dimensionless number. The value of unmixedness degree is higher for less uniform mixtures. As shown in Figure 44, there is a one to one correlation between the value of the unmixedness degree and the given mean equivalence ratio at a particular operating condition. If one knows the value of *S* and the mean equivalence ratio ($\overline{\varphi}$), the value for the standard deviation, σ is determined from equation (94) and the Gaussian (Normal) distribution of equivalence ratio from equation (95).

$$f(\varphi) = \frac{1}{\sqrt{2\pi\sigma^2}} e^{-\frac{(\varphi-\overline{\varphi})^2}{2\sigma^2}} \tag{93}$$

The value of equation (95) gives the fraction of the total mass-flow that exists at equivalence ration φ. From the definition of the probability density function (pdf) the following equation is obtained:

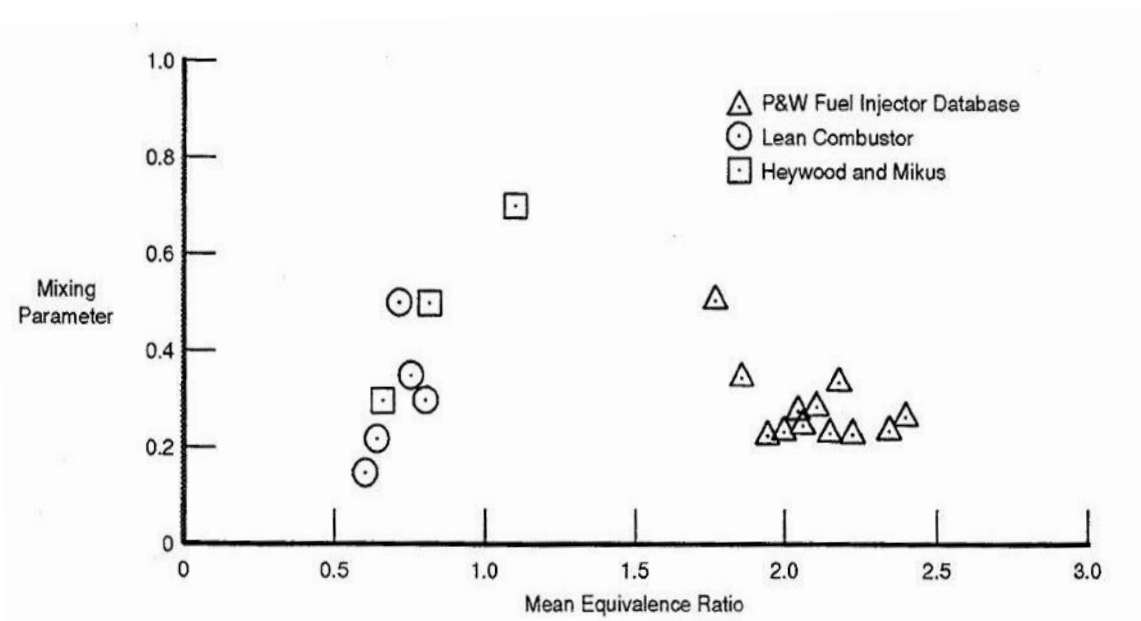

Figure 44: Heywood unmixedness parameter [9]

$$\frac{d\left(\dot{m}_{\varphi}/\dot{m}_{tot}\right)}{d\varphi} = \frac{1}{\sqrt{2\pi\sigma^2}} e^{-\frac{(\varphi-\overline{\varphi})^2}{2\sigma^2}} \tag{94}$$

Unfortunately there is not a unique shape for the unmixedness degree versus mean equivalence ratio and its relation to the physical aspect of the combustor (swirler, injector, etc) is not well defined. Some attempts have been made to correlate this parameter with turbulent flow characteristics inside the combustor [141-142], but they include detail characteristics of combustor and is based on initial parameters whose values is not well-known either. Therefore, the unmixedness parameter acts more like a lumped parameter that contains all the effects in it. The advantage is that the general shape of the unmixedness degree versus the mean equivalence ratio (S-$\overline{\varphi}$ diagram) is similar for all combustors (Figure 44), although they may be shifted, compressed or stretched in vertical or horizontal directions. Each model can have its own S-$\overline{\varphi}$ diagram which should be obtained through experiment and through tuning the model to match the

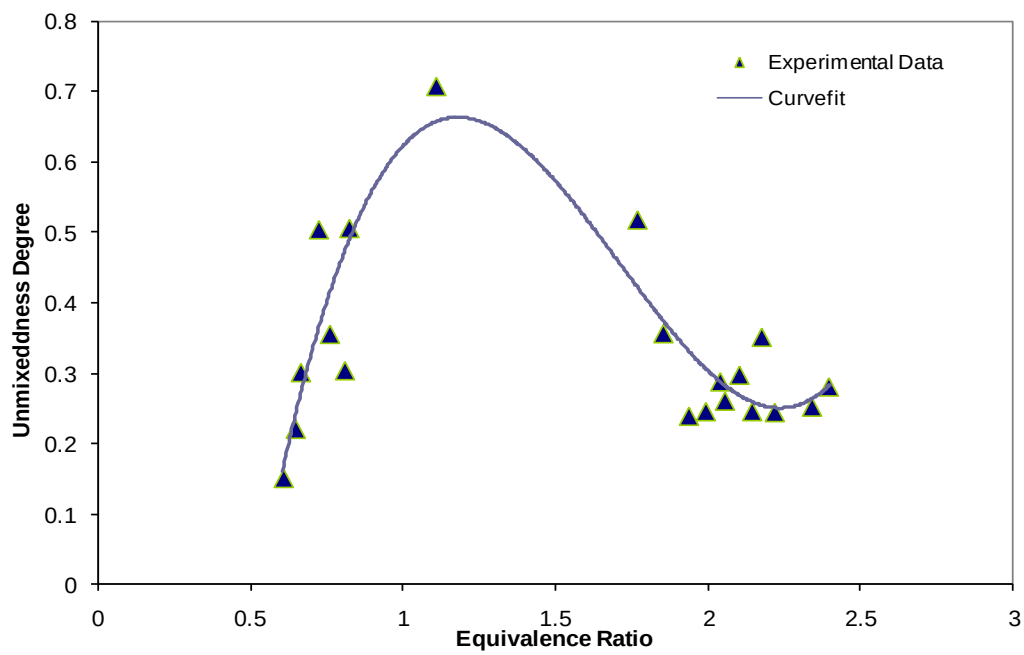

Figure 45: The unmixedness degree diagram [13]

known data [53, 143]. After the combustor model is tuned, it may be used for different combustors. It is possible to perform curve fitting on the S-$\overline{\varphi}$ diagram to obtain a relation between combustor unmixedness degree and mean equivalence ratio (Figure 45).

Equation (94) is a continuous normal distribution that stretches from negative to positive infinity. Clearly such a model cannot exist in reality and it should be truncated and divided into finite number of equivalence ratio intervals (bins) [53, 143]. In this thesis, the distribution is considered for the range between ±3σ which contains 99.99966% of the area under the normal distribution; however, if the lower limit goes below zero (which is impossible since the equivalence ratio cannot be negative), it will be truncated at zero. The value of the lower tail area that is truncated will be distributed to other bins based on their value (i.e., if a bin has a bigger value, the bigger fraction of the truncated area will be assigned to it); by adding these values the total area under the curve is kept equal to one (Figure 46).

After deciding about the number of bins, the width of each bin (Δφ) and the center point of ith bin (φ_i) is obtained. With this information the range of each bin is known (φ_{ilow}, φ_{ihigh}) and the following relation provides the area of the ith bin which corresponds to the fraction of the total flow (fuel and air) at φ_i equivalence ratio.

$$\frac{\dot{m}_{tot}(\varphi_{i,low}\langle\varphi\langle\varphi_{i,high})}{\dot{m}_{tot}} = \frac{\dot{m}_{tot\varphi_i}}{\dot{m}_{tot}} = [CDF(\varphi_{i,high}) - CDF(\varphi_{i,low})](1 + c_{truncated\ tail}) \quad (95)$$
$$i = 1 \ldots n_{bin}$$

where CDF is cumulative distribution function of the normal distribution and where $c_{truncated\ tail}$ is the coefficient that adds the additional value to the bins due to a truncated lower tails. Each bin's share of the truncated tails area is proportional to its value. From the definition of the equivalence ratio (FAR/FAR_{st}), the value of airflow and fuel flow at the given bin can be obtained as:

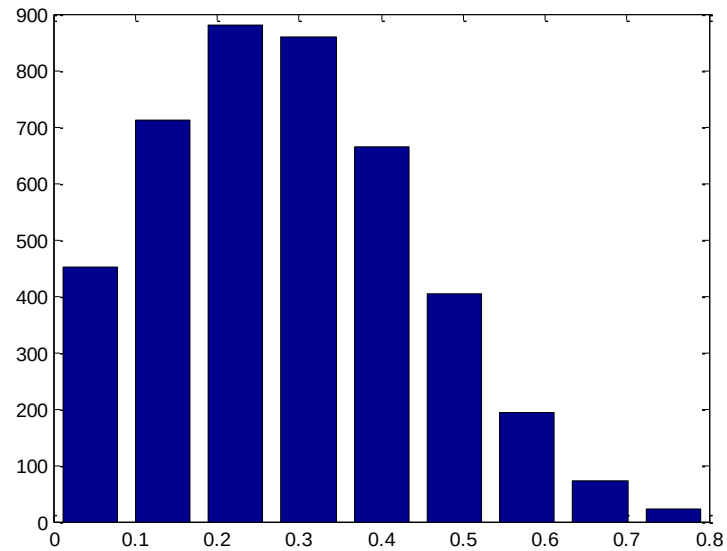

Figure 46: Truncated and discretized normal distribution of equivalence ratio [13]

$$\dot{m}_{air\varphi_i} = \frac{1}{\varphi_i . FAR_{st} + 1} \dot{m}_{tot\varphi_i} \tag{96}$$

$$\dot{m}_{fuel\varphi_i} = \dot{m}_{tot\varphi_i} - \dot{m}_{air\varphi_i} \tag{97}$$

5.4 Chemical Reactors Network Model

The next and last model in the mission prediction model is the chemical analysis model which is based on the finite rate chemistry calculation in the chemical reactors network (CRN). The basics and fundamental of this concept are described in the theoretical background section. The subject of this section is more tailored toward using CRN with a specific structure to model the emissions in the combustor in general and single annular combustor or RQL combustor in particular.

To build the CRN, the CHEMKIN combustion analysis software [144] is used for finite rate analysis. It has all the necessary features that are required for this task such as the ability to create a network of reactor, robust solver and input/output files. In addition to the CRN, CHEMKIN requires a file containing thermodynamics properties (NASA polynomials) of all the species present in the model. It also needs a combustion

mechanism file for a fuel of interest (in this case Jet-A) containing the elementary reactions and the following additional information: 1) the temperature exponent, 2) the pre-exponential factor and, 3) the activation energy of all the elementary reactions to calculate their forward and reverse reaction rate of them.

The structure of the CRN is based on the zones and models that are defined in the 1D internal flow-field model (Figure 47). Wherever there is a zone, it will be replace by a single or set of reactors based on the assumptions and the flow conditions inside the combustor. The 1D internal flow-field model provides all the sizes, volumes and flow properties required by the CRN model.

It is mentioned in the previous section that the mixture's non-uniformity and droplet evaporation/burning needs to be considered in the emissions prediction model. Since almost all the droplets will vaporize or burn in the primary zone, and since unmixedness decays as flow proceeds further downstream in the combustor [145], the unmixedness and droplet evaporation/burning is only considered in the first zone of the

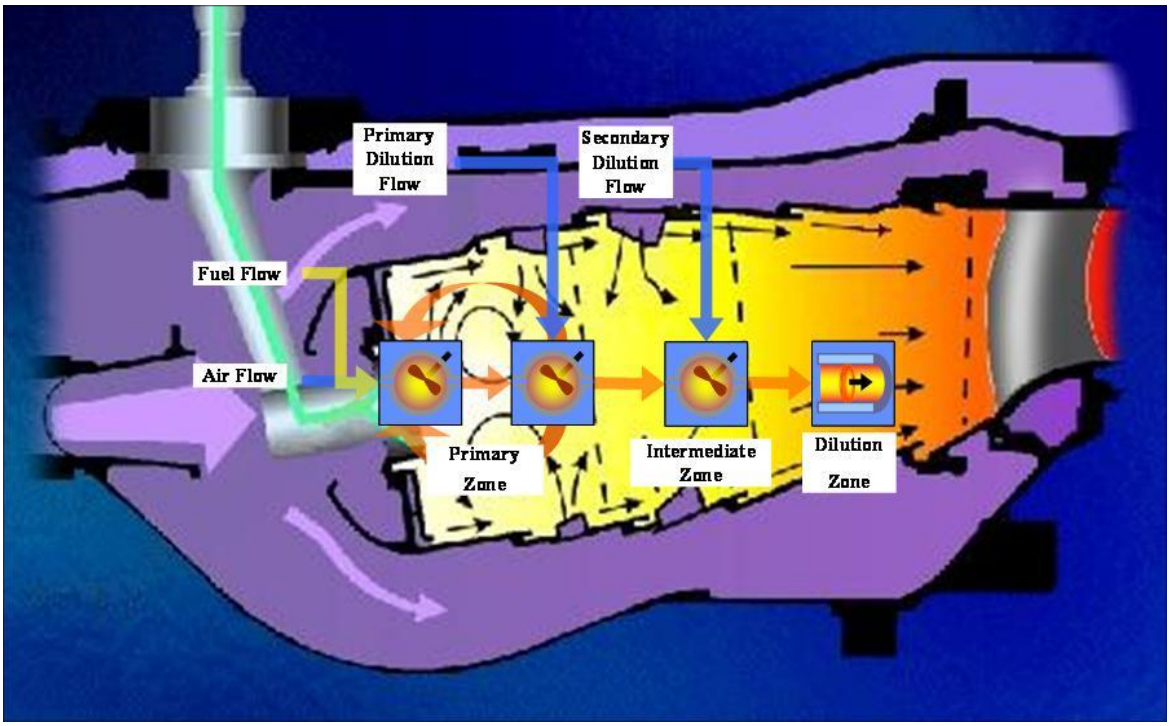

Figure 47: Network of reactors based on combustor zones

combustor which is either primary or rich zone. The rest of the combustor is modeled by single reactors in series. As mentioned above, due to the unmixedness decay, the last zones in the combustor (which is the dilution zone in the SAC and dilution zone or lean zone in the RQL combustor) are modeled by a plug flow reactor (PFR).

In the primary (rich) zone, all the reactors are PSR due to the high turbulent intensity. To consider the diffusion flame (droplet burning), one PSR is assigned for diffusion burning [53]. The amount of the fuel flow is equal to the liquid fuel that has left after the ignition delay time. Additional air is added to the fuel the make the ratio stoichiometric. If the required amount of air is not enough for stoichiometric burning, for the given amount of the air, enough fuel will be assigned to the air to have the stoichiometric burning and the remaining fuel will be sent to the next zone as unburned mixture (a stream with very high equivalence ratio of 30). The volume of the diffusion burning PSR is set to the primary (rich zone) volume based on the assumption that the fuel droplets have all the primary (rich) zone residence time available for the burning.

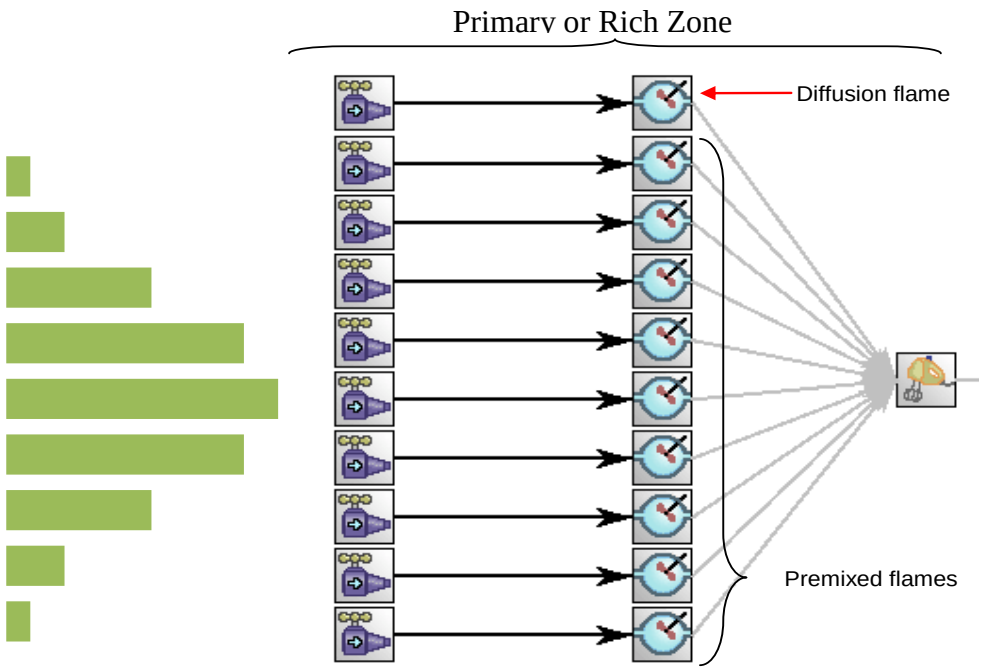

Figure 48: A chemical reactors' network with implementation of diffusion burning and unmixedness degree in CHEMKIN software environment [13]

To implement the concept of non-uniform mixture into the CRN, in addition to the diffusion burning PSR, a set of parallel branches of PSR reactors at the primary zone will be specified. The number of parallel PSR branches is equal to the number of bins in the "Non-Uniform Fuel and Air Mixture" model which is described in the previous section [53, 143]. The volume of PSR's in the pre-mixed flame is proportional to the flow fraction that goes into them and the sum of them will be equal to the primary zone volume. The exhaust of all these branches will go to a single non-reactive gas mixer to mix and go to the next zone (Figure 48). Due to the CHEMKIN limitation, the maximum number of branches (bins) that go to a single reactor cannot be bigger than ten. A sensitivity analysis showed the emission levels sensitivity to the number of branches is negligible beyond 9 [143].

After the first zone (primary or rich zone) the structure of the CRN depends on the combustor type.

5.4.1 A Chemical Reactor's Network Model for Single Annular Combustor

In the SAC CRN, the assumption is that the degree of turbulent intensity still is

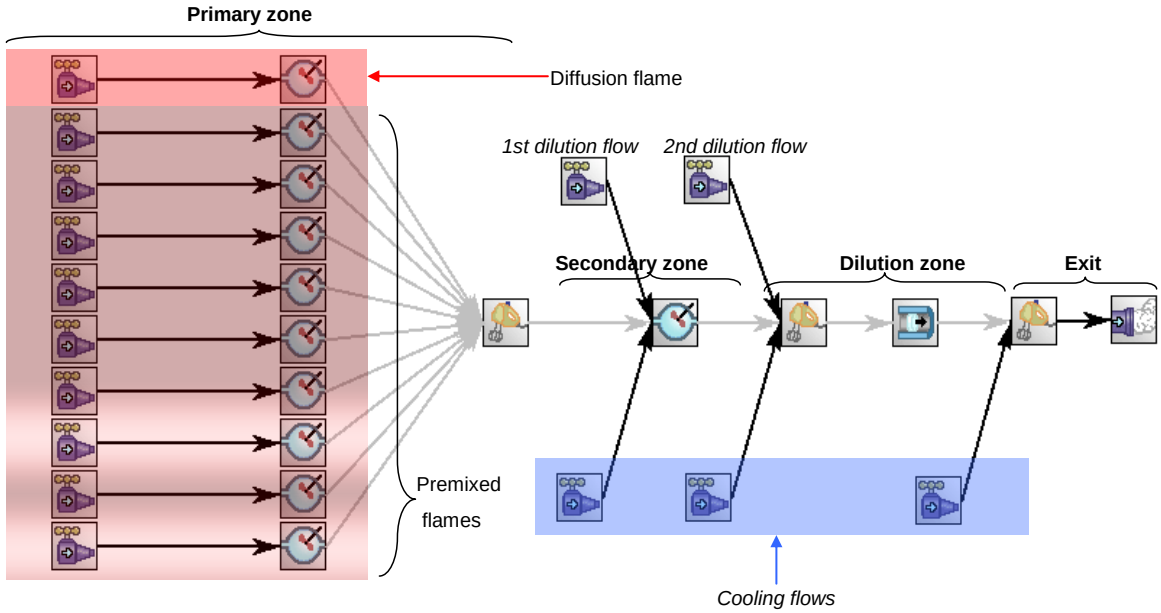

Figure 49: A proposed CRN for the single annular combustor configuration

high enough in the secondary zone to model it with a PSR. The dilution zone is modeled by a PFR with its length and cross section equal to the dilution zone length and cross section. Figure 49 shows the proposed CRN for the SAC combustor concept. After the primary zone, the first dilution flow is added to the PSR which is a representative of the secondary zone. The exhaust of the secondary zone will be mixed with the second dilution flow first (because PFR does not accept more than one inlet) and the mixture will be sent to the dilution zone reactor which is a PFR.

In addition to the first and second dilution flows that are added to the reactors, streams of cooling flow are considered for after each zone. This feature foresees the possibility of capturing the effect of the cooling flow on the emissions. Initially, it had been assumed that cooling flow does remains unmixed throughout the combustor and mixes with the hot section at the exit of the combustor; however, under some conditions, possibly the high power condition, at least part of the cooling flow will be mixed with the hot gases, especially after the dilution flows. Although determining the amount of the cooling flow that is mixed with the core gases requires a high fidelity model, this feature can capture the effect and sensitivity of the cooling flow partition on the emission levels.

5.4.2 A Chemical Reactor's Network Model for RQL Combustor

The beginning (rich zone) and end (dilution) of the CRN model for the RQL is similar to that of the SAC. However, there is a difference in the mid-sections: instead of a secondary zone PSR in the SAC, there is a mixing zone PaSR (Partially Stirred Reactor), gas mixer and lean zone PFR. While the cooling flows and overall dilution and quenching flows structures are the same in both models, the detail modeling of the quenching flow that goes in to the mixing zone is different than the dilution flow model of the secondary or dilution zones.

5.4.2.1 Mixing Zone

In the mixing zone, when a large jet is initially penetrating to the core section, it does not completely mix with the gases and eddies with wide range of size and turn-over time are formed around it that can create local stoichiometric mixtures. In other words, the poor quality of mixing leads to local stoichiometric mixtures around the jet. The other important aspect of mixing in the mixing zone is the micro-mixing. After mixing the quench air with core gases in macro-scales, the quality of the micro-mixing determines the flame temperature and emission levels. To model the whole macro and micro mixing process, the turbulent modeling and chemical kinetic/flow interaction modeling is required. To simplify the model, it is assumed that the size of the energy containing eddies in the mixture at the mixing zone is in the order of the mixing zone height. Based on this assumption, the characteristic mixing time in the mixing zone (τ_{mix}) is defined as:

$$\tau_{mix} = \frac{H_{MZ}^3}{\rho_{MZ}\dot{m}_{MZ}} \tag{98}$$

where H is the mixing zone height. While there is another equation to calculate the mixing time as it is given in the equation (22), this equation needs information about

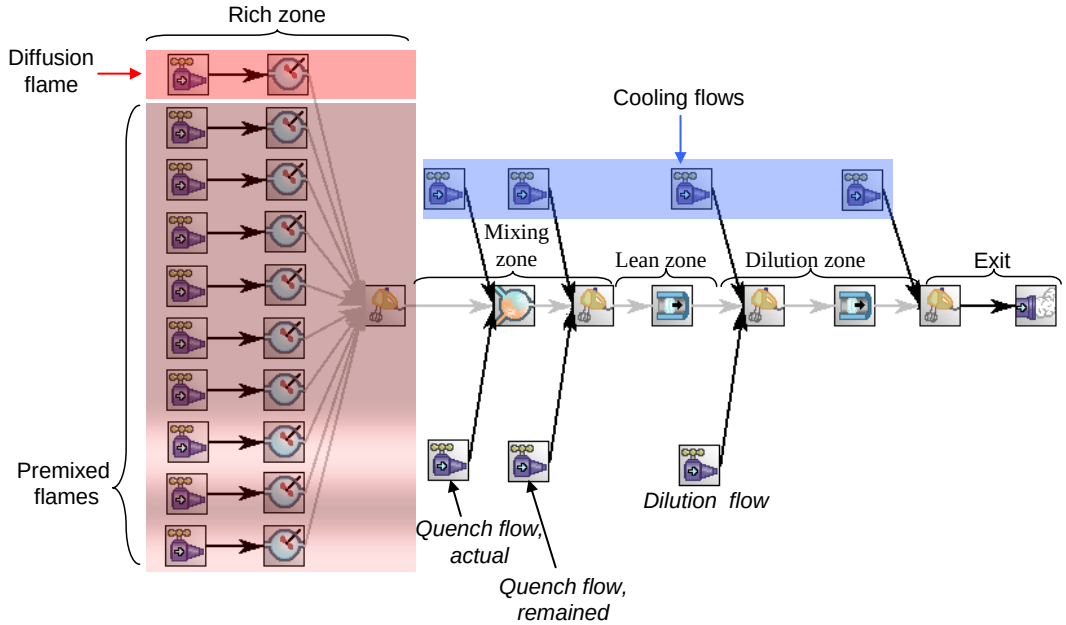

Figure 50: A proposed CRN for the RQL combustor configuration

local turbulent intensity (ε), which is not available in this low fidelity model.

The residence time in the mixing zone is defined as:

$$\tau_{res} = \frac{Vol_{MZ}/2}{A_{MZ}V_{MZ}} \tag{99}$$

The volume is divided by two because half of the mixing zone volume is available for mixing as the mixing flow enters the mixing zone at half a distance down the beginning of the zone. The mixing time (τ_{mix}) and residence time (τ_{res}) can be used in equation (28) to determine the level of unmixedness in the mixing zone. It should be noted the unmixedness in the mixing zone is different from what is defined in the primary zone.

The assumption for developing this model is that the amount of actual mixing of the quench jet and the core flow depends on the mixing quality and the unmixedness degree in the mixing zone. For a perfectly mixed mixture with high mixing quality, the unmixedness value would be one. This mixture will burn in the lean zone at the designed lean zone equivalence ratio (which is below one). As the mixing zone unmixedness increases from zero to one, the actual equivalence ratio (φ_{actual}) of the burning mixture in the PaSR moves toward one. At an unmixedness value of one, the mixture in the PaSR will burn at the stoichiometric ratio. The amount of the quench jet that actually mixes in the PaSR with the coming hot gases is determined based on the obtained actual equivalence ratio (φ_{actual}), and this portion of the quench jet is named *actual quench flow*. The rest of the quenching air that has not been mixed with the core flow in the PaSR will be forwarded to the gas mixer after the PaSR where it mixes with the exhaust of the PaSR, and this portion of the flow is called *remained quench flow*. A linear relationship is assumed between the mixing zone unmixedness value (S_{MZ}, between zero and one) and the equivalence ratio (φ_{PaSR}, between the lean zone equivalence ratio, φ_{LZ} and one).

$$\varphi_{actual} = (1-\varphi_{LZ})S_{MZ} + \varphi_{LZ} \tag{100}$$

From equation (100), the values of *actual quench flow* and *remained quench flow* at the mixing zone are derived as:

$$\dot{m}_{actual\ \ quench} = \dot{m}_{MZ\ actual} = \frac{\dot{m}_{fuel}}{(FAR_{st} - FAR_{LZ})(S_{MZ} - 1) + FAR_{st}} - \dot{m}_{RZ} \tag{101}$$

$$\dot{m}_{remained\ \ quench} = \dot{m}_{MZ\ remained} = \dot{m}_{MZ} - \dot{m}_{MZ\ actual} \tag{102}$$

The mixing zone *actual quench flow* and rich zone output go into the PaSR and the output goes into a gas mixer with the mixing zone *remained quench flow*. Also the total amount of the quenching jet is obtained from the flow partitioning model.

The PaSR reactor has a number of inputs in addition to those required by PaSR (i.e. residence time, equivalence ratio, inlet mass-flow, pressure and inlet temperature). They are: 1) the simulation time, 2) number of Monte Carlo samples and, 3) the simulation marching time step.

The simulation time should be long enough so the solution of the PaSR reaches the steady-state condition at the end of it, but not so long as to make the simulation very slow. It is set to be 5 times of the mixing zone residence time.

$$\tau_{MZ\ simulation} = 5\tau_{MZ\ residence} \tag{103}$$

The number of the Monte Carlo simulation sampling (NPAR) for the PaSR model defines the number of statistical samples that are randomly selected from the joint pdf to model the mixing and reacting process. A number around 200 provides a balance between the accuracy and execution time.

The marching time step of the statistical samples that is required in the Monte Carlo simulation is set to the tenth of the mixing zone residence time.

$$dt_{MCS\ MZ} = \frac{\tau_{MZ\ residence}}{10} \tag{104}$$

5.4.2.2 Lean Zone

The lean zone which is a tube after the mixing zone is modeled by a plug flow reactor (PFR) with the assumption that the flow becomes calm after diverging and exiting from the mixing zone. If the RQL configuration has a dilution zone after the lean zone, the output of the lean zone along with the dilution flow goes in to another plug flow reactor (PFR) representing the dilution zone.

5.5 Post Processing

After running all the mentioned models, the mass fraction of the species (NO, NO_2 and CO) are extracted from the exit file of the last reactor in the CRN. The EI NO_x is obtained by adding the mass fraction of NO and NO_2 together, multiplying it by the total mass flow going out of the combustor (in g/s) and dividing the result by the fuel mass-flow (in kg/s). The same process will be repeated to determine the EI CO value.

5.6 Challenges

After describing the details and important aspects of the proposed methodology, it is a good idea to introduce the challenges and obstacles that lie ahead of implementing the proposed methodology to a real world problem.

5.6.1 Design Perspective versus Analysis Perspective

One of the biggest challenges through this project is the different perspectives that exist between two groups of experts about how to approach a combustion problem and emissions prediction. One school of thought believes that the combustion and emission formation process is such a complex phenomenon that it cannot be dealt with in the conceptual design phase at all. In their view, a highly detailed model of combustor with geometrical information as well as initial and boundary conditions is required to model the internal flow-field, combustion and their related aspects. The other school of thought believes that it is feasible to model the emissions of a combustor based on simplified

models and with enough information available from experiments. Both group's opinions can be justified depending on the perspective that the problem is observed from and the success criteria. If the objective is to perform a detailed modeling of the combustor at the later design phases, the first group's opinion will prevail, whereas if the criterion is to have a tool that helps the conceptual designers and decision makers to have better perspective of the problem, then the second group opinion will prevail. This difference in opinions shows itself in the fidelity level of the models and tools that are available in the field. Some of the tools are very complex and hard to use at conceptual phase and some of them are too simplified.

5.6.2 Disciplinary Models/Tools and Their Integration

As it was discussed in the introduction and literature review of this work, combustion is a highly multidisciplinary phenomena and each disciplinary model has strong interaction with other disciplines; however, many of these models are created for high fidelity analysis and for very specific applications and they cannot be used in the conceptual design phase. Therefore, one of the great challenges of this work is to either find or create a model that it suitable for this design phase. Broad knowledge, component data and extensive literature search is required to create a model with adequate fidelity for this research. Further, the integration of these models with available tools is not a trivial task when those tools have specific requirements for their input and output files. A suitable interface should be created to establish a communication line between these tools and custom-made models.

5.6.3 Limited Available Data

In the proposed methodology some experimental or design data are still required to tune or calibrate the equations and models or validate them. Often, information about

combustors and their components characteristics are not available in the public domain and are considered proprietary property by companies who manufacture them.

5.6.4 Combustion Mechanism

Finding the right combustion mechanism for aviation fuel (Jet-A) is another challenge of this research. In many applications, the combustion mechanism is provided for gaseous fuels and hydrocarbons such as heptane and decane and they are used in combustion chemistry analysis on behalf of the real fuel. Sometimes, these mechanisms are very large in size and complex. When these mechanisms are applied to a complex CRN model, they increase the execution time significantly and sometimes the solver cannot converge to a final solution at all.

In the next section an analogy is provided to show how even a simplified model like the one that is propose in this work, has a potential to provide satisfactory results.

5.7 Emissions Prediction Approach and Skin Friction Coefficient Calculation Analogy

A question that may be asked by field experts is how the model suggested in this thesis can provide reasonably accurate results when it does not specifically address some important issues in the field, such as two-phase flow, shear flow mixing, turbulent models, main and cross-flow jet interaction, etc.

The answer to this question lies in the spatially averaged parameters approach. In this approach, a control volume is considered to average the flow properties across the domain using integral methods. The integral method can be contrasted with the differential equation method, which is applied to find flow properties at a single point (cell) in the domain. The differential equation method is more sensitive to the initial and boundary conditions and requires their precise definition. An example that may further clarify the subject is to calculate the wall skin friction coefficient in viscous fluid

mechanics. In a Newtonian fluid, the shear stress next to the wall (τ_w) in the boundary layer and the skin friction coefficient (c_f) are given by

$$\tau_w = \mu \frac{\partial u}{\partial y}\Big|_{y=0} \tag{105}$$

$$c_f = \frac{\tau_w}{\frac{1}{2}\rho_e u_e^2} \tag{106}$$

where:

μ: absolute (dynamic) viscosity

ρ_e: Free stream density

u: Velocity

u_e: Free stream velocity

One way to obtain wall shear stress, skin friction coefficient and eventually wall drag coefficient (C_D) is to find an analytical solution of the flow governing equations. The best example is the Blasius equation for flat-plate laminar flow which yields an exact analytical solution; however, the answer is not in the form of an explicit equation [146]. Putting aside the exact analytical approach which may not always be available, the second approach involves assuming a boundary layer velocity profile ($u(y)$) and finding the value of its derivative at y=0 to find the quantities of interest (Figure 51). Often the velocity profile that is assumed for the boundary layer is a second order polynomial (parabolic); however, other forms of profiles like the sine function have been used as well. This method is very sensitive to the shape of the function near the wall, and a small change in the shape can cause a great change in its derivative, introducing significant errors to the calculations. Another approach which is still based on an assumed velocity profile utilizes the integral method instead of the differential method. In the integral method, first introduced by Von Karman [147], the integral equations for momentum and displacement are taken over a control volume to find the boundary layer thickness, skin

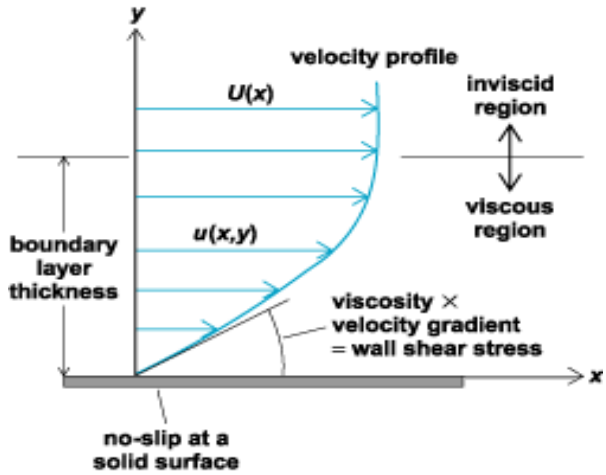

Figure 51: Velocity profile in boundary layer [5]

friction and drag coefficients. In this method, the variation in the velocity profile introduce an error in the final result; however, the error is less than 10 percent, which is considered to be good [146, 148].

By comparing the integral approach to calculate drag coefficient with the control volume emissions-prediction approach, it is clearer why the proposed method has the potential to provide acceptable accuracy without going into modeling all of the details in the combustor. The models being considered in this research are often based on obtaining the average properties of the combustor flow while at the same time keeping an eye on the basic phenomena that exist in the process.

The subject discussed in this section by no means implies that considering detailed phenomena is not useful or that physics-based model can be created without them. The point is that the advantages and disadvantages of each approach should be weighed in the context of the research being conducted to select the best one.

The next chapter explains the steps that are taken and tools that are used to create an integrated frame work to determine the gas turbine emissions in an efficient manner in an integrated platform. This automation can significantly reduce the execution time of the whole process.

CHAPTER 6

INTEGRATED ENVIRONMENT

To automate the whole conceptual combustor sizing and emissions prediction process and to minimize the human interference and set-up time, all models are linked together in an integrated platform (Model Center [149]). The integrated environment may be used to run the design of experiments (DOE), uncertainty and sensitivity studies and perform the parametric studies.

Steps are taken to automate the process in a way that 1D internal flow-field and CRN models run without going to the command prompt window in WINDOWS operating software or software GUI. Therefore, the heart of the this integrated environment in the Model Centre is a group of file-wrappers which take the inputs from the Model Center environment, create an input file for the third party software (i.e., CHEMKIN), execute the software and parse the output file and display them in the Model Center GUI. The file-wrapper utility is used whenever there is not any pre-built plug-in for software that is being used. For example Microsoft Excel, MATLAB and ANSYS have pre-built plug-ins in the Model Center that can be used in the environment directly. They create a link to these softwares without a need to create a file-wrapper. For third-party softwares that do not have a plug-in, there is a feature where a file can be written to communicate with the software and execute it. The precursor to use such a feature is that the third party software can be executed through input files and create an output file of data after finishing the analysis. Every time a file-wrapper is being used, it is necessary to run Analysis Server software in the background. Analysis Server creates a link between the Model Center and the third party software and enables the Model Center to execute cases without going into the software environment. A detailed instruction about how to create a file and what is the task of each section can be found in the Model

Center user manual [149]. For each combustor concept of the SAC and RQL an integrated Model Center environment has been created.

6.1 1D Internal Flow-Field Model

All the elements and components of the 1D flow model are written in MATLAB. Except the main MATLAB script file that uses all the models to run the emission model, all other files are written as MATLAB functions. The list of the files is given in Table 8. There are 26 MATLAB functions that are used by either the RQL or SAC models. The SAC o RQL MATLAB scripts are directly implemented in the Model Center as MATLAB modules. Separation of models and components has made the 1D flow-field model modular enough to model a SAC or RQL combustor by putting the needed elements together to construct the desired architecture. The total size of the codes of the 1D internal flow-field models is about 3800 lines.

The “Droplet Evaporation and Diffusion Burning” and “Non-Uniform Mixture” models are written in four MATLAB files and are directly integrated into the model center.

Table 8: MATHALB functions used in the 1D flow-field Model

CEA Analysis	Flow Property	Combustor Zones	Geometry
burn.m	flow_function.m	annulus.m	
fuel_to_air.m	Mach.m	diffuser.m	combustor_graph.m
gas_properties.m	total_to_static	diffuser_efficiency.m	zone_volume.m
temperature_out.m	velocity.m	droplet_evaporation.m	inner_outer_ annulus_height.m
		droplet_ODE.m	
		Lean_zone.m	
		Mixing_zone.m	
		Primary_zone.m	
		non_Primary_zone.m	
		transition_zone.m	
		zero_diamater_event.m	
		air_distribution_RQL.m	
		air_distribution_SAC.m	

6.2 CRN Model

Integration of the CRN model requires creating a batch file from a set of commands needed to execute the whole CRN model. The steps needed and defined in the batch file to run the CRN are described here and the scripts are provided in Appendix B.

First, the CHEMKIN needs to find the location and name of the thermodynamics properties file and combustion mechanism file. This information is stored in a file named "CK_PreProc_*.input"and a file-wrapper is created to receive the name and address of the thermodynamic and combustion mechanism files from the user to create the file. The name of the file-wrapper is "Combustion_mechanism_selector".

In the next step, CHEMKIN uses the files and creates a chemistry file used by all reactors to perform finite-rate chemistry analysis. Then CHEKIN executes the reactor models in the CRN model one by one in order of the reactor placement. Each reactor model can be run using a specific command followed by the name of input files defined for the reactor. The commands are listed in Table 10. More comprehensive description and detail of the commands can be found in the CHEMKIN user Manual [144].

The input file contains the input information, the address and the name of an xml files containing the information of the previous reactors linked to it. A chemistry file that is created at the beginning, containing the combustion mechanism information of the fuel should be added to the command too. All the reactor models will be executed one by one until the last reactor at the end of the CRN.

After running each reactor, a number of output files are generated. The most comprehensive one is a file with the extension "out". This file has a significant amount of information about the steps that the solver takes to run the model. The file also contains data about convergence and information about species. Usually it is hard to extract the required information from this file because depending on the convergence rate, its size and the location of the desired information vary. An easier way is to use a "GetSolution -nosen -norop -mass –all" command to have the outputs of each reactor in the comma

Table 9: Components of the SAC CRN (left) and RQL CRN (right) model

Component	SAC CRN components
Primary zone	10 inlets
	10 PSR(C1-C10)
	1 upstream inlet
	1 Gas Mixer (C11)
Secondary zone	1 dilution inlet
	1 unburned fuel inlet
	1 cooling flow inlet
	1 upstream inlet
	1 PSR (C12)
Dilution zone	1 upstream inlet
	1 dilution inlet
	1 unburned fuel inlet
	1 cooling flow inlet
	1 Gas Mixer (C13)
	1 upstream inlet
	1 PFR (C14)
Exit	1 upstream inlet
	1 unburned fuel inlet
	1 cooling flow inlet
	1 Gas Mixer (C15)

Component	RQL CRN components
Rich zone	10 Inlets
	10 PSR(C1-C10)
	1 Upstream inlet
	1 Gas Mixer (C11)
Mixing zone	1 Upstream inlet
	1 Actual quench inlet
	1 Cooling flow inlet
	1 PaSR (C12)
	1 Remained quench inlet
	1 Upstream inlet
	1 Cooling flow inlet
	1 Unburned fuel inlet
	1 Gas Mixer (C13)
Lean zone	1 Upstream inlet
	1 PFR (C14)
Dilution zone	1 Upstream inlet
	1 Dilution inlet
	1 Unburned fuel inlet
	1 Cooling flow inlet
	1 Gas Mixer (C15)
	1 Upstream inlet
	1 PFR (C16)
Exit	1 Upstream inlet
	1 Unburned fuel inlet
	1 Cooling flow inlet
	1 Gas Mixer (C16)

separated (csv) format with a universal format for all reactors. It is much easier to parse the needed information from the csv file in an automated fashion because all the output parameters are at predefined location. Another file created after running each reactor is an XMLdata.zip file. This file should be renamed to an appropriate name and saved before running the next reactor because it will be overwritten in the next run. The file should be defined in the input file of the next reactor. This file contain information about the exhaust gases of the reactor which is required if the reactor is linked to another reactor. The name should be provided in the input file of the next reactor in line so the CHEMKIN knows what the upstream flow properties are entering to the next reactor.

There are total of 78 files that are used in the CRN model. Table 10 lists the name of the elementary reactor and important tasks along with their corresponding commands and required files in the CHEMKIN software. Table 10 shows the list of the input files that are required by the reactors in the RQL or SAC CRN model. All of information inside these input files is calculated in the 1D flow-field model, Non-Uniform Mixture model or Droplet Evaporation and Diffusion Burning model. All these commands and process are written in a script file (BATCH file); therefore, by running the script file in the command window, without opening the CHEMKIN GUI, the CRN execution can be performed. This script file is used to automate the CRN analysis in the MODEL CENTER (Appendix B).

To create a file-wrapper for the CRN model to implement it in the Model Center environment, a set of input template files are needed. These file are exactly like the original input file of the reactors. Model Center use this templates to create a new input file for CHEMKIN by replacing pre-specified fields with values that user defines in the MODEL CENTER environment.

The file-wrapper takes the inputs from the MODEL CENTER, creates new set of input files and put them in the pre-defined field and then run the CRN model script file. A new set of output files are created after script file is executed. The file-wrapper then looks into the output files (csv files) to parse the required data. At the end, the parsed data are sent back to MODEL CENTER environment.

Table 10: Main commands used in the CHEMKIN CRN model

Reactor Type or Process	**Command**	**Required Files**
Chemistry run	CKPreProcess.EXE	CKPreProc file(input)
PSR	CKReactorGenericPSR.EXE	Input file (inp), Chemistry file (asc)
PFR	CKReactorGenericPFR.EXE	Input file (inp), Chemistry file (asc)
Gas Mixer	CKReactorMixer.EXE	Input file (inp), Chemistry file (asc)
PaSR	CKReactorGenericPaSR.EXE	Input file (inp), Chemistry file (asc)
CSV solution file	GetSolution	Input file (inp), Chemistry file (asc)

6.3 Linking All Components Together

All the inputs of the CRN model in the Model Center environment are obtained from the output section of the 1D flow-field model, Droplet Evaporation and Diffusion Burning model or Non-Uniform Mixture model. The outputs of these models are linked to the inputs of the CRN model. Also an additional VBA module is added to post-process the data and calculate the NO_x and CO emission indices. An additional MATLAB component is created to plot the combustor axial temperature variations and the probability density function (pdf) of the mixing zone temperature and species (NO, NO_2, CO, CO_2 and H_2O) which are the result of the Monte Carlo simulation in the PaSR.

Figure 52 shows the Model Center integrated environment for the SAC emission model. Also Table 11 to Table 14 show the required inputs for each model (if applicable) and the units and the required on-design and off-design engine cycle parameters at the compressor exit.

Table 11: Design and operating parameters

Condition	Parameters	Unit
On-Design	Compressor exit pressure	psia
	Compressor exit temperature	R
	Compressor exit airflow	lbm/s
	Compressor exit Mach number	-
	Combustor exit Mach number	-
	Fuel flow	lbm/s
	Zone efficiencies	-
	Zone cooling fractions	-
Off-Design	Compressor exit pressure	psia
	Compressor exit temperature	R
	Compressor exit airflow	lbm/s
	Compressor exit Mach number	-
	Combustor exit Mach number	-
	Fuel flow	lbm/s
	Swirler area coefficient	-
	Zone efficiencies	-
	Zone cooling fractions	-

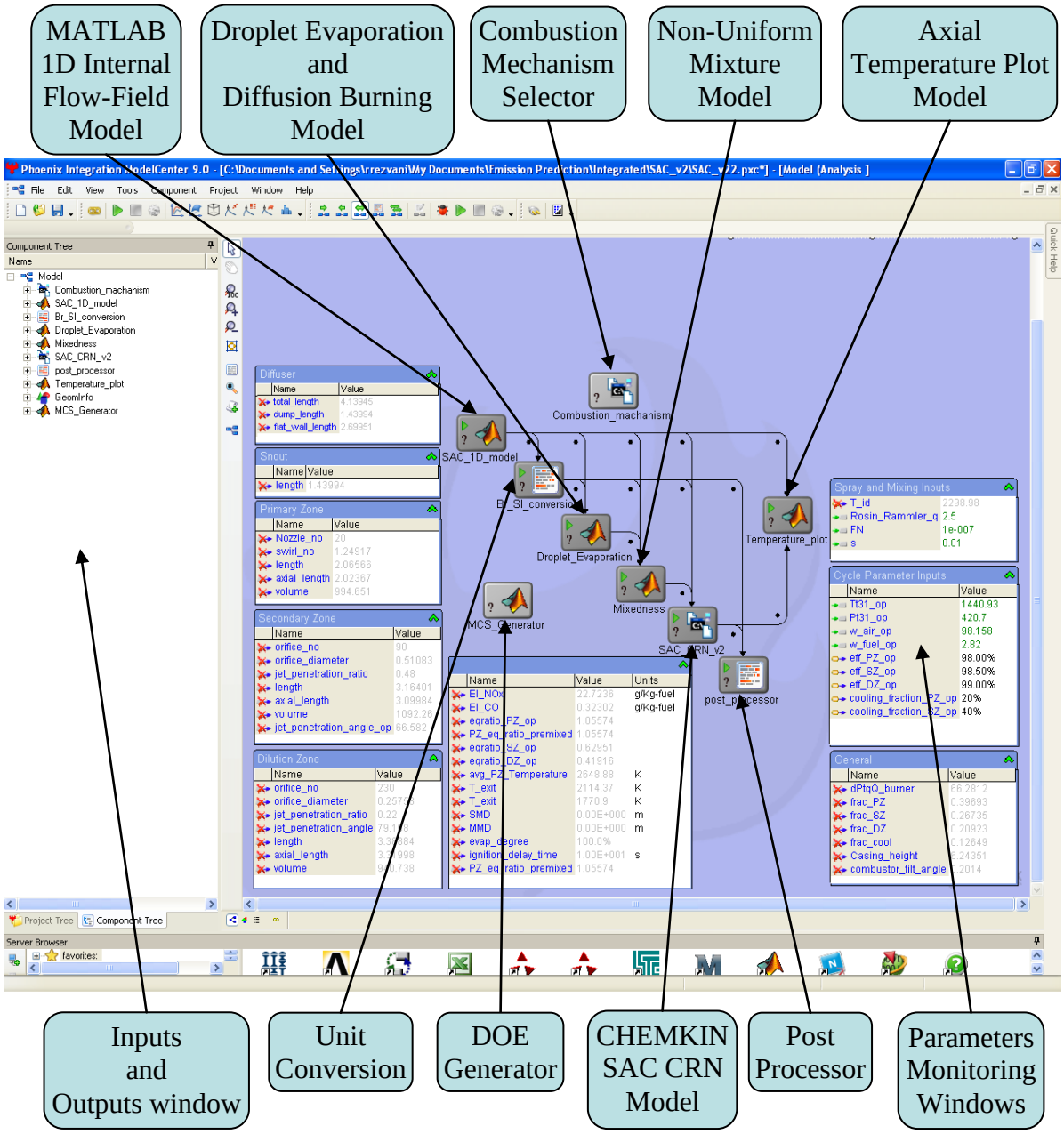

Figure 52: Integrated emission model in the Model Center environment

Table 12: Inputs to the 1D flow-field model

Component		Inputs	unit
Diffuser		Inlet mean radius	in
		Inlet Mach number	-
		Exit Mach number	-
		Half angle	-
		Orientation angle (guess)	-
		Passage number	-
		Sweet spot	-
Burner		Exit mean radius	in
		Exit mach number	-
		Dp/P	-
		T_liner_max	R
		Cooling mechanism factor	-
		T_fuel	R
		Number of injectors	-
		Fuel name	-
		Far_{st}	-
		Configuration	-
	Rich zone	Swirl angle	-
		Swirler discharge coefficient	-
		swirler_hub	in
		W_nozzle_air/W_fuel	-
		Burning efficiency	-
		Equivalence ratio	-
		RZ cooling fraction	-
	Mixing zone	Discharge coefficient	-
		Length ratio	-
		Area_MZ/Area_RZ	-
		Mixing model	-
		Mixing model factor	-
		Mixing mode	-
		Monte Carlo event number	-
		MZ cooling fraction	
	Lean zone	Burning efficiency	-
		Equivalence ratio	-
		Length ratio	-
	Secondary and dilution zones	Burning efficiency	-
		Discharge coefficient	-
		Jet penetration ratio	-
		Length ratio	
		DZ or SZ cooling fraction	-

Table 13: Inputs to the Droplet Evaporation and Diffusion Burning model

Inputs	unit
FN_injector	m^2
Fuel density	kg/m3
q (Rosin-Rammler distribution shape factor)	-
U_turb_fluctuation	m/s
T_fuel	R
Fuel flow	kg/s
Fuel physical properties	-

Table 14: Inputs to the CRN Model

Component	CRN Input Parameters	Unit
Rich or primary zone	Equivalence ratio (array of 10 elements)	-
	Mass-flow (array of 10 elements)	g/s
	Inlet temperature (array of 10 elements)	K
	Inlet fuel name (array of 10 elements)	-
	Pressure (array of 10 elements)	atm
	Volume (array of 10 elements)	cm3
Mixing zone	Volume	cm3
	Pressure	atm
	Residence time	s
	Simulation time	s
	Mixing time	s
	Mixing model	-
	Mixing model factor	-
	Mixing mode (Equil, Chem, Mix)	-
	Monte Carlo events number	-
	Monte Carlo time step	s
Mixing or dilution or cooling flow	Mass-flow	g/s
	Temperature	K
	Composition	gr/s
Lean or dilution zone	Pressure	atm
	Cross section area	cm2
	Start location	cm
	Length	cm
	Equivalence ratio	-
Mixer	Volume	cm3
	Pressure	atm
	Mass-flow	g/s
Secondary zone	Volume	cm3
	Mass-flow	cm
	Pressure	cm

CHAPTER 7

APPROACH IMPLEMENTATION AND RESULTS

To prove or disprove the hypotheses presented in Chapter 3, experiments should be designed. First, the hypotheses are restated here as a reminder.

***Hypothesis 1 (H1)*:** The addition of combustor internal flow-field analysis using modular component modeling approach to the combustion analysis using the chemical reactor network (CRN) approach results in a more versatile and parametric emissions prediction approach for different combustor types, different operating conditions, and different combustor design parameters.

***Hypothesis 2 (H2)*:** An integrated emissions prediction approach with reduced uncertainties can be developed by modeling and integrating important phenomena in the emissions formation process using hybrid models. The most important phenomena are assumed to be Droplet evaporation/burning and air/fuel mixture non-uniformity. An interface provides a line of communication between the disciplines.

Secondary Hypothesis 2A (SH 2A): The following simplified models are expected to reduce epistemic uncertainties of the emissions prediction**:**

- Probabilistic unmixedness model
- Droplet evaporation model
- Diffusion burning based on un-vaporized fuel flow

Secondary Hypothesis 2B (SH 2B): The Monte Carlo analysis can model the epistemic uncertainties. A comparison of the uncertainty analysis of a complete model with deficient models can capture the potential improvements or deterioration of emission uncertainties. A sensitivity analysis can model the aleatory uncertainties and show the effect of the inputs' uncertainty (variation) on the emission levels.

Three experiments are designed to test the validity of the hypotheses. Figure 53 shows the relation between these experiments, the hypotheses and the research questions.

In the first experiment, the proposed methodology will be applied to the combustor of the CFM56 engine to predict its emission levels at different operating conditions. The main objective of the first experiment is to assess the predictive capability of the model, and validate it. To test the parametric capability as well as the predictive capability of the model, it will also be applied to Energy Efficient Engine (E^3) combustor. The CFM56 and E^3 combustors belong to the same single annular combustor family; however, they have different characteristics and emission levels. Two Monte Carlo simulations are performed for each single annular combustor in sub-sections 7.3.1 and 7.3.2. The first Monte Carlo simulation is used to find the right combination of inputs to the 1D flow-field model that provides the same geometrical information and flow fractions as the available data, the inputs distributions are considered to be uniform. The second Monte Carlo simulation (with uniform inputs distribution) is used to test the trend of the cooling flow fractions and unmixedness degree as a function of the power setting and to see if the trends are similar for the two different considered single annular combustors. If the trends are similar, it can be concluded that the model is independent of the two combustors and is able to follow the correct physical trend. The second Monte

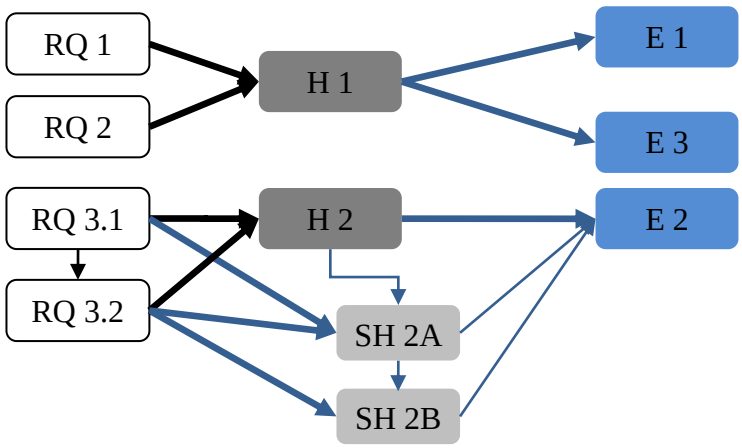

Figure 53: Relation between the research questions, hypotheses and experiments

Carlo simulation is based on the available emission data.

The second experiment is designed in two steps. In the first step, the goal is to investigate if using the proposed methodology reduces the prediction epistemic uncertainties. This experiment is applied to the CFM56 SAC model. In that experiment a distribution of the NO_x and CO emissions are obtained by starting with an emission model without a Non-Uniform Mixture or Droplet Evaporation and Diffusion Burning models. These models then are added to the emission model one by one to assess their effects on the mean and standard deviation of the emission level distributions. Moving the distribution's mean toward actual value and decreasing the standard deviation would be an indication of the improved epistemic uncertainty. In the next step in the second experiment, a sensitivity analysis is performed to study the contribution of the combined combustor characteristics and engine cycle parameters' variations (aleatory uncertainties) on the emission levels.

In the third experiment, the proposed methodology is extended to develop an emission model for an RQL combustor to test the versatility of the approach.

Before the experiments are performed, one more task has to be accomplished which is the creation of a surrogate model for the NASA chemical equilibrium analysis (CEA) model to speed up the 1D internal flow-field model execution. The process is described in the following section. In the section afterward, the combustion mechanisms used or tied in finite-rate chemistry analysis are introduced.

7.1 Surrogate Model for Chemical Equilibrium Analysis

As described earlier, due to the existence of the rich flame in the rich zone, using the simple enthalpy-balanced formula to calculate the flame temperature is not an option and cannot be used for rich combustion. The next best available option is to use CEA. CEA was originally written in the FORTRAN programming language. In addition, Numerical Propulsion System Simulation (NPSS) engine modeling environment

implemented the CEA model in its thermodynamic package. Using the NASA CEA model directly has some integration difficulties. In addition, using the code for all the components, even those that do not need reacting flow calculation (e.g., diffuser) makes the 1D flow-field execution very slow. The solution is to create a surrogate model of the CEA for use in place of the original one.

The NPSS version of the CEA analysis is selected for surrogate modeling. A simple burner object with inlet and exit stations is created in the NPSS environment to run the CEA thermo package. The following command in the file directs the NPSS to use the CEA package:

```
setThermoPackage("CEA","Air","H2O","Jet-A(g)"," "," "," ")
```

The definition of combustion efficiency in CEA is also slightly different from the usual definition. This definition is the ratio of the actual to the maximum mixture temperature rise. Although the model uses a thermodynamics properties file that contains the NASA polynomials for all the available considered reactants and products in the mixture, the fuel inlet enthalpy must be defined explicitly in the model. The formula for calculating the fuel enthalpy based on the Jet-A fuel properties of Prof. Burcat [150]. Figure 54 shows the CEA model structure in the NPSS with its inputs and outputs. The efficiency in the model is set to 100%. The exit temperature is adjusted for user input efficiency by using equation (107) where η is the efficiency and $T_{out\ ideal}$ is the exit

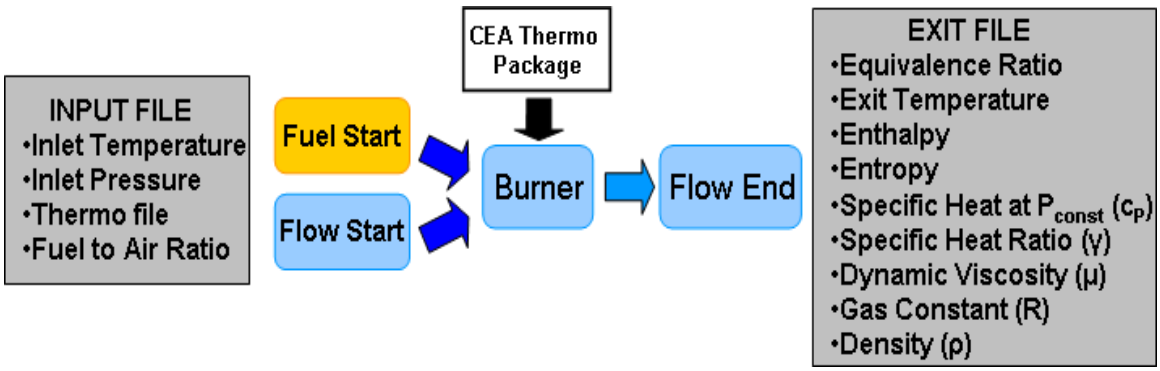

Figure 54: Structure of NPSS model to run CEA analysis

temperature at 100% efficiency.

$$T_{out\ \ actual} = (T_{out\ ideal} - T_{in})\eta + T_{in} \tag{107}$$

A file wrapper in the MODEL CENTER is created to read the inputs from the input file, run the NPSS CEA model and parses the outputs from the output file. The output CEA parameters required in the 1D flow-field model are the specific heat at constant pressure (c_P), specific heat ratio (γ), dynamic viscosity (μ) and mixture gas constant (R). The neural network methodology is selected as surrogate modeling technique due to this methodology's ability to capture possible model non-linearity. The next step is to create a set of training data to train the neural nets. To increase the surrogate models accuracy by reducing the inputs variability, two sets of training data are considered in this step. The first set is for cold flow with zero fuel (zero fuel to air ratio).

Table 15: Input range of training data for the CEA neural network models

Condition	Temperature Range (R)	Pressure Range(psi)	FAR Range	DOE Size
Reacting flow	500-2000	-	-	400
Cold flow	500-2000	14-420	0.05-.15	2000

Due to the lack of reaction, the mixture properties in the first set are independent of the pressure and the fuel to air ratio. The second set is created for the reacting mixture. Table 15 shows the range of input parameters and the training data size for both sets. The neural nets are trained for three cases. The first case is for cold-flow. The second set is for the burned-mixture. In the second case the burned mixture temperature is considered as an input in addition to the pressure and the fuel to air ratio; therefore, the burned mixture properties can be determined for a given temperature, pressure and fuel to air ratio. The third case is trained for the reacting-flow exit temperature as a function of the inlet temperature, pressure and fuel to air ratio. The MATLAB-based BRAINN software developed in the Aerospace Systems Design Laboratory is used to train static feed-forward neural net models with single hidden layer.

Table 16 shows the number of hidden nodes used for each neural net model to obtain the best accuracy. The next set of figures show the training results for cold and reacting-flow cases. The figures shows the error bar in percentage for training and testing data, residual versus neural net model predicted values and actual versus neural net model predicted values. Figure 56 and Figure 55 show the results for the specific heat at constant pressure, specific heat ratio, gas constant and dynamic viscosity for the cold flow case. A pattern is observed in the residual versus predicted pattern of specific heat at constant pressure. Sometimes these behaviors are the result of missing an input or dimension in the training or the result of the numerical accuracy of the solver. Looking at the percentage error range of c_P and γ (0.2% and 0.05%) in their histogram, one can realize that the model is very accurate and the pattern is not the result of the missing behavior. This behavior has not affected the model's predictive capability. Figure 57 and Figure 58 show the result for the same parameters for the reacting-flow case. Again the results show very good accuracy, although some pattern may be observed for the gas constant. Finally, Figure 59 shows the training result for the exit temperature. Again the result shows good accuracy.

Table 16: Number of hidden nodes of the CEA neural network models

Condition	C_P	γ	R	μ	T_{exit}
Reacting flow	25	10	10	10	18
Cold flow	5	5	5	5	-

7.2 Fuel Combustion Mechanism

A fuel combustion mechanism is needed for the finite-rate chemistry calculation in the CRN model. The important criteria for a good fuel combustion mechanism (besides being a realistic mechanism) are the execution time and convergence to the final solution. Four fuel combustion mechanisms are tried in this work. Three of them are detailed mechanisms as follows.

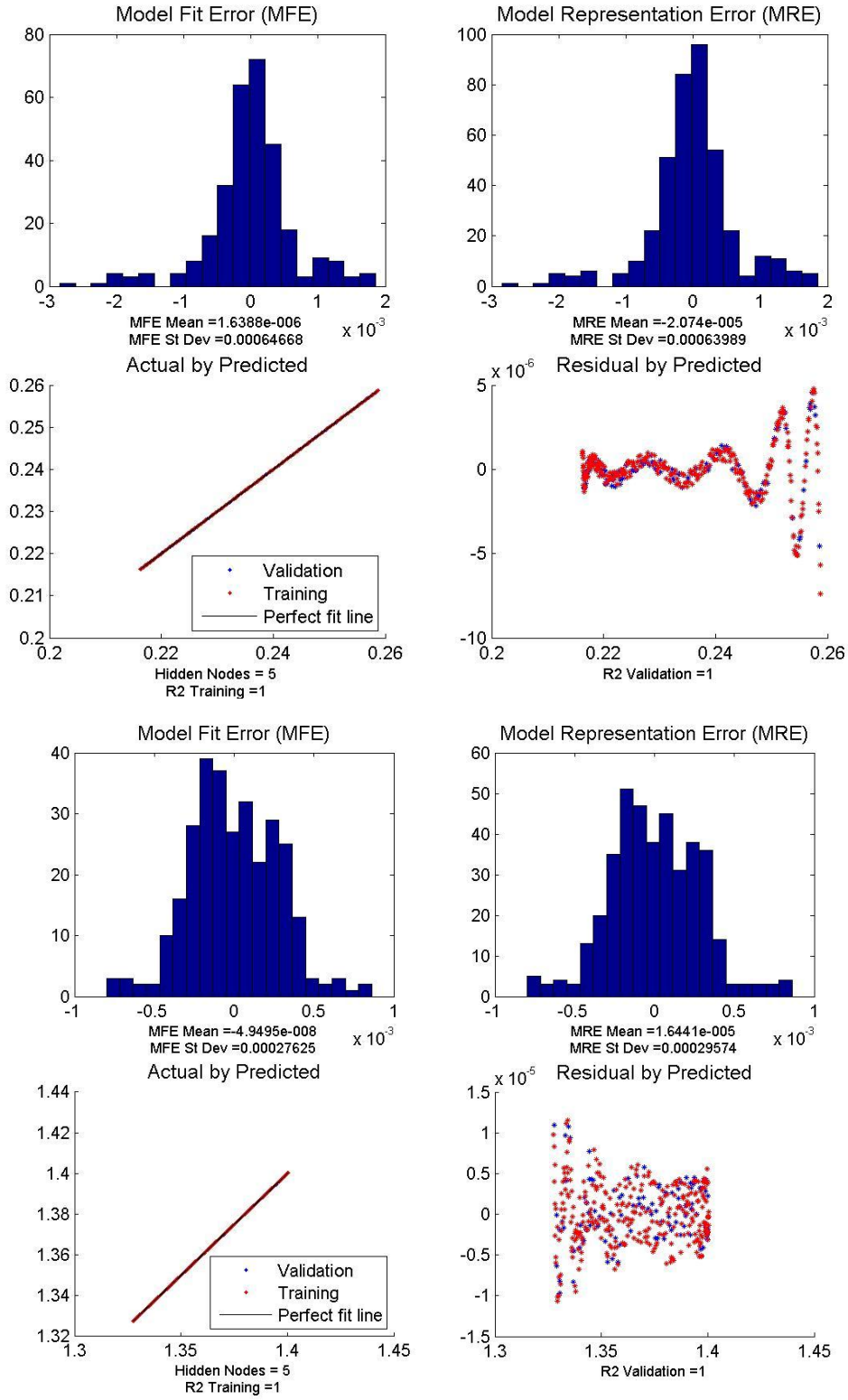

Figure 55: Cold flow neural net training results for c_p (top figure) and γ (bottom figure)

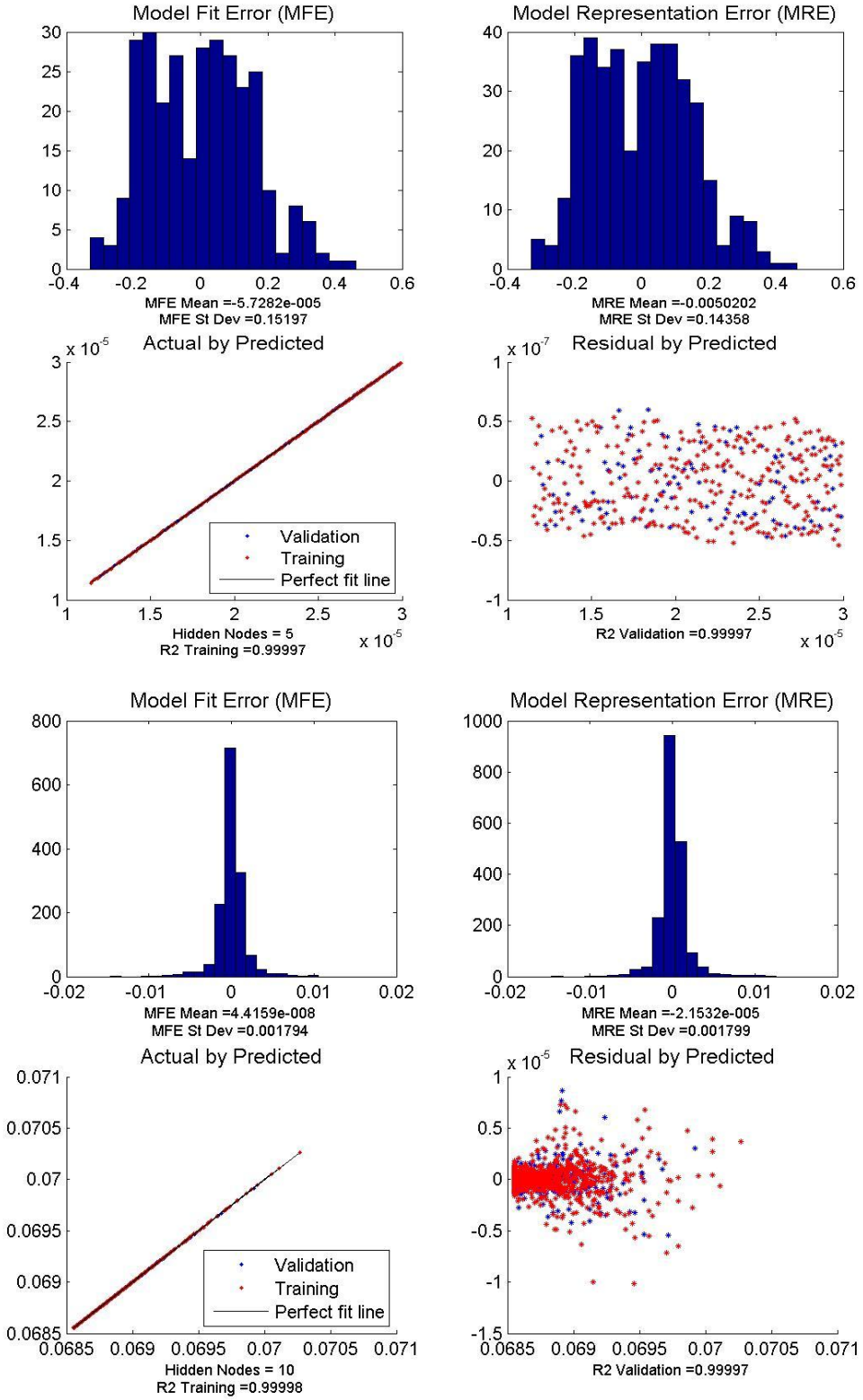

Figure 56: Cold flow neural net training results for μ (top figure) and R (bottom figure)

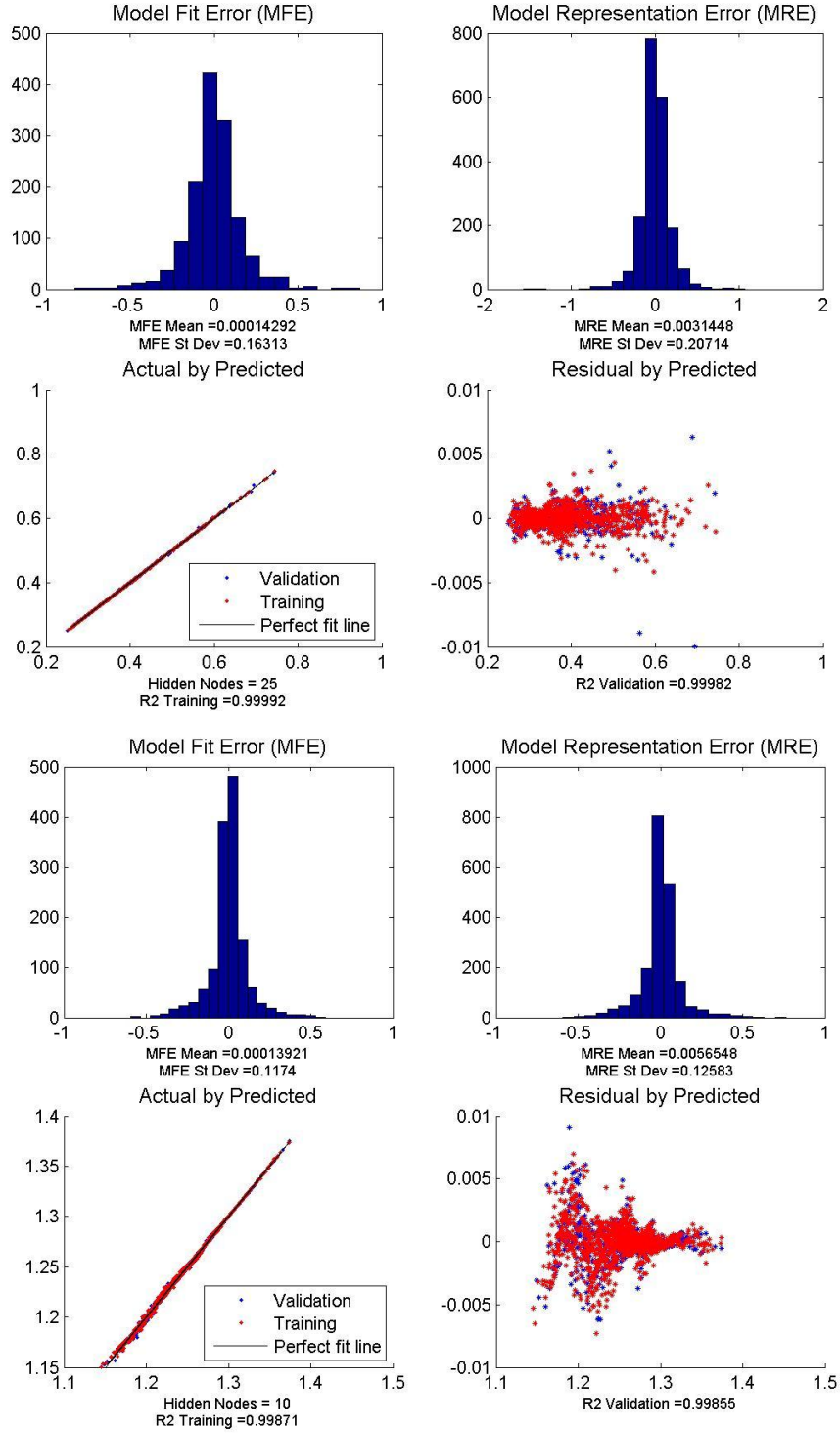

Figure 57: Reacting-Flow neural net training results for c_p (top figure) and γ (bottom figure)

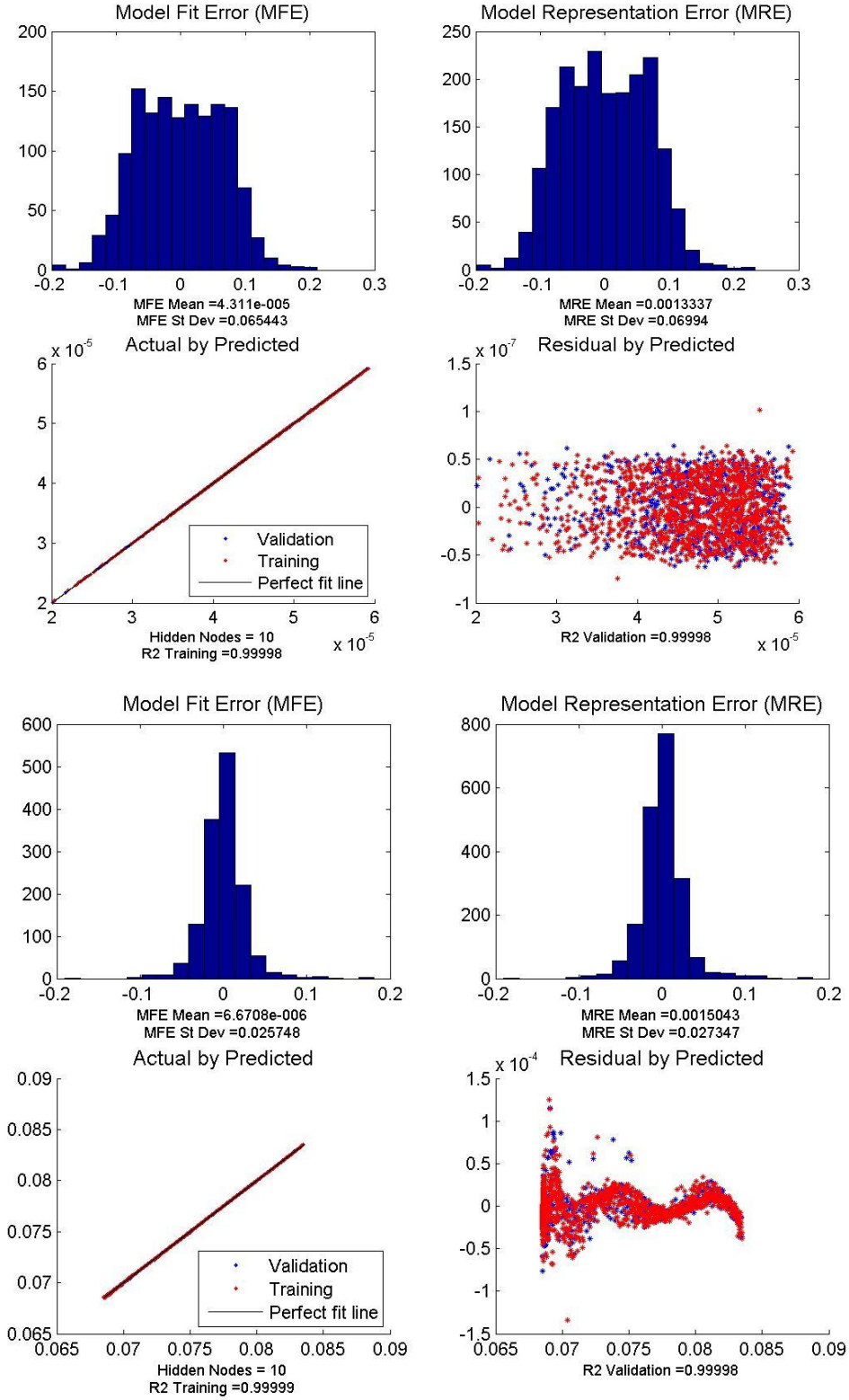

Figure 58: Reacting-Flow neural net training results for μ (top figure) and R (bottom figure)

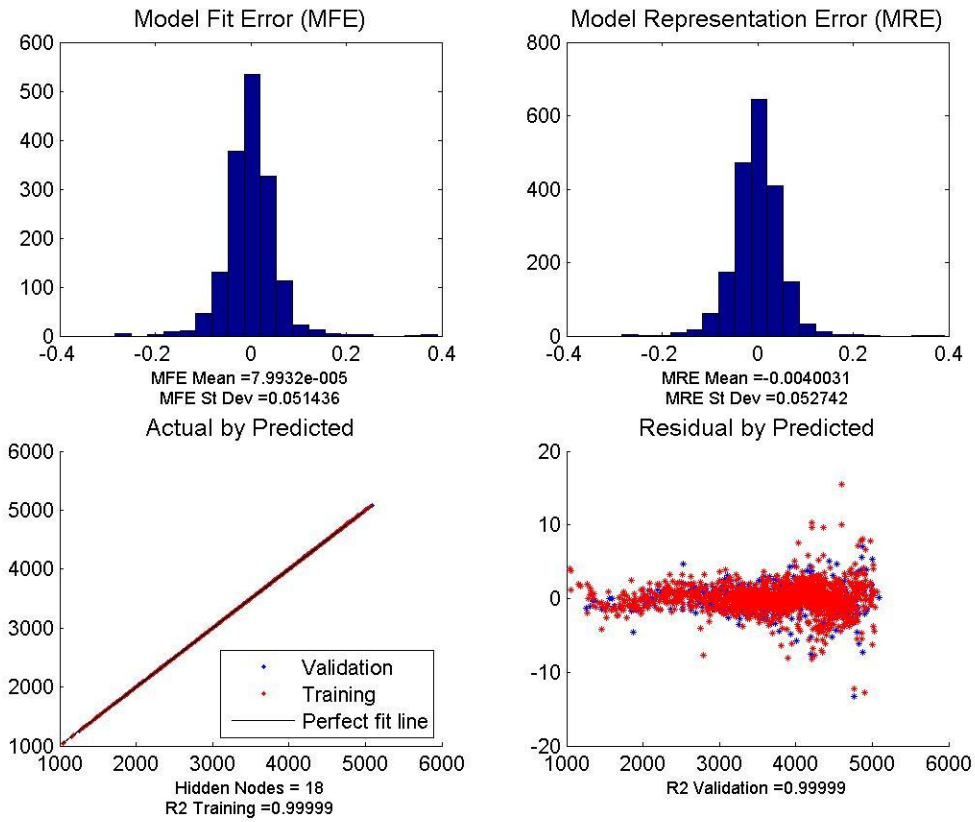

Figure 59: Reacting-Flow neural net training results for exit temperature

- The pressure-dependent Kyne combustion mechanism of n-decane ($C_{10}H_{22}$) [151] containing 63 species and 167 elementary reactions without NO_x formation sub-mechanism.
- The pressure-dependent Aachen combustion mechanism of decane ($C_{10}H_{22}$) containing 120 species and 527 elementary reactions without NO_x formation sub-mechanism [152].
- The combustion mechanism of n-decane containing 178 species and 1199 elementary reactions including the NO_x and aromatics formation sub-mechanisms [94-95].

Two of the above mechanisms do not contain the NO_x formation sub-mechanisms and they should be added to the main mechanisms manually which may introduce solution convergence issues as those sub-mechanisms are not specifically optimized for

the given mechanism. Unfortunately, the use of the above mechanisms resulted in a very long execution time even for a single PSR. Also, at some occasions, they did not converge to the final solution. An alternative mechanism is the simpler pressure-independent Kollrach mechanism (Figure 60), which is selected in this work [97]. This

STEP	REACTION	B_j	N_j	T_j
1.	$C_{12}H_{23} + O_2 \rightarrow 5C_2H_4 + C_2H_3 + O_2$	4.48	1.5	7900
2.	$C_{12}H_{23} + OH \rightarrow 6C_2H_4 + O$	7.3	1.0	4500
3.	$C_2H_4 + H \leftrightarrow C_2H_3 + H_2$	10.48	0.0	9500
4.	$H + H + M \leftrightarrow H_2 + M$	12.3	-1.0	0
5.	$O + O + M \leftrightarrow O_2 + M$	11.0	-1.0	0
6.	$H + OH + M \leftrightarrow H_2O + M$	13.85	-1.0	0
7.	$H + O_2 \leftrightarrow OH + O$	11.35	0.0	8400
8.	$O + H_2 \leftrightarrow OH + H$	10.24	0.0	4730
9.	$CO + OH \leftrightarrow CO_2 + H$	-14.75	7.0	-7000
10.	$H + H_2O \leftrightarrow OH + H_2$	10.92	0.0	10050
11.	$CH_3 + O_2 \leftrightarrow CH_2O + OH$	9.0	0.0	4000
12.	$HO_2 + M \leftrightarrow H + O_2 + M$	12.32	0.0	2300
13.	$HO_2 + H \leftrightarrow 2OH$	9.89	0.0	950
14.	$CH_2O + OH \leftrightarrow H_2O + HCO$	10.90	0.0	2120
15.	$O + H_2O \leftrightarrow 2OH$	10.76	0.0	9000
16.	$N_2 + O \leftrightarrow NO + N$	9.0	0.0	25000
17.	$N + O_2 \leftrightarrow NO + O$	5.0	1.0	2000
18.	$N + OH \leftrightarrow NO + H$	9.0	0.0	0
19.	$HCO + O_2 \leftrightarrow HO_2 + CO$	10.48	0.0	7000
20.	$HCO + OH \leftrightarrow H_2O + CO$	10.30	0.0	0
21.	$C_2H_4 + OH \leftrightarrow C_2H_3 + H_2O$	9.78	0.0	1750
22.	$CH_2O + HO_2 \leftrightarrow HCO + 2OH$	9.0	0.0	4500
23.	$C_2H_2 + HO_2 \leftrightarrow HCO + CH_2O$	9.3	0.0	5500
24.	$C_2H_3 + O_2 \leftrightarrow C_2H_2 + HO_2$	9.23	0.0	5000
25.	$NO + HO_2 \leftrightarrow NO_2 + OH$	3.0	1.0	0
26.	$C_2H_4 + O \leftrightarrow CH_3 + HCO$	9.93	0.0	1500
27.	$C_2H_4 + HO_2 \leftrightarrow CH_3 + HCO + OH$	9.9	0.0	5000
28.	$H_2 + CH_3 \leftrightarrow CH_4 + H$	7.0	-1.5	7140
29.	$C_2H_2 + OH \leftrightarrow CH_3 + CO$	8.2	0.0	2500
30.	$CH_3 + O \leftrightarrow CH_2O + H$	11.11	0.0	1000

Figure 60: Kollrack combustion mechanism for aviation fuel (Jet-A)

reduced mechanism is specifically written for Jet-A combustion ($C_{12}H_{23}$). The mechanism consists of 21 species and 30 reactions and contains the thermal NO_x formation sub-mechanism. The mechanism considers Pyrolysis and global reactions for converting the large Jet-A molecule ($C_{12}H_{23}$) to smaller molecules (C_2H_4 and C_2H_3) and elementary reactions converting the rest of C_2H_4 and C_2H_3 molecules to radicals and products [4, 9, 107, 153].

7.3 Experiment 1: Emissions Prediction of Single Annular Combustor

As mentioned before, first the proposed methodology will be applied to calculate the emission levels of a single annular combustor to test the parametric capability of the methodology. This experiment consists of two parts; and in each part an emission model is developed for a different SAC combustor. After the models are executed, the results are presented and discussed.

A general issue encountered in the first (and third) experiments when creating emission models is the limited amount of available information about combustors. Even if information is available, it is not inclusive enough.

7.3.1 Emission Model for the CFM56-7B27 Combustor

In this research the goal was to find as much information as possible from all public sources. To minimize the number of parameter estimations and eliminate the need to model the whole engine to determine the engine cycle parameters, the single annular combustor of CFM56-7B27 engine is selected. The engine is built by CFM International Company. This combustor is selected due to the availability of some data and reports in the public domain that can be used for this purpose. The emission data of the engine can be obtained from the ICAO engine emission database

The values of some parameters and characteristics in the CFM56-7B27 combustor are not completely known. Also some parameters have an unknown or complex relation

with known parameters in the combustor (i.e. geometry or emissions). An approach (similar to reverse engineering) is required to find the best value for this group of parameters. This approach should be based on estimating the unknown parameters of the combustor using available information and data about the geometry, engine cycle parameters, flow partitions and drawings. The approach for accomplishing this task is Monte Carlo filtering (MCF).

In Monte Carlo filtering, the emission model is executed for combination of inputs obtained by random sampling of inputs with defined range and uniform distribution. Then all the combinations that do not match the required criteria or violate the given constraints are filtered out. The criteria and constraints could be geometrical information and constraints, zone flow fractions and available emissions measurements (such as ICAO/LTO cycle data).

Another data related issue is the absence of the engine cycle parameters at the

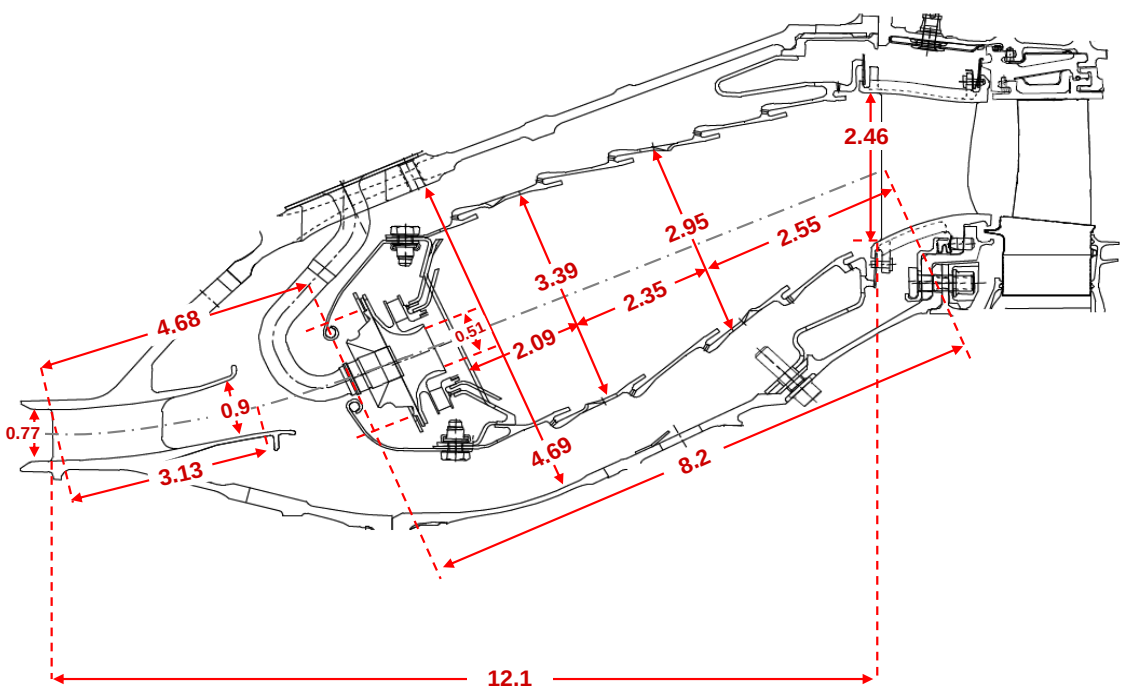

Figure 61: SAC combustor of the CFM56-7B27 engine with dimensions measured in inches [18, 22]

compressor exit; therefore, an engine model is needed to determine the flow parameters and flow path information at its compressor exit and turbine inlet stations. These parameters are available from an engine simulation that is performed in the EDS project for the CFM-56 engine. These parameters have been determined by modeling the engine in the numerical propulsion system simulation (NPSS) and WATE environments (Table 17).

Other parameters provided by the simulation are compressor exit and turbine inlet inner and outer radii, which are assumed to be equal to the combustor inlet and exit radii (neglecting the passages/manifolds that connect the compressor exit and turbine inlet to

Table 17: Cycle parameter values determined in EDS project for the CFM56-7B27

Cycle Parameter	Take-off	Climb	Approach	Idle
Inlet total pressure (atm)	28.62	24.451	11.173	5.52
Inlet total temperature (k)	800.53	763.84	612.63	504.96
Equivalence ratio	0.42	0.39	0.245	0.144
Air mass flow (kg/s)	44.524	39.099	20.870	12.115

Table 18: Measured geometrical information of the CFM56 SAC combustor

Geometrical characteristics	inch
Diffuser inlet mean radius	10.9
Diffuser length	4.68
Diffuser inlet height	0.77
Flat-wall diffuser exit height	0.9
Flat-wall diffuser length	2.19
Casing height	4.96
Injector diameter	0.25
PZ height	3.39
PZ length	2.09
SZ height	2.95
SZ length	2.35
DZ height	2.46
DZ length	2.55
Exit mean radius	13.65
Burner length	8.2
Combustor axial length	12.1

Table 19: Mean radius of compressor exit and turbine inlet of the CFM-56 engine

Station	Mean radius (in)
Inlet	10.86
Exit	34.67

the combustor inlet or exit). The burner length of CFM56 combustor is also available [18] to be equal to 8.2 inches. With this information and a drawing of the combustor [154] the dimensions of the combustor can be obtained by scaling it to its actual size. Figure 65 and Table 18 show the measured dimension of that drawing.

Based on the cycle parameters (Table 17) and diffuser inlet height and mean radius (Table 19), the diffuser area can be obtained and then from the following equation, the inlet Mach number is determined which is needed in the 1D flow-field model:

$$\frac{\dot{m}\sqrt{T_{tot}}}{P_{tot}.A} = \sqrt{\frac{\gamma}{R}} M \left(1 + \frac{\gamma - 1}{2} M^2\right)^{\frac{\gamma+1}{2(\gamma-1)}} \tag{108}$$

where:

$\dot{m}$: Mass flow-rate (kg/s)

T_{tot}: Total temperature (k)

P_{tot}: Total pressure (pa)

A: Cross section (m^2)

γ: Specific heat ratio

R: Air gas constant (287.05 J/kg.K)

Table 20: The CFM56 SAC diffuser inlet Mach number at four ICAO/LTO modes

Power setting	Inlet Mach number
Taxi (7%)	0.22
Approach (30%)	0.20
Climb (85%)	0.198
Take-off (100%)	0.198

M: Mach number

Table 20 shows the value of the diffuser inlet Mach number for the four power settings given in Table 17. The average value of 0.20 is selected for the diffuser inlet Mach number for all conditions.

The next step is to build the 1D flow-field and CRN model for the SAC type combustor. Figure 62 shows the 1D flow-field model and CRN built for the SAC model. They will be used along with the evaporation and mixing models. The 1D flow-field model consists of a diffuser model, primary zone model, and secondary zone and dilution zone models. The chemical reactors' network consists of a primary zone section with nine branches for the premixed flame and one for the diffusion flame. Whenever the entire fuel flow is vaporized, all ten branches are assigned to the premixed flame. All the outputs defined in Chapter 6 must be defined for this model to obtain the emission levels.

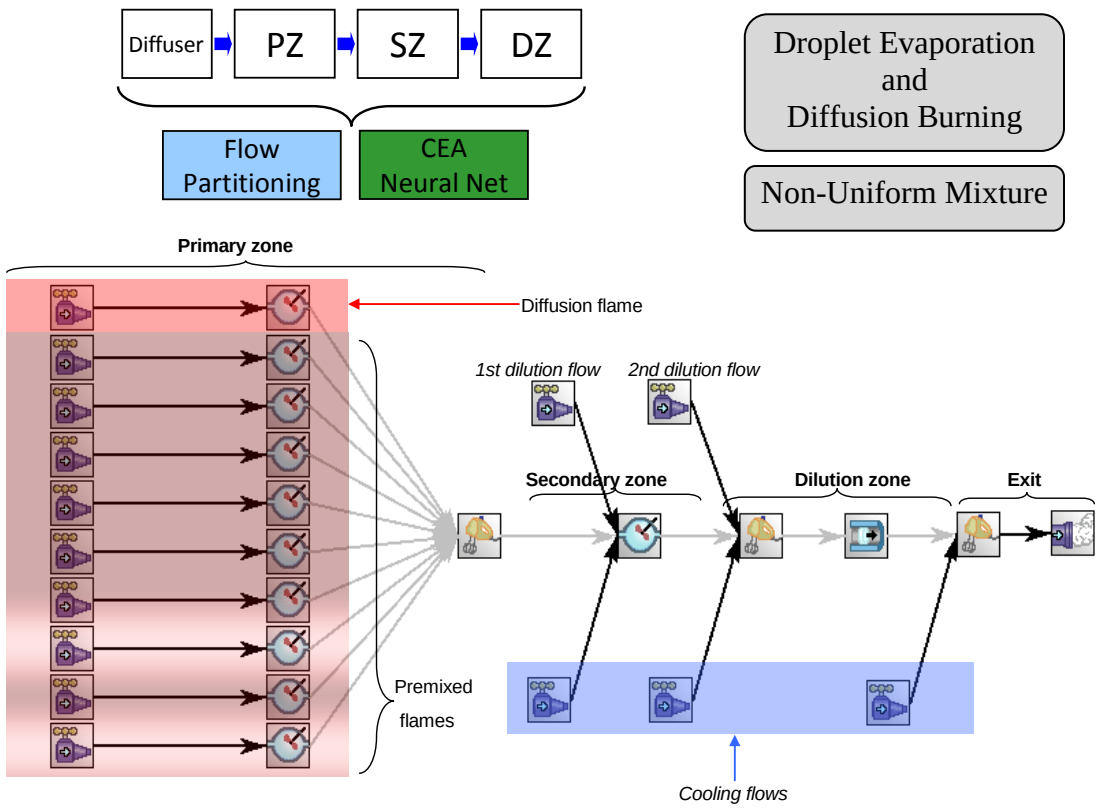

Figure 62: 1D flow-field and CRN models of a single annular combustor in the CHEMKIN

Some of these parameters are based on the information obtained from the literature [18, 84] and they are listed in Table 21; the other parameters must be determined through the Monte Carlo filtering process where a set of input combinations to the 1D flow-field model are determined to provide the same geometry and flow fractions as the available data.

Using Monte Carlo filtering does not mean that the chosen parameters are chosen randomly and they do not have any physical meaning. In this process, the input parameters are selected based on the available range appropriate for the application

Table 21: Known information and parameters of the CFM56 SAC

Component or Parameter	Type or Value
Diffuser type	Straight-wall + Dump
Diffuser passage number	1
Diffuser sweet-spot	1.6
Injector type	Simplex pressure swirl
Number of injectors	20
Injector flow number	1.0e-7 m^2
nozzle airflow/fuel airflow	0
swirler hub radius	0.25 in
Cooling mechanism	Film
Orifice number in the secondary zone	80
Orifice number in the dilution zone	120
Orifices flow coefficient	0.6
Max liner material temperature	2050 K

Table 22: The CFM56 SAC variables considered in the Monte Carlo filtering for geometry matching

Variable Name	Range
Mach liner	0.012-0.022
Mach 32	0.035-0.05
K_{sw}	1.0-2.0
swirl angle	58-66
φ_{PZ}	1.0-1.09
φ_{SZ}	0.60-0.8
$\Delta P/P$ burner	0.04-0.08
SZ jet penetration ratio	0.4-0.6

or around a mean value. Before running MCF, trial and error is performed to find input values to provide outputs inside the constraints. Then the ranges are created and MCS is performed.

A 1000 sample Latin hypercube design is created to perform the MCF process. The MCF sample space is based on the Latin hypercube space filling DOE in which the inputs values are sampled uniformly from the ranges defined in Table 22. After all the points are executed in the sample space, the results must be filtered to find the points that satisfy the geometrical constrains (given information about heights and lengths). Since the secondary zone equivalence ratio value is not known, an additional constraint is considered in the model, which is the number of the secondary zone orifices (80). To achieve that number, both the secondary zone equivalence ratio and the secondary zone jet penetration ratio are considered as inputs in the MCF.

The top picture in Figure 63 shows the scatter plot matrix of inputs and responses (constraints) generated in JMP software. In the same figure, the bottom picture shows the list of constraints considered in the MCF. By incrementally narrowing down the range of the constraints, more of the points that violate the constraints are filtered. The process to narrow down the range continues until a handful of cases remain or the range of variation of constraints is narrowed down to a desired interval. The right set of input combinations that give the correct size of the combustor components can be obtained from the combinations that that do not violate the constraints. Sometime it is not possible to match all the constraints and size due to the modeling fidelity or some unknown design logics that are not considered in the model (combustor zone length etc.).

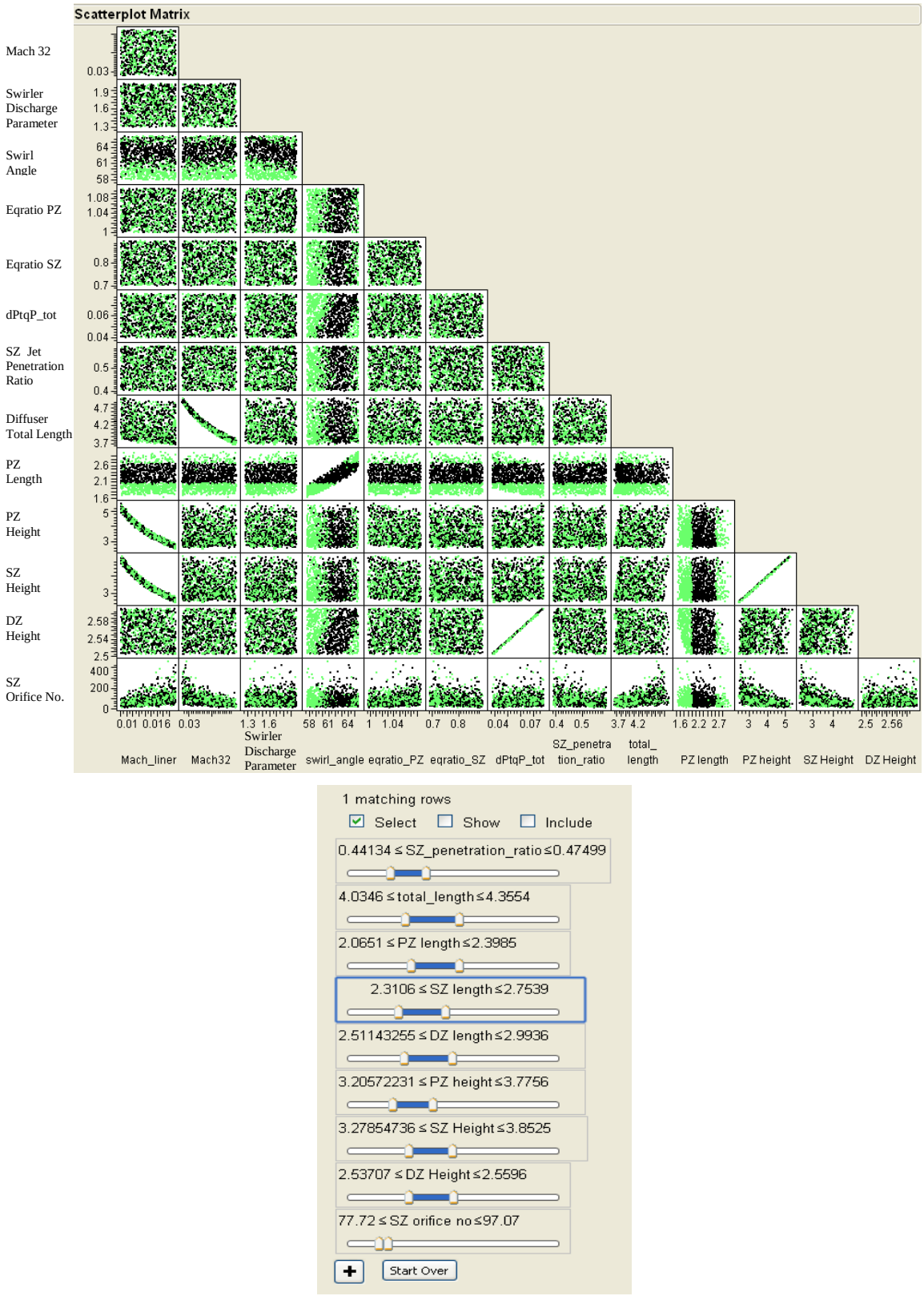

Figure 63: Scatter plot matrix of inputs and outputs of the CFM-56 SAC 1D flow-field model (top figure) and MCF (bottom figure) in JMP

Some parameters such as secondary zone or dilution zone length ratios or dilution zone jet penetrations are not considered in the MCF because there is a one-to-one correlation between these ratios and some of the constraints (number of holes, etc) and they can be tuned manually. Figure 63 shows the MCF environment in JMP software and the selected values for the inputs after the filtering process.

Table 24 shows the final set of inputs for the 1D internal flow-field model that provides almost the same geometry as the CFM56 measured geometries.

Table 23: Filtered set of inputs of the CFM56 SAC 1D flow-field model determined from MCF for geometry matching

Variable Name	MCF Result
Mach liner	0.0149
Mach 32	0.041
K_{sw}	1.48
swirl angle	61.70
φ_{PZ}	1.05
φ_{SZ}	0.8
$\Delta P/P$	0.0504
SZ jet penetration ratio	0.460

Table 24: Final set of inputs of the CFM56 SAC 1D flow-field model

1D Flow-Field Input	Unit	Value
Inlet mean radius	in	10.86
Exit mean radius	in	13.56
Number of injectors	-	20
$T_{Max\ Liner}$	R	2050
Cooling mech. factor	-	0.067
$\Delta P/P$ burner	-	5%
Mach 32	-	0.040
Diffuser half angle	degree	3.5
Diffuser sweet-spot	-	1.6
Diffuser passage no.	-	1
Mach liner	-	0.0149
Swirl angle	degree	61.9
K_{sw}	-	1.48
Swirler hub radius	in	0.25

1D Flow-Field Input	Unit	Value
Injector air/fuel flow	-	0
φ_{PZ}	-	1.05
φ_{SZ}	-	0.8
η_{PZ}	-	98%
η_{SZ}	-	98.7%
η_{DZ}	-	99.9%
$c_{d\ SZ}$ and $c_{d\ DZ}$	-	0.6
Mach 40	-	0.075
SZ length ratio	-	0.7
DZ length ratio	-	0.78
SZ Jet penetration Ratio	-	0.46
DZ jet penetration ratio	-	0.33

Table 25 shows the measured and predicted values of the CFM56 model. Figure 64 shows the two dimensional drawing of the CFM56 produced by the 1D flow-field model and its actual drawing. Now that all the 1D flow-field model inputs are determined and they match the actual data, the next step is to determine the right values in the Droplet Evaporation/Diffusion Burning model and the Non-Uniform Mixture model through another Monte Carlo simulation based on the given emission data. Not too many parameters are user inputs in these models. Many are physical properties of the fuel obtained from the reports [139]. The user-defined parameters are as follows: 1) the Rosin-Rammler shape factor (*q)*, 2) fuel temperature, 3) the unmixedness parameter (*S)* and, 4) the cooling fractions in each zone. Due to the lack of knowledge about the distribution form of the inputs, the uniform distribution is considered for the inputs in the MCS process.

As mentioned earlier, the unmixedness parameter acts like a lumped parameter that takes into account every unknown effect and its value should be defined at this point. In addition, because no physics-based model is provided for the zone's cooling fractions due to the fidelity of the current methodology, cooling fraction at each zone is

Table 25: Comparison of the model predicted and actual geometrical data of the CFM56 SAC

Parameter	Predicted Data	Measured Data
Combustor axial length	12.22	12.12
Burner length	8.33	8.21
Diffuser length	4.14	4.68
Primary zone length	2.21	2.09
Secondary zone length	2.44	2.35
Dilution zone length	2.61	2.55
Primary zone height	3.49	3.39
Secondary zone height	3.35	2.95
Dilution zone height	2.52	2.46
Secondary zone orifice no.	80	80
Dilution zone orifice no.	119	120
Casing height	4.59	4.96

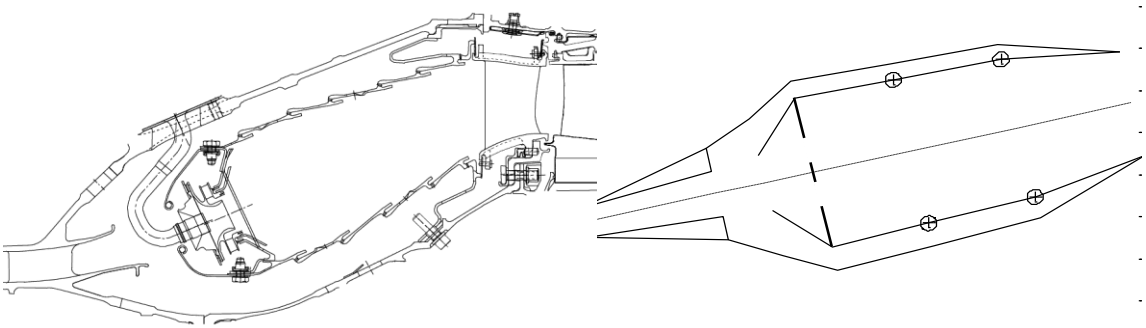

Figure 64: The CFM-56 SAC actual and 1D flow-field model drawings

an unknown parameter that should be provided to the model as an input. The objective at this point is to tune these parameters to match them to the given emission data. The goal is to validate the model by determining the value of the cooling fractions and the unmixedness degree at different power settings and to study whether they follow the physical understanding of the phenomena inside the combustor or the published data [9]. The general steps taken in the Monte Carlo simulation are similar to the MCF process described in the previous part. A set of 500 points at each power setting is performed to find the right value for unmixedness and cooling fractions. Table 26 shows the selected range for the inputs. The cooling flow ranges are based on the experience and knowledge obtained by running the model.

Table 26: Considered range of unmixedness degree and cooling flow fractions for the CFM-56 SAC model in the Monte Carlo simulation

Parameter	Take-off		Climb		Approach		Idle	
	min.	max.	min.	max.	min.	max.	min.	max.
Unmixedness degree	0.1	0.9	0.1	0.9	0.1	0.9	0.1	0.9
q (Rosin-Rammler factor)	1.8	3.0	1.8	3.0	1.8	3.0	1.8	3.0
Fuel temperature	540	558	540	558	540	558	540	558
PZ cooling fraction	0%	30%	0%	30%	0%	20%	0%	10%
SZ cooling fraction	30%	60%	30%	60%	20%	60%	10%	60%

Table 27 shows the obtained value for the unmixedness degree and cooling fractions that provide the best answer when they are compared to the published data of the NO_X and CO emission indices of the CFM56-7B27 for the ICAO/LTO cycle. Using

Table 27: The CFM-56 SAC final set of unmixedness degree and cooling flow fractions

Parameter	Take-off	Climb	Approach	Idle
Unmixedness degree	0.18	0.27	0.844	0.66
q (Rosin-Rammler shape factor)	2.6	2.57	2.56	2.46
Fuel temperature	557	555	549.3	540
PZ cooling fraction	14%	15%	3%	0%
SZ cooling fraction	56%	44%	44%	55%
DZ cooling fraction	30%	41%	53%	45%

values obtained from the MCS, the emission model is executed again to compare its outputs to the ICAO data. In the table the Rosin-Rammler shape factor (q) has a small variation around 2.5. Another observation is the increase of the fuel temperature from low power to high power conditions which is in line with the expectation that as the power setting goes up the fuel temperature entering the combustor goes up too. Finally looking at the cooling fraction that mixes in the primary zone, it can be seen that from the low power to the high power settings, more of the cooling flow is mixed with the core flow.

Table 28 shows the output values obtained using the filtered inputs and their comparison to the actual ICAO emission indices.

The first experiment is performed to demonstrate the model predictability. To test the parametric capability of the model in second part of the first experiment (secondary experiment) the methodology (and the same SAC model) will be applied to a different combustor in the SAC category which is the single annular combustor

Table 28: The CFM-56 SAC predicted emission indices using parameters obtained from the Monte Carlo simulation

Parameter	Take-off	Climb	Approach	Idle
EI NO_x predicted	29.7	23.31	10.61	6.9
EI NO_x actual	30.9	23.7	11	4.8
EI CO predicted	0.41	0.292	0.26	12.77
EI CO actual	0.2	0.5	1.4	17.7

Energy Efficient Engine. At the end, the results of the CFM56 SAC and E^3 SAC emission models are provided and discussed.

7.3.2 Emission Model for the Energy Efficient Engine Combustor

The secondary experiment tests the general predictability of the model as well as its parametric capabilities by applying it to the combustor of the E^3 engine which is a single annular combustor. Information is available about the E^3 single annular combustor in the public domain [18, 20, 25]. Although the available information about the E^3 SAC is comparable or even more than the CFM56 SAC combustor's, the experimental nature of the combustor has made some of its features, definition and parameters vaguely defined. The emissions data published for the E^3 SAC is also based on the sector or full-scale rig tests and not based on the actual operating engine. For that reason, the emission model for the SAC E^3 is selected as the secondary experiment and not the primary experiment.

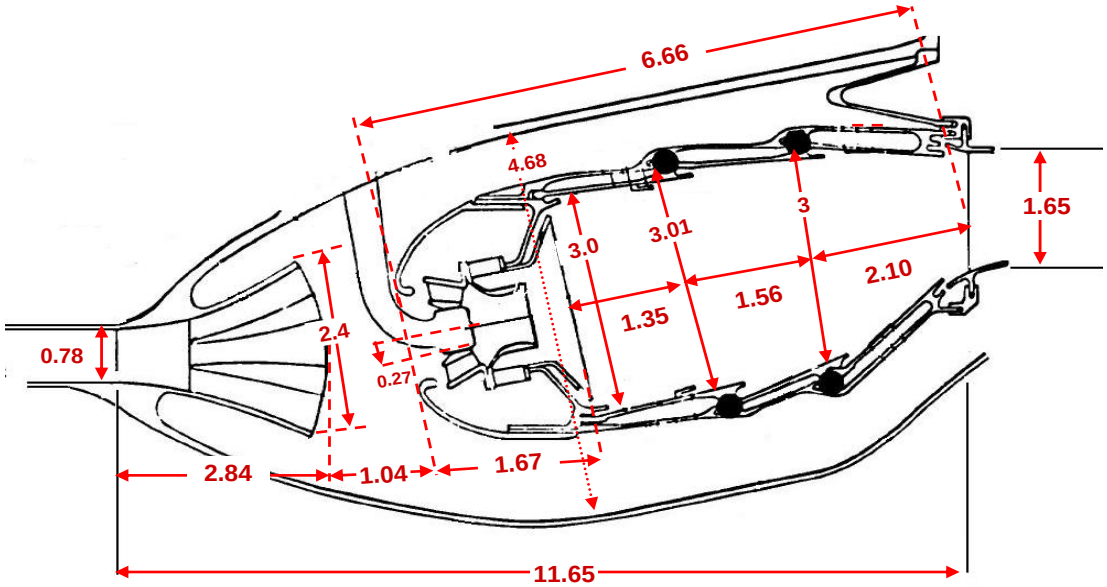

Figure 65: SAC combustor of the E^3 with dimensions measured in inches [20]

Table 29: Measured or published geometrical information of the E^3 SAC

Geometrical characteristics	inch
Diffuser inlet mean radius	11.16
Diffuser length	4.68
Diffuser inlet height	3.88
Flat-wall diffuser length	2.84
Casing height	4.68
Injector diameter	0.27
PZ height	3.01
PZ length	1.35
SZ height	3.00
SZ length	1.56
DZ height	1.65
DZ length	2.10
Exit mean radius	13.17
Burner length	6.66
Combustor axial length	11.65
Turbine exit mean radius	13.17

Since all the procedures used in the CFM56 model are repeated for the E^3 combustor, some of them are briefly recalled here.

The procedure starts with finding the combustor's dimensions. The dimensions of the combustor are obtained by scaling the two-dimensional drawing of the combustor is [154] to actual size. Figure 65 and Table 29 show the measured dimensions of the drawing.

The inlet Mach number is determined using the same method described in the previous experiment using equation (108). Table 31 shows diffuser inlet Mach numbers

Table 30: The E^3 cycle parameter values [18]

Cycle Parameter	Take-off	Climb	Approach	Idle
Inlet total pressure (atm)	29.8	25.91	11.67	3.93
Inlet total temperature (k)	1465.2	1139.4	914.4	860.4
Equivalence ratio	0.36	0.32	0.21	0.20
Air mass-flow (kg/s)	54.9	49.1	25.6	9.0

Table 31: The E^3 SAC diffuser inlet Mach number at four ICAO/LTO modes

Power setting	Inlet Mach number
Taxi (7%)	0.22
Approach (30%)	0.23
Climb out (85%)	0.23
Take-off (100%)	0.22

for the four power settings given in Table 30. The average value of 0.22 is selected for the diffuser inlet Mach number for all conditions.

The same 1D flow-field and CRN models used in the CFM-56 are used here too. The known parameters from the literature [18, 84] are listed in Table 32 and the other parameters are determined through the Monte Carlo filtering.

Monte Carlo filtering similar to the one performed for the CFM-56 is performed

Table 32: Known information and parameters of the E^3 SAC

Parameter or Component	Value or Type
Diffuser type	Straight-wall + Dump
Diffuser passage number	3
Diffuser sweet-spot	2.4
Injector type	Simplex Pressure Swirl
Number of injectors	20
Injector flow number	1.0e-7 m^2
Nozzle airflow/fuel airflow	0
swirler hub radius	0.27 in
Cooling mechanism	Film
Orifice number in the secondary zone	80
Orifice number in the dilution zone	120
Orifices flow coefficient	0.6
Max liner material temperature	2200 K
PZ flow fraction	32.7%
SZ flow fraction	17.9%
DZ flow fraction	27.8%
Cooling flow fraction	21.6%
$\Delta P/P$ burner	4.6%

to find the unknown parameters that provide the geometrical and flow fraction data as the ones given in the report. Additional constraints for the flow-field are considered in the MCF. The uniform distribution is considered for the inputs in the MCF process. The secondary zone equivalence ratio can be obtained from the flow fraction at the secondary zone. Table 33 shows the input variable and the range used in the MCF.

Table 33: The E^3 SAC variables considered in the MCF for geometry matching

Variable Name	Range
Mach liner	0.012-0.022
Mach 32	0.035-0.05
K_{sw}	1-2.0
Swirl angle	50-60
φ_{PZ}	1.0-1.09
φ_{SZ}	0.60-0.8

Figure 66 shows the scatter plot matrix of the inputs and constraints and the filtering environment in JMP software. The filtered input values as a result of the MCF are shown in Table 34.

Table 35 shows the final set of inputs for the 1D internal flow-field model that provides the results shown in Table 36 along with the known data. A difference can be seen between the predicted and actual data in Table 36 for combustor axial length and casing height. The difference comes from the fact that some features in the snout section cannot be simply modeled by the 1D flow-field model. The height of the casing can also be modeled based on some different criteria than what used here, which is the maximum

Table 34: Filtered set of inputs of the E^3 SAC 1D flow-field model determined from MCF for geometry matching

Variable Name	MCF Result
Mach liner	0.017
Mach 32	0.037
K_{sw}	1. 42
Swirl angle	52.2
φ_{PZ}	1.07
φ_{SZ}	0.71

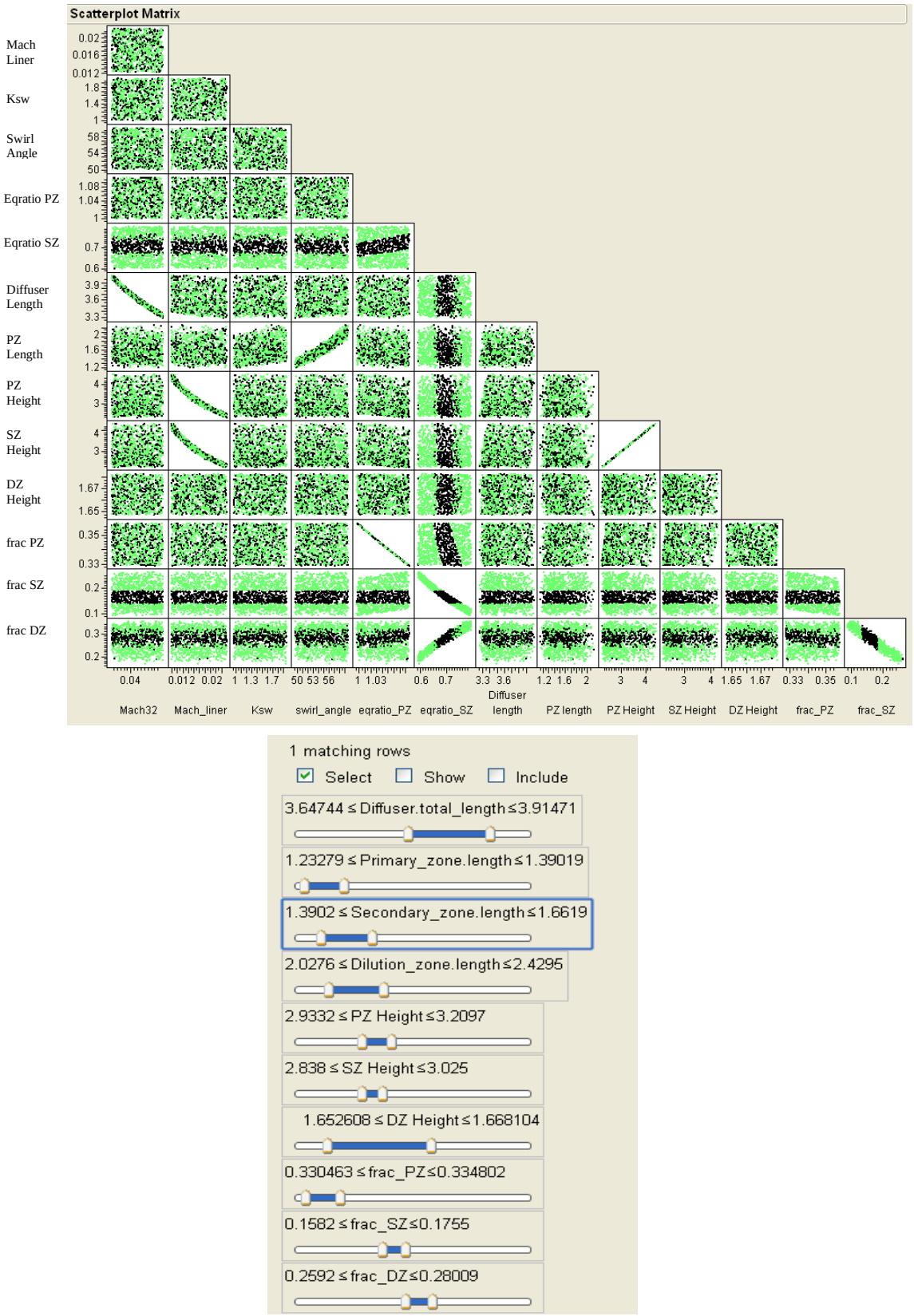

Figure 66: The E^3 SAC 1D flow-field scatter plot matrix (top figure) and MCF (bottom figure) in the JMP

penetration of the dilution jet in the secondary zone (equations (66) and (68)). The two-dimensional drawing of the E^3 SAC combustor produced by the 1D flow-field model and the actual drawing next to it are shown in Figure 67.

Table 35: Final set of inputs of the E^3 SAC 1D flow-field model

Input	Unit	Value
Inlet mean radius	in	11.16
Exit mean radius	in	13.17
Nozzle number	-	20
$T_{max\ \ Liner}$	R	2200
Cooling mech. factor	-	0.067
$\Delta P/P$ burner	-	4.6%
Mach 32	-	0.043
Diffuser half angle	degree	3.5
Diffuser sweet-spot	-	2.4
Diffuser passage no.	-	3
Mach liner	-	0.017
Swirl angle	degree	52.2
K_{sw}	-	1.42
Swirler hub radius	in	0.27

Input	Unit	Value
Injector air/fuel flow	-	0
φ_{PZ}	-	1.07
φ_{SZ}	-	0.71
η_{PZ}	-	97%
η_{SZ}	-	98%
η_{DZ}	-	99.9%
$c_{d\ SZ}$ and $c_{d\ DZ}$	-	0.6
Mach 40	-	0.13
SZ length ratio	-	0.55
DZ length ratio	-	0.80
SZ jet penetration Ratio	-	0.65
DZ jet penetration ratio	-	0.46

Table 36: Comparison of the model predicted and actual geometrical data of the E^3 SAC

Parameter	Predicted Data	Measured Data
Combustor axial length	9.37	11.65
Burner length	5.25	5.87
Diffuser length	3.86	3.88
Primary zone length	1.38	1.35
Secondary zone length	1.62	1.56
Dilution zone length	2.28	2.10
Primary zone height	2.95	3.01
Secondary zone height	2.85	3.0
Dilution zone height	1.66	1.65
Secondary zone orifice no.	79	80
Dilution zone orifice no.	118	120
Casing height	3.97	4.68

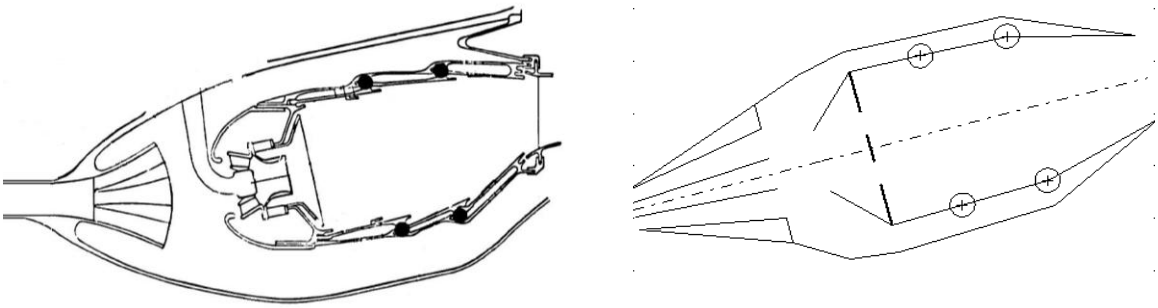

Figure 67: The E^3 actual and 1D flow-field model drawings

Similar to the CFM56 SAC, a Monte Carlo simulation is performed to find the combination of unmixedness degree, fuel temperature and Rosin-Rammler shape factor (q) that gives the same value of emissions as the actual ones. Table 37 shows the range of the mentioned parameters used in the Monte Carlo simulation. The range of the variation of the Rosin-Rammler shape factor (q) is narrowed down based on the results of the CFM56 in the previous experiment. Like the previous MCS process, the uniform distribution is considered for all the inputs.

Table 37: Considered range of unmixedness degree and cooling flow fractions for the E^3 SAC model in Monte Carlo filtering

Parameter	Take-off		Climb		Approach		Idle	
	min.	max.	min.	max.	min.	max.	min.	max.
Unmixedness Degree	0.1	0.9	0.1	0.9	0.1	0.9	0.1	0.9
q (Rosin-Rammler)	2.4	2.6	2.4	2.6	2.4	2.6	2.4	2.6
Fuel temperature	540	558	540	558	540	558	540	558
PZ cooling fraction	0%	30%	0%	30%	0%	20%	0%	10%
SZ cooling fraction	30%	60%	30%	60%	20%	60%	10%	60%

Table 38 shows the MCF result for the unmixedness degree, Rosin-Rammler shape factor (q), fuel temperature and cooling fractions and the comparison of the emission indices predicted based on the MCF result next to the published data. A good degree of accuracy can be seen between the predicted and measured values. The application of the emissions prediction model to the E^3 combustor shows the parametric capability of the model to capture the emission of different combustors.

Table 38: E^3 SAC final set of unmixedness degree and cooling flow fractions

Parameter	Take-off	Climb	Approach	Idle
Unmixedness Degree	0.23	0.4	0.82	0.21
q (Rosin-Rammler shape factor)	2.5	2.5	2.51	2.49
Fuel Temperature	554	551	547	545
PZ cooling fraction	20%	22%	15%	4%
SZ cooling fraction	49%	50%	51%	51%
DZ cooling fraction	31%	28%	34%	45%

Table 39: E^3 SAC predicted emission levels using parameters that are obtained from the Monte Carlo simulation

Parameter	Take-off	Climb	Approach	Idle
EI NO_x predicted	20.85	18.49	9.04	4.04
EI CO predicted	0.31	0.34	0.56	22.1
EI NO_x actual	21.92	18.39	11.96	4.00
EI CO actual	0.15	0.53	4.7	27

In the next step, all the obtained parameters are put together and the emission model is executed for the CFM56 and E^3 combustors and the results and discussion are provided.

7.3.3 SAC Emission Model Results and Discussion

The SAC emission model is executed for the CFM56 and E^3 combustors using the inputs obtained from the MCF or published data. A comprehensive list of model outputs for both combustors is given in Appendix C.

Figure 68 shows the cooling flow distribution between the primary, secondary and dilution zones obtained from the Monte Carlo filtering. At high power settings, there is more cooling flow mixed in the primary zone and this amount decreases to a small fraction at the idle power setting. The cooling flow mixed in the secondary zone is unchanged and finally the rest of the cooling flow goes to the dilution zone. Figure 69 shows the cooling flow distribution obtained from the Monte Carlo filtering for the E^3

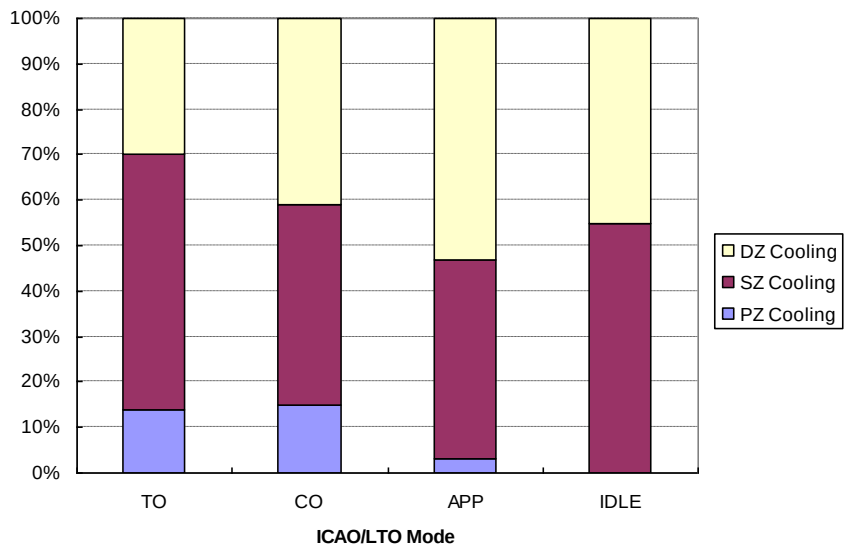

Figure 68: The CFM56 SAC cooling flow budget

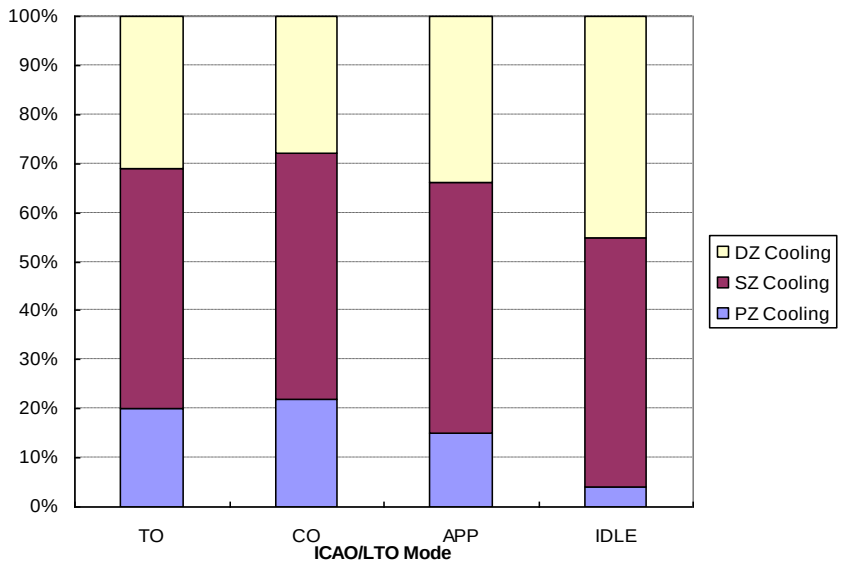

Figure 69: The E^3 SAC cooling flow budget

SAC. The figure shows the similar pattern observed in the CFM56 SAC cooling flow budget in Figure 68.

Figure 70 to Figure 73 show the values of the NO_x and CO emission index versus the engine power setting for the CFM56 and E^3 SACs. As an initial investigation of the effect of the droplet evaporation and non-uniform mixture on the emission levels, additional runs are performed where one or both models are deactivated in the emission model executions and the results are plotted in the same figures. They show the value of

the NO_x and CO emission index versus the engine power setting for: 1) the complete model and, 2) the model in which NUM or both DEDB and NUM are deactivated.

The EI NO_x prediction of both combustors (Figure 70 Figure 71) shows good match with the actual data. These values are obtained based on the unmixedness degree values that are obtained from the Monte Carlo simulation. As it will be shown later, the pattern of the unmixedness degree versus power setting is similar for two combustors under study. The figures demonstrate the ability of the model to capture the emissions of two combustors with different EI NO_x levels. There is an over-prediction in the idle condition of the E^3 combustor which could be due to the fact that the ignition delay temperature (equation (81)) is linked to the bulk primary zone temperature and not local temperature values. In reality, the temperature term in that equation is not a constant term. An interesting behavior can be observed by looking at the EI NO_x prediction for the complete emission model and the model without DEDB or NUM model. At low power, droplet evaporation has a greater contribution than mixture non-uniformity. Moving to higher power levels, the contribution of droplet evaporation decreases and mixture non-uniformity becomes important. At take-off, the contribution of droplet evaporation is minimal and mixture non-uniformity becomes the important contributor.

The EI CO predictions (Figure 72 and Figure 73) are not as good as the EI NO_x predictions. Although the model captures the right physics, the values are either very sensitive to the input parameters which produces a big variability or have little sensitivity. The variability of the EI CO to input parameters at the idle condition is not unexpected as the exponential change of the EI CO level and its high sensitivity to parameters is mentioned in a number of publications. This variability can also be seen as another validation of the methodology that shows the model captures the correct physics of CO emission. Explaining the change in the EI CO level by removing droplet evaporation and non-uniform mixture is harder and more uncertain due to the high sensitivity of the EI CO to input parameters and its low level of accuracy. At high power settings, the EI CO

level is very low and any variation is in the uncertainty or accuracy range of the model. However, at the low power setting of idle in the CFM56, removing either one of the DEDB or NUM model lowers the EI CO level. This is due to the low equivalence ratio of the primary zone of the CFM56 combustor at idle. In general, the source of CO production in the low power setting is the local zones of the high temperature region produced by either droplet diffusion burning or non-uniform mixture. Due to the existence of the cooler regions around these high temperature zones, the CO to CO_2 conversion is quenched. In addition, local flames in low equivalence ratio regions become extinct before CO is converted to CO_2. In the CFM-56, removing either one of the DEDB or NUM model removes every local hot region that is the source of the CO and the quenching effect of the CO to CO_2 process is not a dominant anymore. In the CRN model, some of the PSR branches in the primary zone are the same as the local high temperature regions mentioned above.

Removal of DEDB or NUM models in the E^3 combustor does not create the same trend of CO level at idle condition as it did in the CFM56 combustor. Since the idle primary zone equivalence ratio in the E^3 combustor (0.62) is higher than the one in the CFM56 (0.36), the variation of CO level due to the removal of DEDB or NUM model is less obvious.

Looking at the EI CO, one can see that at the take-off condition, the EI CO level slightly increases in the CFM-56 model's results. The high temperature region and lack of enough oxygen at high power, causes the EI CO level to increase again. This behavior is addressed in the variation of the EI CO versus the temperature or equivalence ratio in other publications as well [4, 7].

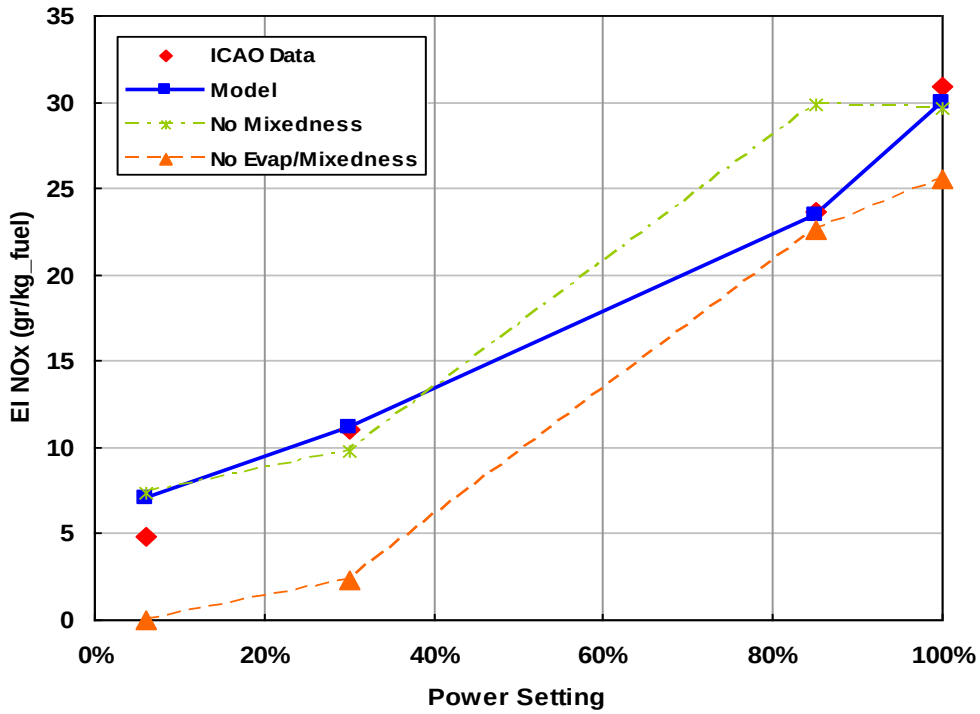

Figure 70: Predicted and actual NO_x emission indices of the CFM56 SAC

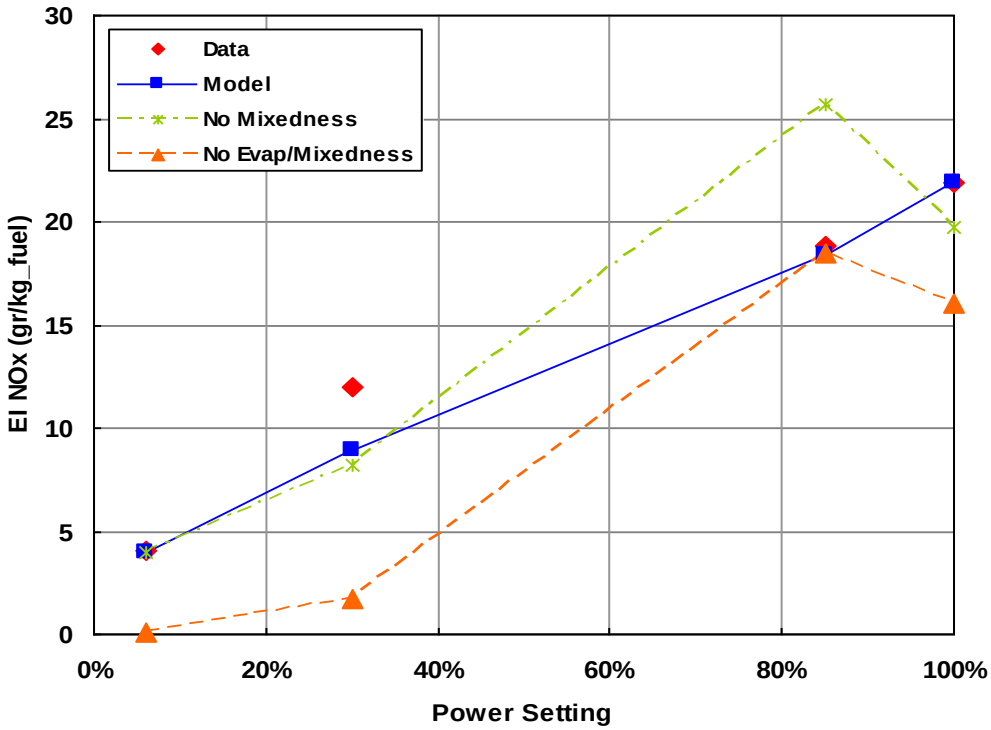

Figure 71: Predicted and actual NO_x emission indices of the E^3 SAC

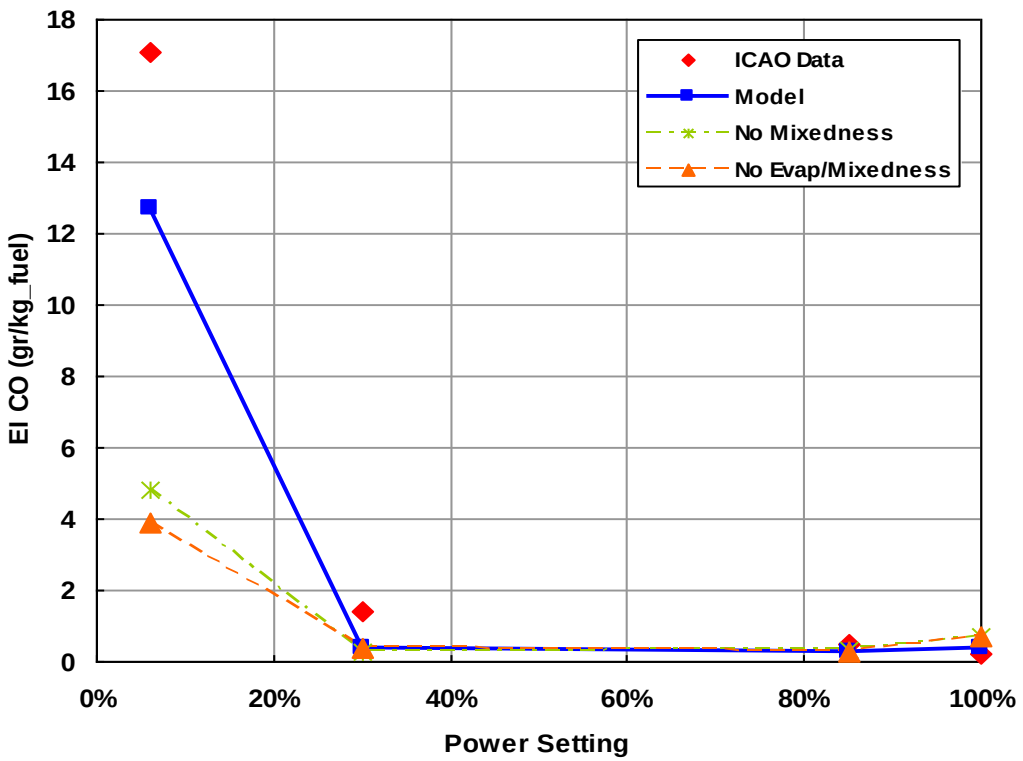

Figure 72: Predicted and actual CO emission indices of the CFM56 SAC

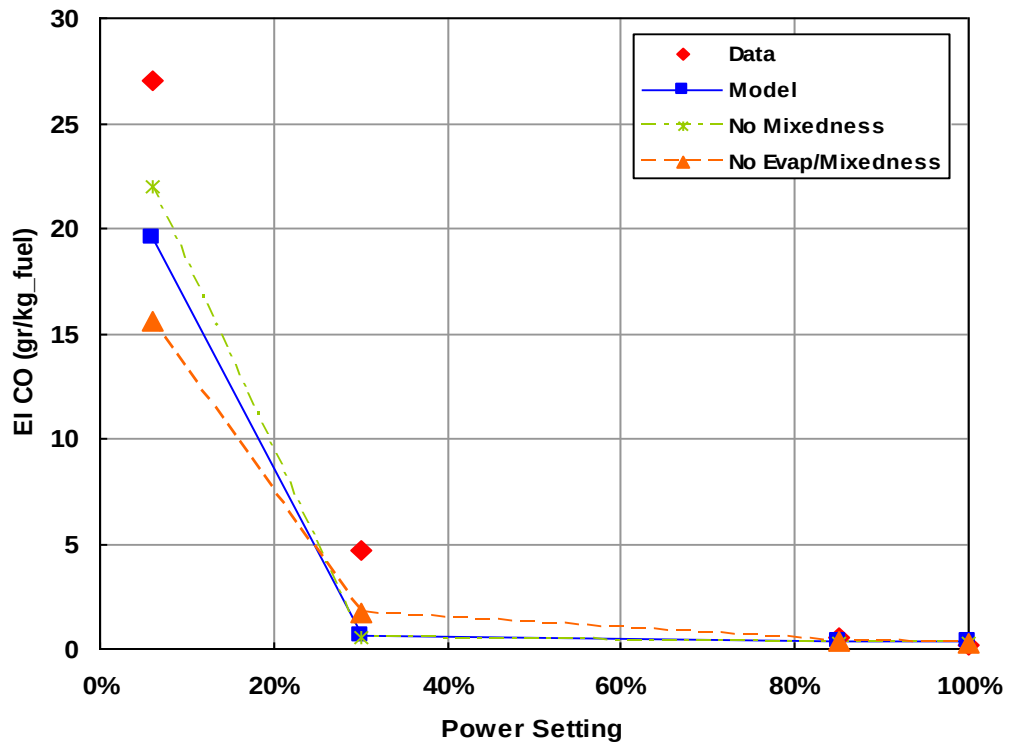

Figure 73: Predicted and actual CO emission indices of the E^3 SAC

Figure 74 to Figure 77 show the droplet size distributions at time zero and their distribution at the time of ignition for four ICAO power settings. The figures also show the variation of the squared of the droplet diameter (D^2). Two other graphs show the variation of the droplet surface temperature and evaporation rate. All these graphs are generated for the droplet whose diameter is the same as the SMD. In all power settings, it can be seen that the droplet has gone through some transient time (heat up period) before the droplet reaches the steady state condition. Often this transient time in the graph is not negligible; therefore, using the well-known D^2 law (Equation (109)) to model droplet evaporation may introduce some error to the model as it considers a constant value for the droplet evaporation constant (k):

$$D^2 = D_0^2 - kt \tag{109}$$

where D_0 is the initial droplet diameter and k is the droplet evaporation constant.

A droplet's surface temperature stops short of the boiling temperature (530 K) due to the droplet evaporation and the heat required [134]. In all figures a general trend is that the amount of vaporized fuel is increased by increasing the power.

A difference can be seen in the amount of liquid fuel at the ignition time at idle condition which relates to the higher primary zone equivalence ratio value of E^3 at idle condition compared to the CFM56. The higher value of the equivalence ratio provides higher temperature and less time for vaporization.

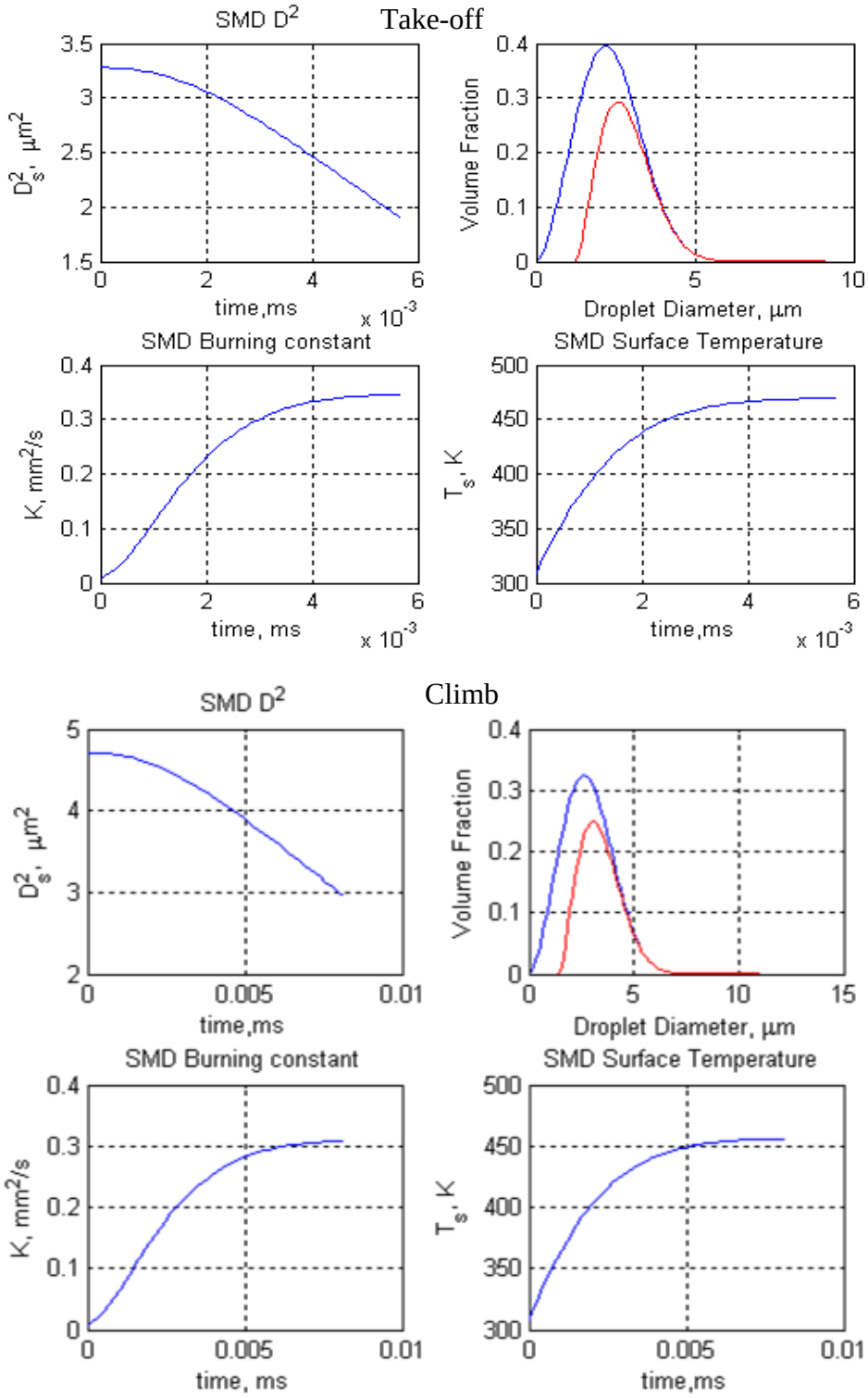

Figure 74: The CFM-56 SAC droplet distribution at time zero (blue) and at the ignition time (red) and the time variation of droplet parameters at take-off and climb

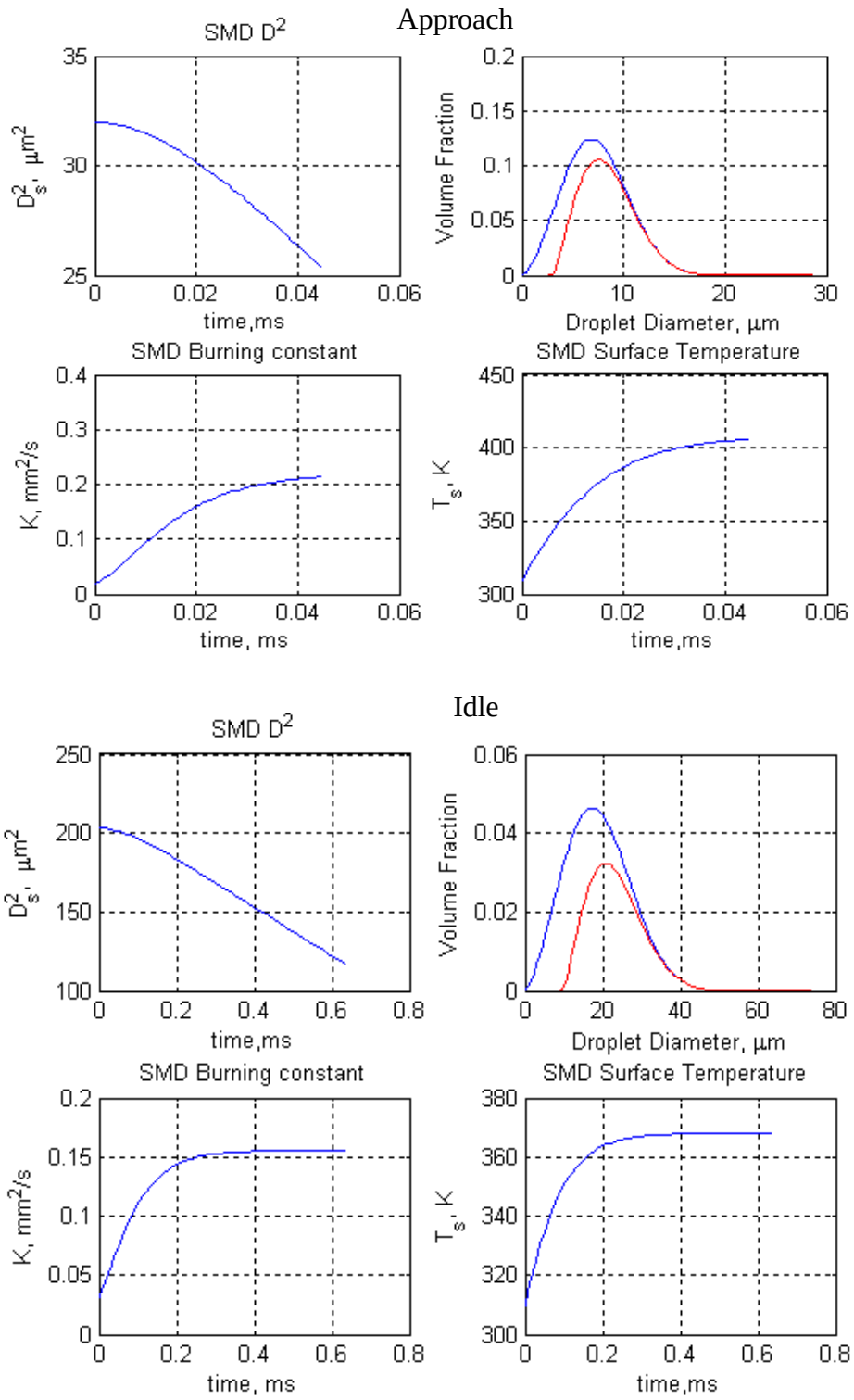

Figure 75: The CFM-56 SAC droplet distribution at time zero (blue) and at the ignition time (red) and the time variation of droplet parameters at approach and idle

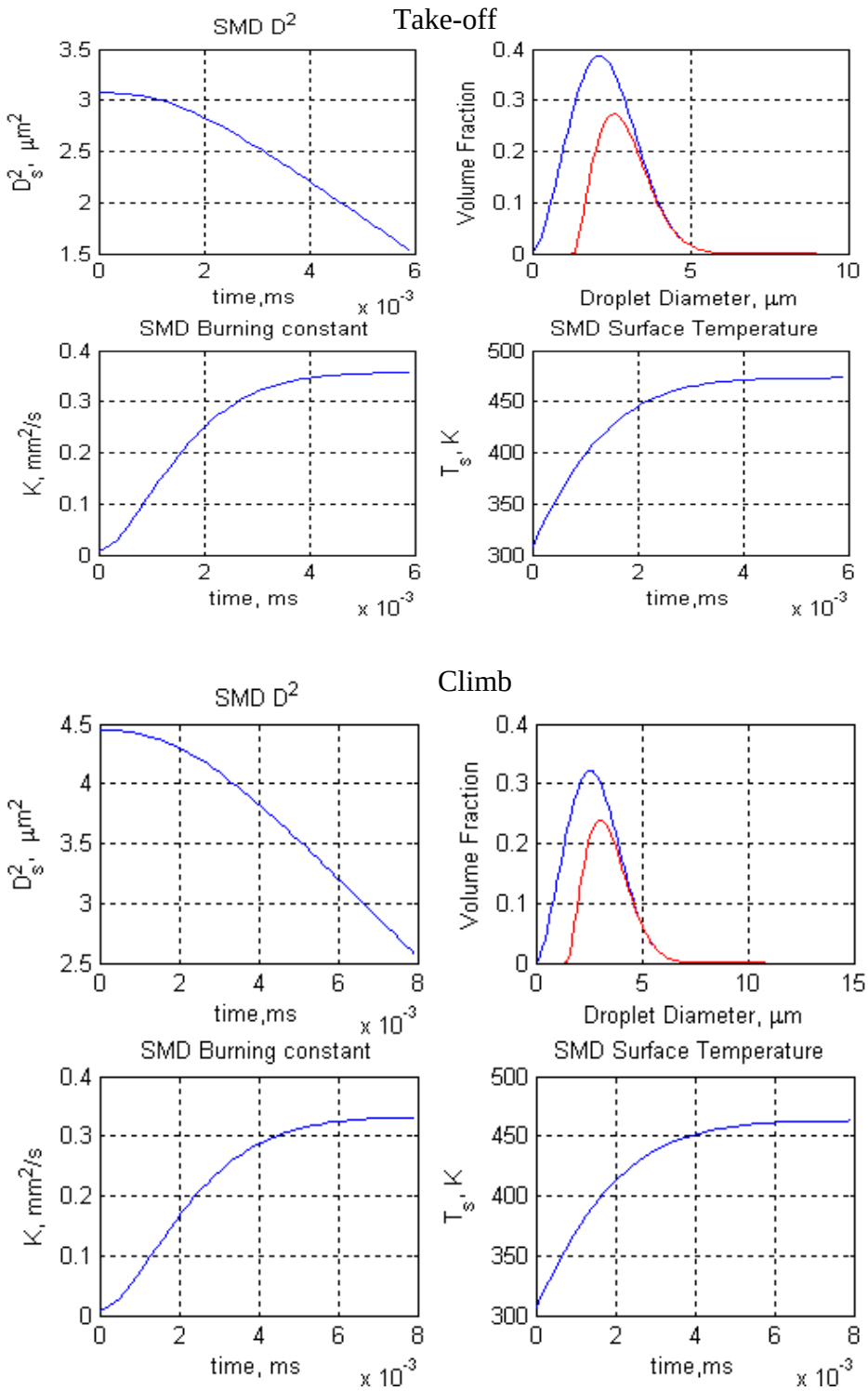

Figure 76: The E3 SAC droplet distribution at time zero (blue) and at the ignition time (red) and the time variation of droplet parameters at take-off and climb

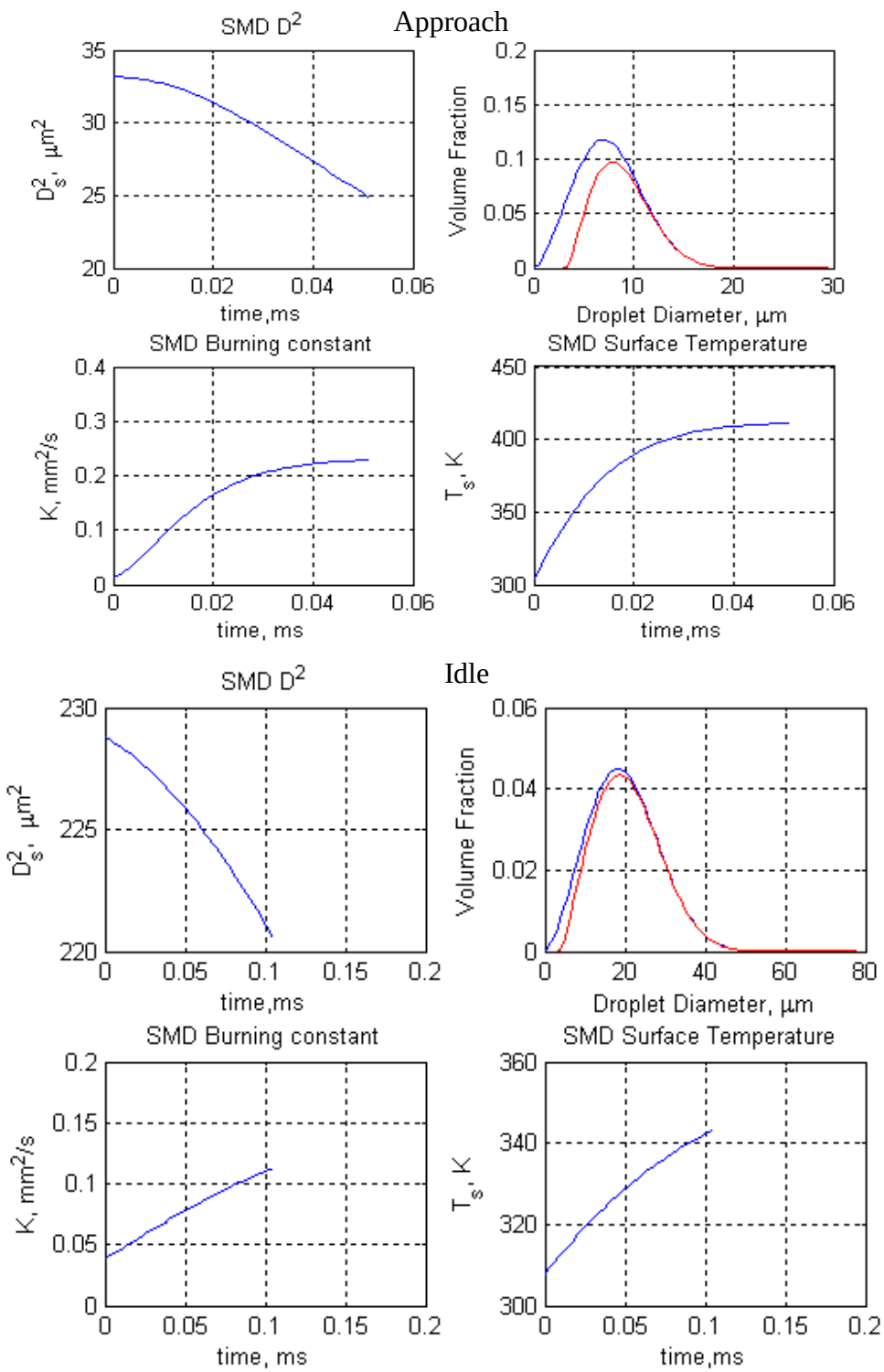

Figure 77: The E^3 SAC droplet distribution at time zero (blue) and at the ignition time (red) and the time variation of droplet parameters at approach and idle

To be able to see the relative change of the droplet distribution as the power setting changes, all of the droplet distributions for the four power settings are plotted in one graph in Figure 78 and Figure 79 for the CFM56 and E^3 combustors. The figures show that as the power setting increases the droplet distribution variation shrinks and the mean decreases. At the same time, due to the increase in the temperature, the ignition delay time decreases as the power setting increases. Therefore the rate at which the droplet distribution decreases and the ignition delay time decreases determines the amount of evaporation.

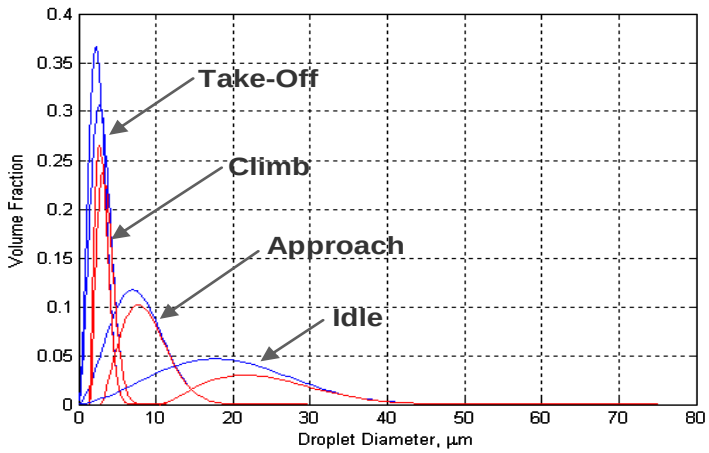

Figure 78: CFM56 SAC droplet distributions

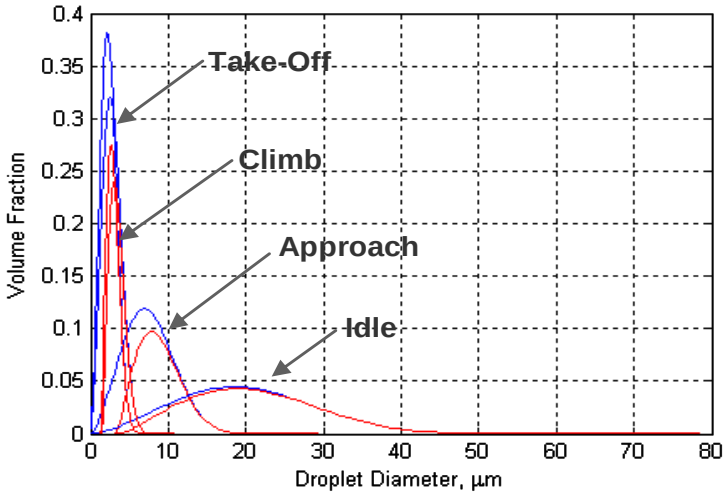

Figure 79: E^3 SAC droplet distributions

Figure 80 and Figure 81 show the equivalence ratio distributions of the premixed mixture at four ICAO/LTO power settings in the CFM56 and E^3 combustors. The horizontal axis shows the equivalence ratio and the vertical axis shows the percentage of the total airflow at a given equivalence ratio. These distributions are based on the unmixedness degree (*S*) and the overall non-premixed equivalence ratio. The unmixedness degrees are obtained in Monte Carlo filtering. The distributions are truncated whenever they go below zero and the truncated area is distributed over the rest of the distribution proportional to the value of S at each given equivalence ratio. With the exception of the idle condition, the range of variation for all of the power settings is almost similar which means their mixing quality is the same.

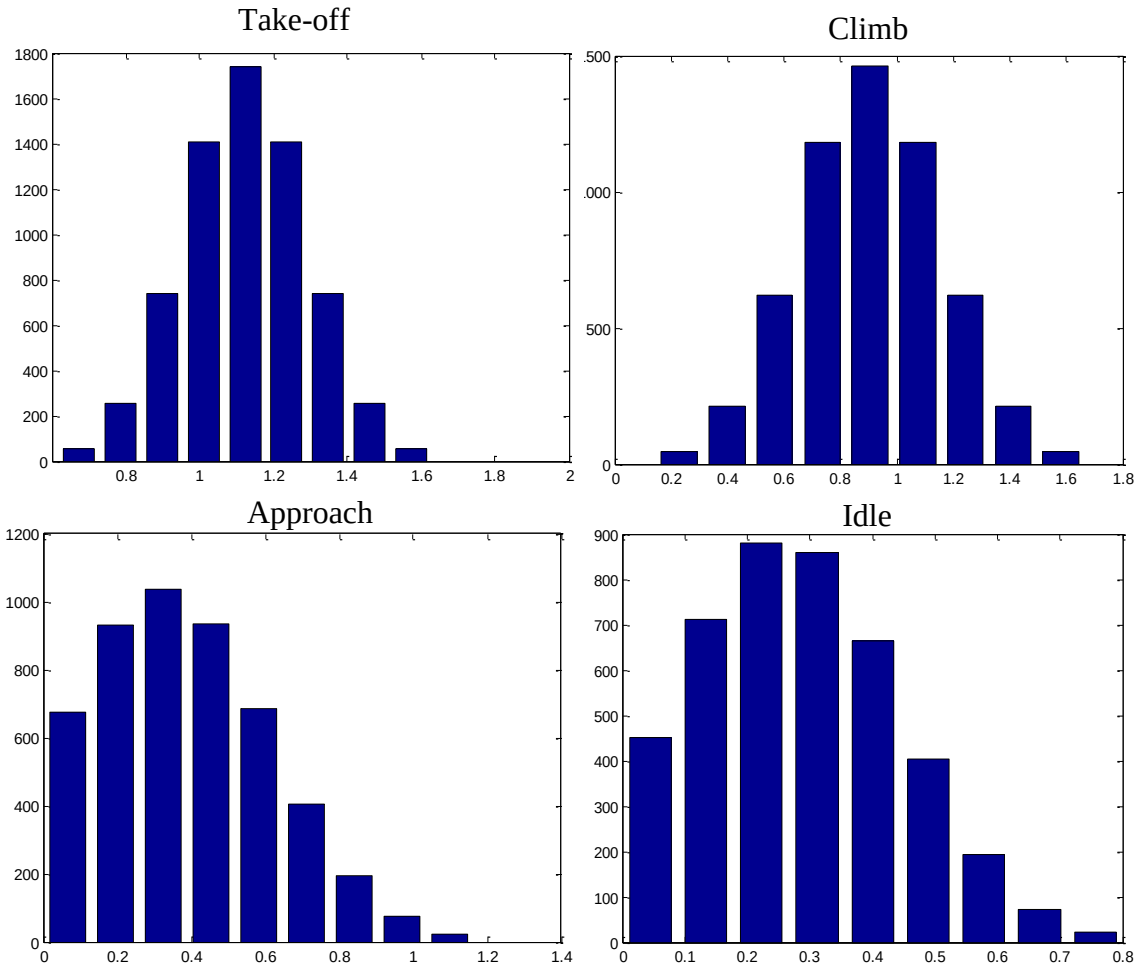

Figure 80: The CFM-56 premixed equivalence ratio distribution in the primary zone

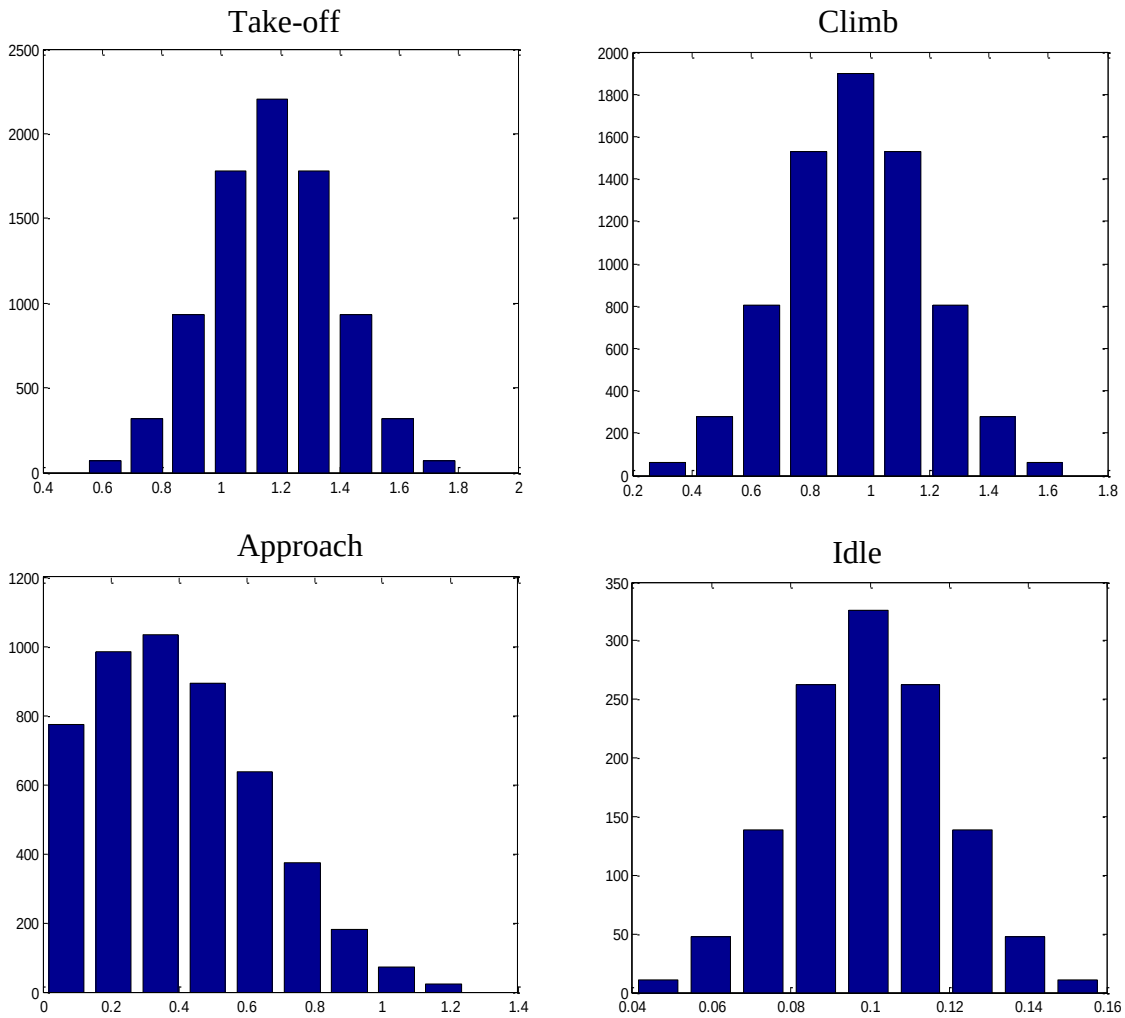

Figure 81: The E^3 premixed equivalence ratio distribution in the primary zone.

Finally, Figure 82 and Figure 83 show the axial temperature variations inside the combustor. Each graph shows two sets of temperature predictions obtained from the 1D flow-field model and the CRN model. The zone efficiencies are adjusted in the 1D flow-field model to match the temperature to the higher fidelity prediction of the CRN model. It is assumed that the efficiencies in the CRN model are implicitly considered in the model through the residence time of the reactors and equivalence ratio distribution, so the temperature prediction of the CRN model is considered as a criterion for iterating the process by changing the zone efficiencies in the 1D flow-field model until the temperature profiles become close. The temperature variations demonstrate a general

pattern in the SACs, where the peak gas temperature exists in the primary zone and gradually goes to lower values as more cooling and dilution flows are added to the core section at downstream locations. The temperature profile shifts upward toward higher temperature values as the power setting (and inlet temperature) increases. This pattern is completely different from the temperature pattern in the RQL combustor as it will be shown in the third experiment. In fact, this difference between the temperature profiles is the main difference between the two combustor types that causes a difference between their NO_x emission level.

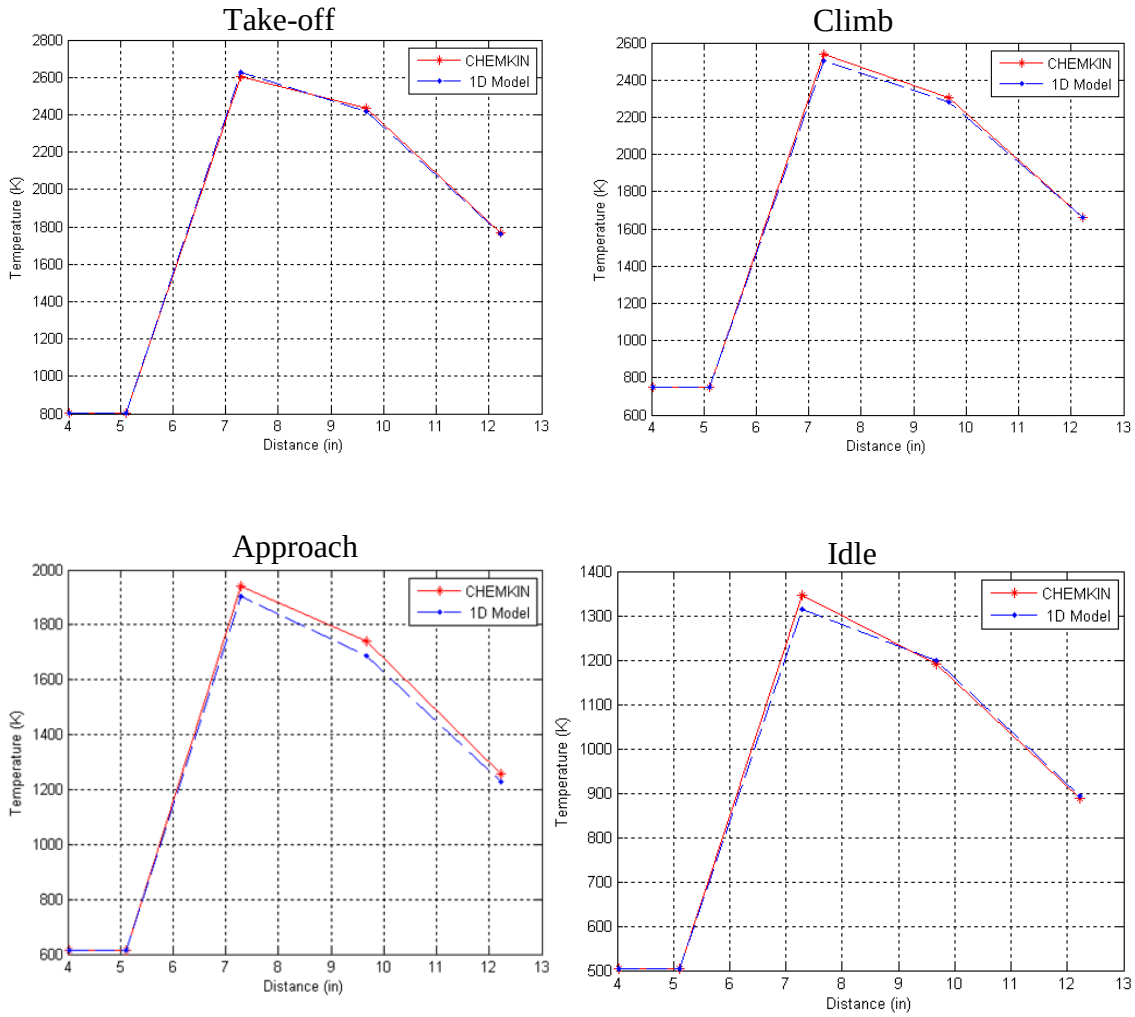

Figure 82: The CFM-56 SAC axial temperature variations across combustor zones

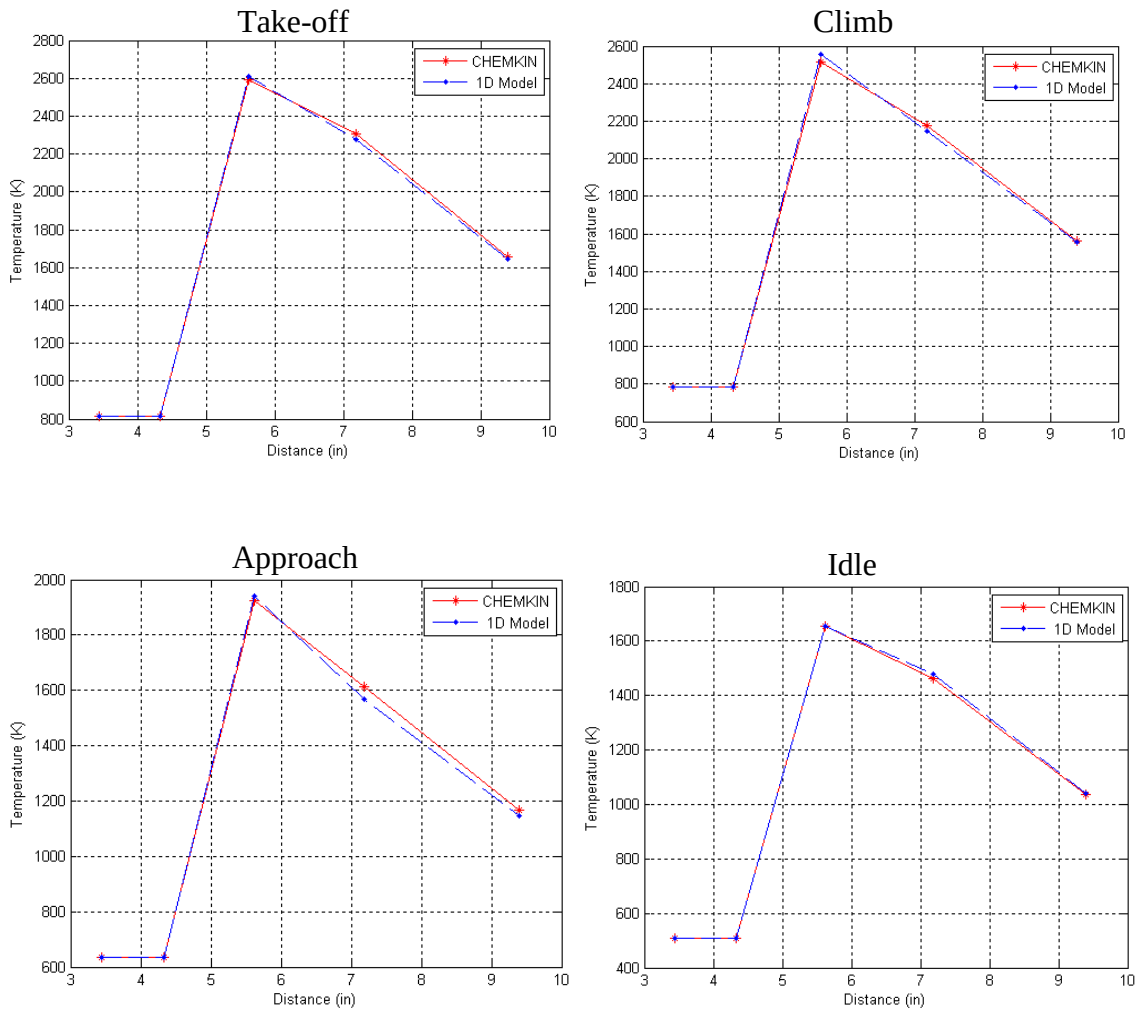

Figure 83: The E^3 SAC axial temperature variations across combustor zones

In this section an emission model is created for the single annular combustor based on the proposed methodology and is applied to two different combustors of the same type. The results showed that the model is able to capture the EI NO_x and EI CO variations. The EI NO_x prediction demonstrates a good accuracy when it is compared to the actual data. The prediction of the EI CO is not as accurate especially at high power settings; however, it captures the correct trends as the actual data.

A valid concern about the SAC emission model is that the unmixedness degrees of the model for different power settings are obtained from the Monte Carlo simulation

process and not based on a physical model. Using this method makes the model dependent on the actual data and reduces its ability to predict the emission of a new combustor. To address this concern, in the next section, the unmixedness degrees of both SAC models determined from the Monte Carlo simulation are combined together to create a model for the unmixedness degree versus the equivalence ratio. It will be shown that the unmixedness values obtained from the Monte Carlo simulation follow a specific trend that can be used to create a general model for the unmixedness degree.

7.3.4 Generalized Non-Uniform Mixture Model

Up to this point, the values used for the unmixedness degree (S) in the Non-Uniform Mixture (NUM) are based on Monte Carlo simulation and tuning the model to match the data. Predicting the emissions of a new combustor based on this approach is not possible and a model should be developed to determine the unmixedness degree for a given power settings or other appropriate parameter. In this work a correlation is found between the unmixedness degree and the equivalence ratio of the premixed mixture (not the total primary zone equivalence ratio); this way the contribution of the diffusion flame is removed from the model and makes the model less dependent on the unmixedness degree.

If all the unmixedness values obtained through the Monte Carlo simulation (Table 27 and Table 38) are plotted against their corresponding premixed equivalence ratios (Figure 84), then a similar trend between the E^3 and CFM56 SACs unmixedness changes is recognized. This similarity shows the general nature of the unmixedness pattern that is the same for two different combustors with different geometry, cycle parameters and emission levels. Figure 84 also is similar in its shape to the published data (Figure 44) [9, 53]; however, it is different in scale. To obtain the unmixedness degree as a function of

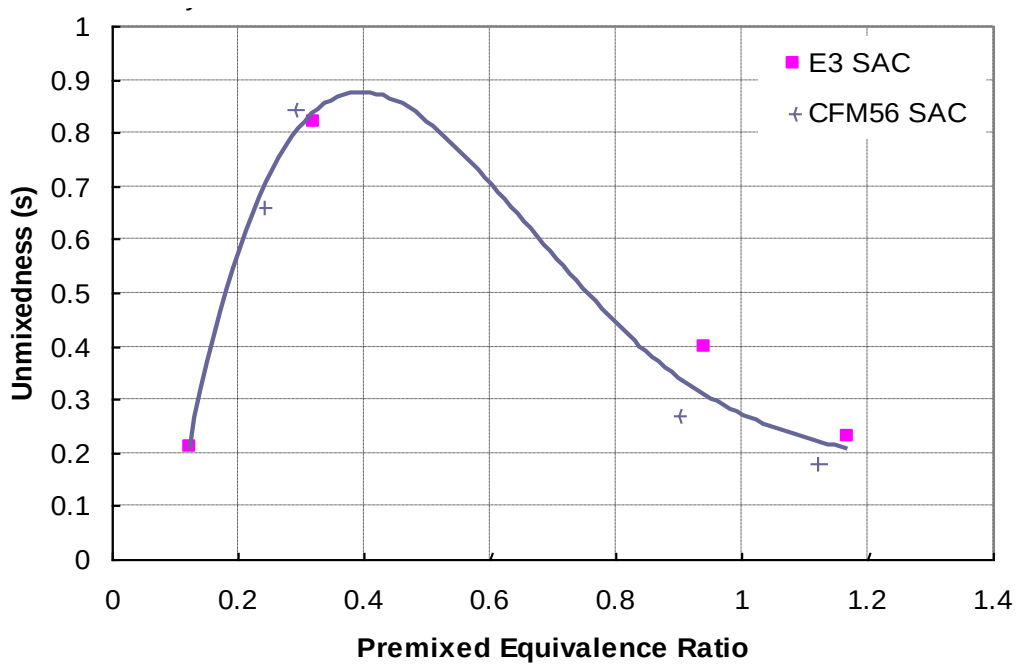

Figure 84: A generalized model for the unmixedness degree

premixed equivalence ratio, a fourth-order polynomial equation is fitted to the points with minimized least squared errors.

The obtained polynomial is:

$$S = -4.9379\varphi^4 + 17.765\varphi^3 - 22.318\varphi^2 + 10.547\varphi - 0.7828 \qquad (110)$$

where φ is the premixed equivalence ratio in the primary zone.

The equation is then used in the CFM56 and E^3 SAC emission models to obtain the value of unmixedness degree as a function of the premixed equivalence ratio in the primary zone.

The emission models for both combustors are executed with the new unmixedness model which is named the Generalized Non-Uniform Mixing (GNUM) model. In the new execution, the fuel temperature for both models is set to 550 R and the Rosin-Rammler shape factor (q) to 2.5 because the Monte Carlo simulation results in the primary and secondary experiments showed a little variation of these two parameters. The results of the emission model execution using the GNUM model are shown in Table 40 and Figure

85 to Figure 88. The variation between the results obtained from the Monte Carlo simulation and the GNUM model are small. This means that the obtained relation between the unmixedness degree and the premixed equivalence ratio provides the same accuracy as the results obtained from the Monte Carlo simulation. Thus, the GNUM model can be used without the need to run the Monte Carlo simulation to obtain the emission of a combustor when no actual emission data is available. Such a model will improve the predictability of the emission model or may be considered an enabler to consider the model as a predictive tool rather than just an analysis tool.

As a conclusion, experiment 1 demonstrated the parametric capability of the model to capture the emissions trend of two different combustors of the same type with the level of accuracy that is considered good at the conceptual phase (especially for NO_x emission prediction) .

The objective of the next experiment is to perform the uncertainty analysis to investigate whether adding the DEDB and GNUM models reduce the epistemic uncertainty of the emissions prediction. The sensitivity analysis is performed to capture the main and second order effects of the variation of the combustor design variables and cycle parameters (aleatory uncertainty) on the NO_x and CO emission levels.

Table 40: E^3 SAC and CFM56 SAC model results based on GNUM model and Monte Carlo simulation unmixedness values

Parameters	Take-off		Climb		Approach		Idle	
	GNUM	MCF	GNUM	MCF	GNUM	MCF	GNUM	MCF
CFM56 EI NO_x	29.91	29.7	23.29	23.31	10.9	10.61	7	6.9
CFM56 EI CO	0.41	0.41	0.29	0.292	0.25	0.26	12.9	12.8
CFM56 unmixedness	0.24	0.18	0.33	0.27	0.80	0.844	0.63	0.66
E^3 EI NO_x	21.1	20.9	19.4	18.5	9.047	9.04	4.04	4.04
E^3 EI CO	0.30	0.31	0.32	0.34	0.567	0.56	21.83	22.1
E^3 unmixedness	0.201	0.23	0.314	0.4	0.847	0.82	0.18	0.21

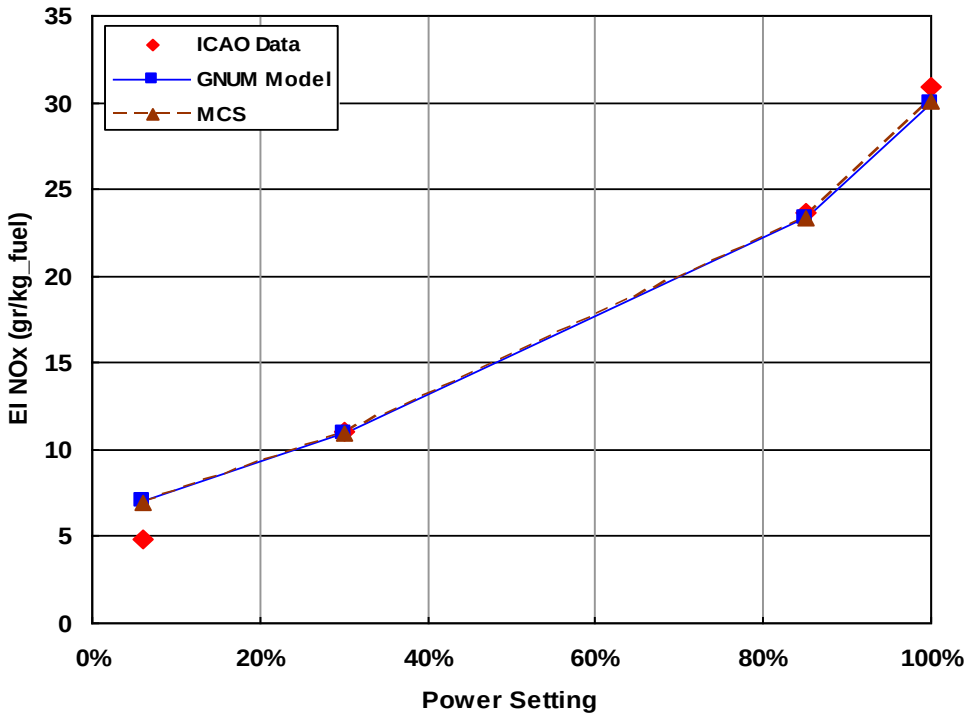

Figure 85: Comparison of the CFM56 SAC EI NO_x values

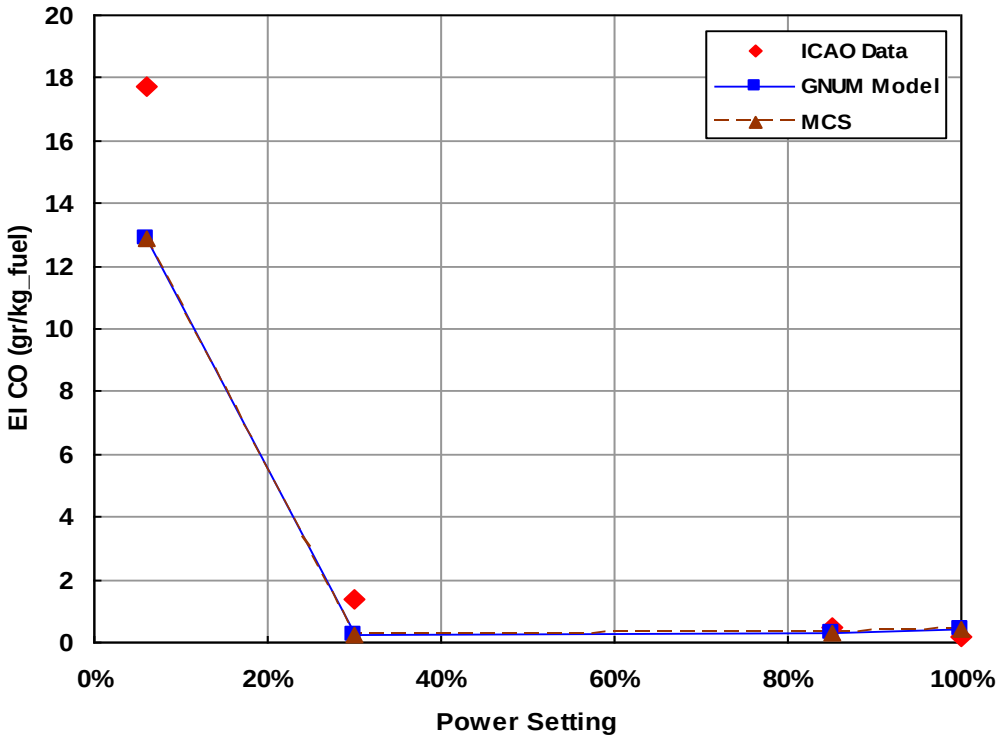

Figure 86: Comparison of the CFM56 SAC EI CO values

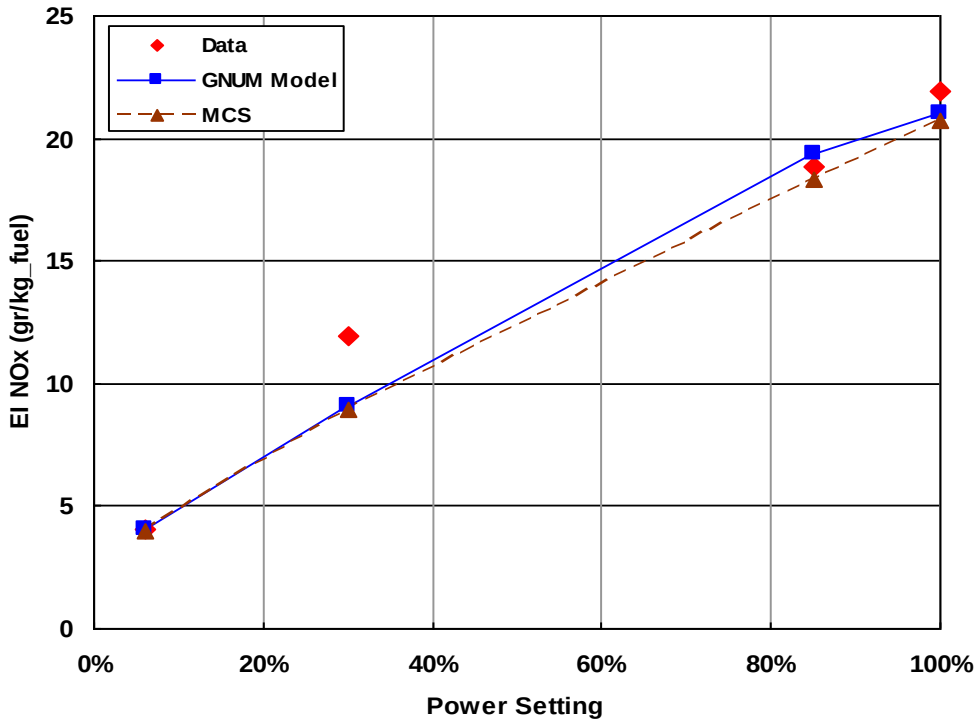

Figure 87: Comparison of the E^3 SAC EI NO_x values

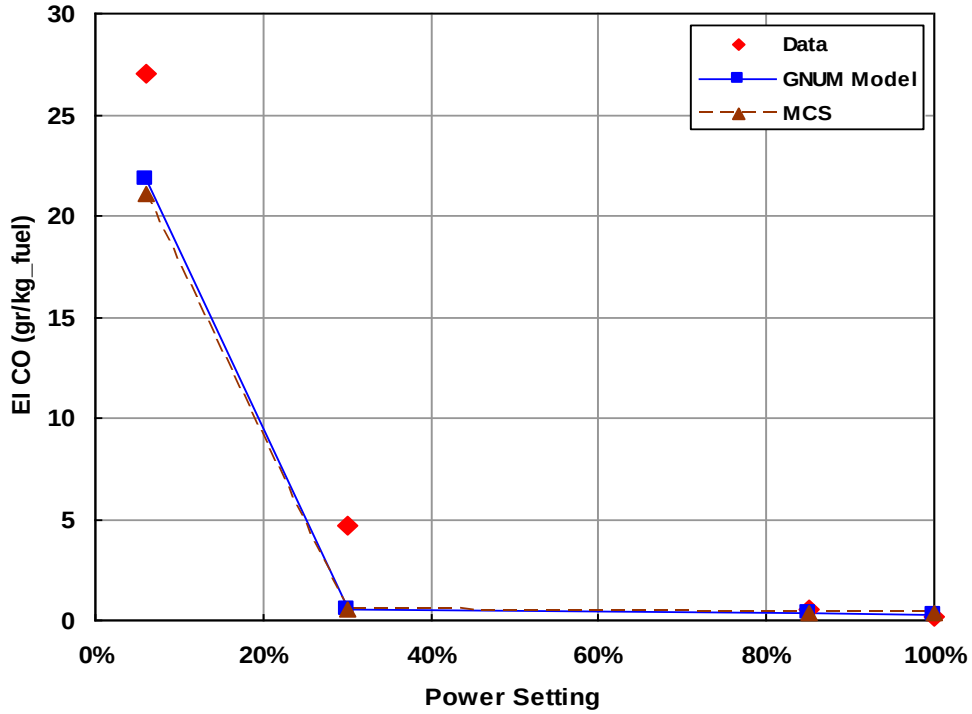

Figure 88: Comparison of the E^3 SAC EI CO values

7.4 Experiment 2: Further Analysis of the CFM56 Combustor Emissions Model

This experiment is composed of two parts. In the first part, a series of Monte Carlo simulations (MCS) are performed on the CFM-56 combustor for four ICAO/LTO power settings to capture the effects of adding the Droplet Evaporation/Diffusion Burning (DEDB) model and the Non-Uniform Mixture (NUM) model on the emissions distribution's mean and variability (standard deviation). The intention of the uncertainty analysis here is to study the effect of the mentioned models on the model epistemic uncertainty compared to a simple model. In the second part, a sensitivity analysis is performed to capture the main and second order effects of the variation (epistemic uncertainty) of the combustor design parameters and engine cycle parameters on the NO_x and CO emission levels.

7.4.1 Uncertainty Analysis

For the uncertainty analysis, a Monte Carlo simulation must be performed. To that end, as has been described in Section 2.4, the range and distribution of the model inputs should be defined. Since the distributions of the inputs are unknown, the uniform distribution is assumed for all of them. Three sets of MCS are performed in this task; the first simulation is performed for the model when both the DEDB and GNUM models are deactivated; the second MCS is performed for the emission model with the addition of the DEDB model but not the GNUM model and the third one is performed for a complete emission model (including the DEDB and GNUM models). The results of the simulations in term of probabilistic graphs (pdf or frequency distribution) are compared to each other at each power setting to assess the effect of the DEDB and GNUM models on the uncertainty of the emission levels.

The inputs to the MCS process are divided into two groups. The first group is those inputs or design variables that are not a function of power settings, i.e. the value of

these inputs is the same for all power settings and is defined at the design condition which is the take-off condition (Table 41). The other group contains the parameters that change with the change in power setting; however, they are not modeled in the current emission model due to their modeling complexity (Table 42). The minimum and maximum values of the parameters are based on the range obtained from literature or reports or 20% perturbation of the nominal parameter values of the CFM56 SAC that are obtained in the previous experiment. In all MCS of the four ICAO/LTO power settings, the first group is present while only that part of the second group appears in the MCS that belong to the specific power setting at which the MCS is being performed.

Table 41: Input ranges and definitions of on-design parameters for the Monte Carlo simulation

Emission Model Inputs	min.	max.
$T_{Max\ Liner}$	2000	2200
T_{Fuel}	540	576
Cooling mechanism factor	0.04	0.07
$\Delta P/P$ burner	0.04	0.08
$\theta_{diffuser}$	3.5	6
Diffuser sweet-spot	1.28	1.92
$Mach_{32}$	0.032	0.048
$Mach_{Liner}$	0.01192	0.018
α_{swirl}	60	64
K_{SW}	1.3	2.0
$r_{hub\ swirler}$	0.2	0.3
Design η_{PZ}	0.9	0.98
φ_{PZ}	1.00	1.09
Design η_{SZ}	0.98	0.99
φ_{SZ}	0.7	0.9
SZ length ratio	0.56	0.84
DZ length ratio	0.624	0.936
Injector flow number (FN)	$0.5*10^{-7}$	$1.5*10^{-7}$
Rosin Rammler shape factor, *q*	1.8	3
Design PZ cooling flow fraction	0.112	0.168
Design SZ cooling flow fraction	0.448	0.672

Only primary and secondary cooling flow fractions are assumed as inputs in the MCS and the DZ cooling flow fraction is obtained by the difference of the sum of two others and one.

Table 42: Input ranges and definitions of off-design parameters for the Monte Carlo simulation

Emission Model Inputs	Idle		Approach		Climb	
	min.	max.	min.	max.	min.	max.
PZ cooling flow fraction	0.0	0.03	0.024	0.036	0.12	0.18
SZ cooling flow fraction	0.44	0.66	0.352	0.528	0.352	0.528
η_{PZ}	0.9	0.95	0.9	0.95	0.9	0.95
η_{SZ}	0.95	0.98	0.95	0.98	0.95	0.98
η_{DZ}	0.98	0.999	0.98	0.999	0.8	0.999

For each power setting of idle, approach, climb and take-off, three MCS's are performed, each one with the size of 500 samples. To deactivate the GNUM model, its effect is eliminated by setting the unmixedness degree to a very small value (0.01) and to deactivate the effect of the DEDB, the final value of evaporation degree is set to 100% which means all fuel droplets are vaporized in all operating conditions. Figure 89 to Figure 92 demonstrate the results of the MCS at four power settings for three models (No DEDB and GNUM, No GNUM and complete). They show the frequency distribution of the NO_X and CO emission indices which are the approximation of their pdf. The general trend of the results is in agreement with the initial investigation of the effects of the DEDB and NUM models on the emission levels (Figure 70 to Figure 73).

Figure 89 shows the frequency distribution of the EI NO_x and EI CO at the take-off condition. The mean value of EI NO_x distribution moves closer to the target by the addition of the DEDB model and the variability is increased. This means that droplet burning is still important at the take-off condition. The addition of the GNUM model does not have a significant effect on the NO_x distribution's mean but, decreases its variability. The EI CO distribution is unaffected by the addition of the models.

Figure 90 shows the importance of the DEDB and GNUM models on EI NO_x level at the climb condition. The addition of the DEDB model alone moves the EI NO_x distribution's mean beyond the target and increases the variability. The addition of GNUM model moves the EI NO_x distribution's mean back to the target value and reduces its variability as well. The EI CO distribution is remained unaffected by the addition of the models.

Figure 91 shows the frequency distribution of the EI NO_x and EI CO at the approach condition. It is clear from the figure that adding the DEDB model significantly improves the prediction of EI NO_x by moving the EI NO_x distribution's mean closer to the target value. At the same time, adding the DEDB model increases the variability of the EI NO_x distribution. Addition of the GNUM model does not change the EI NO_x distribution's mean value; however, it reduces its variability. For EI CO prediction, adding the models moves the distribution's mean closer to the target and reduces the variability; however, it is hard to assess the changes at this low level of EI CO as it falls outside of the model's accuracy range.

Finally, Figure 92 shows the frequency distribution of the EI NO_x and EI CO at the idle condition. The EI NO_x prediction improves significantly by the addition of the DEDB model. Similar to the approach condition, the DEDB model moves the EI NO_x distribution's mean toward the actual value by significant amount and the GNUM model reduces its variability. Adding the DEDB or GNUM model at the idle condition also has a clear effect on the EI CO distribution. It shows that addition of DEDB and GNUM models increase the mean of the EI CO distribution and move it toward the target value. The EI CO distribution's variability of the complete model is increased compared to the incomplete model, and this shows the sensitivity of the EI CO level to the inputs variation which is in consistence with the physical understanding of the high sensitivity of the CO emission level to inputs condition.

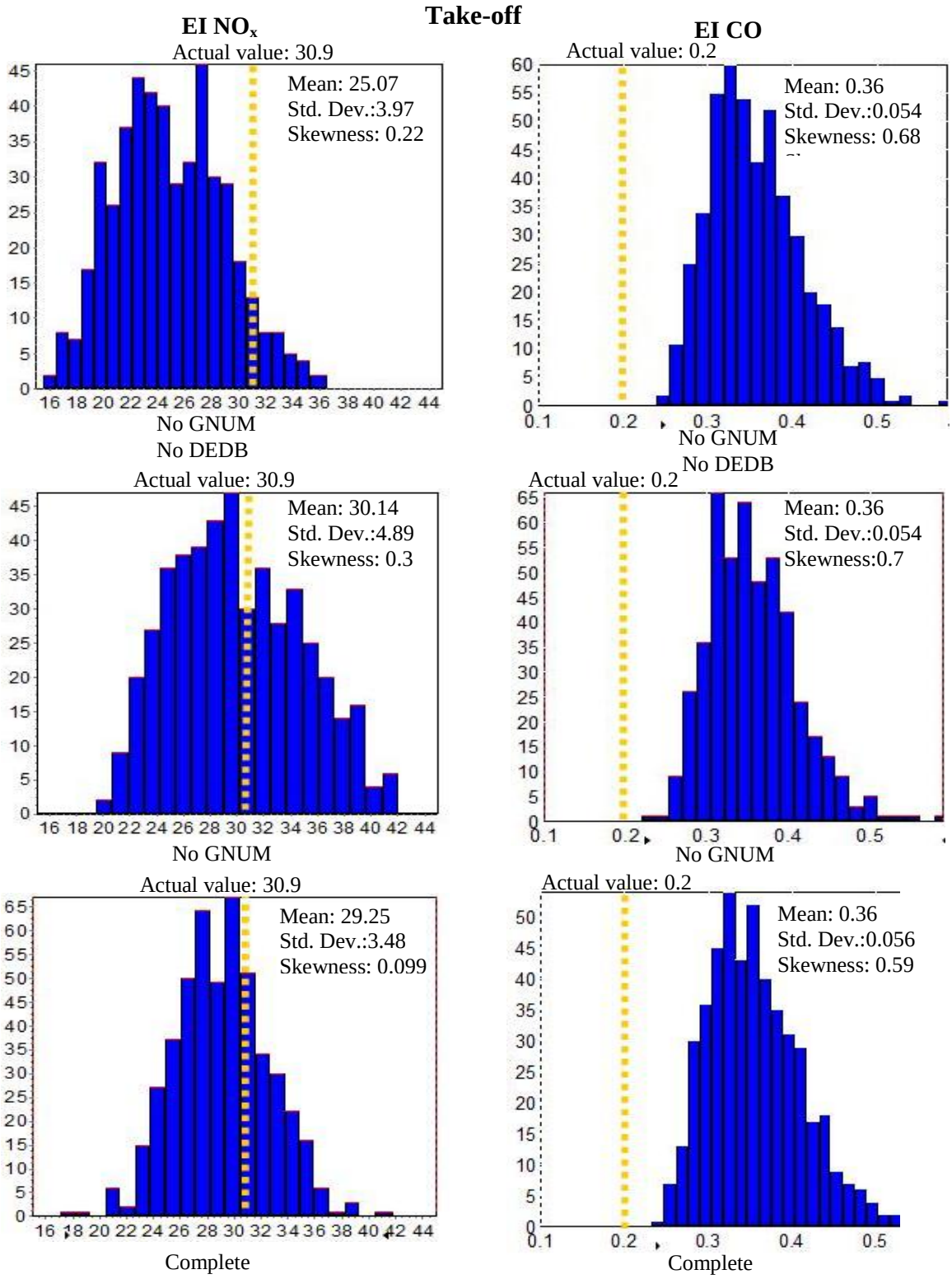

Figure 89: Frequency distribution of EI NO_x and EI CO at take-off

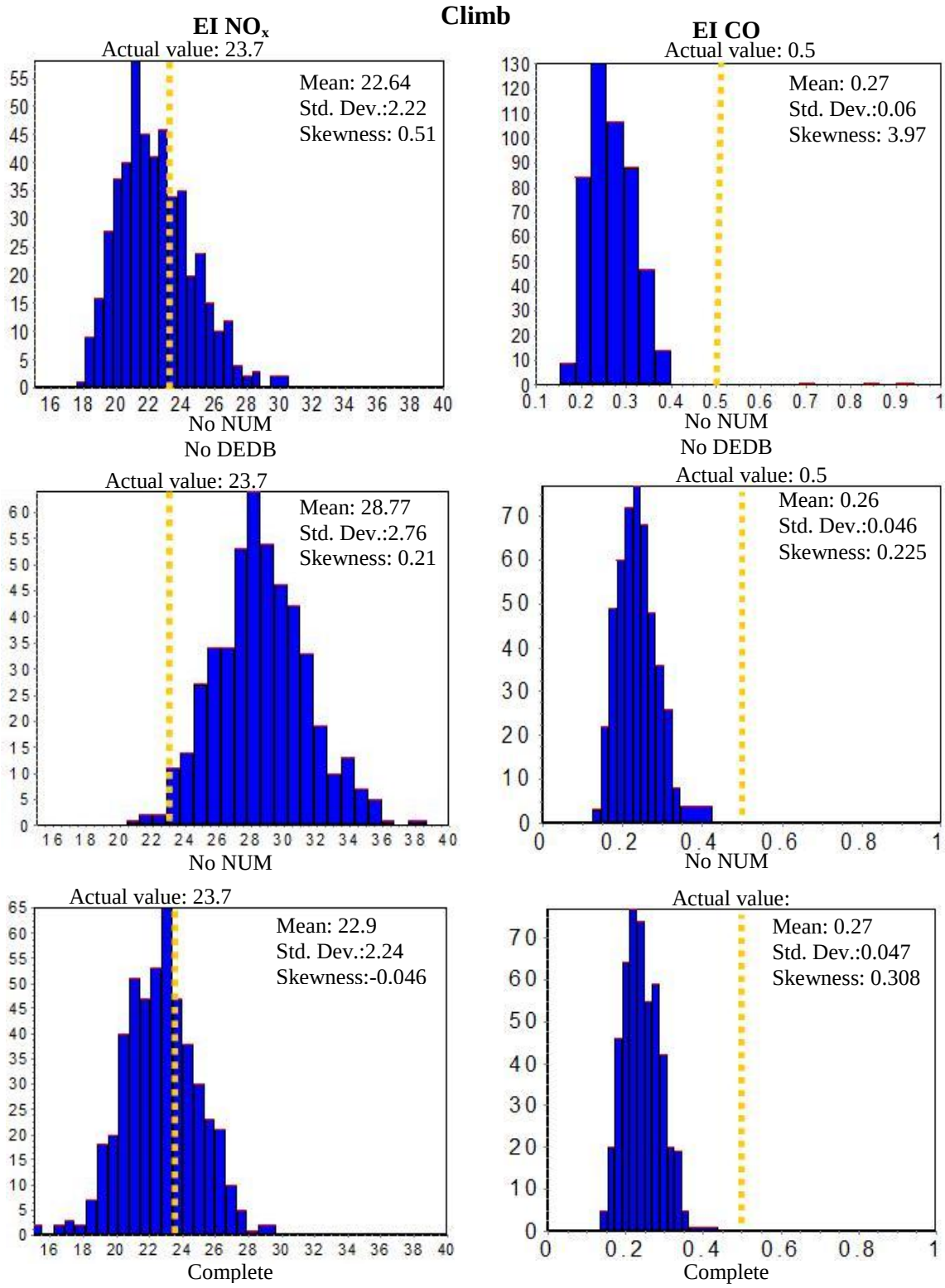

Figure 90: Frequency distribution of EI NO_x and EI CO at climb

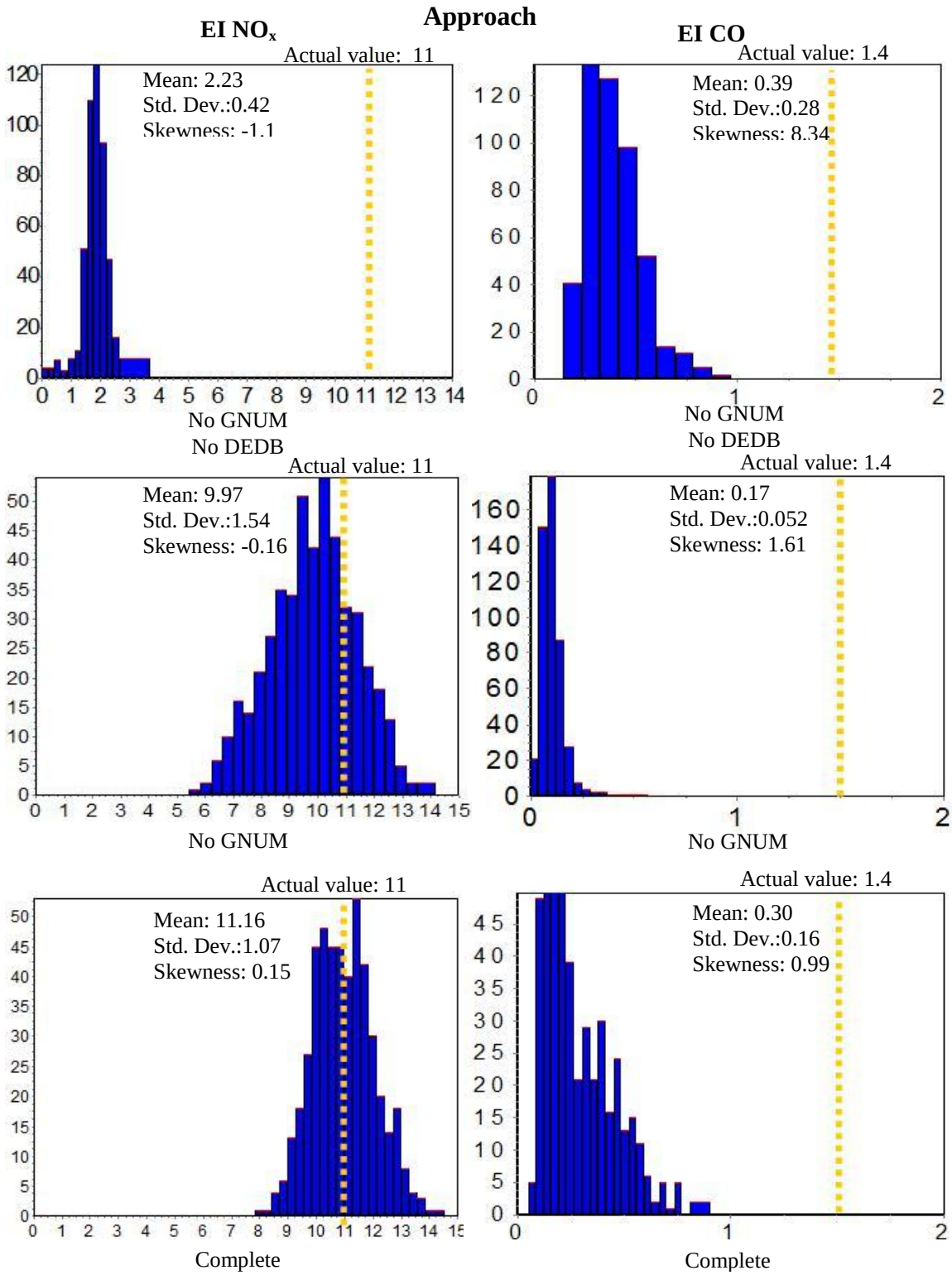

Figure 91: Frequency distribution of EI NO_x and EI CO at approach

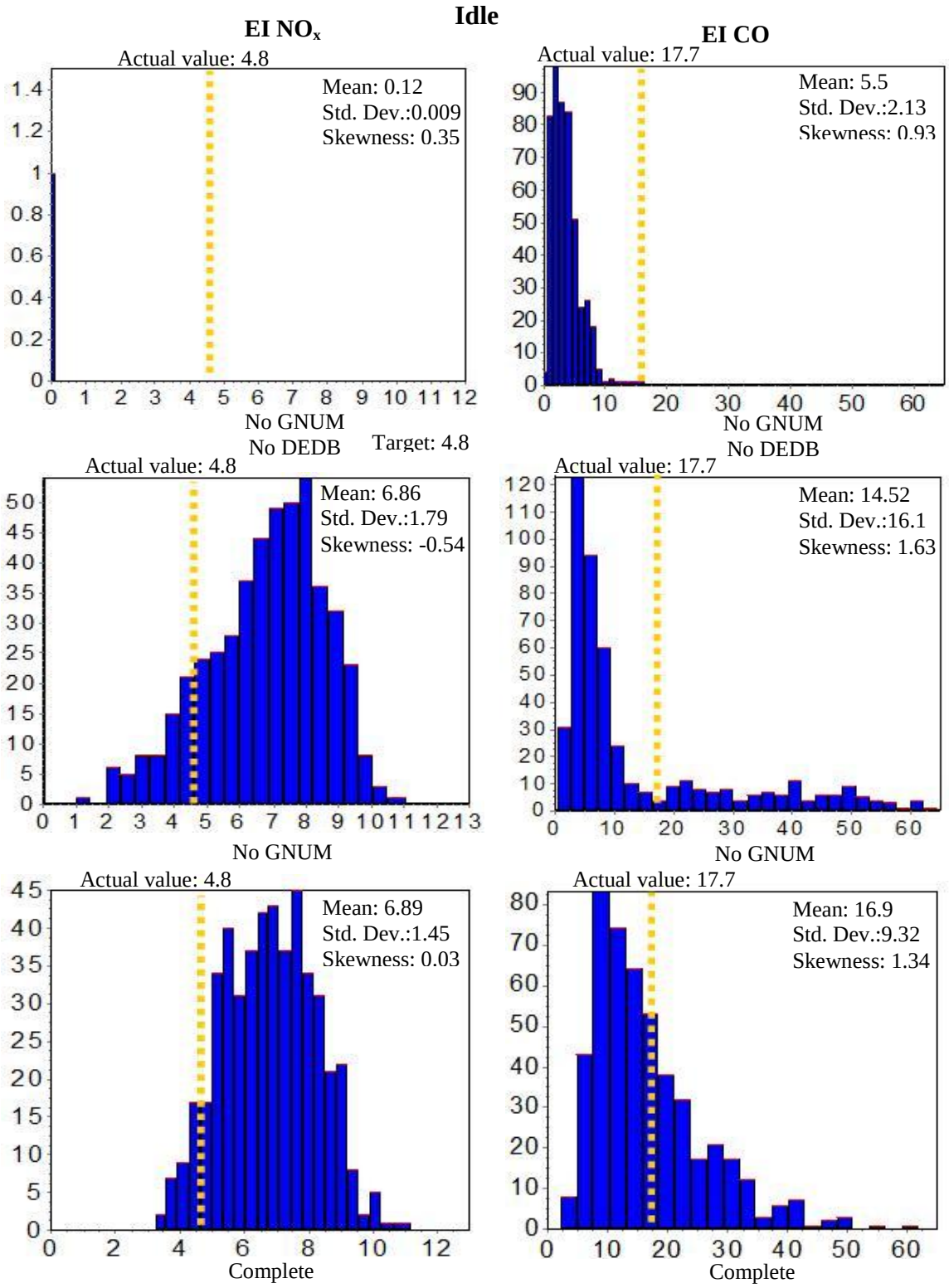

Figure 92: Frequency distribution of EI NO_x and EI CO at idle

The results of this section show that in general, adding the DEDB model increases the distribution variability and adding GNUM model on top of that reduces the variability. The overall effect is the slight reduction in the distribution's variability. The addition of DEDB or GNUM models moves the distribution's mean of EI NO_x closer to the actual value at all power settings and distribution's mean of EI CO prediction toward the actual value at idle. It is not possible to assess the effects of adding DEDB and GNUM models on the EI CO distributions at the take-off, climb and approach conditions due to the very low value of CO emissions which are probably outside of the accuracy range of the model.

7.4.2 Sensitivity Analysis

To capture the relative effects of the emission model inputs on the emission levels, a sensitivity analysis is performed. The inputs are based on the input values of the CFM-56 combustor that are perturbed by 4%. Table 43 shows the list of inputs range that are considered for this sensitivity study. A fractional factorial screening design of experiments (DOE) is selected to study the main and some crossing effects of the combustor characteristics and engine cycle parameters on the emission levels. The engine cycle parameters are considered in the analysis to compare their contributions to the contribution of other combustor parameters.

Unlike the uncertainty analysis where most of the inputs range are defined based on the available ranges, in the sensitivity analysis the input range should be based on equal amounts of perturbation from the nominal value for all inputs. By keeping the variation of the input the same, it is possible to assess the contribution of each input to the emission levels variability and compare them to each other. This requirement puts some constraint on the perturbation magnitude. For example, if the magnitude of the perturbation is larger than a particular value, the efficiencies of the primary and secondary zones will have an overlap that causes the 1D flow-field model to issue an

Table 43: Range of on-design parameters for the sensitivity analysis

Emission Model Inputs	Take-off	
	min.	max.
$T_{Max\ Liner}$	1968	2132
T_{Fuel}	528	572
Cooling mechanism factor	0.0643	0.0700
$\Delta P/P_{burner}$	0.048	0.052
$\theta_{Diffuser}$	3.54	3.84
Diffuser sweet spot	1.54	1.66
$Mach_{32}$	0.038	0.042
$Mach_{Liner}$	0.0143	0.0155
α_{swirl}	59.24	64.34
K_{SW}	1.42	1.54
$r_{hub\ swirler}$	0.24	0.26
Design η_{PZ}	0.9024	0.96
Design η_{SZ}	0.96	0.987
Design φ_{PZ}	1.008	1.092
Design φ_{SZ}	0.77	0.83
SZ length ratio	0.67	0.73
DZ length ratio	0.749	0.811
Injector flow number	9.6e-8	1.04e-7
Rosin-Rammler shape factor, *q*	2.4	2.6
Design PZ cooling flow fraction	0.001	0.0104
Design SZ cooling flow fraction	0.528	0.572
Design P_{31}	403.9	437.53
Design T_{31}	1383.3	1498.6
Design $\dot{m}_{air}$	94.23	102.08
Design $\dot{m}_{fuel}$	2.71	2.93

error and stop. The reason is that the efficiency in each zone should be larger than the preceding zone as the combustion efficiency cannot decrease as the combustion process proceeds toward the end (or at least it is the assumption here).In addition, the efficiency of the dilution zone cannot be bigger than one. These constraints should be considered when creating a DOE for the sensitivity analysis and that is why a perturbation of 4% is selected for the analysis. After each sensitivity analysis is performed, the result is processed in JMP software to study the main and cross effects of the inputs on the

emission levels. Then the Pareto plot of the input contributions is generated at each case for EI NO_x and EI CO.

The efficiency of the dilution zone is 99.9% and any variation would make it greater than one or smaller than the secondary zone efficiency; therefore, the dilution zone efficiency is not considered in the sensitivity analysis. In addition, the parameters of the dilution zone have very small effects on the emission level and removing dilution zone efficiency does not affect the final results. The efficiency of the primary and secondary zones at take-off, climb and approach are very close to each other and they are considered the same as the take-off efficiency.

The sensitivity analysis is performed for four ICAO/LTO power settings for the complete model. Like the uncertainty analysis, there are two groups of parameters; the first group contains design parameters that remain unchanged in all power settings (Table 43). The second group contains the operating (off-design) combustor and the engine cycle parameters that are the function of the power setting (Table 44). The input ranges are provided for both groups and the ranges are used to design a screening DOE in JMP software.

Something that should be clarified here is the difference between on-design and operating (off-design) engine cycle parameters, especially at the take-off condition. The on-design parameters (at take-off) are used to size the combustor and its components; however, it is possible to operate the engine at the take-off condition with engine cycle parameters that are different from the given on-design engine cycle parameters. For that reason, always two sets of engine cycle parameters are considered in the sensitivity analysis. The first set is the design engine cycle parameters (without any subscript, e.g., T_{31}) and the second set is the operating engine cycle parameters (with subscript "op", e.g., $T_{31\ op}$) of the condition at which the engine is actually operating.

A total of 129 runs are performed for each power setting. The results of each power setting are transformed back to JMP for further analysis where a sensitivity

analysis is performed on the results and the inputs or input interactions whose p-value is smaller than 0.1 (10% significance level) are considered statistically significant.

In the next step, all the inputs are used to create a second order model and from that, a Pareto plot of the inputs contribution at each power setting for EI NO_x and EI CO are generated.

Table 44: Range of off-design parameters for the sensitivity analysis

Emission Model Inputs	Idle		Approach		Climb	
	min.	max.	min.	max.	min.	max.
Operating PZ cooling fraction	0.009	0.010	0.029	0.031	0.144	0.156
Operating SZ cooling fraction	0.528	0.572	0.422	0.458	0.422	0.458
Operating η_{PZ}	0.883	0.957	0.902	0.96	0.902	0.96
Operating η_{SZ}	0.96	0.987	0.96	0.987	0.96	0.987
Operating P_{31}	77.89	84.39	157.67	170.8	345.05	373.8
Operating T_{31}	872.9	945.3	1058.6	1146.8	1293.9	1401.8
Operating air mass flow	25.63	27.77	44.17	47.85	82.75	89.64
Operating fuel mass $flow_1$	0.256	0.278	0.742	0.804	2.21	2.39

The Pareto plots in Figure 93, Figure 94, Figure 95 and Figure 96 show the contribution of the emission model inputs on EI NO_x at four ICAO/LTO power settings. The first observation is that the combustor characteristics are as important as engine cycle parameters. Also many inputs have contribution to the emission levels indicating the complexity of the model. For that reason only the few top contributors (often the first seven inputs) are discussed here.

In all four figures, the contribution of the diffuser parameters on the EI NO_x is very small or none. There is a low sensitivity of EI NO_x to secondary and dilution zone length ratios. This result can be seen as a justification for simplifying the length calculation in the secondary and dilution zones by defining the length to height ratio as an input to find the length of the zones.

At all operating conditions, the compressor exit temperature at the operating condition is the number one contributor. The compressor exit temperature at the design

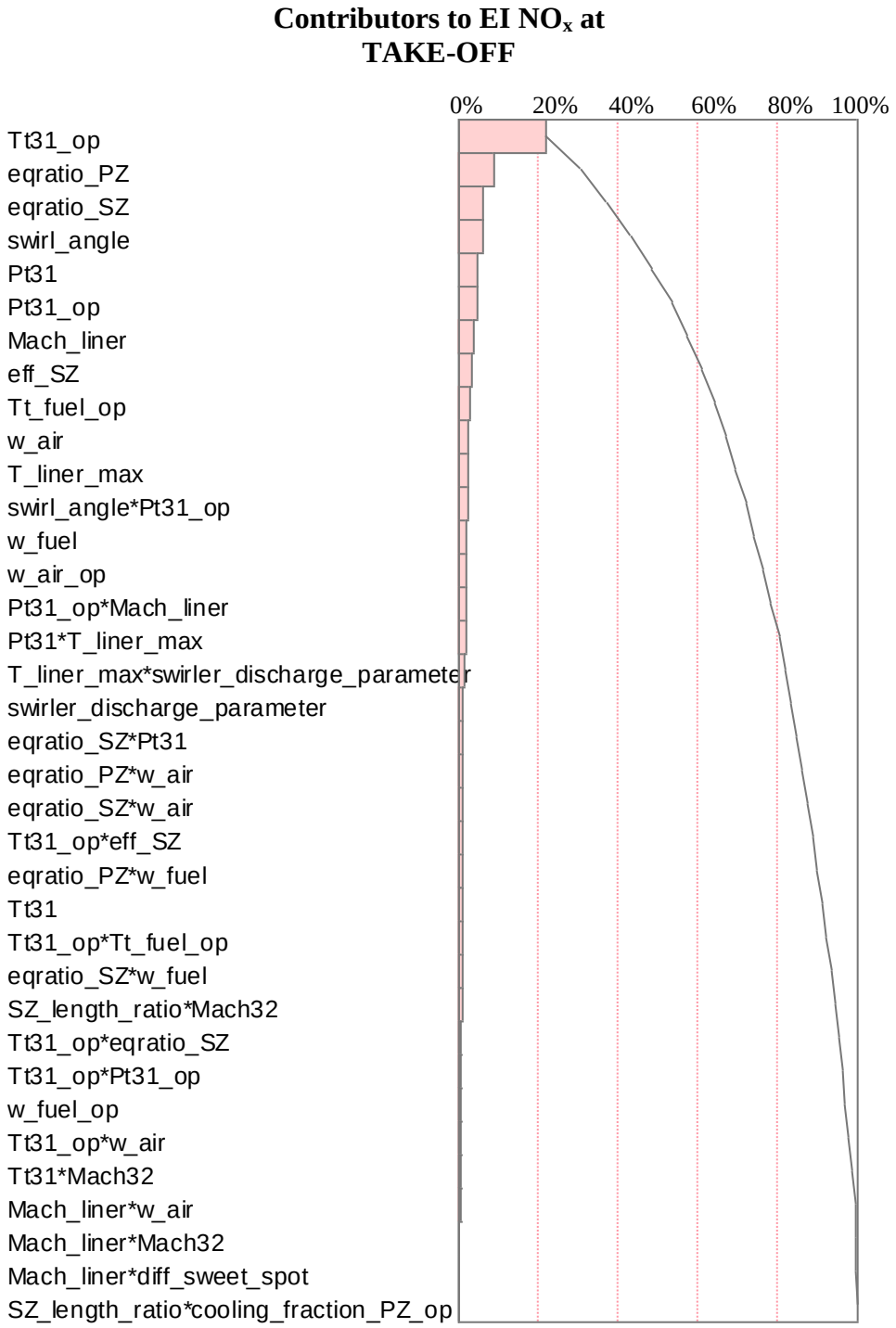

Figure 93: Relative contribution of input parameters to EI NO_x at take-off

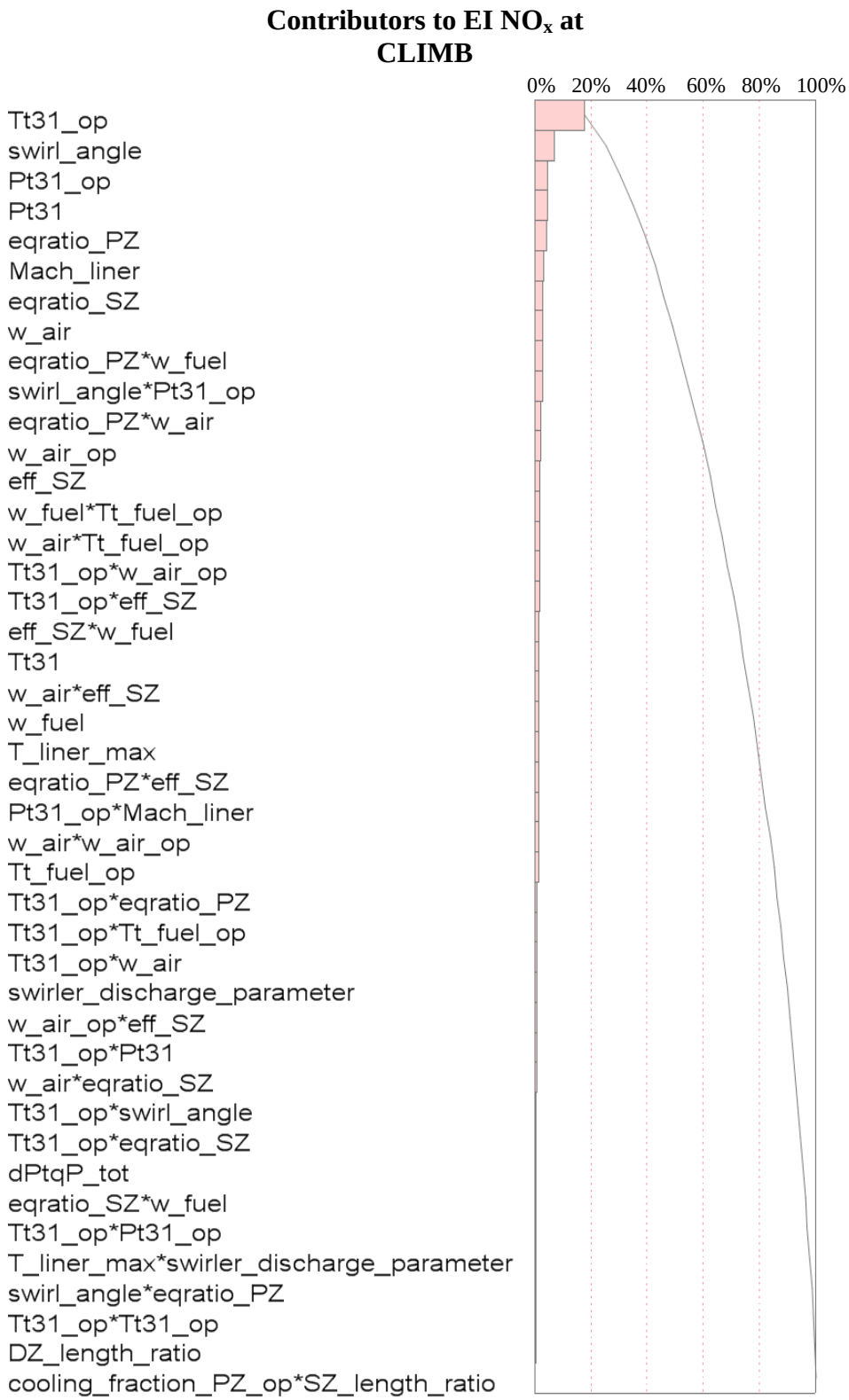

Figure 94: Relative contribution of input parameters to EI NO_x at the climb condition

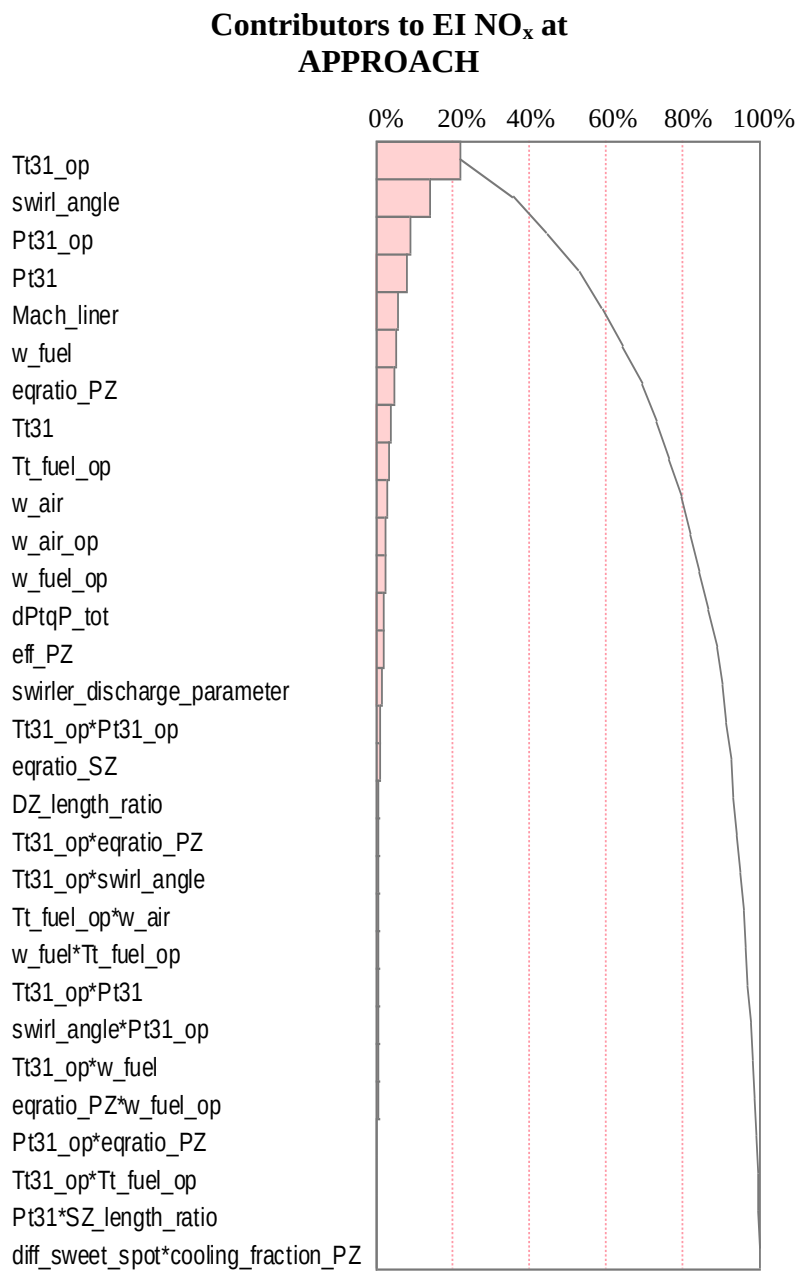

Figure 95: Relative contribution of input parameters to EI NO_x at the approach condition

condition is not a significant contributor. The large temperature rise at the take-off condition reduces the effect of the compressor exit temperature change on combustor geometry at the on-design condition; however, the operating temperature affects the combustion chemistry and residence time and that justifies the operating compressor exit

Contributors to EI NO_X at IDLE

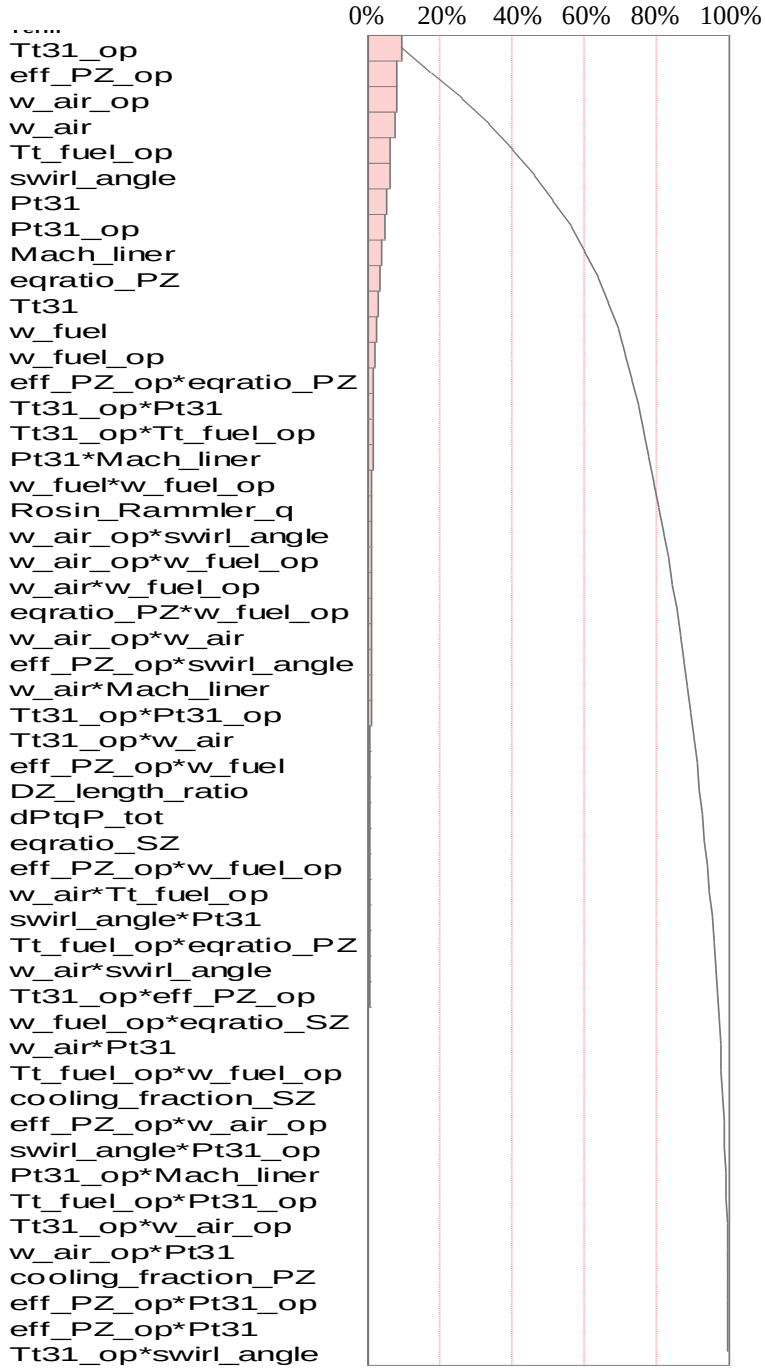

Figure 96: Relative contribution of input parameters to EI NO_x at the idle condition

temperature's first place. It also enhances the droplet evaporation as well as reducing the ignition time, both of which can affect the EI NO_x levels.

The contribution of the design and operating pressures should be looked at with caution as the current combustion mechanism (Kollrack) is pressure independent. At the design condition, the change in the compressor exit pressure changes the cross section area of the combustor and consequently the volume. At operating power settings, the pressure change affects the residence time in each zone and therefore the EI NO_x level.

In all power settings, the, swirl angle maintains its place among the first six contributors in all power settings. It has a direct effect on the primary zone length at the design condition and the primary zone volume. The effect of the primary and secondary zone equivalence ratios go down as the power setting decreases. This is in consistence with the fact that the EI NO_x is directly linked to the flame temperature and consequently the equivalence ratio. At high power settings the primary and secondary zone equivalence ratios are high and near the stoichiometric value which results in high thermal NO_x formation. However, this is not the case in low power settings.

The liner Mach number is another significant contributor as it derives the size of the combustor cross section area. A lower liner Mach number provides a larger cross section area and larger volume.

Fuel temperature is a significant contributor at the idle condition where evaporation and diffusion flame effects become important and the difference between the surrounding temperature (the compressor exit temperature) and the fuel temperature is smaller than the other cases.

Many input interactions are seen in the climb condition. In experiments 1, Figure 70 and Figure 71 show the importance of the Non-Uniform Mixing model on the EI NOx level. The GNUM model is a non-linear model that that has complex interaction with other parameters through the premixed equivalence ratio and is the cause of the high level of input interactions in the climb condition.

In general, the effects of the combustor characteristics and on-design or operating engine cycle parameters on the EI NO_x are through the change in the primary zone geometry, residence time or combustion.

The Pareto plots in Figure 97, Figure 98, Figure 99 and Figure 100 show the contribution of the combustor characteristics and engine cycle parameters on the EI CO level. Since the EI CO prediction at high power settings is very small and in the scale of the model accuracy, some of the contributors in those power settings may not make a real contribution to the EI CO and are the result of the low fidelity of the model. The high level of the interaction terms may also be related to the model fidelity and CO formation process complexity as well. For that reason only the few top contributors (often the first four inputs) are discussed for CO emission index sensitivity analysis.

Some general observations can be made from the EI CO Pareto plots which are described in the following paragraphs. At the approach condition, many of the inputs or their interactions are removed because their p-values are bigger than 0.1. In this case the higher order effects should be considered at the approach condition.

Similar to the EI NO_x Pareto plots, diffuser parameters and the secondary and dilution zone length to height ratios do not have important effect on the EI CO level. Unlike the EI NO_x, the liner Mach number and Swirl angle have moderate effect at best. The reason is the reaction rate of CO which is fast (unlike NO) and therefore less dependent on the residence time. At take-off and climb, the maximum liner temperature is an important contribution too as it derives the amount of the cooling flow.

In addition, the compressor exit temperature at the operating condition and other engine cycle parameters are often significant. Finally at idle and approach the coupling between different parameters is strong and none of them can be identified as a dominant contributor; however, at idle for which the model has better prediction compared to other power settings, the fuel temperature and primary zone and secondary zone equivalence

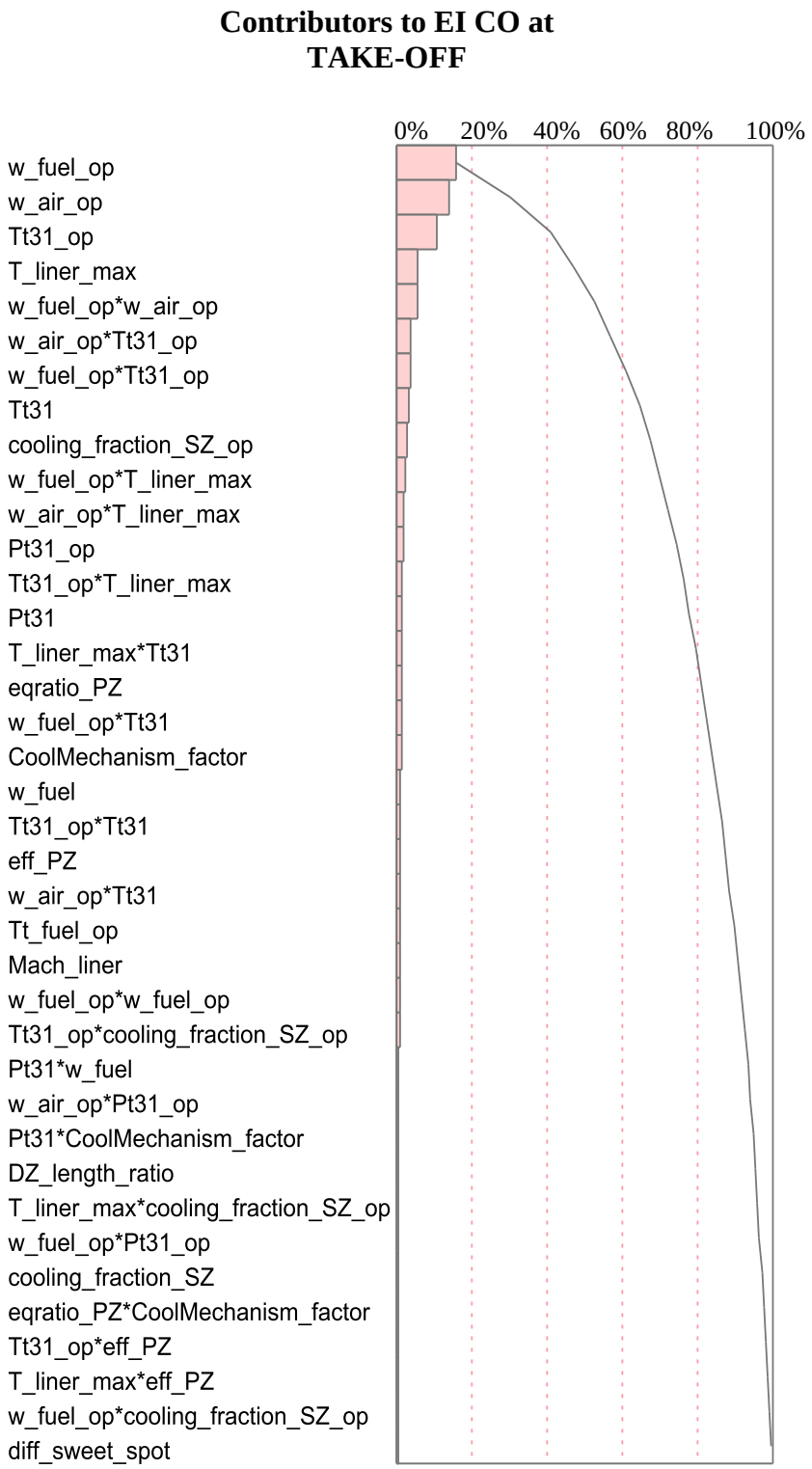

Figure 97: Relative contribution of input parameters to EI CO at the take-off condition

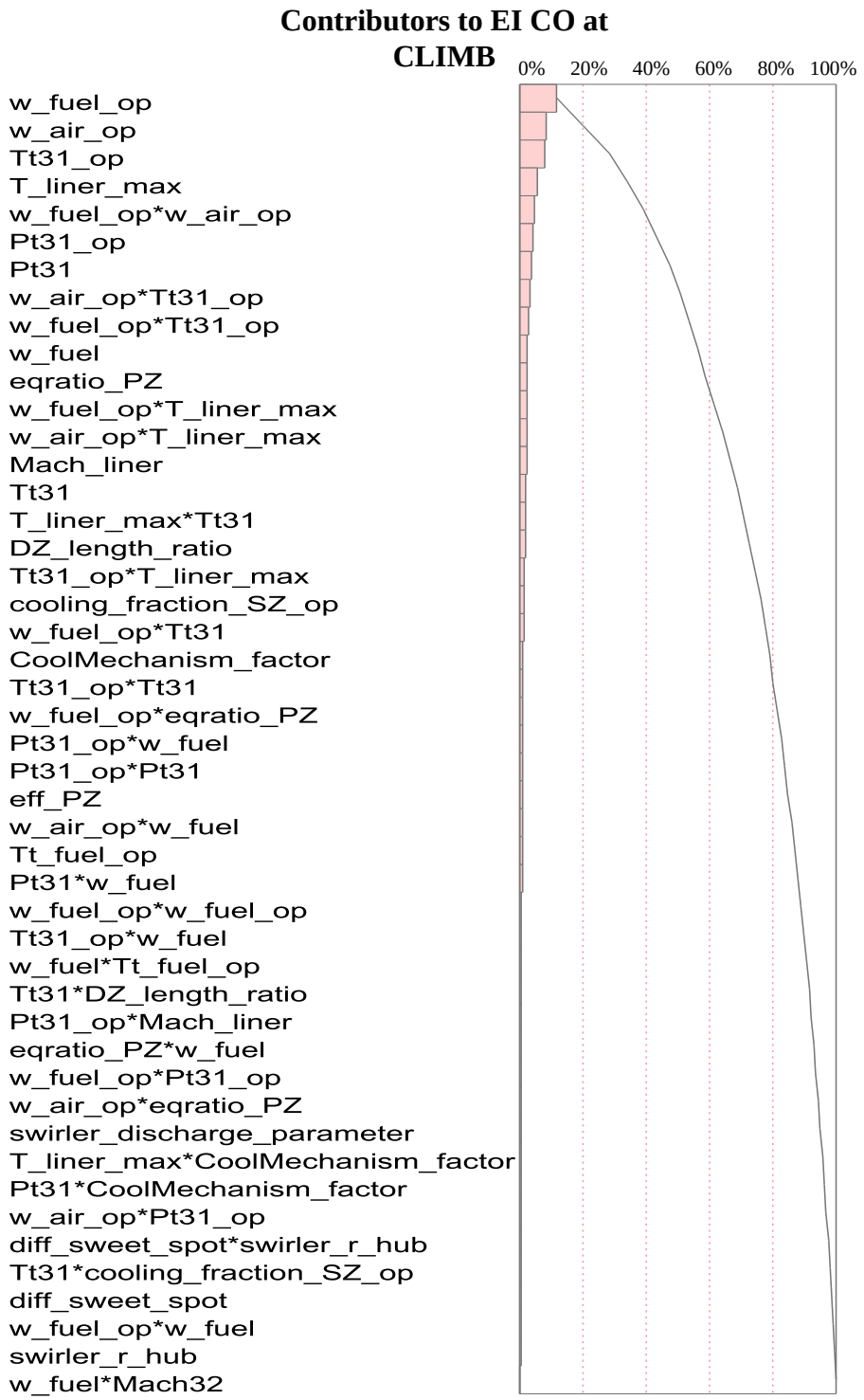

Figure 98: Relative contribution of input parameters to EI CO at the climb condition

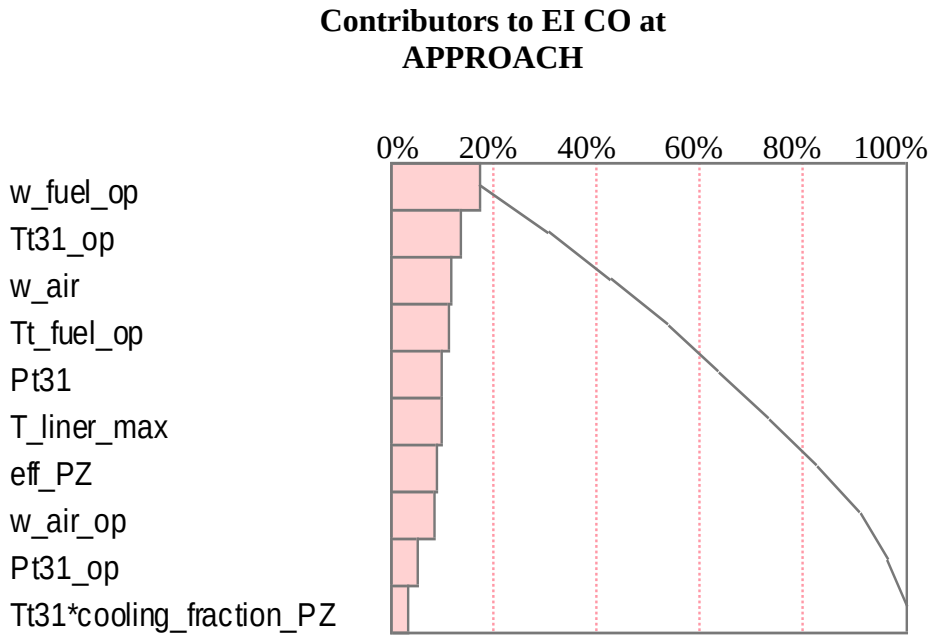

Figure 99: Relative contribution of input parameters to EI CO at the approach condition

ratios are significant contributors. All of these parameters derive the level of CO formations in the primary zone and secondary zone.

Operating fuel flow and air flow are also among the top contributors. Their effect on the EI CO level should be seen through their effect on the primary and secondary zone equivalence ratios as well as cooling flow fraction as they change in operating conditions by changing the fuel or airflow.

In the next experiment, the versatility of the approach is tested. To that end, an emission model is created for an RQL combustor.

7.5 Experiment 3: Emissions Prediction of an RQL Combustor

After the parametric capability and uncertainty reduction capability of the proposed methodology have tested, the last experiment tests the methodology's versatility. For that reason, modeling a different combustor type based on this methodology is required. An unconventional RQL combustor is selected for this purpose. The goal in an RQL combustor is that by quick mixing and quenching the rich mixture, the stoichiometric

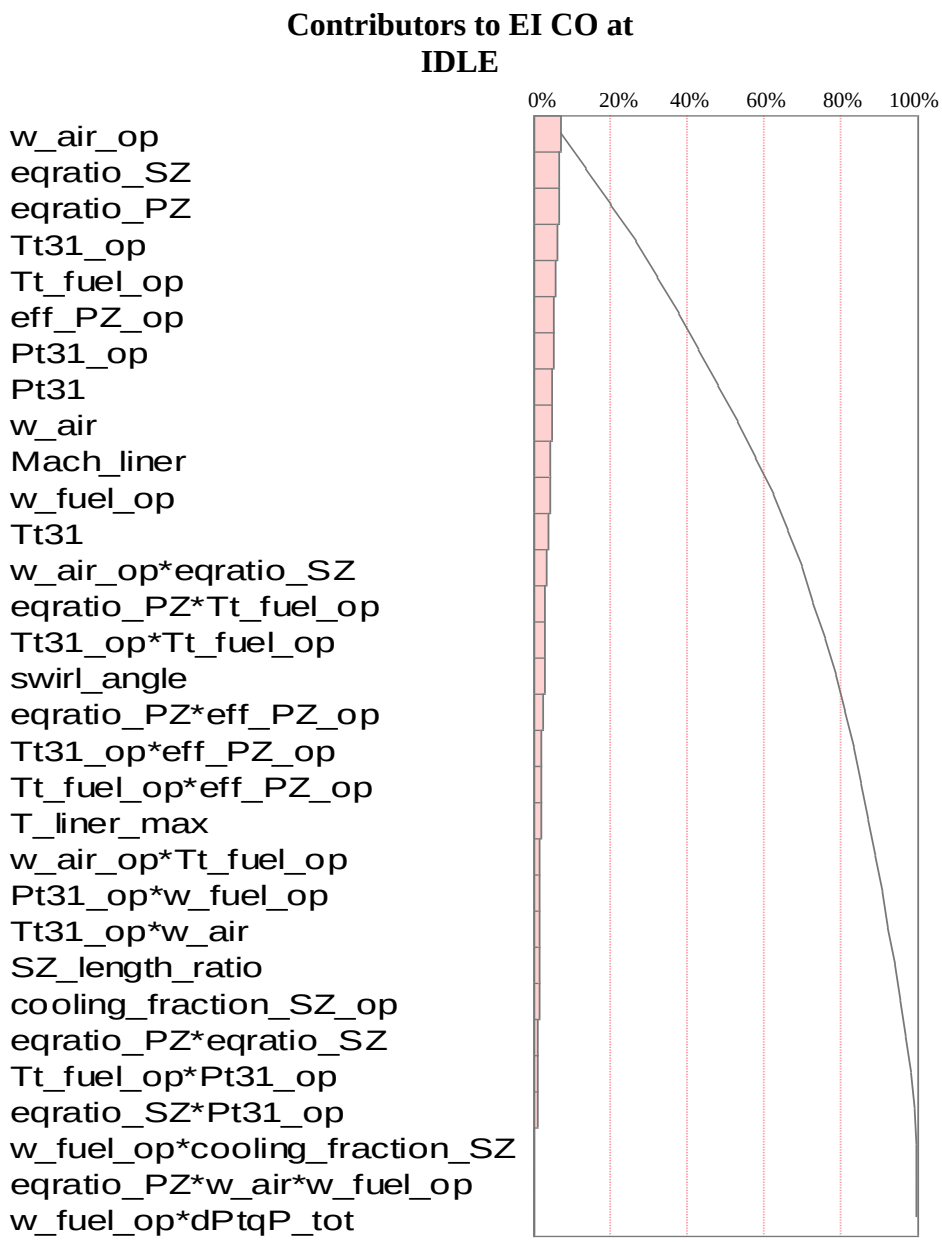

Figure 100: Relative contribution of input parameters to EI CO at the idle condition

flame region that corresponds to the high level of thermal NO_x is bypassed (Figure 101).

Unlike the SAC, where there is information about experimental (E^3 SAC) and operational (CFM56) concepts that could be used to validate the model, it is harder to validate the RQL emission model due to the lack of available information. One of the reports about an RQL combustor in the public domain is the one prepared for the NASA high speed research (HSR) program [1] for LDI and RQL combustors.

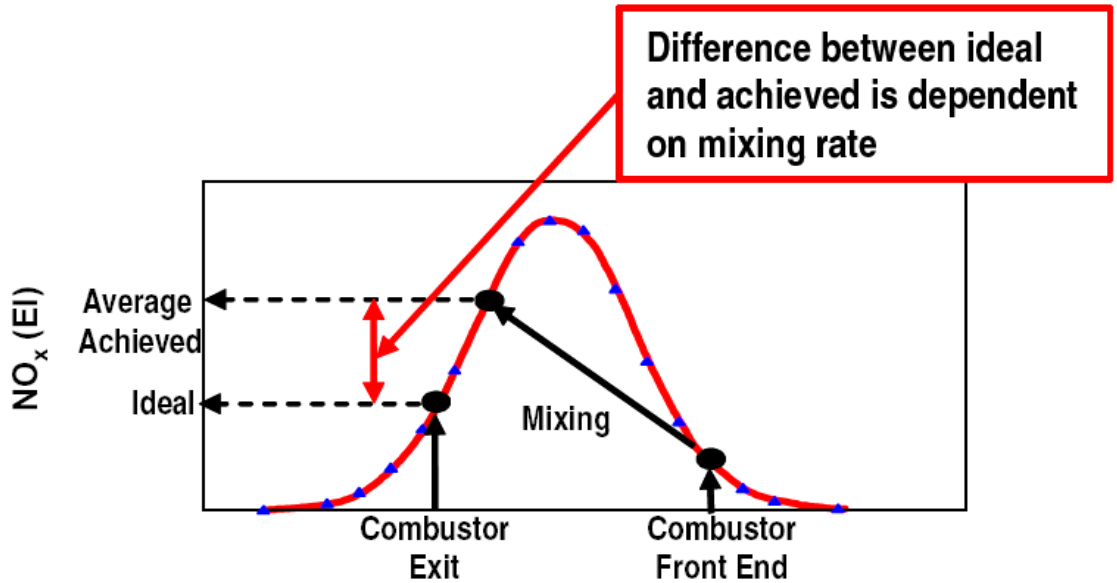

Figure 101: Quick mixing in RQL combustor to bypass the high NO_x stoichiometric region [17]

It contains a description of the size and operating conditions of each type. Three RQL concepts that are described in Chapter 4 are tested and their results are provided in the report. Two of these concepts (reduced scale quench) have a complex geometry and flow-field. Some of these concepts are also constructed in the form of the dual annular combustor which requires a different 1D flow-field model composed of both dual annular and RQL concepts. Moving toward such concepts before testing the simpler and more basic model is not justified in this research. The other RQL combustor, the tubular Wall-Jet concept, is simpler to model and it is selected in this research. Unfortunately the emission data for the Wall-Jet concept is provided only for a single point of the supersonic condition. Although not enough, only this single point is used in this research for the validation.

The NASA Wall-Jet RQL combustor is a tubular combustor composed of a rich zone, a Mixing zone and a lean zone. There is not any apparent indication about the existence of the dilution zone in this type of combustor. The final configuration has 12 tubular modules (Figure 102).

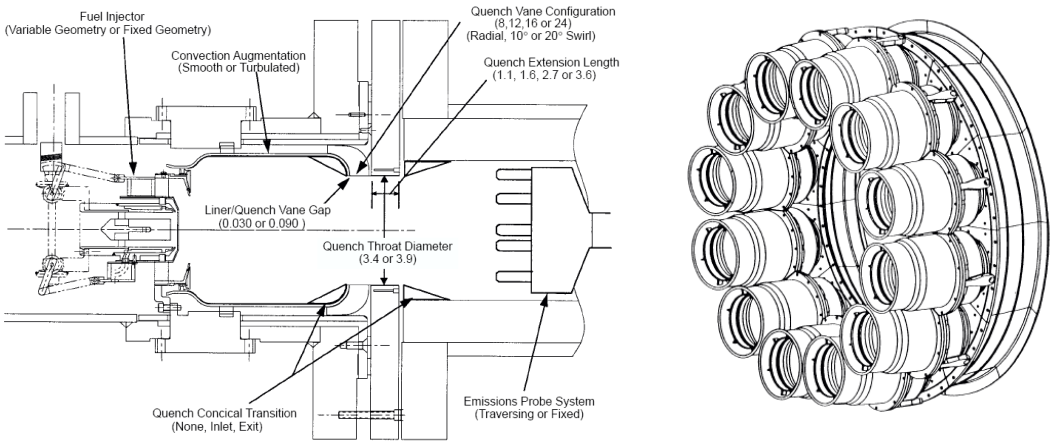

Figure 102: The NASA HSR Wall-Jet RQL single module and final configuration [1]

Table 45 shows the dimensions and some other data of the Wall-Jet RQL combustor. The length of the rich zone and the lean zone includes the transition sections between the rich zone and the mixing zone and the transient section between the mixing zone and the lean zone.

Table 45: Geometry information of the Wall-Jet RQL combustor [1]

Dimensions	RZ	MZ	LZ
Diameter (in)	5	3.4	5
Length (in)	5.42(3.82+1.6)	3.4	5.1(3.2+1.9)
Equivalence ratio	1.6-2	0.5-0.6	0.44
Orifice number	-	8-24	-
Orifice inner diameter (in)	-	0.719-0.41	-
Air fractions at supersonic cruise	22% -%24	71%-73%	71%-73%
Cooling	0	0	5%

Table 46 shows the engine cycle parameters of the high-speed airplane propulsion system at the compressor exit. The parameter values are obtained from different pages, tables and graphs. As mentioned earlier, the emission values of the Wall-Jet concept are given just for a single point of the supersonic cruise condition.

Similar to the SAC emission model, the RQL emission model consists of two major components of 1D flow-field model and CRN model with additional models for droplet evaporation and diffusion burning (DEDB) and non-uniform mixture (NUM) (Figure 103).

Table 46: RQL combustor engine cycle parameters [1].

Test Conditions	T_3 (R)	P_3 (psia)	FAR	W_{air} (lb/s)	W_{fuel} (lb/s)	EI NO_x	EI CO
Supersonic cruise	1660	150	0.03	39.6	1.18	13.6	4-20
100% Thrust (take-off)	1379	301	0.0329	79.2	2.6	-	-
65% Thrust (climb)	1200	212	0.0248	39.6	0.98	-	-
34% Thrust (approach)	1048	134	0.0187	38.4	0.72	-	-

The 1D flow-field model consists of the rich zone element connected to the mixing zone with the transition zone between them. The mixing zone element is connected to the lean zone element with another transition zone between them. At the end, the lean zone element is connected to the dilution zone element. Although the dilution zone does not exist in the Wall-Jet RQL combustor, adding this zone at the end

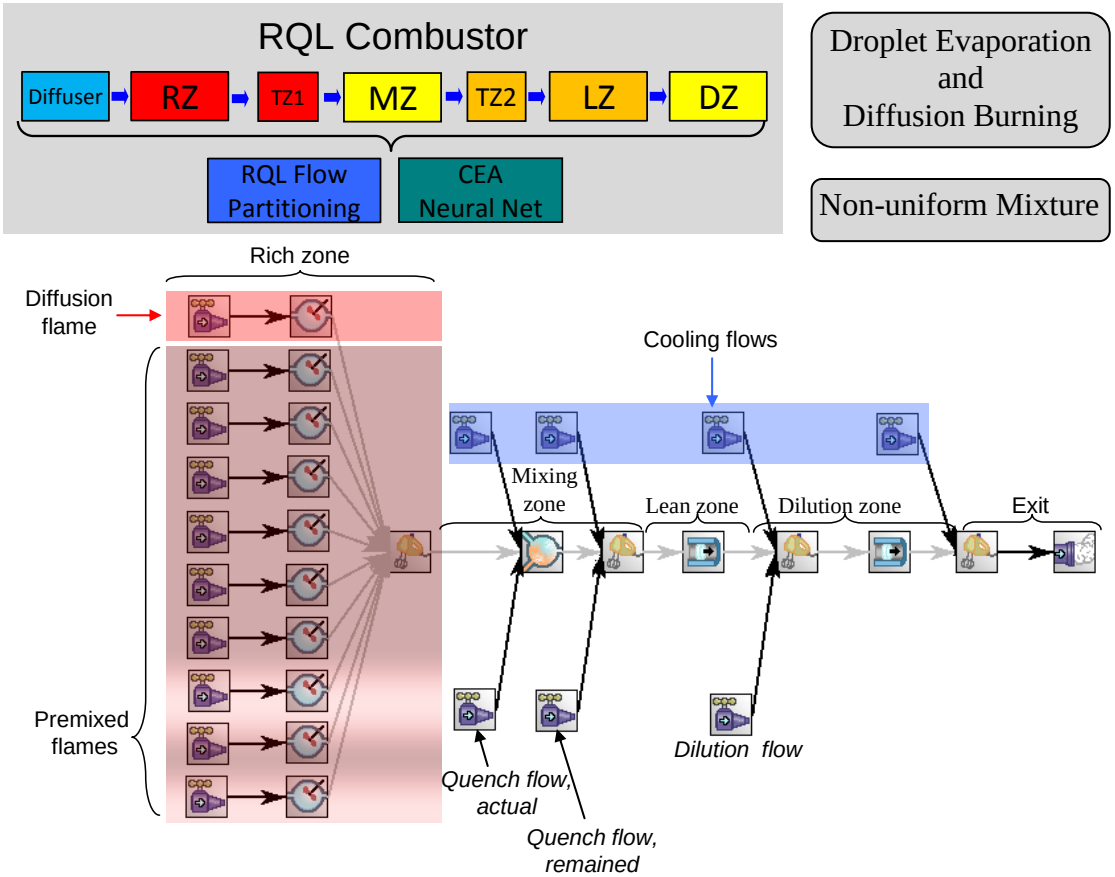

Figure 103: The 1D flow-field and CRN models of the RQL combustor configuration in CHEMKIN

of the combustor model can make the 1D flow-field model more generic and applicable to other RQL concepts that have the dilution zone. For the current Wall-Jet model; however, inputs are defined in a way that makes the dilution flow and dilution zone length negligible.

The inputs to the 1D flow-field model are set in a way to provide the size and the flow distribution given in Table 46. In the Wall-Jet RQL combustor, a combined high shear swirler and air-blast atomizer is used to achieve a good mixing; however, no simple mathematical model has been found for this injector type to be used in the emission model. Consequently, the same type of injector (simplex pressure swirl) which is used for the SAC emission model is used here with the same characteristics (same SMD model, shape factor of 2.5 and flow number of 1e-7 m^2). The fuel temperature is also set to the nominal value of 550 R. The unmixedness degree, is based on the GNUM model obtained from the experiment one and values for an RQL combustor from the unmixedness curve [9]. For the premixed equivalence ratios beyond the validity range of equation (110), the unmixedness degree is assumed to be 0.18 (the value at the higher end of the equation (110) due to the required good mixing quality in the rich section of the RQL. This low value is close to the value shown in [9].

The design point is selected to be the take-off condition and the rich zone equivalence ratio is 1.8 at that point and the value of 0.52 is obtained for the lean zone equivalence ratio at the take-off condition. For the rest of the power settings, the variable geometry swirler area varies to keep the rich zone equivalence ratio either at the rich condition (φ=1.8-2) which is for the high power setting conditions or at the lean condition (φ=0.7) for low power settings. The equivalence ratio scheduling is adopted from the information provided in Figure 24 [1]. The goal is to find the smaller change in the swirler area to achieve the rich or lean equivalence ratio in the rich zone. At the supersonic condition, the swirler area coefficient should be set to 0.8 (20% reduction in

the swirler area compared to the design condition to achieve the value provided for the rich zone flow fraction (0.22) that corresponds to the equivalence ratio of 1.93.

The cooling mechanism of the Wall-Jet RQL combustor is based on conductive cooling in the first sections and conventional film cooling in the rest of the combustor. Exact modeling of the cooling requires more data and detailed modeling. For the Wall-Jet RQL, the same cooling model as in the previous experiments is used. The gas temperature is assumed to be the average of the rich and lean zone temperatures. Since the rich and mixing zone sections of this model do not have any cooling flow going into the core section, all the cooling flow (100%) goes to the lean zone section. Although the take-off condition is selected to be the design point, the critical cooling requirement occurs in the supersonic condition where the combustor inlet temperature is maximum (1660R) and the cooling requirement should be satisfied at that condition too. To satisfy the cooling requirement at the supersonic condition, first the material temperature is set to 2500 R and the take-off cooling flow is varied by a coefficient (changing the effective cooling holes area) until the supersonic requirement is met. As a result the cooling flow at the take-off condition is increased by 15% to satisfy the supersonic cooling requirement; in addition the cooling mechanism factor is changed until the value of 5% is obtained at the supersonic condition.

There are not too many parameters to necessitate the use of Monte Carlo filtering in this experiment. Most of the inputs are either known, obtained from the previous experiments or can be determined. The results are shown in Table 47. No information is provided about the diffuser; therefore, the inputs to the diffuser model are based on the previous experiments and are provided to the 1D flow-field model because they are required by it; otherwise, they could be excluded. Also in the same table, the length of the transition zone from rich to mixing is included in the length of the rich zone and the length of the transition zone from mixing to lean zones is included in the length of the lean zone.

Table 47: Inputs of the RQL combustor 1D flow-field model

Input Parameter	Value	Input Parameter	Value
Inlet mean radius	15	Cooling mechanism factor	0.03
Exit mean radius	15	η_{PZ}	0.98
Mach 31	0.22	φ_{PZ}	1.8
Mach 32	0.056	RZ to MZ convergence angle	32
Mach liner	0.013	$c_{D\,MZ}$	0.55
Diffuser half angle	3.5	MZ length ratio	1
Passage number	1	$\text{Area}_{MZ}/\text{Area}_{PZ}$	0.46
K_{SW}	1.5	Mixing model $_{MZ}$	CURL
Swirl angle	59	Mixing model factor $_{MZ}$	2
Swirler hub radius	1	Mixing mode $_{MZ}$	CHEM
Number of injectors	12	MZ to LZ divergence angle	-17
$\dot{m}_{air\ nozzle}/\dot{m}_{fuel}$	0	η_{LZ}	0.997
$\Delta P/P$ burner	0.08	φ_{LZ}	0.51
T_{fuel}	550	LZ length ratio	0.5
$T_{Max\ Liner}$	2500	Mach 40	0.06

Figure 104 shows the 2D drawing of the Wall-Jet RQL combustor created by the 1D flow-field model and the actual 2D drawing of the combustor. Table 48 shows the geometry and flow fractions of the 1D flow-field model compared to the actual values. Table 49 shows the variation of the swirler and corresponding rich and lean zones equivalence ratios, burner pressure loss coefficient and burner pressure drop. As described in section 5.1.5, for the RQL combustor with variable geometry, the pressure loss coefficient and pressure drop are variable and a function of the geometry variation.

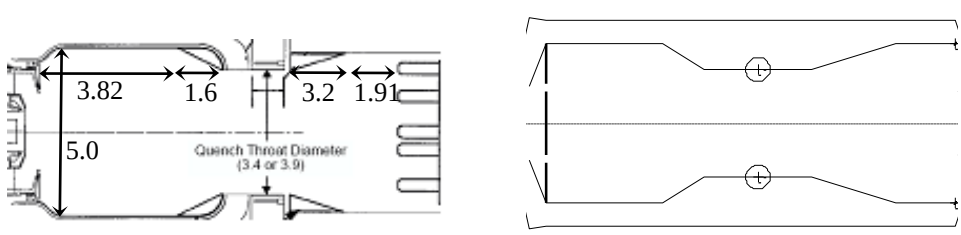

Figure 104: The Wall-Jet RQL combustor actual and 1D flow-field model produced drawings

Table 48: Comparison of the 1D flow-field model outputs and actual values

Geometry	Actual	Predicted
Quench orifices number per module / diameter (in)	8-24 (0.719-0.41)	8 (0.77)
Rich zone height (in)	5	5.07
Rich zone length (in)	5.42	5.04
Quench zone height (in)	3.4	3.44
Quench zone length (in)	3.4	3.44
Lean zone height (in)	5	5.00
Lean zone length (in)	5.1	4.5
RZ fraction (Supersonic)	22% - 24%	22.6%
LZ fraction (Supersonic)	71%-73%	71.7%
Cooling fraction (Supersonic)	5%	5.2%

Table 49: swirler area and associated parameters' variation

Power Setting	$\Delta A_{SW}/A_{SW\ TO}$	φ_{RZ}	φ_{LZ}	$\Delta P/P$	$\Delta P/Q$
Supersonic cruise	-20%	1.93	0.47	10%	40.6
100% Thrust (Take-off)	0	1.8	0.52	7%	36
65% Thrust (Climb)	-30%	1.8	0.39	4%	43
34% Thrust (Approach)	+70%	0.72	0.29	4.9%	25.7

Table 50 shows the model outputs for the unmixedness degree, EI NO_x and EI CO. More model outputs are provided in Appendix C.

Figure 105 shows the emission indices of NO_x and CO for the approach, supersonic cruise, climb and take-off conditions. The results are shown with fuel flow in the abscissa. At the supersonic condition (1.18 lb/s) the model can predict the EI NO_x with acceptable accuracy. A significant reduction is observed in the EI NO_x form the supersonic (fuel flow of 1.18 lb/s) to the take-off condition (fuel flow of 2.6 lb/s). Since

Table 50: Predicted emission indices and unmixedness degrees of the Wall-Jet RQL combustor

Test Conditions	EI NOx	EI CO	Unmixedness
Supersonic cruise	14.60	2.61	0.18
100% Thrust (Take-off)	4.18	0.65	0.18
65% Thrust (Climb)	12.03	0.18	0.18
34% Thrust (Approach)	12.97	0.21	0.85

the rich zone temperature at all conditions is relatively constant (Figure 109), this change is more related to the reduced evaporation due to the increased droplet size. The great reduction of the fuel flow from the take-off to other condition is the reason for the increased droplet size, which leaves a high fraction of the fuel in liquid form. Figure 106 helps to better understand this phenomenon. The figure shows that the droplet distribution variation is smaller at the take-off compared to other power settings droplet distributions that are similar in scale and shape (blue curves). Also most of the droplets are vaporized at the take-off condition while this is not the case at other power settings (red curves). The high degree of fuel evaporation at the take-off condition is the reason of low EI NO_x at this power setting. The EI NO_x decrease from the supersonic cruise condition (fuel flow of 1.18 lb/s) to the climb condition (fuel flow of 0.98 lb/s) or the approach condition (fuel flow of 0.72 lb/s) can be the result of the reduction in the inlet temperature (having the similar degree of evaporation). The close values of the EI NO_x at the climb and approach conditions is the result of the competition between the increase in the ignition delay time (temperature and equivalence ratio decrease) and the increase in

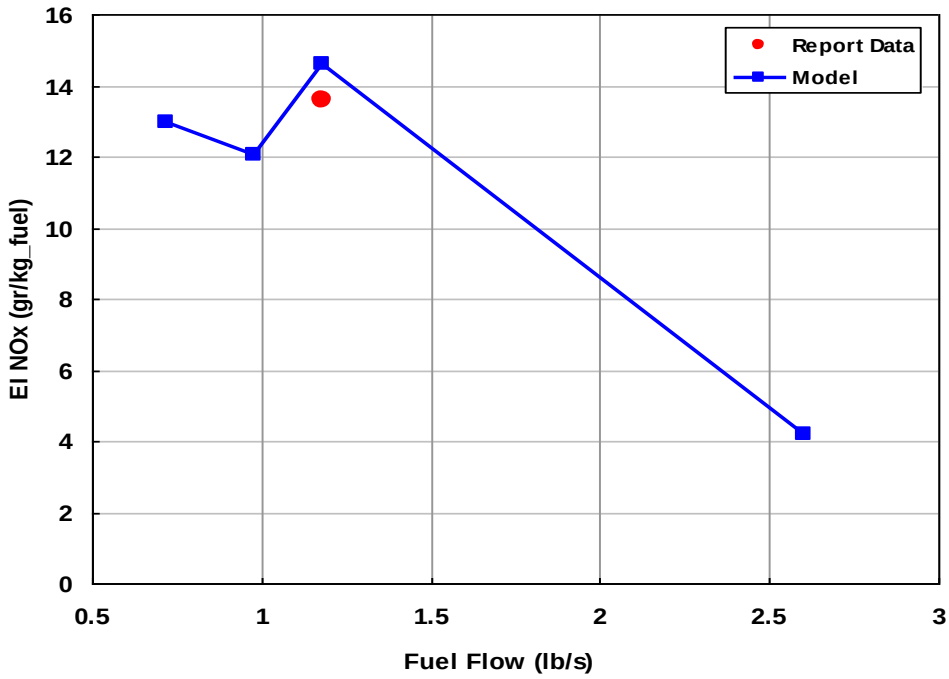

Figure 105: The Wall-Jet RQL combustor predicted and actual NO_x emission indices

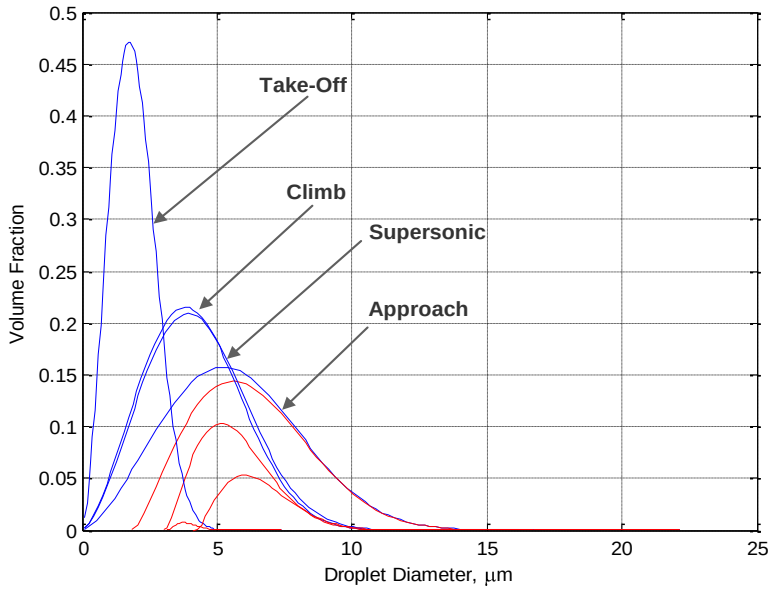

Figure 106: The Wall-Jet RQL combustor droplet distributions

the droplet size. Using a better injector model may reduce this big difference as it could provide a more realistic droplet evaporation model and evaporation degree at all power settings.

Similar to the SAC model, capturing the EI CO level is more challenging; however, the model prediction at the supersonic condition has the same order of magnitude as the given data (Figure 107). Experimental results or data are not available to compare the result of the model with them at other power settings. The change of the CO level for this RQL combustor is not known, although it is expected that the EI CO level increases at low power settings when there is a higher possibility of the flame extinction and local quenching and the result is against such an expectation. One reason is the presence of a different flow-field and air staging in the RQL that affects the chemistry of the combustion. The reason can be traced back to the way that the structure of the CRN is created as well as the complexity of capturing the CO emission level with this methodology. The current CRN has enough fidelity to qualitatively model flame extinction and quenching in the SAC primary zone, however since the model in the mixing and lean zones is simplified, it is unable to capture the quenching effect in those

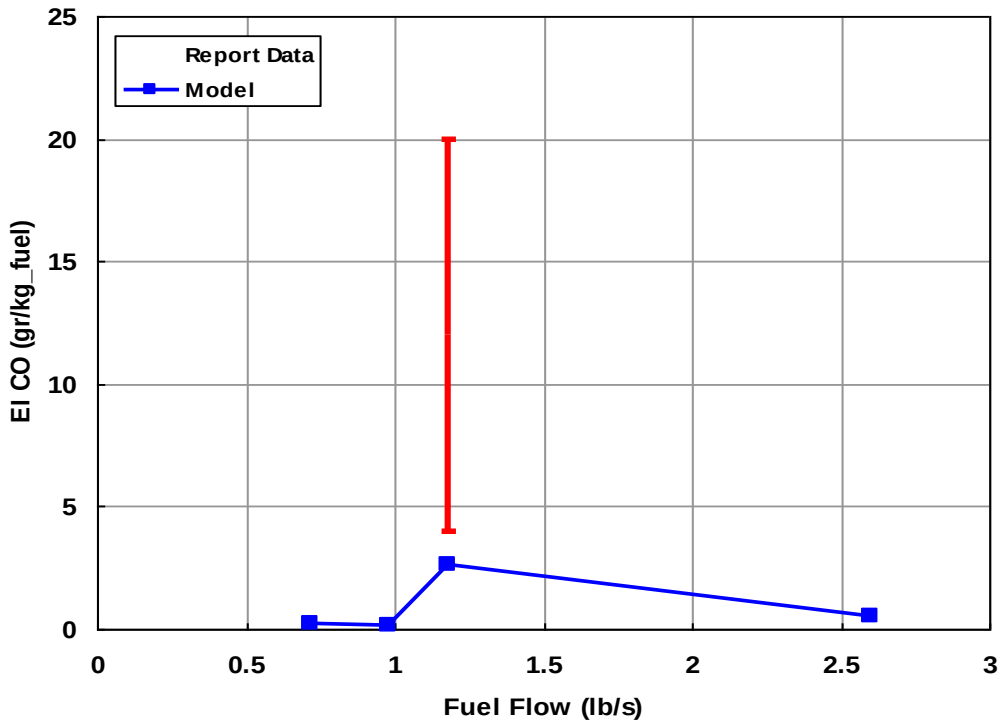

Figure 107: The Wall-Jet RQL combustor predicted and actual CO emission indices

sections where it has a high contribution to EI CO level in RQL combustor. In the current Wall-Jet combustor, the rich zone often operates away from the low equivalence ratio, where its CO production level can be captured by the current CRN. The main source of CO production in the RQL is the mixing zone and the lean zone where the dilution jets freeze the CO to CO_2 reaction. The capability of the current model for CO prediction is limited here as the quenching effect of the jet in the mixing zone cannot be captured by the current one dimensional CRN model and single reactors in the mixing and lean zones.

Figure 108 shows the equivalence ratio distribution of the premixed mixture at four power settings. Since the variable geometry feature keeps the rich zone equivalence ratio at the rich condition, the take-off, climb and approach conditions are distributed over the rich interval. The equivalence ratio at the approach condition is kept away from the stoichiometric region by keeping the ratio at lean condition (equivalence ratio of 0.7) and therefore the equivalence ratio is distributed over the lean to the stoichiometric interval.

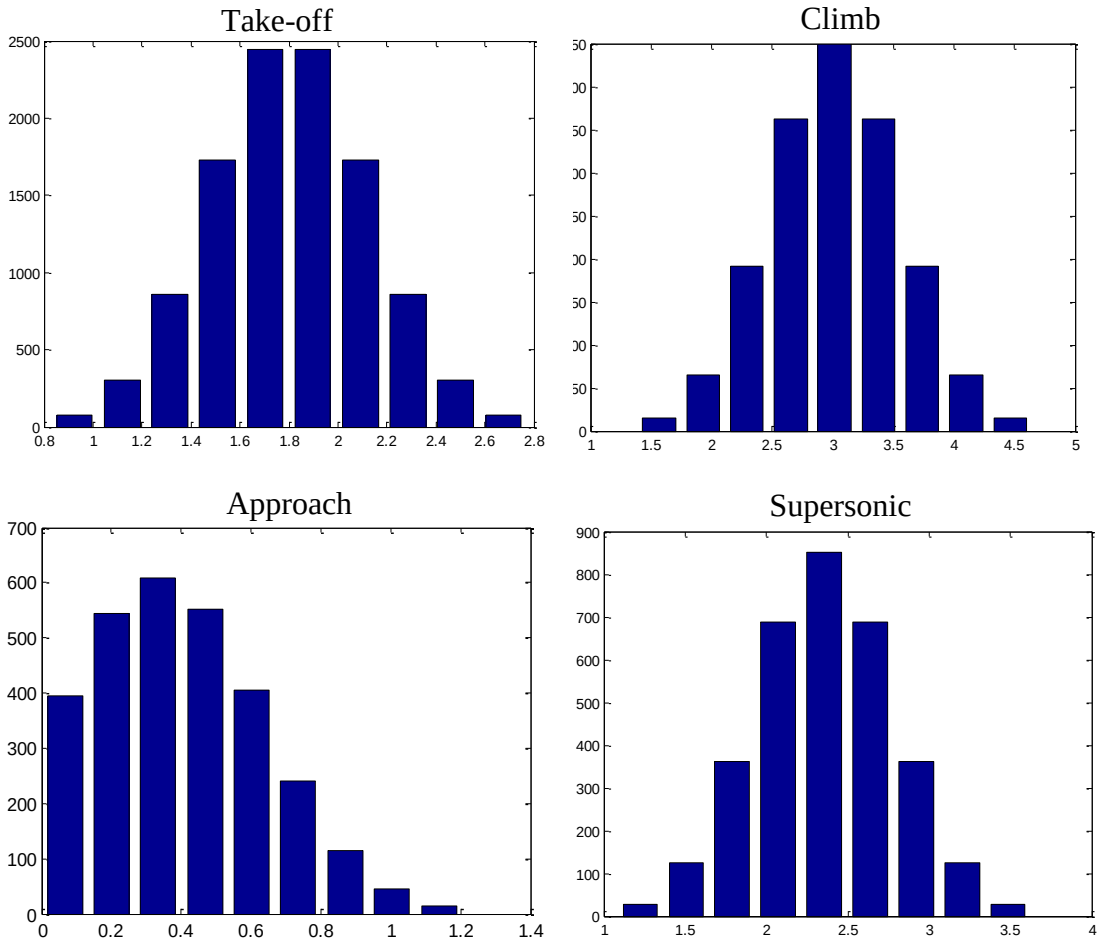

Figure 108: The Wall-Jet RQL combustor premixed equivalence ratio distribution in the rich zone

Figure 109 shows the axial temperature variation in the combustor calculated by 1D flow-field and CRN models. A general pattern can be seen in all power settings where there is an initial temperature rise in the rich zone followed by a temperature drop due to the quick mixing of the quenching jets with the hot core gases. There is an additional temperature increase in the lean zone due to lean combustion. This up-and-down trend is unique to the RQL concept. In the SAC model, the temperature variation trend monotonically decreases from the primary zone to the dilution zone as it is shown in the experiment 1 (Figure 83). Another difference between the RQL and SAC temperature profile is the difference between their peak temperature levels. In the RQL combustor, the maximum temperature level in all power settings is around the same level and given

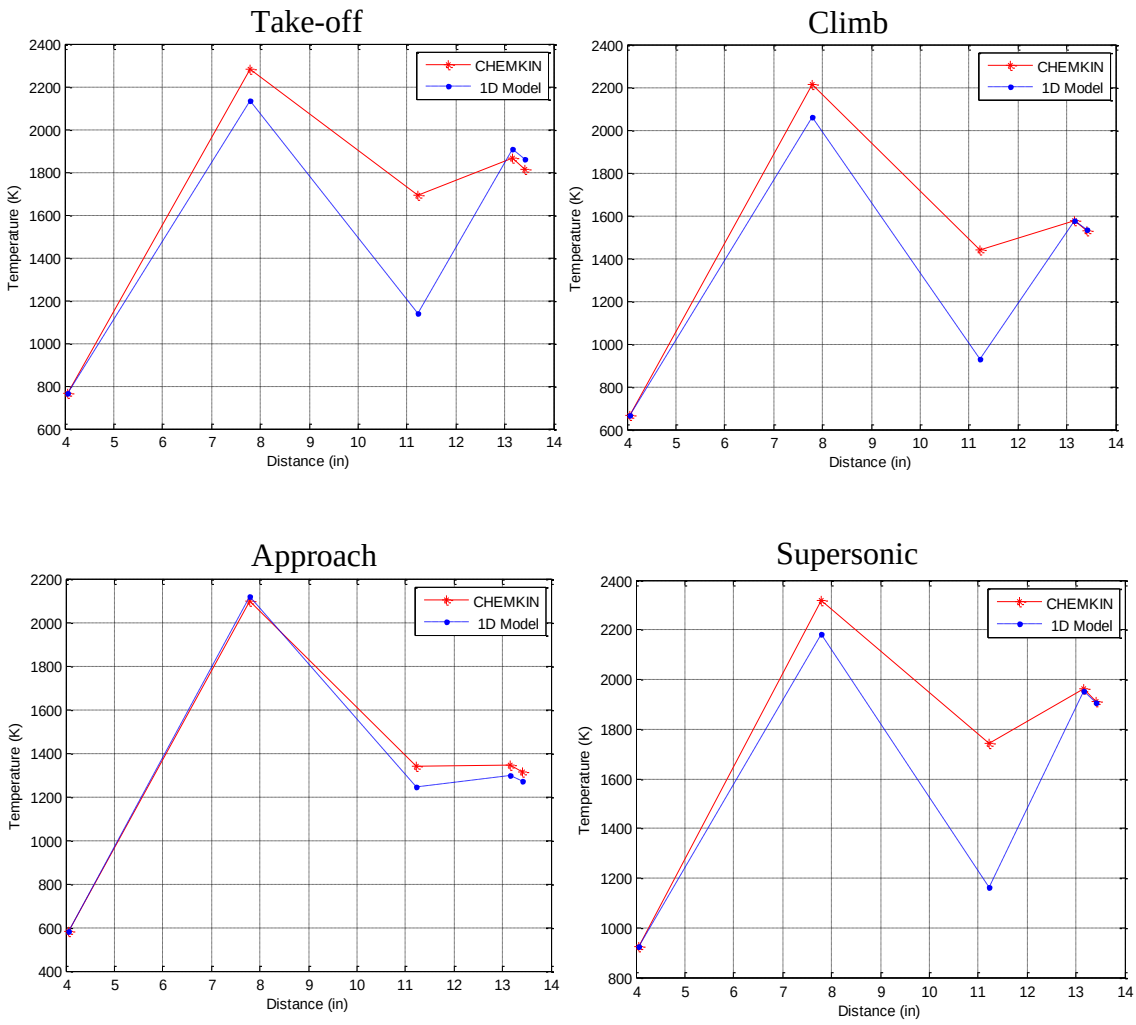

Figure 109: The Wall-Jet RQL combustor axial temperature variation across combustor zones

the same condition, they will be lower than the SAC combustor due to rich (or lean at low power settings) combustion.

A noticeable gap is seen between the 1D flow-field model and the CRN model temperature predictions in the mixing zone. It is explained by the type of the mixing in the mixing zone assumed in 1D flow-field and CRN models. Due to the lack of fidelity, in the 1D flow-field model the assumption is that quench jets mix with the hot gases perfectly without any combustion taking place in the zone (non-reactive mixing) and equation (75) is used to calculate this temperature; however, in the CRN model, the finite rate chemistry model is employed to calculate the exit temperature of the mixing zone.

The higher temperature of the mixing zone in the CRN model is based on the fact that a degree of combustion is present in the mixing zone that results in a higher temperature level. The small temperature drop at the end is the result of the addition of the cooling flow, which lowers the exit temperature.

Figure 110 shows an example of the PaSR reactor output in the mixing zone which is the pdf of the temperature, NO, CO, CO_2 and H_2O at the PaSR exit for the supersonic condition. They show that for each output parameter, there is a range of values instead of a single deterministic value that is the result of the Monte Carlo simulation performed in the PaSR. Unfortunately, it is not possible to use these pdf's as input for the next reactor (and this is also one reason for bad EI CO prediction); therefore, the mean value of these pdf's is used as the input for the next reactor.

As additional study and validation, the variation of the EI NO_x and EI CO are obtained as a function of the mixing to rich zone area ratio and Figure 111 shows the result. The figure shows that increasing the mixing zone area (for the fixed rich zone area) would increase the emissions. This behavior is consistent with the physical phenomena inside the combustor. As the area of the mixing zone increases, the size of the

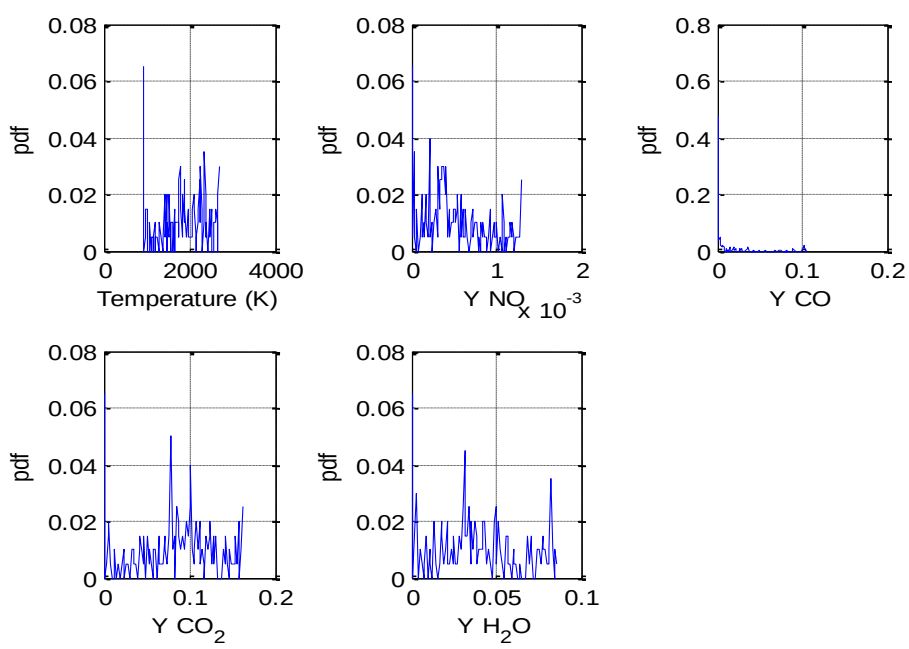

Figure 110: The pdf of temperature, NO, CO, CO2 and H2O at the output of the PaSR at supersonic cruise condition

largest eddies increases too, which deteriorates the mixing quality in the mixing zone (decreasing the mixing zone unmixedness). The reduction of the mixing quality increases the level of NO_x and CO emissions. The variation of the EI NO_x demonstrates a linear relation with the change in the area ratio; however, the EI CO variation with the area ratio is non-linear and its rate of change increases with the increase of the area ratio.

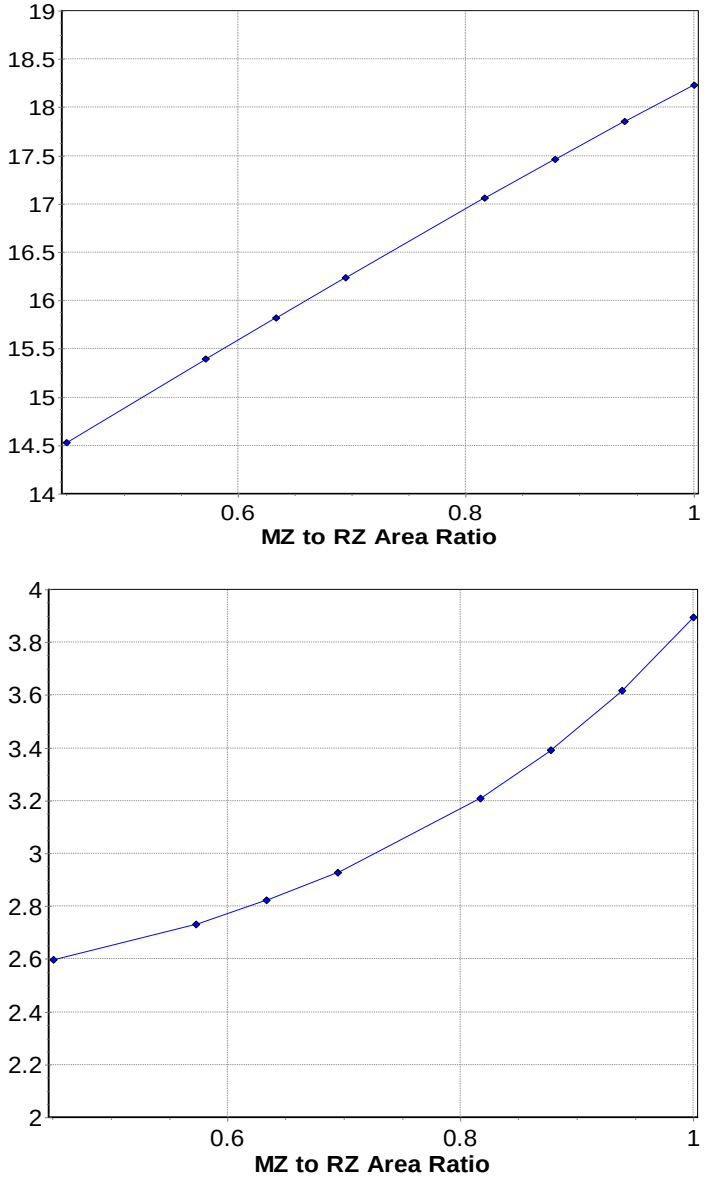

Figure 111: Effect of changing the mixing to rich zone area ratio on the emission indices

The third experiment demonstrated that the model may be used for a combustor with different architecture. Although due to the limited available data and component models, the model assessment is not comprehensive, for the given limited data, the model shows acceptable results.

CHAPTER 8

DISCUSSION AND CONCLUSION

This chapter provides an overview of the research conducted in this thesis and the implemented methodology. First a brief review of the motivation, research objective, research questions and formulated hypotheses is provided. For each stated hypothesis, a process that has led to prove (or disprove) that hypothesis is described. A contributions of the research conducted in this thesis is provided next followed by the limitation of the model. The discussion of the limitations opens the way to provide the recommendations for the future work and areas that need improvement and the last section of this chapter and this thesis is the final remarks.

8.1 Review

The motivation for the present research is derived from the need to develop a methodology to predict gas turbine emissions at the conceptual design phase. A parametric and versatile emission model is needed to be integrated with engine and aircraft models to assess the effect of design or operating parameters on the emission levels and to capture the interaction between those parameters and emission levels. Such an integrated framework is needed to study the effect of the future aircraft fleet on the environment around the airports and at cruising altitudes. The goal is more focused to capture the trend rather than accurately predict the emission levels at this early design phase.

To address those needs, a methodology is provided to model combustor emissions by considering a simplified model of two main disciplines which are one dimensional internal flow-field and finite rate chemistry. Additional models are assumed to have important effect on the accuracy of the model which are droplet evaporation and non-

uniform mixture. A literature and background search is performed to find appropriate models or methods to be used for the mentioned disciplines and phenomena.

8.2 Revisiting Research Questions and Hypotheses

In this section, the research questions and hypotheses are provided again and it is discussed whether the proposed hypotheses could answer the research questions.

8.2.1 Research Questions

The following research questions have been posed in Chapter 1 and restated in Chapter 3 and are provided here as well.

Research Question 1(RQ 1): How can an emissions prediction approach be made more parametric in a way that a variation in a combustor design parameter is reflected in the emission levels?

Research Question 2(RQ2): How can different combustor architectures be accommodated in an emissions prediction approach and their effects on emission levels be captured at different operating conditions?

Research Question 3.1 (RQ 3.1): How can the uncertainties of emissions prediction model be reduced in the conceptual design phase?

Research Question 3.2 (RQ 3.2): How can the uncertainties in the emissions-prediction model be captured and quantified?

8.2.2 Hypotheses

The Hypothesis 1 is based on the research questions 1 and 2:

***Hypothesis 1 (H1)*:**The addition of combustor internal flow-field analysis using modular component modeling approach to the combustion analysis using

the chemical reactor network (CRN) approach results in a more versatile and parametric emissions prediction approach for different combustor types, different operating conditions, and different combustor design parameters.

To test the first hypothesis, major components in single annular combustor and RQL combustor were identified and modeled. A library of these components was created as MATLB files that can be used to construct new combustor architecture. In Sections 0 and 7.4 these components were put together to create a 1D flow-field model of SAC and RQL combustor internal flow-fields. A network of elementary chemical reactors (PSR, PFR, Mixer and PaSR) was also constructed to model the finite rate chemistry of the combustion process. Also the Droplet Evaporation and Diffusion Burning (DEDB) and Non-Uniform Mixture (NUM) models were added to the emission model. In the first experiment, to tests the parametric capability of the approach, the emission model was applied to CFM56 and E^3 single annular combustors. The results (especially EI NOx) showed good agreement between the prediction and experiments or available data.

To test the versatility of the approach, the emission model of NASA Wall-Jet RQL combustor was developed. Lack of analytical model and data was a major obstacle for creating a comprehensive model and assessment of the results. For the provided single point data, the model showed acceptable performance for the NO_x emission index. The intention of this experiment was to test the versatility of the model which was proved to some extent.

The hypothesis 2 is based on the research questions 3.1 and 3.2:

***Hypothesis 2 (H2)*:** An integrated emissions prediction approach with reduced uncertainties can be developed by modeling and integrating important phenomena in the emissions formation process using hybrid models. The most important phenomena are assumed to be droplet evaporation/burning and air/fuel

mixture non-uniformity. An interface provides a line of communication between the disciplines.

- *Secondary Hypothesis 2A*: The following simplified models are expected to reduce epistemic uncertainties of the emissions prediction**:**
    - Probabilistic unmixedness model
    - Droplet evaporation model
    - Diffusion burning based on un-vaporized fuel flow
- *Secondary Hypothesis 2B*: The Monte Carlo analysis can model the epistemic uncertainties. A comparison of the uncertainty analysis of a complete model with deficient models can capture the potential improvements or deterioration of emission uncertainties. A sensitivity analysis can model the aleatory uncertainties and show the effect of the input uncertainties (variations) on the emission levels.

A Generalized Non-Uniform Mixture (GNUM) model was created to find the relation between the unmixedness degree and premixed equivalence ratio. The emission model of the CFM56-7B27 SAC was used to assess the uncertainty of the inputs on the emissions prediction accuracy and variability. It was shown that removing anyone of the DEDB or GNUM models will increase the prediction variability (standard deviation) and reduce the accuracy (distribution mean). The effects were not the same at different power settings; at low power settings the DEDB model was more important than GNUM while at higher power settings the GNUM model had more effect. The changes were more visible on EI NOx prediction than EI CO prediction. The variability of the EI CO at idle was increased by adding DEDB and GNUM models however the distribution moved closer to the target. The large variability of EI CO at the idle condition, showed the high level of EI CO sensitivity to the inputs.

The experiments showed that by addition of DEDB and GNUM the uncertainties were reduced (especially for the EI NO_x prediction).

A sensitivity analysis of emission model inputs was also performed on the model. The analysis showed the importance of many inputs (not just a few) on the emission levels as well as the importance of combustor characteristics besides the engine cycle parameters. The results showed that the model captured the right inputs as important contributors to the EI NO_x (cycle parameters, swirl angle and some primary and secondary zone parameters). The results also showed the important contribution of the cycle parameters at all power settings and primary and secondary equivalence ratios at idle to the EI CO.

8.3 Contributions

The attempt in this research is focused to narrow the gap between the combustion field and system design field. The experts and researchers in each group have different expectation from an emission model which is stemmed from the nature of the field they are working on. On the one hand, for those who work in combustion field, combustion in the gas turbine engine is so complicated that often nothing short of high fidelity analysis (i.e. CFD) would provide acceptable results and even those tools sometimes are unable to achieve their goal. In their perspective, sometime a results that has the same order of magnitude as the actual data is acceptable. On the other hand, system design experts often look for a model that is robust enough to be used in extreme conditions for design space exploration and their accuracy requirements are more stringent. As a result, criteria for an emissions prediction model to be a good model is different based on who defines it. There are many simplifications in this research that could affect the results; however, without those simplifications, it is not possible to have an emission model that can be used in the conceptual design phase.

In this research an emission prediction methodology in the conceptual design phase is developed that provides a way to develop a combustor emission model to estimate the emissions of the gas turbine engine in the conceptual design phase in a short time. Different models and methods are put together from different sources and simplified to be able to use them in this research. Due to the approach versatility, many of these models have the potential to be replaced by a better model when they are available. The models created based on the proposed methodology are modular enough so that each component in them can easily be replaced by a newer and better or higher fidelity one. This feature also potentially provides zooming capability so the user can zoom into different components and gain more information about the performance of that component.

The creation of a modular 1D flow-field model based on a library of components is another contribution. Some features that are available in the 1D flow-field model (like the annulus height, number of holes, etc) have the potential to be used in the future more advanced models. The author of this thesis has put efforts to create a comprehensive 1D model that could be used in many applications. Simplified acoustic model, liner and casing structural analysis, simple 2D CFD analysis are among those applications. The 1D flow model can be used as the first building block in those applications.

Creation of NO_x and CO emission models for SAC and RQL combustors based on the 1D flow-field model, the CRN model along with the Droplet Evaporation and Diffusion Burning (DEDB) and Generalized Non-Uniform Mixture (GNUM) models together is another contribution.

The sensitivity analysis validated the approach, capturing the importance of the combustor characteristics besides the engine cycle parameters provides some insight about what should be the major focus in developing an emission model.

Based on the proposed methodology, a framework is created that has established a line of communication between different disciplines and codes. It may look a trivial and

easy task to integrate a code (e.g. CHEMKIN) with another disciplinary code after such a task is done; however, finding an efficient way for the integration, creating the right input and output files and lines of commands needs much more time and efforts than it looks at the first glance. Around 90 files are involved in each emission model and these files are used to transfer the data between different models. Sometimes a hidden feature or bug stopped the advancement of this research for a long time. Creating a knowledge-base for integration of these disciplines is a valuable asset that can be employed in other researches and applications.

8.4 Limitations and Future Works

The proposed methodology does not model fine details of the internal flow-field or the combustion process, since neither it is the objective of this research, nor it is possible to conduct such a task in the conceptual design phase. Also it is not intended to design a combustor using this methodology. The objective is to use the model to predict combustor emissions at the conceptual design phase, where there is not enough information to employ high fidelity codes to capture the emission levels. The simplicity and execution speeds are two important characteristics of a conceptual design tool; however, there is a price to be paid for the simplification of the models in this research. The ability of the model to capture some effects and model them is limited as a result of those simplifications. It should be noted that some of these effects are hard to capture even using the high fidelity models. Following is the list of the limitations:

- Ability to correctly capture the flame lean blow-out
- Ability to model combustion dynamics
- Accurate CO prediction
- Modeling the pressure drop across the combustor as a result of friction and mixing
- Turbulent mixing model

- Injector/ swirler interaction
- Heat loss through the liner walls

The result of this dissertation showed that the level of the combustor NO_x emission can be predicted satisfactorily in the early design phase with minimal information about a combustor. The emission results of SAC model are more satisfactory than the RQL combustor due to the better knowledge about its flow-field. The RQL combustor emissions prediction results could not be verified and validated except at one point. Additional emission information is needed to fully assess the predictability of the RQL model. Also, to improve the RQL combustor emission model, physical models beyond those that are used here are needed.

In general, predicting the level of CO emission index proved to be more challenging than NO_x emission index; although, the physical trend of the CO emission index can be captured using this methodology. The reason is the strong link between the CO emission and local flow-field variations due to the strong link between the CO-CO_2 conversion and heat release process. This link in turn creates an interaction with the local flow-field. Such fidelity to model these local events does not exist in the emission models used in this thesis.

The performance of the emission models in this thesis is a function of the performance and accuracy of its 1D internal flow-field, CRN, DEDB and GNUM models. The accuracy of the emission models improves by having access to better and more realistic models.

Following is the list of areas which can be the focus of the future works to improve the model predictability and reduce its uncertainty, especially in case of EI CO prediction and RQL combustor emission model.

Better Combustion Mechanism of Aviation Fuel

The 30 reactions, 21 species Kollrack mechanism is the best option that could be found to satisfy the required criteria. However, this mechanism has number of weaknesses. It is based on the Pyrolysis of the big Jet-A fuel molecule ($C_{12}H_{23}$) to smaller molecules (C_2H_4 and C_2H_5) and it does not include the CH radical which is an initiator branch for the prompt NO_x formation. As a result, the mechanism does not have the prompt NO_x formation mechanism which could be important in the rich burning flame.

More comprehensive combustion mechanisms are available (most of them for gaseous fuels (e.g. heptane), but using them in a complex CRN model would significantly increase the execution time of the emissions prediction process. The convergence of the stiff ODE's of the CRN model to the final solution is another issue when using complex combustion mechanism. One way to address this problem is to employ a combustion mechanism reduction scheme that reduces the number of species and reactions of a large mechanism based on a given criteria.

Improving the CRN Structure

One way to improve the EI CO prediction as well as the general prediction capability of the RQL combustor emission model is to improve the structure of the chemical reactors network. The PSR's in the CRN in the regions where there is a partial mixing may be replaced by the PaSR's. By doing this, it is possible to better model the unmixedness in the CRN. However, this necessitates the addition of a mixing model for those zones that employ PaSR. Also the issues related to the execution time and convergence of the CRN should be resolved as well.

The CRN structure can be improved beyond of what is proposed in this thesis, by using a simple CFD analysis applied to the output of the 1D flow-field model. If using such a CFD model is not possible, addition of a branch to the CRN that models the near-wall reaction where CO to CO_2 conversion reaction becomes frozen can improve the CO

prediction. Addition of such a branch necessitates the use of additional models for the cooling flow and its related phenomena near the liner wall (e.g., shear layer, mixing and etc.). Using multiple parallel branches in the secondary and dilution zones in combination with mixing model can capture the CO production in the RQL better than the current model.

Cooling Flow and Dilution Jet Mixing Models

It is beneficial to develop a mixing model for the dilution jets and cooling flows and use them in conjunction with the improved CRN model. In fact an improved CRN model and mixing model are mutually dependent on each other in an emission model. Using these two models together can improve the EI CO prediction capability of the model. The byproduct of using such a model is the ability of the model to determine the quality of mixing for the given length downstream of the dilution orifices.

Injector and swirler Models

In the current research, only one injector model (simplex pressure swirl) is used. Many of the current combustors use more advanced injectors such as air-assisted, air-blast atomizers which have better performance at all operating conditions. High-shear atomizer/swirler is also used in RQL combustor. Using an appropriate atomizer/swirler will improve the accuracy of the model.

Analytical Model for the Unmixedness Degree

The proposed approach of correlating the unmixedness degree to the premixed equivalence ratio reduced the dependency of the emission model to this parameter; however, a better was (if possible) is to link the unmixedness degree to physical parameter(s) in the combustor would reduce the uncertainty around unmixedness degree and makes it independent from experimental data.

Better Droplet Ignition Delay Time Model

The ignition delay time model used in this thesis is a simple exponential model. It does not consider the time in which the droplets are travelling in the swirler or recirculation bubble before they are exposed to the hot gases in the primary zone. It also considers a bulk temperature of the primary zone in the ignition delay time model. Finding a way to consider these additional times and modify the bulk temperature assumption could provide better prediction results.

8.5 Final Remarks

The research conducted in this thesis is the first step toward creating a more comprehensive emission model. Extent of the work made it impossible for a PhD student to develop a perfect model with everything taken into account; however, the provided framework and the proposed methodology can be used as a road-map toward a more advanced model. Some of the findings in the sensitivity analysis may be known facts, but they can be considered as a validation case for the proposed methodology.

A huge obstacle that sometimes had a paralyzing effect was the lack of industrial data and support to calibrate and tune the models. An emission model is as good as its components are and it is an unrealistic expectation to ask for a good emission model with bad component models. However, the opposite is true to have a bad model with good component models. A performance and accuracy of the model would definitely improve if its sub-models are verified and tuned using the actual data.

At the end, it should be added that the proposed methodology has the potential to be applied to other combustor types such as LPP or Direct Lean Injection (DLN) or to model broader range of emissions like soot or SO_x produced by different fuel types besides the aviation fuels (e.g. alternative fuels). Also it can be applied to land-based gas turbine engines or power plants which have significant contribution to the global

emission levels. The methodology may be used or implemented in other tools to study the effect of combustor types on emission levels in system level and eventually their effects on the environment.

Appendix A

Transient Droplet Evaporation Model

In this dissertation, calculation of droplet diameter and surface temperature as a function of time and related equations are based on the method provided in references 67 and 133. A MATLAB code named "*droplet_ODE.m*" is written which provides a system of ODE's based on the initial conditions and physical fuel properties. This system of ODE's is solved in another MATLAB code named "*droplet_evaporation.m*" for given initial condition for droplet diameter distribution to determine the amount of vaporized fuel.

As an approximation to determine the physical properties of the fuel vapor around a droplet, the reference temperature (T_{ref}) is defined as:

$$T_{ref} = T_s + \frac{(T_\infty - T_s)}{3} \tag{111}$$

where T_∞ is the temperature far from droplet (compressor exit temperature) and droplet T_s is the droplet surface temperature.

In the model, the fluid physical properties are divided into four groups of air, liquid fuel, fuel vapor and gas (fuel vapor + air) properties. The fuel or gas properties are either obtained from the CEA surrogate model or from the equations described in the following.

The dynamic viscosity (Poise, Pa.s) is the product of the fuel density (kg/m^3) and the kinematic viscosity (Stokes, m^2/s) is defined as:

$$\mu_{fuel} = \rho_{fuel} \nu_{fuel} = \rho_{fuel} 10^{\left(A_1 + \frac{B_1}{T} + C_1 T + D_1 T^2\right)} 10^{-6} \tag{112}$$

where fuel density value is at 298 K which is assumed to be the nominal temperature of the fuel. This equation is based on the information obtained from reference [139] with an

exponential curve-fit applied to it. From the same source, the fuel surface tension (σ, N/m) is obtained.

$$\sigma_{fuel} = A(1 - \frac{T_s}{T_{cr}})^n \tag{113}$$

where T_{cr} is the fuel critical temperature and A and n are constants for the given fuel.

The liquid fuel properties are latent heat (h_{fg}), specific heat at constant pressure and fuel density:

$$h_{fg\ f} = h_{fg@T_b}(\frac{T_{cr} - T_s}{T_{cr} - T_b}) \tag{114}$$

$$\rho_f = \rho_{f@298}[1 - 1.8.C_{ex}(T_s - 288.6) - 0.09(\frac{T_s - 288.6}{T_{cr} - 288.6})^2] \tag{115}$$

$$c_{P\ f} = \frac{760 + 3.35T_s}{\sqrt{0.001\rho_f}} \tag{116}$$

The air specific heat at constant pressure is obtained from the CEA surrogate model. The air heat conductivity (k, W/m^2.K), density and dynamic viscosity (μ, Pa.s) are obtained at the reference temperature (T_{ref}). The air density is obtained from the ideal gas law:

$$k_a = \frac{40.7 \times 10^{-3}}{700}(T_{ref} - 300) + 26 \times 10^{-3} \tag{117}$$

$$\mu_a = [\frac{18(T_{ref} - 400)}{600}] \times 10^{-6} \tag{118}$$

The fuel vapor properties are obtained from the following equations(with the same units as those stated above).

$$c_{P\ v} = (363 + 0.467T_{ref}(5 - 0.001\rho_{f@298}) \tag{119}$$

$$k_v = 0.001[13.2 - 0.0313(T_b - 273)](\frac{T_{ref}}{273})^{n_k} \text{ where } n_k = 2 - 0.0372(\frac{T_{ref}}{T_b})^2 \quad (120)$$

$$\rho_v = \frac{P_{Fs@T_b} \times 10^3}{\frac{R_u}{MW_f} T_{ref} P} \quad (121)$$

where R_u is the universal gas constant, P is the pressure, MW_f is the fuel molecular weight and $P_{f\ S@Tb}$ is the fuel vapor partial pressure at droplet surface at the boiling temperature (T_b) obtained from the following equation:

$$P_{fS@Tb} = e^{a_h - \frac{b_h}{T_b - 43}} \quad (122)$$

The value of experimental constants a_h and b_h are obtained for the fuel of interest. After determining the properties of fuel vapor and air, the next step is to combine them to find the average properties of the gas surrounding the droplet using the following equations:

$$P_{fs} = e^{\frac{a_h - b_h}{T_s - 43}} \quad (123)$$

$$Y_{f\ S} = [1 + (\frac{P_\infty}{P_{fs}} - 1)\frac{MW_a}{MW_f}]^{-1} \quad (124)$$

$$Y_{f\ ref} = \frac{2}{3} Y_{f\ S} \quad (125)$$

$$Y_{a\ ref} = 1 - Y_{f\ ref} \quad (126)$$

The partial pressure of the fuel at the droplet surface is used to determine the fuel mass fraction. Then the reference mass fraction of the fuel (2/3 of the fuel mass fraction) and air mass fraction at the droplet surface are obtained to determine the gas properties at the droplet surface as the weighted average of the fuel-vapor and air properties. The equations are:

$$c_{P\ g} = Y_{a\,ref} c_{P\,a} + Y_{v\,ref} c_{P\,v} \tag{127}$$

$$k_g = Y_{a\,ref} k_a + Y_{v\,ref} k_v \tag{128}$$

$$\rho_g = [\frac{Y_{a\,ref}}{\rho_a} + \frac{Y_{v\,ref}}{\rho_v}]^{-1} \tag{129}$$

$$\mu_g = Y_{a\,ref} \mu_a + Y_{v\,ref} \mu_v \tag{130}$$

Now that all the properties of the gas around the droplet are available, the following system of ODE's can be constructed.

$$\begin{bmatrix} \frac{dD}{dt} \\ K(t) \\ \frac{dT_s}{dt} \end{bmatrix} = \begin{bmatrix} -4k_g\, ln(\frac{1+B_M}{\rho_f c_{P\,g} D}) \\ -8Dk_g\, ln(\frac{1+B_M}{\rho_f c_{P\,g} D}) \\ \dot{m}_{fD} h_{fg} \frac{B_T}{(B_M - 1) c_{P\,f} m_D} \end{bmatrix} \tag{131}$$

where K is the droplet evaporation constant and B_M and B_T are Spalding transfer numbers based on the mass and heat transfer which are function of temperature themselves. $\dot{m}_{fD}$ is the evaporation rate of fuel from the droplet surface and m_D is the mass of the fuel droplet. The relevant equations are:

$$B_M = \frac{Y_{fS}}{1 - Y_{fS}} \tag{132}$$

$$B_T = c_{Pg} \frac{T_\infty - T_s}{h_{fg}} \tag{133}$$

$$\dot{m}_{fD} = 2\pi D \frac{k_g}{c_{Pg}} ln(1 + B_M) C_{convection} \tag{134}$$

$$m_D = \pi\rho \frac{D^3}{6} \tag{135}$$

The convection coefficient $C_{convection}$ modifies the evaporation rate in the non-stationary conditions based on the convective heat transfer. It is a function of droplet Reynolds and Prandtl numbers and is defined as follows.

$$C_{convection} = 1 + 0.3\, Re_D^{\;0.5}\, Pr_g^{\;0.33} \tag{136}$$

The Reynolds number is defined based on the droplet diameter and the turbulent fluctuating velocity (U_{turb}) and both Reynolds and Prandtl numbers are based on the gas properties.

Appendix B

Component Scripts and Codes

B.1 Annular Volume Calculation

Following code is a MATLAB function to calculate the zone volumes in annular and tubular configurations. In annular case, it calculates the volume of incomplete cones produced by the inner and outer liners and front and rear faces of the zone. Depending on combustor orientation, the code, add the incomplete cone's volumes to or subtract them from each other to calculate the volume contained between them which is the volume of the zone in annular configuration. Also it calculates the additional volume that is created by the inclined penetrating jets. For penetrating jets in front of the zone, the volume is subtracted and for the jets at the back, the volume is added to the total volume. Following is the list and the description of the inputs:

- Mean radius of the inlet and exit of the zone: rm1 and rm2
- Height at the inlet and exit of the zone: H1 and H2
- Zone length: length
- Jet penetration angle at the front and rear of the zone measured from horizontal axes in degrees
- Number of nozzles: Nozzle_no
- Configuration of the combustor (annular or tubular)
- Combustor orientation angle: alpha (in radians)

The function to calculate the volume of the incomplete cone is given below.

$$V_{incomplete\,cone} = \pi(r_b^2 + r_b r_t + r_t^2)\frac{h}{3} \tag{137}$$

where r_b, r_t and h are the base and top radius and cone's height.

Following is the main body of the code to calculate the zone volumes.

```
**********************************************************************

function vol=zone_volume(rm1,H1,rm2,H2,length,theta1,theta2,Nozzle_no,
configuration,alpha)
%Calculates the volume of the combustor zones, given their mean radius and
%height at beginning and end and the length of the zone and orientation angle
%(alpha is in radians), the shape of the zone is the volume between two
%concentric incomplete cones whit an inflated or deflated front and rear faces
 % theta 1 and 2 are jet penetration angles at the front and rear dilution
 % holes which reduce and increase the total volume respectively
alpha=alpha*180/pi;
if alpha>=0
   j=1;
else
   j=-1;
end

if theta1 > (90 - abs(alpha))
   if alpha > 0
      a1 = 1;
      b1 = 1;
   else
      a1 = -1;
      b1 = -1;
   end
else
   a1 = 1;
   b1 = -1;
end

if theta2 > (90 - abs(alpha))
   if alpha > 0
      a2 = 1;
      b2 = 1;
   else
      a2 = -1;
      b2 = -1;
   end
else
   a2 = 1;
   b2 = -1;
end

if strcmpi(configuration,'annular')
         %coordinates of front face of the zone
```

```
 xo1=-H1/2*sin(alpha*pi/180);
xi1=H1/2*sin(alpha*pi/180);
ro1=rm1+H1/2*cos(alpha*pi/180);
ri1=rm1-H1/2*cos(alpha*pi/180);
length_axial = length * cos(alpha*pi/180);
%coordinates of rear face of the zone
 xo2=length_axial-H2/2*sin(alpha*pi/180);
xi2=length_axial+H2/2*sin(alpha*pi/180);
ro2=rm2+H2/2*cos(alpha*pi/180);
ri2=rm2-H2/2*cos(alpha*pi/180);

front_face_volume=incomplete_cone_volume(ro1,ri1,abs(xo1-xi1));
rear_face_volume=incomplete_cone_volume(ro2,ri2,abs(xo2-xi2));
outer_liner_volume=incomplete_cone_volume(ro1,ro2,abs(xo1-xo2));
 inner_liner_volume=incomplete_cone_volume(ri1,ri2,abs(xi1-xi2));
%The total volume of the zone without considering volumes produced by angled
penetrating jets
V_base=outer_liner_volume-inner_liner_volume+j*(rear_face_volume-
front_face_volume);

%Front station
dy1_jet = H1/2 * tan ((90 - theta1)* pi /180) * sin (alpha*pi/180);
% Vertical difference between mean-line and upper and lower jet intersections
dx1_jet = H1/2 * tan ((90 - theta1)* pi /180) * cos ( alpha*pi/180);
% Horizontal difference between mean-line and upper and lower jet intersections
 rm1_jet = rm1 + dy1_jet;
xm1_jet = dx1_jet;

v1_o_jet=incomplete_cone_volume(ro1,rm1_jet,abs(xo1-xm1_jet));
v1_i_jet=incomplete_cone_volume(rm1_jet,ri1,abs(xm1_jet-xi1));
% Volume produced by jets
V1_jet =  a1 * v1_o_jet + b1 * v1_i_jet - j * front_face_volume;

%Rear station
dy2_jet = H2/2 * tan ((90 - theta2)* pi /180) * sin (alpha*pi/180);
% Vertical difference between mean-line and upper and lower jet intersections
dx2_jet = H2/2 * tan ((90 - theta2)* pi /180) * cos (alpha*pi/180);
% Horizontal difference between mean-line and upper and lower jet intersections
rm2_jet = rm2 + dy2_jet;
xm2_jet = length_axial + dx2_jet;

v2_o_jet=incomplete_cone_volume(ro2,rm2_jet,abs(xo2-xm2_jet));
v2_i_jet=incomplete_cone_volume(rm2_jet,ri2,abs(xm2_jet-xi2));
% Volume produced by jets
V2_jet =  a2 * v2_o_jet + b2 * v2_i_jet - j * rear_face_volume;
```

```
        %The total volume of the zone considering volumes produced by angled
        penetrating jets
        vol = V_base + V2_jet - V1_jet;

elseif strcmpi(configuration,'tubular')
        %The total volume of the zone without considering volumes produced by angled
        penetrating jets
        V_base=incomplete_cone_volume(H1/2,H2/2,length);

         %Volume produced by jets

        % Front Face
        dx1_jet = H1/2 * tan ((90 - theta1)* pi /180);
        V1_jet = incomplete_cone_volume(H1/2,0,dx1_jet);

        % Rear Face
         dx2_jet = H2/2 * tan ((90 - theta2)* pi /180);
        V2_jet = incomplete_cone_volume(H2/2,0,dx2_jet);

        %The total volume of the zone considering volumes produced by angled
        penetrating jets
        vol = Nozzle_no * (V_base + V2_jet - V1_jet);
end % if
end % function

*********************************************************************
 function v=incomplete_cone_volume(rb,rt,h)
% rb and rt are radius of the circles at the top and bottom of the incomplete cone and h is
%height of the cone
        v=pi*(rb^2+rb*rt+rt^2)*h/3;
end  %function
```

B.2 Droplet Evaporation Model

The following code ”droplet_evaporation” uses a MATLAB function “droplet_ODE” to determine the distribution of droplet size at the end of the ignition delay time. The ‘Droplet_ODE” code is based on the method described in Appendix A; therefore, it is not provided here. The droplet distributions at the beginning and end of ignition delay time are integrated to determine the amount of vaporized fuel and its ratio to the total fuel flow. The fuel properties are either provided Jet-A aviation fuel or n-

dodecane wherever the Jet-A properties are not available [137, 139, 155]. The inputs to the model are listed below.

- Critical temperature of the fuel, T_cr , 659 K for Jet-A
- Boiling temperature of the fuel, T_bn, 530 K for Jet-A
- Fuel Molecular weight, MW_fuel, 167 for Jet-A
- Fuel density at 298 K, rho_f_298, 687.6 kg/m^3 for Jet-A
- Fuel coefficient of thermal expansion to be used in fuel density calculation, C_ex, 7.5e-4 for Jet-A
- Latent heat at boiling temperature, Latent_heat_Tbn, 371800 J/kg
- Universal gas constant, R, 1.9858775 kcal/g-mole
- Coefficient for kinematic viscosity (equation (112)), A1, -8.8225 for Jet-A
- Coefficient for kinematic viscosity (equation (112)), B1, 1547.6 for Jet-A
- Coefficient for kinematic viscosity (equation (112)), C1,1.6525e-2 for Jet-A
- Coefficient for kinematic viscosity (equation (112)), D1, for Jet-A
- Surface Tension Parameter (equation (113)), A, 0.04722 for Jet-A [139]
- Surface Tension Parameter (equation (113)), n, 0.86 for Jet-A [139]
- Fuel temperature, T_in_fuel
- Injector flow number , FN (m^2)
- Total pressure at compressor exit, Ptot32
- Fuel flow, w_fuel (kg/s)
- Air flow, w_air (kg/s)
- Air density, air_density (kg/m3)
- Primary zone equivalence ratio, eq_ratio_PZ_
- Temperature in the ignition delay time equation, T_id(K), assumed to be the same as the primary zone bulk temperature

- Shape factor (q) in Rosin-Rammler droplet distribution, Rosin_Rammler_q
- Turbulent velocity fluctuation in the primary zone, U_turb_fluc (m/s), set to be 20 m/s [75]
- Partial pressure constants a_h and b_h (equation (122)), 4.3896 and 3209.45 for $T_s<T_b$ and 14.2146 and 3151.68 for $T_s<T_b$.

Following is the main body of "droplet_evaporation" code:

```
**********************************************************************

cd (directory_address);
% Conversion to kPa
P_inf = Ptot32 *101.325
T_id = T_id + T_ig_adder;
% Temperature around droplets same as the compressor exit temperature
T_surr = Ttot32;

if T_in_fuel < T_cr
        % Ignition delay time
        t_ig = 10^-4 * exp(21000/( R * T_id))/eq_ratio_PZ_op/1000;
        kin_viscosity=10^(A1+B1/T_in_fuel+C1*T_in_fuel+D1*T_in_fuel^2)*1e-6;
        surface_tension=A*(1-T_in_fuel/T_cr)^n;
        dyn_viscosity=rho_f_298*kin_viscosity;
        del_P = (w_fuel/1000/injector_number)^2 / ( FN * rho_f_298 ^ 0.5)^2.0 /1e6;
         SMD = 2.25*surface_tension^0.25*dyn_viscosity^0.25*(w_fuel/1000 /
        injector_number)^0.25*(1e6*del_P)^-0.5*air_density^-0.25;
        % Mass median diameter or a diameter where 50% of the droplets (in volume)
        have diameter smaller than that
        MMD = SMD * 0.693 ^ (1/Rosin_Rammler_q) * gamma(1-
        1/Rosin_Rammler_q);
        Rosin_Rammler_X = MMD / (-log(0.5))^(1/Rosin_Rammler_q);
        D_max = 4*MMD;
        D_min = 0.1*1e-6;
        dD = (D_max - D_min)/100;
        Di = D_min:dD:D_max;
        Di2 = Di.^2;

        options = odeset('RelTol',1e-5,'Refine',5,'Events',@zero_diameter_event);
        for i=1:max(size(Di))
                [t,y,te,ye,n] = ode45(@(t,y)
                droplet_ODE(t,y,T_cr,T_bn,P_inf,T_surr,MW_fuel,rho_f_298,C_ex,Late
                nt_heat_Tbn,U_turb_fluc),[0 t_ig],[T_in_fuel; Di(i) ; Di2(i)],options);
```

```
        tf(i) = t(end);
        Tsf = y(end,1);
        Df(i) = y(end,2);
        D2f(i) = y(end,3);
end
n_ig = find(tf < t_ig);
n_ig(isempty(n_ig))=[1];
Df = Df(n_ig(end):end);
Di = Di(n_ig(end):end);
Df(imag(Df)~= 0 | Df < 0 )= 0;

[t1,y1,te1,ye1]= ode45(@(t,y)
droplet_ODE(t,y,T_cr,T_bn,P_inf,T_surr,MW_fuel,rho_f_298,C_ex,
Latent_heat_Tbn,U_turb_fluc),[0 t_ig],[T_in_fuel; SMD ; SMD^2], options);
for j=1:size(t1)
        x = droplet_ODE(t1(j),[y1(j,1);y1(j,2)],T_cr,T_bn,P_inf,T_surr,
        MW_fuel,rho_f_298,C_ex,Latent_heat_Tbn,U_turb_fluc);
        burning_constant(j) =-x(3,1);
end

subplot(2,2,1);
plot(t1*1e3,y1(:,3)*1e12);
ylabel('D^2_s,  \mum^2');
xlabel('time,ms');
title('SMD D^2');
grid on

subplot(2,2,3);
plot(t1*1e3,burning_constant*1e6);
ylabel('K, mm^2/s');
xlabel('time, ms');
title('SMD Burning constant');
grid on

pdf_reduced_volumei=  wblpdf(Di,Rosin_Rammler_X,Rosin_Rammler_q).
*(1-(Df./Di).^3);
% Total percentage of volume reduction due to ignition delay
evap_degree = 1-exp(-(Di(1)/Rosin_Rammler_X)^Rosin_Rammler_q) +
trapz(Di , pdf_reduced_volumei);

D = (D_min:dD:D_max)*1e6;
vol_fractioni = wblpdf(D,Rosin_Rammler_X*1e6,Rosin_Rammler_q);

subplot(2,2,2);
plot(D,vol_fractioni);
grid on;
```

```
        hold on;

        vol_fractionf=wblpdf(Di*1e6,Rosin_Rammler_X*1e6,Rosin_Rammler_q).*
        Df./Di).^3;
        plot(Di*1e6,vol_fractionf,'r');
        grid on
        xlabel('Droplet Diameter, \mum');
        ylabel('Volume Fraction');

        subplot(2,2,4);
        plot(t1*1e3,y1(:,1));
        grid on
        ylabel('T_s, K');
        xlabel('time,ms');
        title('SMD Surface Temperature ');
        hold off
else
        Rosin_Rammler_X = 0;
        del_P = 0;
        kin_viscosity=0;
        fuel_density=0;
         surface_tension=0;
        dyn_viscosity=0;
        SMD=0;
        MMD = 0;
        evap_degree=1;
        t_ig = 10;
end
```

B.3 The Unmixedness Model

Inputs to the Non-Uniform Mixture model are:

- Fraction of vaporized fuel to total fuel: evap_degree
- Fuel mass-flow: w_fuel(kg/s)
- Stoichiometric fuel to air ratio: far_stoichiometric
- Primary zone mass-flow: w_PZ (g/s)
- Primary zone volume: vol_PZ (cm^3)

Following is the main body of the code.

```
**********************************************************************
if  evap_degree > 0.99
```

```
        evap_degree = 1.0
end
% Vaporized fuel which creates premixed flame
w_fuel_premixed  = evap_degree * w_fuel;
% Liquid fuel which creates diffusion flame
w_fuel_diffusion = w_fuel - w_fuel_premixed;
w_air_diffusion  = w_fuel_diffusion / far_stoichiometric;
w_air_premixed   = w_PZ - w_air_diffusion;
if w_air_premixed <0
        w_fuel_diffusion = w_PZ * 0.99 *far_stoichiometric;
        w_fuel_premixed = w_fuel - w_fuel_diffusion;
        w_air_diffusion = w_PZ * 0.99 ;
        w_air_premixed = w_PZ * 0.01 ;
end
PZ_eq_ratio_premixed=w_fuel_premixed/w_air_premixed/far_stoichiometric;
PZ_air_flow_distribution(1) = w_air_diffusion;
fuel_flow_distribution(1) = w_fuel_diffusion;
PZ_flow_distribution(1) = w_air_diffusion+w_fuel_diffusion;
PZ_phi_distribution(1) = 1;
% Considering the total combustor volume for droplets burning in diffusion flame mode
PZ_vol_distribution(1) = vol_PZ;
PZ_eq_ratio = w_fuel / w_PZ / far_stoichiometric;
if (PZ_eq_ratio_premixed <1.2 && PZ_eq_ratio_premixed >0.05 )
        Unmixedness_degree=polyval([-4.9379 ,17.765 , -22.31 , 10.547 , -0.7828
        ],PZ_eq_ratio_premixed);
else
        Unmixedness_degree = 0.18;
end
Unmixedness_degree = Unmixedness_degree * mixedness_var_coeff;
std  = PZ_eq_ratio_premixed*Unmixedness_degree;
variance= std^2;
Phi_l = PZ_eq_ratio_premixed - 3*std;
Phi_u= PZ_eq_ratio_premixed + 3*std;
if Phi_l <0
        Phi_l = 0.0;
end

if  evap_degree ~= 1
% A condition that checks if there is a fuel flow in the first reactor or not (the reactor that
%assigned to liquid fuel)to prevent CHEMKIN crash. If the flow is zero then it means all
%the fuel is vaporized and all the reactors (10) can be assigned to vapor fuel distribution
        increment=(Phi_u-Phi_l)/9;
        % Middle value of equivalence ratio at each interval
        PZ_phi_distribution(2)=Phi_l+increment/2;
        for index=3:10
        % Middle value of equivalence ratio at each interval
```

```
            PZ_phi_distribution(index)=PZ_phi_distribution(index-1)+increment;
        end
        %Area of left tail before Phi(1)
        left_tail_area = normcdf(Phi_l,PZ_eq_ratio_premixed,std);
        %Area of right tail after Phi(9)
        right_tail_area = 1-normcdf(Phi_u,PZ_eq_ratio_premixed,std);
         tails_area = left_tail_area+right_tail_area;
        % Correction factor to correct the area under the truncated normal curve to unity
        correction_factor = tails_area/(1-tails_area);
%-----------------------------------------------------------------------------------------------------------
        for index=2:10
            PZ_flow_distribution(index)=(w_air_premixed+w_fuel_premixed)*(norm
            cdf(PZ_phi_distribution(index)+increment/2,PZ_eq_ratio_premixed,std)-
            normcdf(PZ_phi_distribution(index)-
            increment/2,PZ_eq_ratio_premixed,std))*(1+correction_factor);
            PZ_vol_distribution(index)=vol_PZ*(normcdf(PZ_phi_distribution(index)
            +increment/2,PZ_eq_ratio_premixed,std)-
            normcdf(PZ_phi_distribution(index)-
            increment/2,PZ_eq_ratio_premixed,std))*(1+correction_factor);
             if PZ_vol_distribution(index) <= 0.01
                        PZ_vol_distribution(index)=0.01;
            end
            if PZ_flow_distribution(index) <= 0.01
                        PZ_flow_distribution(index)=0.01;
            end
        end

        PZ_air_flow_distribution=
        PZ_flow_distribution./(PZ_phi_distribution*far_stoichiometric+1);
        PZ_fuel_flow_distribution = PZ_flow_distribution - PZ_air_flow_distribution;
        bar(PZ_phi_distribution(2:end),PZ_flow_distribution(2:end),0.75)
else
        increment=(Phi_u-Phi_l)/10;
        %Middle value of equivalence ratio at each interval
        PZ_phi_distribution(1)=Phi_l+increment/2;
        for index=2:10
            PZ_phi_distribution(index)=PZ_phi_distribution(index-1)+increment;
            %Middle value of equivalence ratio at each iterval
        end
        %Area of left tail before Phi(1)
         left_tail_area = normcdf(Phi_l,PZ_eq_ratio_premixed,std);
        %Area of right tail after Phi(9)
        right_tail_area = 1-normcdf(Phi_u,PZ_eq_ratio_premixed,std);
        tails_area = left_tail_area+right_tail_area;
        % Correction factor to correct the area under the truncated normal distribution to
        %unity
```

```
        correction_factor = tails_area/(1-tails_area);
%-----------------------------------------------------------------------------------------------------------
        for index=1:10
                PZ_flow_distribution(index)=(w_air_premixed+w_fuel_premixed)*(norm
                cdf(PZ_phi_distribution(index)+increment/2,PZ_eq_ratio_premixed,std)-
                normcdf(PZ_phi_distribution(index)-
                increment/2,PZ_eq_ratio_premixed,std))*(1+correction_factor);
                PZ_vol_distribution(index)=vol_PZ*(normcdf(PZ_phi_distribution(index)
                +increment/2,PZ_eq_ratio_premixed,std)-
                normcdf(PZ_phi_distribution(index)-
                increment/2,PZ_eq_ratio_premixed,std))*(1+correction_factor);
                if PZ_vol_distribution(index) <= 0.01
                        PZ_vol_distribution(index)=0.01;
                end
                if PZ_flow_distribution(index) <= 0.01
                        PZ_flow_distribution(index)=0.01;
                end
        end

        PZ_air_flow_distribution=
        PZ_flow_distribution./(PZ_phi_distribution*far_stoichiometric+1);
        PZ_fuel_flow_distribution = PZ_flow_distribution - PZ_air_flow_distribution;
        bar(PZ_phi_distribution,PZ_flow_distribution,0.75)
end
```

B.4 CHEMKIN CRN Model Scripts

The following scripts are a set of commands written in a BACH file (BAT) to execute CHEMKIN CRN models with given input files (.inp and .asu). It produces output files with extension “out”, “CSV” and “xml”. There is one file for each of the SAC and RQL CRN models. The files eliminate the need to go to the CHEMKIN environment to execute the model. They are used in the MODEL CENTER environment to automate the process.

B.3.1 SAC CRN Model

```
*************************************************************************

rem Chemical Reactors Network Batch file for CHEMKIN software automation
rem By: Reza Rezvani  June 2010
rem Aerospace Systems Design Lab
cls
CALL "c:\Program Files\Reaction\chemkin41_pc\bin\run_chemkin_env_setup.bat"
```

```
SET JAVA_ID=94060983
rem Define the path
SET model_path=C:\Documents and Settings\rrezvani\My Documents\Emission
Prediction\ Integrated\SAC_v2
rem define the CHEMKIN runtime environment
rem delete any data files left from previous runs
DEL "%model_path%\XMLdata*.zip"
DEL "%model_path%\XMLrestart*.zip"
DEL "%model_path%\XMLdata*.xml"
DEL "%model_path%\CKSolnInfo*.txt"
DEL "%model_path%\CKsoln*.CSV"
DEL "%model_path%\SAC_CRN_v2_*.OUT"
DEL "%model_path%\SAC_CRN_v2_gas.*"
DEL "%model_path%\SAC_CRN_v2_*.csv"
DEL "%model_path%\SAC_CRN_v2.xml"
cd %mechanism_path%
rem create Chemistry file of  *_gas.asc,  *_gas.asu  and  *_gas.out from defined input
and output files in  CKPreProc_*.input
CKPreProcess.EXE -i "%model_path%\CKPreProc_SAC_CRN_v2.input"
rem  copy  chemkindata.dtd to current folder
COPY "%reaction_dir%\chemkin41_pc\data\chemkindata.dtd" "%model_path%"
rem model center seems does not work without "cd"ing to the desired path, even though
CHEMKIN and cmd environment have no problem without doing it !!!!!!!!!!!!!!!!!!!!
cd %model_path%
rem run cluster 1 to 10 parallel branches
rem run cluster 1(PSR)
CKReactorGenericPSR  -i "%model_path%\SAC_CRN_v2_c1.inp" -o "%model_path%\
SAC_CRN_v2_c1.out" -c "%model_path%\SAC_CRN_v2_gas.asc"
rem  GetSolution extracts the information from XMLData.ZIP file and puts it in CSV
format under the name CKSoln.ckcsv.
GetSolution -nosen -norop -mass -all
RENAME "XMLdata.zip" "XMLdata_SAC_CRN_v2_Cluster1C1.zip"
rem By default the CHEMKIN  uses restart.xml to run the next model if it cannot find a
xml file that is defined in the input file
RENAME "CKSoln.ckcsv" "SAC_CRN_v2_C1.csv"
rem run cluster 2(PSR)
CKReactorGenericPSR -i "%model_path%\SAC_CRN_v2_c2.inp" -o "%model_path%\
SAC_CRN_v2_c2.out" -c "%model_path%\SAC_CRN_v2_gas.asc"
GetSolution -nosen -norop -mass -all
RENAME "XMLdata.zip" "XMLdata_SAC_CRN_v2_Cluster2C2.zip"
RENAME "CKSoln.ckcsv" "SAC_CRN_v2_C2.csv"
rem run cluster 3(PSR)
CKReactorGenericPSR -i "%model_path%\SAC_CRN_v2_c3.inp" -o "%model_path%\
SAC_CRN_v2_c3.out" -c "%model_path%\SAC_CRN_v2_gas.asc"
GetSolution -nosen -norop -mass -all
RENAME "XMLdata.zip" "XMLdata_SAC_CRN_v2_Cluster3C3.zip"
```

```
RENAME "CKSoln.ckcsv" "SAC_CRN_v2_C3.csv"
rem run cluster 4(PSR)
CKReactorGenericPSR -i "%model_path%\SAC_CRN_v2_c4.inp" -o "%model_path%\
SAC_CRN_v2_c4.out" -c "%model_path%\SAC_CRN_v2_gas.asc"
GetSolution -nosen -norop -mass -all
RENAME "XMLdata.zip" "XMLdata_SAC_CRN_v2_Cluster4C4.zip"
RENAME "CKSoln.ckcsv" "SAC_CRN_v2_C4.csv"
rem run cluster 5(PSR)
CKReactorGenericPSR -i "%model_path%\SAC_CRN_v2_c5.inp" -o "%model_path%\
SAC_CRN_v2_c5.out" -c "%model_path%\SAC_CRN_v2_gas.asc"
GetSolution -nosen -norop -mass -all
RENAME "XMLdata.zip" "XMLdata_SAC_CRN_v2_Cluster5C5.zip"
RENAME "CKSoln.ckcsv" "SAC_CRN_v2_C5.csv"
rem run cluster 6(PSR)
CKReactorGenericPSR -i "%model_path%\SAC_CRN_v2_c6.inp" -o "%model_path%\
SAC_CRN_v2_c6.out" -c "%model_path%\SAC_CRN_v2_gas.asc"
GetSolution -nosen -norop -mass -all
RENAME "XMLdata.zip" "XMLdata_SAC_CRN_v2_Cluster6C6.zip"
RENAME "CKSoln.ckcsv" "SAC_CRN_v2_C6.csv"
rem run cluster 7(PSR)
CKReactorGenericPSR -i "%model_path%\SAC_CRN_v2_c7.inp" -o "%model_path%\
SAC_CRN_v2_c7.out" -c "%model_path%\SAC_CRN_v2_gas.asc"
GetSolution -nosen -norop -mass -all
RENAME "XMLdata.zip" "XMLdata_SAC_CRN_v2_Cluster7C7.zip"
RENAME "CKSoln.ckcsv" "SAC_CRN_v2_C7.csv"
rem run cluster 8(PSR)
CKReactorGenericPSR -i "%model_path%\SAC_CRN_v2_c8.inp" -o "%model_path%\
SAC_CRN_v2_c8.out" -c "%model_path%\SAC_CRN_v2_gas.asc"
GetSolution -nosen -norop -mass -all
RENAME "XMLdata.zip" "XMLdata_SAC_CRN_v2_Cluster8C8.zip"
RENAME "CKSoln.ckcsv" "SAC_CRN_v2_C8.csv"
rem run cluster 9(PSR)
CKReactorGenericPSR -i "%model_path%\SAC_CRN_v2_c9.inp" -o "%model_path%\
SAC_CRN_v2_c9.out" -c "%model_path%\SAC_CRN_v2_gas.asc"
GetSolution -nosen -norop -mass -all
RENAME "XMLdata.zip" "XMLdata_SAC_CRN_v2_Cluster9C9.zip"
RENAME "CKSoln.ckcsv" "SAC_CRN_v2_C9.csv"
rem run cluster 10(PSR)
CKReactorGenericPSR -i "%model_path%\SAC_CRN_v2_c10.inp" -o "%model_path%\
SAC_CRN_v2_c10.out" -c "%model_path%\SAC_CRN_v2_gas.asc"
format under the Rename CKSoln.ckcsv.
GetSolution -nosen -norop -mass -all
RENAME "XMLdata.zip" "XMLdata_SAC_CRN_v2_Cluster10C10.zip"
RENAME "CKSoln.ckcsv" "SAC_CRN_v2_C10.csv"
rem run cluster 11 (Gas Mixer)
```

```
CKReactorMixer  -i "%model_path%\SAC_CRN_v2_c11.inp" -o "%model_path%\
SAC_CRN_v2_c11.out" -c "%model_path%\SAC_CRN_v2_gas.asc"
GetSolution -nosen -norop -mass -all
RENAME "XMLdata.zip" "XMLdata_SAC_CRN_v2_Cluster11C11.zip"
RENAME "CKSoln.ckcsv" "SAC_CRN_v2_C11.csv"
rem run cluster 12(PSR)
CKReactorGenericPSR -i "%model_path%\SAC_CRN_v2_c12.inp" -o "%model_path%\
SAC_CRN_v2_c12.out" -c "%model_path%\SAC_CRN_v2_gas.asc"
format under the name CKSoln.ckcsv.
GetSolution -nosen -norop -mass -all
RENAME "XMLdata.zip" "XMLdata_SAC_CRN_v2_Cluster12C12.zip"
RENAME "CKSoln.ckcsv" "SAC_CRN_v2_C12.csv"
rem run cluster 13 (Gas Mixer)
CKReactorMixer  -i "%model_path%\SAC_CRN_v2_c13.inp" -o "%model_path%\
SAC_CRN_v2_c13.out" -c "%model_path%\SAC_CRN_v2_gas.asc"
GetSolution -nosen -norop -mass -all
RENAME "XMLdata.zip" "XMLdata_SAC_CRN_v2_Cluster13C13.zip"
RENAME "CKSoln.ckcsv" "SAC_CRN_v2_C13.csv"
rem run cluster 14 (PSR)
CKReactorPlugFlow -i "%model_path%\SAC_CRN_v2_c14.inp" -o "%model_path%\
SAC_CRN_v2_c14.out" -c "%model_path%\SAC_CRN_v2_gas.asc"
GetSolution -nosen -norop -mass -all
RENAME "XMLdata.zip" "XMLdata_SAC_CRN_v2_Cluster14C14.zip"
RENAME "CKSoln.ckcsv" "SAC_CRN_v2_C14.csv"
rem run cluster 15 (Gas Mixer)
CKReactorMixer  -i "%model_path%\SAC_CRN_v2_c15.inp" -o "%model_path%\
SAC_CRN_v2_c15.out" -c "%model_path%\SAC_CRN_v2_gas.asc"
GetSolution -nosen -norop -mass -all
RENAME "XMLdata.zip" "XMLdata_SAC_CRN_v2_Cluster15C15.zip"
RENAME "CKSoln.ckcsv" "SAC_CRN_v2_C15.csv"
EXIT /B
```

B.3.2 RQL CRN Model

```
**********************************************************************

rem RQL Chemical Reactors Nerwork Batch  command file for Chemikin software
automization
rem By: Reza Rezvani  May 2010
rem Aerospace Systems Design Lab
cls
CALL "c:\Program Files\Reaction\chemkin41_pc\bin\run_chemkin_env_setup.bat"
SET JAVA_ID=636031262
rem define the path
SET model_path=C:\Documents and Settings\rrezvani\My Documents\Emission
Prediction\Integrated\RQL_v3
```

```
REM get the Chemkin runtime environment defined
REM Delete any data files left from previous runs
DEL "%model_path%\XMLdata*.zip"
DEL "%model_path%\XMLrestart*.zip"
DEL "%model_path%\XMLdata*.xml"
DEL "%model_path%\CKSolnInfo*.txt"
DEL "%model_path%\CKsoln*.CSV"
DEL "%model_path%\RQL_CRN_v3_*.OUT"
DEL "%model_path%\RQL_CRN_v3_gas.*"
DEL "%model_path%\RQL_CRN_v3_*.csv"
DEL "%model_path%\RQL_CRN_v3.xml"

rem model center seems to not work without "cd"ing to the desired path, even though
CHEMKIN and cmd environment have no problem without doing it !!!!!!!!!!!!!!!!!!!!!!
cd %mechanism_path%
rem create Chemistry file of  *_gas.asc,  *_gas.asu  and  *_gas.out from defined input
and output files in  CKPreProc_*.input
CKPreProcess.EXE -i "%model_path%\CKPreProc_RQL_CRN_v3.input"
rem  copy  chemkindata.dtd to current folder
COPY "%reaction_dir%\chemkin41_pc\data\chemkindata.dtd" "%model_path%"
rem model center seems does not work without "cd"ing to the desired path, even though
CHEMKIN and cmd environment have no problem without doing it !!!!!!!!!!!!!!!!!!!!!
cd %model_path%

rem run cluster 1 to 10 parallel branches

rem run cluster 1(PSR)
CKReactorGenericPSR -i "%model_path%\RQL_CRN_v3_c1.inp" -o
"%model_path%\RQL_CRN_v3_c1.out" -c "%model_path%\RQL_CRN_v3_gas.asc"
rem  GetSolution extracts the information from XMLData.ZIP file and puts it in CSV
format under the name CKSoln.ckcsv.
GetSolution -nosen -norop -mass -all
RENAME "XMLdata.zip" "XMLdata_RQL_CRN_v3_Cluster1C1.zip"
rem By default the CHEMKIN  uses restart.xml to run the next model if it cannot find a
xml file that is defined in the input file
RENAME "CKSoln.ckcsv" "RQL_CRN_v3_C1.csv"
rem run cluster 2(PSR)
CKReactorGenericPSR -i "%model_path%\RQL_CRN_v3_c2.inp" -o
"%model_path%\RQL_CRN_v3_c2.out" -c "%model_path%\RQL_CRN_v3_gas.asc"
GetSolution -nosen -norop -mass -all
RENAME "XMLdata.zip" "XMLdata_RQL_CRN_v3_Cluster2C2.zip"
RENAME "CKSoln.ckcsv" "RQL_CRN_v3_C2.csv"
rem run cluster 3(PSR)
CKReactorGenericPSR -i "%model_path%\RQL_CRN_v3_c3.inp" -o
"%model_path%\RQL_CRN_v3_c3.out" -c "%model_path%\RQL_CRN_v3_gas.asc"
```

```
GetSolution -nosen -norop -mass -all
RENAME "XMLdata.zip" "XMLdata_RQL_CRN_v3_Cluster3C3.zip"
RENAME "CKSoln.ckcsv" "RQL_CRN_v3_C3.csv"
rem run cluster 4(PSR)
CKReactorGenericPSR -i "%model_path%\RQL_CRN_v3_c4.inp" -o
"%model_path%\RQL_CRN_v3_c4.out" -c "%model_path%\RQL_CRN_v3_gas.asc"
GetSolution -nosen -norop -mass -all
RENAME "XMLdata.zip" "XMLdata_RQL_CRN_v3_Cluster4C4.zip"
RENAME "CKSoln.ckcsv" "RQL_CRN_v3_C4.csv"
rem run cluster 5(PSR)
CKReactorGenericPSR -i "%model_path%\RQL_CRN_v3_c5.inp" -o
"%model_path%\RQL_CRN_v3_c5.out" -c "%model_path%\RQL_CRN_v3_gas.asc"
GetSolution -nosen -norop -mass -all
RENAME "XMLdata.zip" "XMLdata_RQL_CRN_v3_Cluster5C5.zip"
RENAME "CKSoln.ckcsv" "RQL_CRN_v3_C5.csv"
rem run cluster 6(PSR)
CKReactorGenericPSR -i "%model_path%\RQL_CRN_v3_c6.inp" -o
"%model_path%\RQL_CRN_v3_c6.out" -c "%model_path%\RQL_CRN_v3_gas.asc"
GetSolution -nosen -norop -mass -all
RENAME "XMLdata.zip" "XMLdata_RQL_CRN_v3_Cluster6C6.zip"
RENAME "CKSoln.ckcsv" "RQL_CRN_v3_C6.csv"
rem run cluster 7(PSR)
CKReactorGenericPSR -i "%model_path%\RQL_CRN_v3_c7.inp" -o
"%model_path%\RQL_CRN_v3_c7.out" -c "%model_path%\RQL_CRN_v3_gas.asc"
GetSolution -nosen -norop -mass -all
RENAME "XMLdata.zip" "XMLdata_RQL_CRN_v3_Cluster7C7.zip"
RENAME "CKSoln.ckcsv" "RQL_CRN_v3_C7.csv"
rem run cluster 8(PSR)
CKReactorGenericPSR -i "%model_path%\RQL_CRN_v3_c8.inp" -o
"%model_path%\RQL_CRN_v3_c8.out" -c "%model_path%\RQL_CRN_v3_gas.asc"
GetSolution -nosen -norop -mass -all
RENAME "XMLdata.zip" "XMLdata_RQL_CRN_v3_Cluster8C8.zip"
RENAME "CKSoln.ckcsv" "RQL_CRN_v3_C8.csv"
rem run cluster 9 (PSR)
CKReactorGenericPSR -i "%model_path%\RQL_CRN_v3_c9.inp" -o
"%model_path%\RQL_CRN_v3_c9.out" -c "%model_path%\RQL_CRN_v3_gas.asc"
GetSolution -nosen -norop -mass -all
RENAME "XMLdata.zip" "XMLdata_RQL_CRN_v3_Cluster9C9.zip"
RENAME "CKSoln.ckcsv" "RQL_CRN_v3_C9.csv"
rem run cluster 10 (PSR)
/BELOWNORMAL
CKReactorGenericPSR -i "%model_path%\RQL_CRN_v3_c10.inp" -o
"%model_path%\RQL_CRN_v3_c10.out" -c "%model_path%\RQL_CRN_v3_gas.asc"
GetSolution -nosen -norop -mass -all
RENAME "XMLdata.zip" "XMLdata_RQL_CRN_v3_Cluster10C10.zip"
RENAME "CKSoln.ckcsv" "RQL_CRN_v3_C10.csv"
```

```
rem run cluster 11 ( Non reactive gas mixer)
CKReactorMixer  -i "%model_path%\RQL_CRN_v3_c11.inp" -o
"%model_path%\RQL_CRN_v3_c11.out" -c "%model_path%\RQL_CRN_v3_gas.asc"
GetSolution -nosen -norop -mass -all
RENAME "XMLdata.zip" "XMLdata_RQL_CRN_v3_Cluster11C11.zip"
RENAME "CKSoln.ckcsv" "RQL_CRN_v3_C11.csv"

rem run cluster 12 (Partially stireed reactor) using initialization from previous 9 parallel
clusters
CKReactorGenericPaSR -i "%model_path%\RQL_CRN_v3_c12.inp" -o
"%model_path%\RQL_CRN_v3_c12.out" -c "%model_path%\RQL_CRN_v3_gas.asc"
GetSolution -nosen -norop -mass -all
RENAME "XMLdata.zip" "XMLdata_RQL_CRN_v3_Cluster12C12.zip"
RENAME "CKSoln.ckcsv" "RQL_CRN_v3_C12.csv"
rem run cluster 13 ( Non reactive gas mixer)
CKReactorMixer  -i "%model_path%\RQL_CRN_v3_c13.inp" -o
"%model_path%\RQL_CRN_v3_c13.out" -c "%model_path%\RQL_CRN_v3_gas.asc"
GetSolution -nosen -norop -mass -all
RENAME "XMLdata.zip" "XMLdata_RQL_CRN_v3_Cluster13C13.zip"
RENAME "CKSoln.ckcsv" "RQL_CRN_v3_C13.csv"
rem run cluster 14 (Plug Flow reactor)
CKReactorPlugFlow  -i "%model_path%\RQL_CRN_v3_c14.inp" -o
"%model_path%\RQL_CRN_v3_c14.out" -c "%model_path%\RQL_CRN_v3_gas.asc"
GetSolution -nosen -norop -mass -all
RENAME "XMLdata.zip" "XMLdata_RQL_CRN_v3_Cluster14C14.zip"
RENAME "CKSoln.ckcsv" "RQL_CRN_v3_C14.csv"
rem run cluster 15 (Non reactive gas mixer)
CKReactorMixer  -i "%model_path%\RQL_CRN_v3_c15.inp" -o
"%model_path%\RQL_CRN_v3_c15.out" -c "%model_path%\RQL_CRN_v3_gas.asc"
GetSolution -nosen -norop -mass -all
RENAME "XMLdata.zip" "XMLdata_RQL_CRN_v3_Cluster15C15.zip"
RENAME "CKSoln.ckcsv" "RQL_CRN_v3_C15.csv"
rem run cluster 16 (Plug flow reactor)
CKReactorPlugFlow  -i "%model_path%\RQL_CRN_v3_c16.inp" -o
"%model_path%\RQL_CRN_v3_c16.out" -c "%model_path%\RQL_CRN_v3_gas.asc"
GetSolution -nosen -norop -mass -all
RENAME "XMLdata.zip" "XMLdata_RQL_CRN_v3_Cluster16C16.zip"
RENAME "CKSoln.ckcsv" "RQL_CRN_v3_C16.csv"
rem run cluster 17 ( Non reactive gas mixer)
CKReactorMixer  -i "%model_path%\RQL_CRN_v3_c17.inp" -o
"%model_path%\RQL_CRN_v3_c17.out" -c "%model_path%\RQL_CRN_v3_gas.asc"
GetSolution -nosen -norop -mass -all
RENAME "XMLdata.zip" "XMLdata_RQL_CRN_v3_Cluster17C17.zip"
RENAME "CKSoln.ckcsv" "RQL_CRN_v3_C17.csv"
EXIT /B
```

Appendix C

Emission Models Outputs

The following tables show the major output parameters of the emission models executed for CFM-56 SAC, E^3 SAC and Wall-Jet RQL combustors. The temperature of the zones in these tables are the temperatures after the cooling flow at each zone is mixed with the core flow; therefore, they may be slightly different from the axial temperature graphs that are provided in the experiments in Chapter 7, where the core temperatures without cooling flow mixing is provided.

As it is expected for CFM56 and E3 the pressure loss coefficients and flow fractions do not change due to the fix geometry of the combustor; however, the pressure loss percentage changes. In RQL combustor the swirler geometry changes to keep the rich zone equivalence ratio at a certain limit and the change in the geometry changes the flow distribution, burner pressure loss coefficient and burner pressure loss. These changes can be seen in Table 53.

Table 51: Additional outputs of the CFM56-7B27 SAC emission model

Output Parameter	unit	TO	CL	APP	ID
Primary zone temperature	K	2603	2524	1942	1311
Secondary zone temperature	K	2347	2214	1724	1215
Dilution zone temperature	K	1768	1662	1256	902
Primary zone flow fraction	-	0.4	0.4	0.4	0.4
Secondary zone flow fraction	-	0.12	0.12	0.12	0.12
Dilution zone flow fraction	-	0.18	0.18	0.18	0.18
Cooling flow fraction	-	0.29	0.29	0.29	0.29
Primary zone equivalence ratio	-	1.05	0.97	0.61	0.36
Secondary zone equivalence ratio	-	0.8	0.74	0.47	0.28
Dilution zone equivalence ratio	-	0.419	0.39	0.24	0.14
Primary zone efficiency	-	0.98	0.95	0.94	0.91
Secondary zone efficiency	-	0.99	0.98	0.98	0.98
Dilution zone efficiency	-	0.9998	0.9998	0.9998	0.9998
Liner cross section area	in^2	276.4	276.4	276.4	276.4
Primary zone cross section area	in^2	276.4	276.4	276.4	276.4
Secondary zone cross section area	in^2	276.4	276.4	276.4	276.4
Dilution zone cross section area	in^2	217.9	217.9	217.9	217.9
Liner Mach number	-	0.015	0.015	0.015	0.017
Primary zone Mach number	-	0.033	0.033	0.03	0.029
Secondary zone Mach number	-	0.047	0.045	0.043	0.036
Dilution zone Mach number	-	0.075	0.074	0.073	0.073
Primary zone unmixedness	-	0.18	0.27	0.844	0.66
Diffuser pressure loss percentage	%	0.47	0.47	0.52	0.6
Diffuser pressure loss coefficient	-	0.17	0.17	0.17	0.17
Burner pressure loss percentage	%	4.54	4.49	5.02	5.72
Burner pressure loss coefficient	-	42.0	42.0	42.0	42.0
Ignition delay time	se-6	5.79	8.2	44.9	789
Sauter Mean Diameter (SMD)	me-6	1.81	2.17	5.78	15
Evaporation degree	%	42.9	39.5	26.6	46.9

Table 52: Additional outputs of the E^3 SAC emission model

Output Parameter	unit	TO	CL	APP	ID
Primary zone temperature	K	2591	2501	1939	1646
Secondary zone temperature	K	2206	2068	1564	1447
Dilution zone temperature	K	1656	1561	1172	1035
Primary zone flow fraction	-	0.33	0.33	0.33	0.33
Secondary zone flow fraction	-	0.17	0.17	0.17	0.17
Dilution zone flow fraction	-	0.26	0.26	0.26	0.26
Cooling flow fraction	-	0.23	0.23	0.23	0.23
Primary zone equivalence ratio	-	1.07	0.98	0.61	0.62
Secondary zone equivalence ratio	-	0.71	0.65	0.40	0.41
Dilution zone equivalence ratio	-	0.36	0.33	0.20	0.21
Primary zone efficiency	-	0.97	0.97	0.97	0.82
Secondary zone efficiency	-	0.98	0.98	0.98	0.98
Dilution zone efficiency	-	0.99	0.99	0.99	0.985
Liner cross section area	in^2	235	235	235	235
Primary zone cross section area	in^2	235.0	235.0	235.0	235.0
Secondary zone cross section area	in^2	235.0	235.0	235.0	235.0
Dilution zone cross section area	in^2	143.1	143.1	143.1	143.1
Liner Mach number	-	0.017	0.018	0.018	0.017
Primary zone Mach number	-	0.04	0.04	0.037	0.034
Secondary zone Mach number	-	0.058	0.058	0.056	0.054
Dilution zone Mach number	-	0.13	0.129	0.126	0.124
Primary zone unmixedness	-	0.23	0.4	0.82	0.21
Diffuser pressure loss percentage	%	0.15	0.15	0.17	0.15
Diffuser pressure loss coefficient	-	0.047	0.047	0.047	0.050
Burner pressure loss percentage	%	35.8	35.8	35.8	35.8
Burner pressure loss coefficient	-	4.47	4.5	4.9	4.3
Ignition delay time	se-6	5.9	8.0	51	105
Sauter Mean Diameter (SMD)	me-6	1.75	2.11	5.8	15
Evaporation degree	%	45.6	41.5	31.3	8.6

Table 53: Additional outputs of the Wall-Jet RQL combustor emission model

Output Parameter	unit	APP	CL	SS	TO
Rich zone temperature	K	2098.5	2210.7	2319.4	2281
Mixing zone temperature	K	1338.9	1437.8	1742.1	1691.42
Lean zone temperature	K	1346.3	1574.9	1960.9	1863.6
Exit temperature	K	1315.6	1528.0	1909.6	1812.9
Rich zone flow fraction	-	0.38	0.20	0.23	0.27
Mixing zone flow fraction	-	0.57	0.73	0.72	0.68
Cooling flow fraction	-	0.042	0.054	0.052	0.050
Rich zone equivalence ratio	-	0.72	1.78	1.93	1.8
Mixing zone equivalence ratio	-	0.29	0.39	0.46	0.51
Lean zone equivalence ratio	-	0.29	0.39	0.46	0.51
Liner cross section area	in^2	242.1	242.1	242.1	242.1
Rich zone cross section area	in^2	242.1	242.1	242.1	242.1
Mixing zone cross section area	in^2	111.3	111.3	111.3	111.3
Lean zone cross section area	in^2	242.1	242.1	242.1	242.1
Rich zone efficiency	-	0.99	0.99	0.99	0.99
Lean zone efficiency	-	0.995	0.995	0.995	0.995
Liner Mach number	-	0.017	0.006	0.012	0.013
Rich zone Mach number	-	0.036	0.014	0.024	0.027
Mixing zone Mach number	-	0.14	0.078	0.14	0.13
Lean zone Mach number	-	0.068	0.049	0.08	0.08
Primary zone unmixedness	-	0.854	0.18	0.18	0.18
Burner pressure loss percentage	%	4.9	3.9	10	7.7
Burner pressure loss coefficient	-	25.7	43.04	40.64	36.4
Ignition delay time	se-6	20.5	42.6	51.4	37.3
Sauter mean diameter (SMD)	me-6	4.31	3.15	3.24	1.44
Evaporation degree	%	20	67.5	83.9	99.3
Mixing zone mixing time	s	1.36e-4	3.35e-4	1.81e-4	1.64e-4
Mixing zone (PaSR) unmixedness	-	0.132	0.150	0.155	0.139

REFERENCES

1. *Critical Propulsion Components, Volume 2: Combustor*. 2005, NASA.
2. Glassman, I. and R. Yetter, *Combustion*. 2008: Academic Pr
3. Committee on Aviation Environmental Protection, *CAPE/7 Working Paper*. 2007.
4. Mattingly, J.D., W.H. Heiser, and D.T. Pratt, *Aircraft engine design*. 2002: AIAA
5. Answers.com. *Boundary Layer Description*. [cited 2010 Nivember]; Available from: http://www.answers.com/topic/boundary-layer.
6. Dieter, G.E., *Engineering Design: A Materials and Processing Approach*. 3 ed. 2000: McGraw-Hill
7. Lefebvre, A.H., *Gas Turbine Combustion*. 2 ed. 1999, Philadelphia, PA: Taylor & Francis
8. Roby, R., et al., *High Fuel-Air Ratio (FAR) Combustor Modeling*. 2003, Storming Media.
9. Smith, R., et al., *Advanced Low Emissions Subsonic Combustor Study*. 1998, NASA Center: Glenn Research Center.
10. Penner, J.E. and others, *Aviation and the Global Atmosphere*. 1999: Cambridge University Press Cambridge
11. Rohde, J., *Overview of the NASA AST and UEET Emissions Reduction Projects*. 2002, Presentation.
12. Federal Aviation Administration, *Aviation & Emissions: A Primer*. 2005, Federal Aviation Administration, Office of Environment and Energy. p. 25.
13. Rezvani, R., R. Denny, and D. Mavris. *A Design-Oriented Semi-Analytical Emissions Prediction Method for Gas Turbine Combustors*. in *Aerospace Science Meeting*. 2009. Orlando, Fl: American Institute of Aeronautics and Astronautics
14. Mongia, H.C., *Combining Lefebvre's Correlations with Combustor CFD*, in *40th AIAA/ASME/SAE/ASEE Joint Propulsion Conference and Exhibit*. 2004, AIAA: Fort Lauderdale,FL.
15. Samuelson, S., *Rich Burn, Quick-Mix, Lean Burn (RQL) Combustor*, in *The Gas Turbine Handbook*, National Energy Technology Laboratory, Editor. 2006, U.S. Department of Energy, Office of Fossil Energy.

16. Wood, C.P., et al., *Development and application of a surrogate distillate fuel.* Journal of Propulsion and Power, 1989. **5**(4): p. 399–405
17. McKinney, R.G., et al., *The Pratt & Whitney TALON X Low Emissions Combustor: Revolutionary Results with Evolutionary Technology*, in *45th AIAA Aerospace Sciences Meeting and Exhibit*. 2007: Reno, NV.
18. Burrus, D., P.E. Sabla, and D.W. Bahr, *Energy Efficient Engine (E3): Component Development and Integration of Single-Annular Combustor Technology*. 1980, NASA Center. p. 118.
19. Brasseur, G.P., et al., *European scientific assessment of the atmospheric effects of aircraft emissions.* Atmospheric Environment, 1998. **32**(13): p. 2329--2418
20. Burrus, D.L., et al., *Energy Efficient Engine (E3): Combustion System Component Technology Performance*. 1984, NASA Center. p. 494.
21. Despierre, A., P.J. Stuttaford, and P.A. Rubini. *Preliminary gas turbine combustor design using a genetic algorithm*. in *Int. Gas Turbine and Aeroengine Congress & Exhibition,*. 1997. Orlando, FL, USA: ASME, New York, NY, USA
22. Dodds, W., *Engine and Aircraft Technologies To Reduce Emissions*, in *UC Technology Transfer Symposium "Dreams of Flight"*. 2002: San Diego.
23. Motsamai, O.S., J.A. Visser, and R.M. Morris, *Multi-disciplinary design optimization of a combustor.* Engineering Optimization, 2008. **40**(2): p. 137-156
24. Eberius, K.H. and T. Just. *Atmospheric Pollution by Jet Engines*. 1973
25. Burrus, D.L., et al., *Energy Efficient Engine (E3): Combustor Test Hardware Detailed Design*. 1984, NASA Center. p. 474.
26. Shakariyants, S.A., et al. *Generic airplane and aero-engine simulation procedures for exhaust emission studies*. in *ASME Turbo Expo, Power for Land, Sea and Air*. 2007. Montreal, Que., Canada: American Society of Mechanical Engineers, New York, NY 10016-5990, United States
27. Bellan, J.R., P.T. Harsha, and R.B. Edelman, *State of The Art Combustion Modeling (Part B: Analytical Modeling)*, Sicence Applications, Inc. (SAI): Woodland Hills, CA. p. 138.
28. Sturgess, G.J., et al., *Emissions Reduction Technologies for Military Gas Turbine Engines.* Journal of Propulsion and Power, 2005. **21**(2): p. 193-217

29. *International Civil Aviation Organization (ICAO).* [cited 2010 October]; Available from: www.icao.org.

30. Ballal, D.R. and J. Zelina, *Progress in aeroengine technology(1939-2003).* Journal of Aircraft, 2004. **41**(1): p. 43--50

31. Penner, J., et al., *Aviation and the Global Atmosphere, Intergovernmental Panel on Climate Change Special Report*. 1999, Cambridge University Press, Cambridge, UK.

32. National Research Council, *Assessing NASA's High Speed Research Program*. 1997: National Academy Press, Washington, DC

33. Williams, M. *Emission Levels of the Olympus 593 Engine at the Supersonic Cruise Conditions of the Concorde Aircraft*. 1973

34. Wulff, A. and J. Hourmouziadis, *Technology review of aeroengine pollutant emissions.* Aerospace science and technology, 1997. **1**(8): p. 557-572

35. Schmucker C. P, *Zum Potential zukünftig Überschall-Verkehrsflugzeuge*, in *DGLR Annual Meeting*. 1996: Dresden, Germany.

36. Kandebo, S.W., *HSCT Propulsion Studies Focus on Reducing Emissions, Noise.* . Aviation Week & Space Technology, July 10, 1989.

37. Wesoky, L., U. Schumann, and D. Wurzel, *Lingering uncertaintly about aviation's impact addressed by growing body of scientific data.* ICAO Journal, 1996. **51**(2)

38. Shaw, R.J. *Propulsion challenges for a 21 st century economically viable, environmentally compatible High-Speed Civil Transport*. in *10th ISABE*. 1991. Nottingham, UK

39. Peter Belobaba, Amedeo Odoni, and Cynthia Barnhart, *The Global Airline Industry*. 2009, West Sussex, UK: Wiley Ltd. 509

40. National Research Council, *A Review of NASA's Atmospheric Effects of Stratospheric Aircraft Project*. 1999, Washington DC: National Academy Press

41. Waitz, I., et al., *Report to the United States Congress: Aviation and the Environment, A National Vision, Framework for Goals and Recommended Actions.* Partnership for AiR Transportation Noise and Emissions Reduction, MIT, Cambridge, MA, 2004

42. Norman, Q., *Development of the technical basis for a new emission parameter covering the whole aircraft operation*, NEPAIR, final technical report, 35-63.

43. FAA Website. *Aviation Environmental Models*. 2007 [cited 2010 November]; Available from: http://www.faa.gov/about/office_org/headquarters_offices/aep/models/.

44. Kirby, M.R., et al., *Advanced Vehicles Modeling for the Next Generation Air Transportation System (NextGen Vehicle Integration NRA)*, in *9th AIAA Aviation Technology, Integration, and Operations Conference (ATIO)* 2009, AIAA: Hilton Head, South Carolina.

45. Kirby, M.R., P.A. Barros, and D.N. Mavris, *Enhancing the Environmental Policy Making Process with the FAA's EDS Analysis Tool*, in *47th AIAA Aerospace Sciences Meeting Including The New Horizons Forum and Aerospace Exposition*. 2009, AIAA: Orlando, Florida.

46. Mellor, A.M., *Design of Modern Turbine Combustors*. 1990, San Diego, CA: Academic Press

47. Mellor, A.M., *Semi-empirical correlations for gas turbine emissions, ignition, and flame stabilization.* Progress in Energy and Combustion Science, 1980. **6**(4): p. 347-358

48. Mongia, H.C., *Recent Progress in Comprehensive Modeling of Gas Turbine Combustion*. 2008.

49. Stubbs, R. and N. Liu. *Preview of the National Combustion Code*. in *33rd AIAA/ASME/SAE/ASEE Joint Propulsion Conference & Exhibit* 1997. Seattle, WA: AIAA

50. Danis, A., D. Burrus, and H. Mongia, *Anchored CCD for gas turbine combustor design and data correlation.* Journal of Engineering for Gas Turbines and Power, 1997. **119**: p. 535

51. Lefebvre, A.H., *Gas Turbine Combustor Design Problems*. 1978, Washington, D.C: Hemisphere Publishing

52. Rizk, N., *Fuel Atomization Effects on Combustor Performance*, in *40 th AIAA/ASME/SAE/ASEE Joint Propulsion Conference and Exhibit*. 2004: Fort Lauderdale, Florida.

53. Rizk, N.K., et al., *Predictions of NO Formation Under Combined Droplet and Partially Premixed Reaction of Diffusion Flame Combustors.* Journal of Engineering for Gas Turbines and Power, 2002. **124**: p. 31

54. Shakariyants, S.A., J.P. Van Buijtenen, and W.P.J. Visser. *Aero-gas turbine emission reduction and simulation technology: Philosophy and approach*. in *Proceeding of ASME TURBO EXPO, Power for Land, Sea and Air*. 2004. Vienna, Austria: American Society of Mechanical Engineers, New York, NY 10016-5990, United States

55. Shakariyants, S.A., J.P. Van Buijtenen, and W.P.J. Visser. *Generic geometry definition of the aircraft engine combustion chamber*. in *ASME Turbo Expo, Power for Land, Sea and Air*. 2004. Vienna, Austria: American Society of Mechanical Engineers, New York, NY 10016-5990, United States

56. Shakariyants, S.A., et al. *A Generic Approach to Aero-Engine Exhaust Emission Simulation*. in *ISABE 2005 - The 17th Symposium on Air Breathing Engines*. 2005. Munich, Germany: American Inst. of Aeronautics and Astronautics

57. Shakariyants, S.A., et al. *A multidisciplinary aero-engine exhaust emission study*. in *ASME Turbo Expo, Power for Land, Sea and Air*. 2006. Barcelona, Spain: American Society of Mechanical Engineers, New York, NY 10016-5990, United States

58. Swithenbank, J., et al., *Combustion Design Fundamentals.* Fourteenth Symposium (International) on Combustion, 1973: p. 627-638

59. Rizk, N.K. and H.C. Mongia. *Lean Low NOx Combustion Concept Evaluation*. in *23rd Symposium (International) on Combustion*. 1990: The Combustion Institute

60. Rizk, N. and H. Mongia. *3-D combustor performance validation with high density fuels*. 1989

61. Lebedev, A.B., et al., *Modeling study of gas-turbine combustor emission*, in *Proceedings of the Combustion Institute*. 2009. p. 2941-2947.

62. Greyvenstein, G. and D. Laurie, *A segregated CFD approach to pipe network analysis.* International Journal for Numerical Methods in Engineering, 1994. **37**(21): p. 3685-3706

63. Stuttaford, P.J. and P.A. Rubini, *Preliminary Gas Turbine Combustor Design using a Network Approach.* Journal of Engineering for Gas Turbines and Power, 1997. **119**(3)

64. Rodriguez, C.G. and W.F. O'Brien, *One-dimensional, steady model for Straight and Reverse Flow Gas Turbine Combustors*. 1997.

65. Davis, M. *A stage-by-stage post-stall compression system modeling technique*. 1987

66. Andreini, A. and B. Facchini, *Gas Turbines Design and Off-Design Performance Analysis with Emissions Evaluation.* Journal of Engineering for Gas Turbines and Power-Transactions of the Asme, 2004. **126**(1): p. 83-91

67. Chigier, N., *Energy, combustion, and environment*. 1981: McGraw-Hill Companies

68. Turns, S.R., *An introduction to combustion*. 2 ed. 1996, New York: McGraw-Hill

69. Chen, R.H. *The role of the recirculation vortex in improving fuel-air mixing within swirling flames*. in *Symposium(International) on Combustion, 22 nd*. 1988. Seattle, WA: The Combustion Institute

70. Chigier, N.A. and J.M. Beer. *Velocity and static-pressure distributions in swirling air jets issuing from annular and divergent nozzles*. in *ASME Meeting FE-8, May 18-21 1964*. 1964. New York, NY, United States: American Society of Mechanical Engineers (ASME)

71. Pompei, F. and J.B. Heywood, *The role of mixing in burner-generated carbon monoxide and nitric oxide.* Combustion and Flame, 1972. **19**: p. 407-418

72. Hsiao, G. and H. Mongia, *Swirl cup modeling part III: Grid independent solution with different turbulence models.* AIAA Paper, 2003. **1349**: p. 2003

73. Hsiao, G., H. Mongia, and A. Vij, *Swirl cup modeling part II: inlet boundary conditions.* AIAA Paper, 2003. **1350**

74. Jeng, S.M., N.M. Flohre, and H.C. Mongia, *Swirl Cup Modeling-Atomization.* 2004

75. Mongia, H.C., et al., *Swirl Cup Modeling Part I.* AIAA Paper, 2001. **3576**: p. 2001

76. Fu, Y., et al. *Characteristics of the swirling flow generated by a counter-rotating swirler*. in *43rd AIAA/ASME/SAE/ASEE Joint Propulsion Conference*. 2007. Cincinnati, OH, United States: American Institute of Aeronautics and Astronautics Inc., Reston, VA 20191-4344, United States

77. Mongia, H.C., *Aero-thermal design and analysis of gas turbine combustion systems - Current status and future direction* in *34th AIAA/ASME/SAE/ASEE Joint Propulsion Conference and Exhibit,* . 1998, AIAA: Cleveland, OH.

78. Gogineni, S., et al., *Combustion Air Jet Influence on Primary Zone Characteristics for Gas Turbine Combustors.* Journal of Propulsion and Power, 2002. **18**(2): p. 407-416

79. Holdeman, J., D. Liscinsky, and D. Bain, *Mixing of Multiple Jets With a Confined Subsonic Crossflow: Part II—Opposed Rows of Orifices in Rectangular Ducts.* Journal of Engineering for Gas Turbines and Power, 1999. **121**: p. 551

80. Holdeman, J., et al., *Mixing of Multiple Jets With a Confined Subsonic Crossflow: Part I—Cylindrical Duct.* Journal of Engineering for Gas Turbines and Power, 1997. **119**: p. 852

81. Peters, N., *Turbulent combustion*. 2000: Cambridge University Press

82. Fluent Inc., *Fluent User Manual*. 2003, Lebanon, New Hampshire

83. Held, T. and H. Mongia. *Application of a partially premixed laminar flamelet model to a low emissions gas turbine combustor*. in *International Gas Turbine & Aeroengine Congress & Exhibition*. 1998. Stockholm, Sweden: ASME

84. Stevens, E.J., T.J. Held, and H.C. Mongia, *Swirl Cup Modeling Part VII: Partially-premixed Laminar Flamelet Model Validation and Simulation of a Single-cup Combustor with Gaseous N-heptane.* AIAA Paper-2003-0488, 2003

85. Held, T. and M. Mueller, *A data-driven model for NOx, CO and UHC emissions for a dry low emissions gas turbine combustor*, in *37th AIAA/ASME/SAE/ASEE Joint Propulsion Conference and Exhibit*. 2001: Salt Lake City, UT.

86. Longwell, J., E. Frost, and M. Weiss, *Flame stability in bluff body recirculation zones.* Industrial & Engineering Chemistry, 1953. **45**(8): p. 1629-1633

87. Tsang, W., *Progress in the development of combustion kinetics databases for liquid fuels.* Data Science Journal, 2004. **3**(0): p. 1-9

88. Held, T., A. Marchese, and F. Dryer, *A semi-empirical reaction mechanism for n-heptane oxidation and pyrolysis.* Combustion Science and Technology, 1997. **123**(1): p. 107-146

89. Westbrook, C. and W. Pitz, *Comprehensive chemical kinetic reaction mechanism for oxidation and pyrolysis of propane and propene.* Name: Combust. Sci. Technol, 1984

90. Park, T., et al., *Development of a Detailed Chemical Kinetic Mechanism for Combustion of JP-7 Fuel*, in *39th AIAA/ASME/SAE/ASEE Joint Propulsion Conference and Exhibit*. 2003: Huntsville, Al.

91. Montgomery, C.J., et al., *Reduced Chemical Kinetic Mechanisms for JP-8 Combustion*, in *40th AIAA Aerospace Science Meeting and Exhibit*. 2002, AIAA: Reno, NV.

92. Violi, A., et al., *Experimental Formulation and Kinetic Model for JP-8 Surrogate Mixtures.* Combustion Science and Technology, 2002. **174**(11): p. 399-417

93. Edwards, T. and L.Q. Maurice, *Surrogate mixtures to represent complex aviation and rocket fuels.* Journal of Propulsion and Power, 2001. **17**(2): p. 461-466

94. Maurice, L.Q., et al., *Emissions from Combustion of Hydrocarbons in a Well-Stirred Reactor*, in *AIAA/ASME/SAE/ASEE Joint Propulsion Conference and Exhibit, 37th*. 1999: Salt Lake City, UT. p. 99-1038.

95. Lindstedt, R.P. and L.Q. Maurice, *Detailed Chemical–Kinetic Model for Aviation Fuels.* Journal of Propulsion and Power, 2000. **16**(2): p. 187-195

96. Montgomery, C.J., et al., *Reduced Chemical Kinetic Mechanisms for Hydrocarbon Fuels.* Journal of Propulsion and Power, 2002. **18**(1): p. 192-198

97. Roberts, R., et al., *An Analytical Model for Nitric Oxide Formation in a Gas Turbine Combustor.* AIAA Journal, 1972. **10**(6): p. 820-826

98. Fenimore, C.P. in *13th Symposium on Combustion*. 1971: The Combustion Institute

99. Chen, J., *Stochastic modeling of partially stirred reactors.* Combustion Science and Technology, 1997. **122**(1): p. 63-94

100. Bragg, S., *Application of Reaction Rate Theory to Combustion Chamber Analysis*. 1953, Aeronautical Research Council London (United Kingdom).

101. Correa, S.M., *Turbulence-chemistry interactions in the intermediate regime of premixed combustion.* Combustion and Flame, 1993. **93**(1-2): p. 41-60

102. Hottel, H.C. and G.C. Williams. *Kinetic studies in stirred reactors -- Combustion of carbon monoxide and propane*. in *10th Symposium on Combustion, 1965*. 1965

103. Kee, R.J., et al., *CHEMKIN 4 User Manual*. 2005, Reaction Design: San Diego, CA.

104. Pope, S., *PDF methods for turbulent reactive flows.* Progress in Energy and Combustion Science, 1985. **11**(2): p. 119-192

105. Pope, S., *A Monte Carlo method for the PDF equations of turbulent reactive flow.* Combustion Science and Technology, 1981. **25**(5): p. 159-174

106. Borghi, R., *Turbulent combustion modelling.* Progress in Energy and Combustion Science, 1988. **14**(4): p. 245-292

107. Sturgess, G.J. and D.T. Shouse, *A Hybrid Model for Calculating Lean Blowouts in Practical Combustors*, in *ASME, SAE, and ASEE, Joint Propulsion Conference and Exhibit*. 1996 AIAA: 32nd, Lake Buena Vista, FL.

108. Tonouchi, J., T. Held, and H. Mongia, *A semi-analytical finite rate two-reactor model for gas turbine combustors.* Journal of Engineering for Gas Turbines and Power, 1998. **120**: p. 495

109. Mellor, A.M. and K.J. Fritsky, *Turbine combustor preliminary design approach.* Journal of Propulsion and Power, 1990. **6**(3): p. 334-343

110. Novosselov, I., et al. *Chemical reactor network application to emissions prediction for industrial DLE Gas Turbine*. in *ASME Turbo Expo: Power for Land, Sea and Air*. 2006. Barcelona, Spain

111. Novosselov, I.V., *Chemical Reactor Networks for Combustion Systems Modeling*, in *Department of Mechanical Engineering*. 2006, University of Washington: Washington. p. 322.

112. Vedula, V., et al. *Sector rig test of a Ceramic Matrix Composite (CMC) combustor liner*. in *ASME Turbo Expo 2006 Power for Land, Sea and Air*. 2006. New York, NY 10016-5990, United States: American Society of Mechanical Engineers

113. Beven, K. and A. Binley, *Future of distributed models: Model calibration and uncertainty prediction.* Hydrological Processes, 1992. **6**(3): p. 279-298

114. Penmetsa, R.C. and R.V. Grandhi, *Uncertainty Propagation Using Possibility Theory and Function Approximations.* Mechanics Based Design of Structures and Machines, 2003. **31**(2): p. 257-279

115. Helton, J., J. Johnson, and W. Oberkampf, *An exploration of alternative approaches to the representation of uncertainty in model predictions.* Reliability Engineering & System Safety, 2004. **85**(1-3): p. 39-71

116. Oberkampf, W., et al., *Mathematical representation of uncertainty.* Seattle, WA, April, 2001: p. 2001-1645

117. Guo, J. and X. Du, *Sensitivity Analysis with Mixture of Epistemic and Aleatory Uncertainties.* AIAA Journal, 2007. **45**(9): p. 2337

118. Helton, J.C., *Uncertainty and sensitivity analysis techniques for use in performance assessment for radioactive waste disposal.* Reliability engineering & systems safety, 1993. **42**(2-3): p. 327-367

119. National Energy Technology Laboratory, *The Gas Turbine Handbook.* 2006: U.S. Department of Energy, Office of Fossil Energy

120. Peterson, C., W. Sowa, and G. Samuelsen, *Performance of a Model Rich Burn-Quick Mix-Lean Burn Combustor at Elevated Temperature and Pressure.* 2002

121. Holdeman, J.D., *Mixing of multiple jets with a confined subsonic crossflow.* Progress in Energy and Combustion Science, 1993. **19**(1): p. 31-70

122. Chen, K.S. and J.Y. Hwang, *Experimental study on the mixing of one- and dual-line heated jets with a cold crossflow in a confined channel.* AIAA journal, 1991. **29**(Compendex): p. 353-360

123. Chang, Y.R. and K.S. Chen, *Prediction of opposing turbulent line jets discharged laterally into a confined crossflow.* International Journal of Heat and Mass Transfer, 1995. **38**(9): p. 1693-1703

124. *Combustor*, in *Critical Propulsion Components*. 2005, NASA.

125. McBride, B., S. Gordon, and M. Reno, *Coefficients for Calculating Thermodynamic and Transport Properties of Individual Species, NASA, Report No*. 1993, TM-4513.

126. Gordon, S. and B. McBride, *Computer program for calculation of complex chemical equilibrium compositions, rocket performance, incident and reflected shocks, and Chapman-Jouguet detonations.* 1976

127. Tai, J., *A Multidisciplinary Design Approach to Size Stopped Rotor/Wing Configuration Using Reaction Drive and Circulation Control*, in *Aerospace Engineering*. 1998, Georgia Institute of Technology: Atlanta. p. 254.

128. Norster, E., *Jet penetration and mixing studies.* Unpublished work, College of Aeronautics, Cranfield,

129. Knight, H.A. and R.B. Walker, *The Component Pressure Losses in Combustion Chambers*, in *Aeronautical Research Council Reports and Memoranda* 1957, Aeronautical Research Council (A.R.C): LONDON. p. 36.

130. Tacina, R.R. and J. Grobman, *Analysis of Total Pressure Loss and Airflow Distribution for Annular Gas Turbine Combustors*. 1969, NASA.

131. Pratt, D.T., *An Analytical Investigation of the Pressure Loss in a Cylindrical Gas Turbine Combustor*. 1962, University of California: Berkeley.

132. Spadaccini, L. and J. Tevelde, *Autoignition characteristics of aircraft-type fuels.* Combustion and Flame, 1982. **46**: p. 283-300

133. Rosin, P. and E. Rammler, *The laws governing the fitness of powdered coal.* Journal of the Institute of fuel, 1933. **7**(31): p. 29-36

134. Lefebvre, A., *Atomization and sprays*. 1989: CRC

135. Faeth, G., *Current status of droplet and liquid combustion.* Progress in Energy and Combustion Science, 1977. **3**(4): p. 191-224

136. Faeth, G.M., *Evaporation and combustion of sprays.* Progress in Energy and Combustion Science, 1983. **9**(1-2): p. 1-76

137. Sazhin, S.S., et al., *Models for droplet transient heating: effects on droplet evaporation, ignition, and break-up.* Int J Thermal Science, 2005. **44**: p. 610–622

138. Bae, J.H. and C.T. Avedisian, *Jet fuel droplet combustion with and without the convection*, in *37th Intersociety Energy Conversion Engineering Conference (IECEC)*. 2002, IECEC: Washington, WA, USA.

139. Coordinating Research Council, *Handbook of Aviation Fuel Properties*. 1983, Society of Automotive Engineers (SAE): Atlanta, Ga. p. 113.

140. Heywood, J.B. and T. Mikus, *Parameter Controlling Nitric Oxide Emissions from Gas Turbine Combustors*, in *AGARD Propulsion and Energetic Panel 41st Meeting on Atmospheric Pollution by Aircraft Engines*. 1973: London, England.

141. Corrsin, S., *Simple theory of an idealized turbulent mixer.* AIChE Journal, 1957. **3**(3): p. 329-330

142. Corrsin, S., *The isotropic turbulent mixer: Part II. Arbitrary Schmidt number.* AIChE Journal, 1964. **10**(6): p. 870-877

143. Allaire, D.L., *A Physics-Based Emissions Model for Aircraft Gas Turbine Combustors*, in *Aerospace Engineering*. 2006, Massachusetts Institute of Technology: Boston, MA. p. 105.

144. Reaction Design. *CHEMKIN 4* [cited 2010 October]; Available from: http://www.reactiondesign.com/products/open/chemkin.html.

145. Syed, K.J., K. Roden, and P. Martin, *A Novel Approach to Predicting NOX Emissions from Dry Low Emissions Gas Turbines.* Journal of Engineering for Gas Turbines and Power-Transactions of the Asme, 2007. **129**(3): p. 672-679

146. White, F., *Viscous fluid flow*. 1991: McGraw-Hill New York

147. von Karman, T., *Uber laminare und turbulente Reibung.* Z. Angew. Math. Mech, 1921. **1**(4): p. 233–253

148. Thwaites, B., *Incompressible aerodynamics*. 1960: Clarendon Press

149. Phoenix Integration, *Model Center 9.0.*

150. Burcat, A. *Prof. Burcat's Thermodynamic Data* [cited 2010 November]; Available from: http://garfield.chem.elte.hu/Burcat/burcat.html.

151. Kyne, A.G., et al., *Prediction of premixed laminar flame structure and burning velocity of aviation fuel-air mixtures*, in *ASME Turbo Expo: Power for Land, Sea and Air*. 2001, ASME: New Orleans, USA.

152. Honnet, S., et al., *A surrogate fuel for kerosene.* Proceedings of the Combustion Institute, 2009. **32**(1): p. 485-492

153. Sturgess, G.J. *Assessment of an abbreviated jet-A/JP-5/JP-8 reaction mechanism for modeling gas turbine engine gaseous emissions (1402 KB)* in *AIAA/ASME/SAE/ASEE Joint Propulsion Conference and Exhibit 33rd*. 1997. Seattle, WA: AIAA

154. Dodds, W., *Twin Annular Premixing Swirler (TAPS) Combustor, Power Point Presentation.* 2005

155. Borman, G., J. Johnson, and S.o.A. Engineers, *Unsteady vaporization histories and trajectories of fuel drops injected into swirling air*. 1962: Society of Automotive Engineers